SOFT TISSUE BIOMECHANICS IN WOUND HEALING AND PREVENTION

EDITED BY: Yih-Kuen Jan, Matthew J. Major, Fang Pu and Sharon Eve Sonenblum

PUBLISHED IN: Frontiers in Bioengineering and Biotechnology

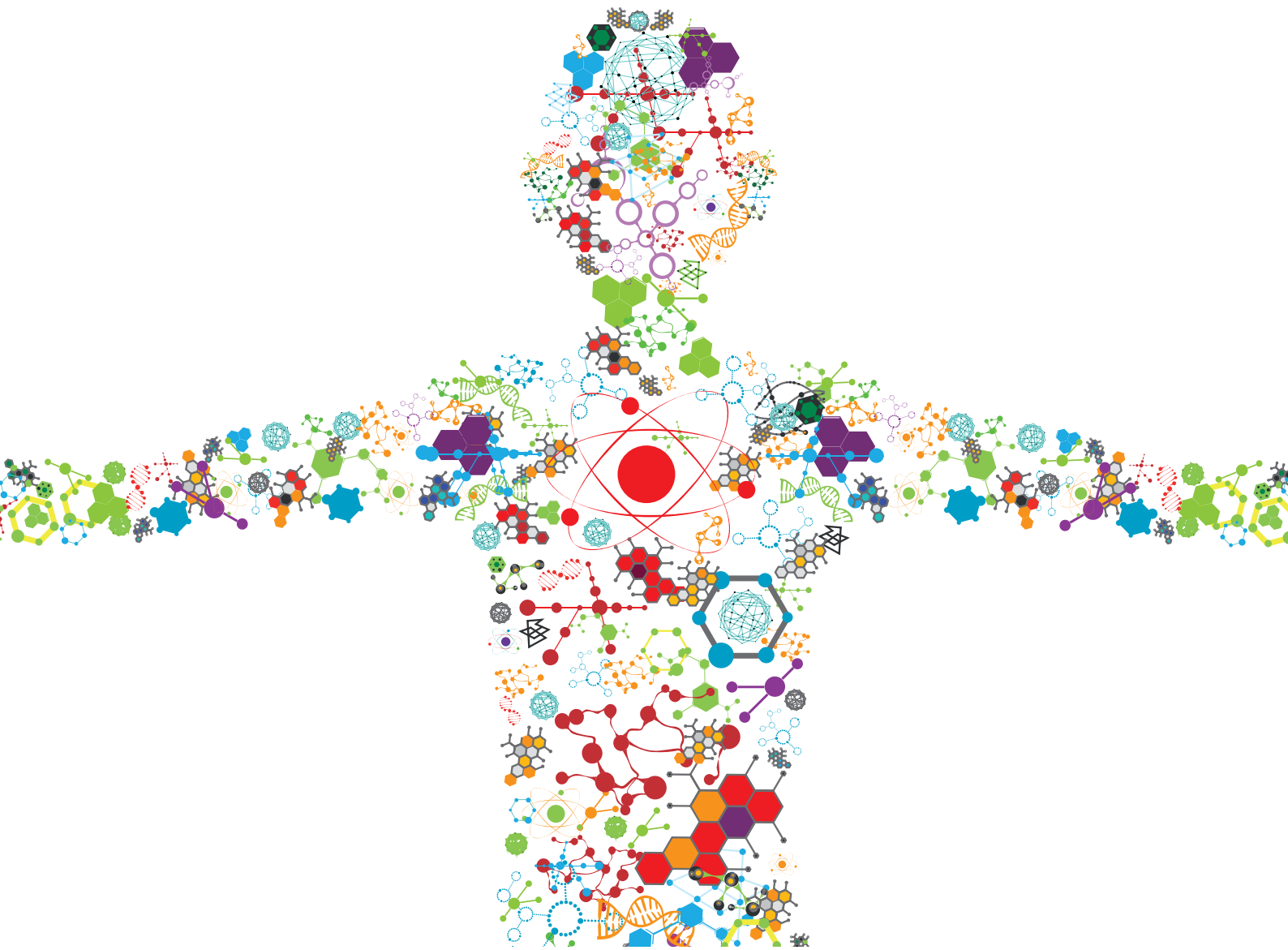

frontiers Research Topics

ISSN 1664-8714
ISBN 978-2-88976-028-2
DOI 10.3389/978-2-88976-028-2

About Frontiers

Frontiers is more than just an open-access publisher of scholarly articles: it is a pioneering approach to the world of academia, radically improving the way scholarly research is managed. The grand vision of Frontiers is a world where all people have an equal opportunity to seek, share and generate knowledge. Frontiers provides immediate and permanent online open access to all its publications, but this alone is not enough to realize our grand goals.

Frontiers Journal Series

The Frontiers Journal Series is a multi-tier and interdisciplinary set of open-access, online journals, promising a paradigm shift from the current review, selection and dissemination processes in academic publishing. All Frontiers journals are driven by researchers for researchers; therefore, they constitute a service to the scholarly community. At the same time, the Frontiers Journal Series operates on a revolutionary invention, the tiered publishing system, initially addressing specific communities of scholars, and gradually climbing up to broader public understanding, thus serving the interests of the lay society, too.

Dedication to Quality

Each Frontiers article is a landmark of the highest quality, thanks to genuinely collaborative interactions between authors and review editors, who include some of the world's best academicians. Research must be certified by peers before entering a stream of knowledge that may eventually reach the public - and shape society; therefore, Frontiers only applies the most rigorous and unbiased reviews.
Frontiers revolutionizes research publishing by freely delivering the most outstanding research, evaluated with no bias from both the academic and social point of view. By applying the most advanced information technologies, Frontiers is catapulting scholarly publishing into a new generation.

What are Frontiers Research Topics?

Frontiers Research Topics are very popular trademarks of the Frontiers Journals Series: they are collections of at least ten articles, all centered on a particular subject. With their unique mix of varied contributions from Original Research to Review Articles, Frontiers Research Topics unify the most influential researchers, the latest key findings and historical advances in a hot research area! Find out more on how to host your own Frontiers Research Topic or contribute to one as an author by contacting the Frontiers Editorial Office: frontiersin.org/about/contact

SOFT TISSUE BIOMECHANICS IN WOUND HEALING AND PREVENTION

Topic Editors:
Yih-Kuen Jan, University of Illinois at Urbana-Champaign, United States
Matthew J. Major, Northwestern University, United States
Fang Pu, Beihang University, China
Sharon Eve Sonenblum, Georgia Institute of Technology, United States

Citation: Jan, Y.-K., Major, M. J., Pu, F., Sonenblum, S. E., eds. (2022). Soft Tissue Biomechanics in Wound Healing and Prevention. Lausanne: Frontiers Media SA. doi: 10.3389/978-2-88976-028-2

Table of Contents

frontiers | Frontiers in Bioengineering and Biotechnology

EDITORIAL
published: 05 April 2022
doi: 10.3389/fbioe.2022.897860

Editorial: Soft Tissue Biomechanics in Wound Healing and Prevention

Yih-Kuen Jan[1]*, *Matthew J. Major*[2,3], *Fang Pu*[4] and *Sharon Eve Sonenblum*[5]

[1]Rehabilitation Engineering Lab, Department of Kinesiology and Community Health, University of Illinois at Urbana-Champaign, Champaign, IL, United States, [2]Departments of Physical Medicine and Rehabilitation and Biomedical Engineering, Northwestern University, Chicago, IL, United States, [3]Jesse Brown VA Medical Center, Chicago, IL, United States, [4]Beijing Advanced Innovation Center for Biomedical Engineering, School of Biological Science and Medical Engineering, Beihang University, Beijing, China, [5]Rehabilitation Engineering and Applied Research Laboratory, The George W. Woodruff School of Mechanical Engineering, Georgia Institute of Technology, Atlanta, GA, United States

Keywords: blood vessel, constitutive properties, diabetic foot ulcers, pressure injury, pressure ulcers, skin breakdown, viscoelasticity, wound

Editorial on the Research Topic

Soft Tissue Biomechanics in Wound Healing and Prevention

Wound healing and prevention of chronic wounds are challenging issues in public health. Chronic wounds often result from pressure ulcers/injuries, diabetic foot ulcers, and skin breakdown of the residual limb in the case of limb deficiency. Pressure ulcers occur in people with limited mobility and impaired sensation, such as people with spinal cord injury, Alzheimer disease, and Parkinson disease (Sprigle et al., 2020). Diabetic foot ulcers are the result of complications caused by diabetes, including diabetic neuropathy and peripheral artery disease. Skin breakdown of the residual limb occurs due to repetitive loads transferred from the encapsulating prosthetic socket during load-bearing physical activities. Unfortunately, even after decades of efforts on the prevention and treatment of these wounds their incidence remains largely unchanged (Brienza et al., 2022).

Wounds are thought to result from prolonged, repetitive mechanical loads which may be either compressive or shear forces. The current clinical practice emphasizes the decrease of mechanical loads by providing support surfaces (wheelchair cushions, hospital mattresses, novel prosthetic socket materials and designs, and therapeutic insoles) to relieve points of high interface pressure between the device and the soft tissues of the individual. However, interface pressure alone does not fully describe the risk of wound development and thus preventive and treatment interventions based on this principle may not be fully effective (Jan and Brienza, 2006; Bader and Worsley, 2018; Gefen, 2019). In addition, current approaches often ignore the detailed biomechanical properties of compressed soft tissues consisting of the skin, subcutaneous tissue, fat, fascia, muscles, and blood vessels that are nonlinear, viscoelastic materials (Jan et al., 2013).

Computational and theoretical models can provide new insights on the development of wounds as well as optimization of the current clinical interventions. Rankin et al. used a high-velocity environmental debris in an animal cadaveric model to study mechanisms of traumatic amputation due to blast injury. The authors showed that high velocity sand blast is an independent mechanism of injury causing traumatic amputation. Kelly et al. explored the use of forefoot computational models from people with rheumatic arthritis (RA) to predict patient outcomes. Their magnetic resonance based models showed promise on predicting real life events in people with RA. Wang et al. performed a thermal analysis to predict blood flow of a foot using a vessel-porous media model and demonstrated exciting findings using thermal analysis to predict blood flow in 31 diabetic patients. These models allow for better understanding of the mechanisms of wound development and personalized prediction of outcomes.

Edited and reviewed by:
Markus O. Heller, University of Southampton, United Kingdom

***Correspondence:**
Yih-Kuen Jan
yjan@illinois.edu

Specialty section:
This article was submitted to Biomechanics, a section of the journal Frontiers in Bioengineering and Biotechnology

Received: *16 March 2022*
Accepted: *18 March 2022*
Published: *05 April 2022*

Citation:
Jan Y-K, Major MJ, Pu F and Sonenblum SE (2022) Editorial: Soft Tissue Biomechanics in Wound Healing and Prevention. Front. Bioeng. Biotechnol. 10:897860. doi: 10.3389/fbioe.2022.897860

Theoretically, a single mechanical overload can cause soft tissue damage, while repetitive sub-maximal mechanical loads can trigger adaptation (Liao et al., 2018). The adaptive response is known to be rate-dependent and is also affected by the magnitude of the mechanical loads and tissue viability of the individual. Various mechanical interventions, including exercise, have shown promise on improving wound healing and reducing risk for pressure injury. Roberts et al. showed a novel application of using low intensity vibration to improve angiogenesis and wound healing in diabetic mice. Ren et al. explored whether weight-bearing exercise increases risk for diabetic foot ulcers. The authors compared plantar microvascular function and tissue hardness in 80 participants with different volumes of weight bearing exercise. Their study demonstrated that higher volumes of exercise are associated with better microvascular function and lower plantar tissue hardness in people with type 2 diabetes. Duan et al. investigated the relationship between plantar tissue hardness and peak plantar pressure and pressure-time integral in people with and without Diabetic Peripheral Neuropathy. They provide evidence of the effect of soft tissue hardness on plantar pressure patterns.

Different patient populations and different sites of soft tissues can demonstrate very different structures, properties, and hence stress-strain relationships that respond differently to mechanical loads. Furthermore, the current understanding of soft tissue biomechanics is based primarily on the behavior of ligaments, tendons, and muscles under tension rather than on the mechanics of bulk soft tissue (consisting of skin, subcutaneous tissue, fat, fascia, muscle and blood vessels) under compression. Sonenblum et al. explored the relationship between adipose characteristics and pressure injury history in 43 wheelchair users. The adipose characteristics were obtained from MRI in a seated posture. The authors demonstrated that wheelchair users with a history of pressure injury had different subcutaneous fat characteristics than wheelchair users without a history of pressure injury. Similar to the findings of Duan et al., tissue properties, specifically intramuscular adipose, varied with years since injury or long term exposure to load. Qian et al. investigated the role of morphology and mechanical properties of plantar fascia in flexible flatfoot and plantar injury using B-mode and elastographic ultrasound. Another study conducted by Choi et al. used an optical coherence tomography-based air-jet indentation system to investigate the correlation between the indentation stiffness and type I collagen abundance, and organization of a wound in diabetic rats. Their study showed evidence of the relationship between indentation stiffness and collagen content of a diabetic wound.

Assessing microvascular networks embedded in the soft tissues can be used to evaluate risk for ischemic injury and wounds (Liao et al., 2013). Balasubramanian et al. reviewed skin blood flow in response to occlusion, pressure and temperature with the intention to establish the link between impaired skin perfusion and the development process of diabetic foot ulcers. Yeh et al. explored the use of cross-correlation and chaotic analyses of blood pressure and blood flow velocity to predict cardiovascular dysfunction and stroke. Their results show promise of using cardiovascular dynamics for early detection of cardiovascular related diseases.

It is evident from the articles in this research topic that biomechanical properties of soft tissues, including microvasculature embedded in soft tissues, affect the risk of developing pressure injury as well as wound healing. It is imperative to assess the changes of soft tissue in various pathological conditions as well as microvasculature in addition to traditional risk assessments, such as interface pressure. Mechanical stimulations (e.g., vibration and exercise induced mechanical stress to the weight-bearing tissue) show promise on promoting wound healing and decreasing plantar tissue stiffness associated with diabetes. More studies will be needed in order to translate these findings into clinical practice.

AUTHOR CONTRIBUTIONS

All authors listed have made a substantial, direct, and intellectual contribution to the work and approved it for publication.

ACKNOWLEDGMENTS

The authors thank Dr. Markus Heller for his valuable suggestions on developing this research topic.

REFERENCES

Bader, D. L., and Worsley, P. R. (2018). Technologies to Monitor the Health of Loaded Skin Tissues. *Biomed. Eng. Online* 17, 40. doi:10.1186/s12938-018-0470-z

Brienza, D. M., Campbell, K. E., and Sprigle, S. (2022). The Past, Present, and Future of Pressure Injury Prevention in Patients with Spinal Cord Injury. *Adv. Skin Wound Care* 35, 84–86. doi:10.1097/01.asw.0000803604.78848.11

Gefen, A. (2019). How Medical Engineering Has Changed Our Understanding of Chronic Wounds and Future Prospects. *Med. Eng. Phys.* 72, 13–18. doi:10.1016/j.medengphy.2019.08.010

Jan, Y.-K., and Brienza, D. (2006). Technology for Pressure Ulcer Prevention. *Top. Spinal Cord Inj. Rehabil.* 11, 30–41. doi:10.1310/26r8-unhj-dxj5-xg7w

Jan, Y.-K., Lung, C.-W., Cuaderes, E., Rong, D., and Boyce, K. (2013). Effect of Viscoelastic Properties of Plantar Soft Tissues on Plantar Pressures at the First Metatarsal Head in Diabetics with Peripheral Neuropathy. *Physiol. Meas.* 34, 53–66. doi:10.1088/0967-3334/34/1/53

Liao, F., An, R., Pu, F., Burns, S., Shen, S., and Jan, Y. K. (2018). Effect of Exercise on Risk Factors of Diabetic Foot Ulcers: A Systematic Review and Meta-Analysis. *Am. J. Phys. Med. Rehabil.* 98, 103–116. doi:10.1097/PHM.0000000000001002

Liao, F., Burns, S., and Jan, Y.-K. (2013). Skin Blood Flow Dynamics and its Role in Pressure Ulcers. *J. Tissue Viability* 22, 25–36. doi:10.1016/j.jtv.2013.03.001

Sprigle, S., Mcnair, D., and Sonenblum, S. (2020). Pressure Ulcer Risk Factors in Persons with Mobility-Related Disabilities. *Adv. Skin Wound Care* 33, 146–154. doi:10.1097/01.asw.0000653152.36482.7d

Conflict of Interest: The authors declare that the research was conducted in the absence of any commercial or financial relationships that could be construed as a potential conflict of interest.

Publisher's Note: All claims expressed in this article are solely those of the authors and do not necessarily represent those of their affiliated organizations or those of the publisher, the editors, and the reviewers. Any product that may be evaluated in this article, or claim that may be made by its manufacturer, is not guaranteed or endorsed by the publisher.

frontiers in Bioengineering and Biotechnology

ORIGINAL RESEARCH
published: 04 March 2021
doi: 10.3389/fbioe.2021.648453

Indentation Stiffness Measurement by an Optical Coherence Tomography-Based Air-Jet Indentation System Can Reflect Type I Collagen Abundance and Organisation in Diabetic Wounds

*Harry Ming Chun Choi[1], Alex Kwok-Kuen Cheung[1], Michelle Chun Har Ng[1], Yongping Zheng[2], Yih-Kuen Jan[3] and Gladys Lai Ying Cheing[1]**

[1] Department of Rehabilitation Sciences, The Hong Kong Polytechnic University, Kowloon, Hong Kong, [2] Department of Biomedical Engineering, The Hong Kong Polytechnic University, Kowloon, Hong Kong, [3] Department of Kinesiology and Community Health, University of Illinois at Urbana-Champaign, Urbana, IL, United States

OPEN ACCESS

Edited by:
Bahman Anvari,
University of California, Riverside,
United States

Reviewed by:
Elisa Cinotti,
Hôpital Nord, France
Kamran Avanaki,
University of Illinois at Chicago,
United States
Roger Lewis,
The University of Sheffield,
United Kingdom

***Correspondence:**
Gladys Lai Ying Cheing
Gladys.cheing@polyu.edu.hk

Specialty section:
This article was submitted to Biomechanics, a section of the journal Frontiers in Bioengineering and Biotechnology

Received: 31 December 2020
Accepted: 09 February 2021
Published: 04 March 2021

Citation:
Choi HMC, Cheung AK-K, Ng MCH, Zheng Y, Jan Y-K and Cheing GLY (2021) Indentation Stiffness Measurement by an Optical Coherence Tomography-Based Air-Jet Indentation System Can Reflect Type I Collagen Abundance and Organisation in Diabetic Wounds. Front. Bioeng. Biotechnol. 9:648453. doi: 10.3389/fbioe.2021.648453

There is a lack of quantitative and non-invasive clinical biomechanical assessment tools for diabetic foot ulcers. Our previous study reported that the indentation stiffness measured by an optical coherence tomography-based air-jet indentation system in a non-contact and non-invasive manner may reflect the tensile properties of diabetic wounds. As the tensile properties are known to be contributed by type I collagen, this study was aimed to establish the correlations between the indentation stiffness, and type I collagen abundance and organisation, in order to further justify and characterise the *in vivo* indentation stiffness measurement in diabetic wounds. In a male streptozotocin-induced diabetic rat model, indentation stiffness, and type I collagen abundance and organisation of excisional wounds were quantified and examined using the optical coherence tomography-based air-jet indentation system and picrosirius red polarised light microscopy, respectively, on post-wounding days 3, 5, 7, 10, 14, and 21. The results showed significant negative correlations between indentation stiffness at the wound centre, and the collagen abundance and organisation. The correlations between the indentation stiffness, as well as collagen abundance and organisation of diabetic wounds suggest that the optical coherence tomography-based air-jet indentation system can potentially be used to quantitatively and non-invasively monitor diabetic wound healing in clinical settings, clinical research or preclinical research.

Keywords: biomechanical properties, collagen, diabetic wounds, non-invasive measurement, diagnostic device

INTRODUCTION

Diabetes mellitus is a metabolic disease characterised by hyperglycaemia. Peripheral polyneuropathy, regional ischaemia in the limbs and foot ulceration are common diabetes-related complications. Due to impaired sensation and circulation, people with diabetes are susceptible to repeated cutaneous injuries and possible wound infection, which may result in delayed healing and chronic foot ulcers (Jeffcoate and Harding, 2003; Bjarnsholt et al., 2008).

Chronic diabetic foot ulcers may subsequently result in lower limb amputation and thus require prompt medical attention.

Precise, objective, reliable, and quantitative measurements of wounds are needed to determine prognosis and ensure best strategies adopted in treating and preventing the development of ulcers. Common clinical assessments for diabetic ulcers include gross observation of wound size, colour, and depth (tendon/capsule/bone involvements), as well as the presence of gangrene, infection, and/or ischaemia (Oyibo et al., 2001; Gul et al., 2006). However, these assessments rely only on the observation of the wound appearance, which are not shown to reflect the underlying histology and the biomechanical strength. During wound healing, collagen, which is a major protein in the cutaneous extracellular matrix, is deposited, organised, and contributing to the biomechanical properties as well as the integrity of the skin. The biomechanical properties can thus be a potential quantitative measurement for chronic wounds such as diabetic ulcers to reflect the functional histological integrity of the wounds. Conventional tensile testing is a common strategy to measure the tensile biomechanical properties which are dependent on the abundance, alignment and orientation of collagen, in particular type I collagen (Silver et al., 1992). Therefore, tensile testing is useful in assessing wound healing and recovery of collagen histology in the literature (Howes et al., 1929; Dogan et al., 2009; Dadpay et al., 2012; Minossi et al., 2014; Lau et al., 2015). Preclinical studies have consistently concluded that impaired wound healing in diabetic condition is characterised by decreased tensile strength, as well as reduced collagen abundance and organisation (Yue et al., 1987; Davidson et al., 1997; Schäffer et al., 1997; Reddy et al., 2001; Immonen et al., 2013; Minossi et al., 2014; Zhang et al., 2016). Nevertheless, both tensile testing and histological examination are not feasible in clinical settings because the excision of tissue samples from the subject is required. Optical coherence tomography (OCT) has been applied to assess *in vivo* skin in real time and non-invasively. Advanced OCT systems were also developed to even image the skin in human at high resolution but only required brief contact (Monnier et al., 2020). Recently, our research team conducted a pilot study utilising an OCT-based air-jet indentation system to assess the indentation stiffness of diabetic wounds in a non-contact manner (Choi et al., 2015). By using the air-jet as an indenter, deformation of the wounds can be achieved by a small force in a non-contact manner, which minimises the risk of contamination or damage due to direct contact. We have demonstrated that the OCT-based air-jet indentation system can accurately and reliably measure the indentation force and deformation in the plantar tissues of patients with diabetes (Chao et al., 2011). Unlike tensile testing that involves the extraction and rupture of specimens, the OCT-based air-jet indentation system reversibly deforms the wounds inward to measure their indentation stiffness at low load and strain (i.e., it does not disrupt the wound tissue). The load of indentation is mainly absorbed by the cutaneous proteoglycans in the extracellular matrix (Silver et al., 1992), which participate in regulating collagen deposition and maturation (Raghow, 1994; Reed and Iozzo, 2002) as well as in the whole wound healing process (Werner and Grose, 2003; Schultz and Wysocki, 2009). Together with our earlier study that demonstrated the negative correlations between the tensile strength and indentation stiffness of a diabetic rat wound model (Choi et al., 2015), we hypothesised that the indentation stiffness is also associated with the recovery of type I collagen histology during wound healing.

The objective of the present study was therefore to establish the correlations between indentation stiffness, and type I collagen abundance and organisation in a diabetic rat wound model.

MATERIALS AND METHODS

Animal Handling and Diabetes Induction

The protocol of this study was approved by the Animal Subjects Ethics Sub-Committee of the Hong Kong Polytechnic University. All the rats received humane care and the protocols were in compliance with the guidelines and regulations from the Animal Subjects Ethics Sub-Committee and Institutional Animal Care and Use Committee[1]. Ten-week-old male (300–400 g) Sprague-Dawley rats used in this study were obtained from the Centralised Animal Facilities of The Hong Kong Polytechnic University. The rats were kept at 21°C and 60% relative humidity under a 12-h light-dark cycle. They were fed with a standard laboratory diet and sterile water *ad libitum*. Before diabetes induction, the rats were fasted for 12 h and their blood glucose level was measured to exclude any abnormally hyper- or hypoglycaemic animals from the study. Intra-peritoneal injection of streptozotocin (50 mg/kg; Sigma-Aldrich, St. Louis, MO, United States) in sterile citrate buffer (pH 4.4) was given to induce diabetes in the rats. After 7 days, the blood glucose level of the rats was measured and monitored once a week throughout the experiment to ensure diabetes was successfully induced and sustained in these rats. Any rats with a blood glucose level lower than 16.7 mM were excluded from the study (King, 2012; Lei et al., 2020).

Wound Induction

Prior to wound induction, the rats were anaesthetised by an intra-peritoneal injection of a mixture of ketamine (100 mg/kg) and xylazine (3.33 mg/kg). After shaving and cleansing the skin, wounds were induced with a 6 mm biopsy punch on the lateral side of each hind limb (about 3 mm distal to the fibular head). The wounds were left opened without dressing. The rats were then housed individually to prevent cannibalism. At the time points of harvest, photos of the wounds were taken and the wound area was estimated by Fiji software (Schindelin et al., 2012). Percentage of wound area was defined as the area of the wound at a particular time point divided by the initial wound area (post-wounding day 0).

OCT-Based Air-Jet Indentation Assessment

Wounds were randomly selected for assessment using the OCT-based air-jet indentation system (Choi et al., 2015) on post-wounding days 3, 5, 7, 10, 14, and 21 so that data from various

[1]http://www.polyu.edu.hk/ro/forms/Attachment%202_Guidelines%20for%20the%20assessment%20&%20mgmt%20of%20pain.pdf

phases of wound healing could be collected. Immediately before the assessment, the rats were anaesthetised by ketamine and xylazine injection as mentioned. The technical details of the OCT-based air-jet indentation system have been documented in our previous studies (Huang et al., 2009; Choi et al., 2015). The schematic diagram is shown in **Figure 1**.

Briefly, the probe of the OCT device consisted of a 1-mm air-jet bubbler together with a super-luminescent diode light source (Dense Light, DL-CS3055A, Singapore) operating at a central wavelength of 1,310 nm, a nominal −3 dB spectral bandwidth of 50 nm, and a nominal output power of 5 mW. The OCT unit provided an axial resolution of 18 μm and an imaging depth of approximately 2 to 3 mm in highly scattered materials. An electronic proportional valve with pressure feedback (ITV 1030-311L-Q, SMC Corporation, Tokyo, Japan) at a measurement range of 0.5 MPa was installed. In-house OCT software was used to collect the signals and to control the air valve with a step motor.

The system was used to measure the indentation stiffness of the wounds *in vivo*. There were five measurement sites including one at the centre of the wound with reference to the wound margin, and four at the periphery (proximal, distal, medial, and lateral to the wound with reference to the fibula, 3 mm from the centre of the wound). Two measurements were made at each site with a 5 min resting interval between each measurement; a total of ten measurements were taken for each wound. Three cycles of loading and unloading at an indentation rate of around 0.13 mm/s were applied and recorded, which lasted for approximately 30 s in total. The maximum indentation force was approximately 0.012 N. The deformation was measured by the OCT probe as the inward displacement of the surface of the wound, in accordance with the shift of the OCT signal corresponding to the tissue surface. The stiffness coefficient presented as force/deformation ratio (N/mm) was calculated to represent indentation stiffness. The first loading and unloading cycle was the preconditioning cycle. The indentation stiffness measurements calculated in the loading phases of the second and third cycles were averaged. The typical load-deformation curve including both loading and unloading phases in each cycle is illustrated in **Supplementary Figure 1**.

Histological Analysis of Collagen

The full-thickness wounds of randomly selected rats were harvested on post-wounding days 3, 5, 7, 10, 14, and 21 with 8 mm biopsy punches. The wound tissues were then fixed, processed, embedded in paraffin wax, and then sectioned into 5 μm thickness. The sections of the wound centre, which is defined by the sections with the largest wound gap between morphologically mature epidermis and dermis amongst the series of consecutive sections, were deparaffinised and stained with picrosirius red (Sigma-Aldrich, St. Louis, MO, United States) according to the standard procedures (Kiernan, 2002). Type I collagen is the only type of collagen to appear red upon the staining and examination under a polarised light microscope (Nikon Eclipse 80i, Nikon Corporation, Tokyo, Japan) (Kiernan, 2002). Images of the wound centre were captured using a digital camera (Spot Flex 15.2 64 Mp Shifting Pixel, Diagnostic Instruments Inc., Sterling Heights, MI, United States). The quantification of collagen was executed by Fiji software. The red channel of the images was converted to 8-bit colour depth for analysis. The amount of collagen was quantified as area. The percentage of collagen abundance was represented by the amount of collagen normalised by the area of dermis, where collagen is normally present. The intensity of the staining was measured to represent the alignment of collagen fibrils as better aligned collagen fibrils have a higher degree of birefringence and thus generate brighter image under polarised light microscope (Montes and Junqueira, 1991). Greater Feret length indicates greater continuation of a collagen fibre and also reflects greater degrees of orientation and anisotropy (Melis et al., 2002; Noorlander et al., 2002). The average Feret length of the top ten longest collagen fibres of the wound was calculated to represent the orientation of the collagen fibres (Melis et al., 2002; Noorlander et al., 2002). By selecting six representative regions of interest in the dermis, the energy and coherency values from the Fiji plug-in, OrientationJ, were also obtained as parameters of orientation and anisotropy of collagen fibres by structure tensor evaluation (Rezakhaniha et al., 2012). Briefly, the coherency value ranges from 0 to 1, where a coherency value that is close to 1 indicates coherently oriented fibres of the same direction (Fonck et al., 2009); the energy value, consistent to the coherency value, reflects the directionality of the fibres, but is also a function of the area of fibres (Rezakhaniha et al., 2012).

Statistical Analysis

Intraclass correlation (ICC) [3, 2] analysis was performed to assess the test-retest reliability. Two-way analysis of variance with *post hoc* Tukey's tests was conducted to examine differences between indentation stiffness measured at the wound centre and periphery over time. Spearman's Rho was conducted to explore the correlations between the indentation stiffness, and collagen abundance and organisation. The two-sided significance level was set at 0.05. The ICC coefficient was generated by IBM SPSS Statistics for Windows version 21.0 (Armonk, NY, United States: IBM Corp.). The other statistics were performed by GraphPad Prism version 6.00 for Windows (GraphPad Software, La Jolla, CA, United States)[2]. Data were displayed as individual data points and mean ± standard error of mean.

RESULTS

The diabetic rat model was induced using streptozotocin injection. The streptozotocin injection led to 21.8% mortality. Among the surviving rats, 4.4% did not develop hyperglycaemia.

Wound Size, Indentation Stiffness, and Type I Collagen Deposition

Excisional wounds were inflicted on the hind limbs of the rats for the assessment of indentation stiffness, and collagen abundance and organisation. By 14 days, all wounds were grossly closed without notable infection (**Figure 2**).

[2]www.graphpad.com

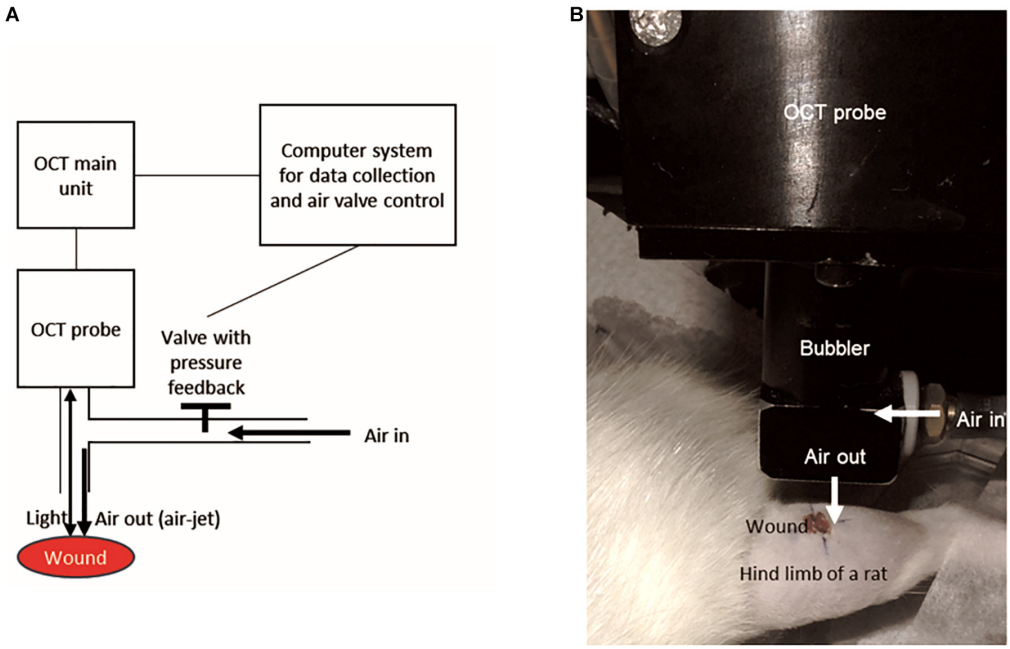

FIGURE 1 | The design of the OCT-based air-jet indentation system used for measuring indentation stiffness of wounds. **(A)** Schematic diagram showing that air-jet whose pressure or flow was controlled by a valve with pressure feedback and a computer system. The air-jet was used as an indenter while the reflected light signal is captured by the OCT probe so that the displacement was detected by the computer system. **(B)** A wound on a hind limb of a diabetic rat was assessed by the OCT-based air-jet indentation system.

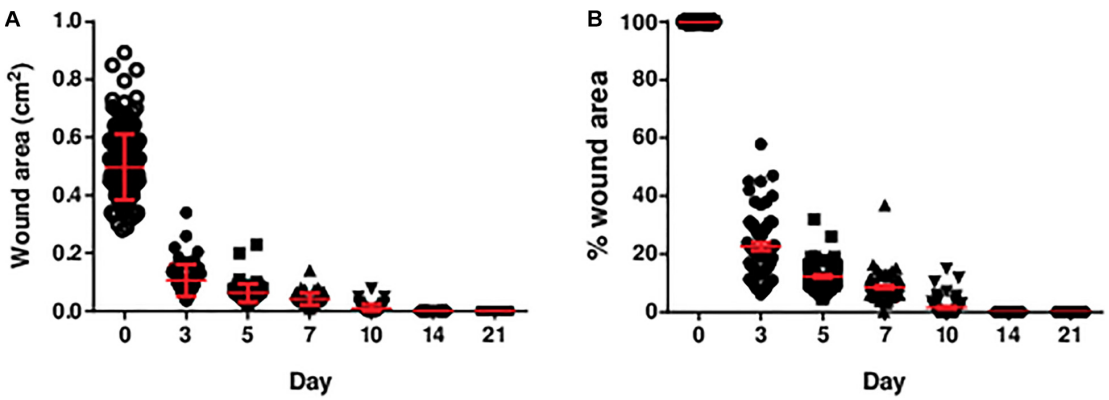

FIGURE 2 | The **(A)** area and **(B)** percentage of area of the diabetic wounds measured over 3 weeks. The area and percentage of area of the diabetic wounds decreased over time. All wounds were closed by post-wounding day 14. The percentage of wound area was the wound area on the specific day divided by the initial wound area (day 0). Data are expressed as individual data points as well as mean ± standard error of mean. Day 0: n = 191 wounds, 96 rats; day 3: n = 68 wounds, 34 rats; day 5: n = 68 wounds, 34 rats; day 7: n = 64 wounds, 32 rats; day 10: n = 56 wounds, 28 rats; day 14: n = 56 wounds, 28 rats; and day 21: n = 56 wounds, 28 rats.

Intraclass correlation [3, 2] analysis indicated an excellent test-retest reliability of the indentation stiffness measurement at both the centre and periphery of 46 randomly selected wounds at different time points [ICC (3, 2) = 0.92]. This finding shows that the measurement made in current experimental setting was reliable.

At the wound centre, the indentation stiffness was comparable in the early phase (days 3, 5, and 7; **Figure 3**). However, it significantly dropped in the later phase (days 10, 14, and 21; $P < 0.0001$). In contrast, the indentation stiffness at the wound periphery demonstrated negligible change over time and was consistently smaller as compared to the wound centre.

Picrosirius red staining was performed to visualise type I collagen fibres (appear in red under polarised light), which is the main contributor to the tensile strength of the wounds and the skin. Images taken at the centre of the wounds harvested on post-wounding days 3, 5, 7, 10, 14, and 21 revealed that the majority of the staining appeared red indicating type I

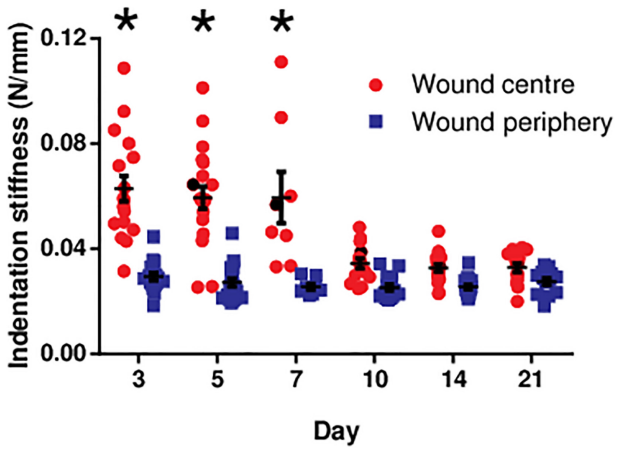

FIGURE 3 | The indentation stiffness measured at the centre and periphery of the diabetic wounds over 3 weeks. The indentation stiffness measurements at the wound centre on days 3, 5, and 7 were significantly greater than those measured on days 10, 14, and 21 (*$P < 0.0001$). Data are expressed as individual data points as well as mean ± standard error of mean. Day 3: $n = 17$ wounds, 9 rats; day 5: $n = 20$ wounds, 11 rats; day 7: $n = 8$ wounds, 4 rats; day 10: $n = 14$ wounds, 7 rats; day 14: $n = 16$ wounds, 9 rats; and day 21: $n = 14$ wounds, 8 rats.

collagen fibres. However, green signals, which indicates thinner and less aligned collagen fibres, such as type III, were negligible in abundance. Type I collagen fibres were quantified in terms of collagen abundance, fibril alignment and fibre orientation (**Figure 4**). The collagen abundance showed an notable increase from day 7 to day 21. However, there were no substantial changes in collagen organisation (i.e., fibril alignment, fibre orientation, and anisotropy) throughout the study period.

Correlations Between Indentation Stiffness, and Type I Collagen Abundance and Organisation

As type I collagen is the major structural protein in the extracellular matrix underlying biomechanical properties, correlations were established between the indentation stiffness and the abundance and organisation of type I collagen. The indentation stiffness at the wound centre was significantly negatively correlated with the collagen abundance (absolute abundance and percentage abundance) and organisation (fibril alignment, fibre orientation, energy of anisotropy, and coherency of anisotropy; **Figure 5**). As a negative control, the indentation stiffness at the wound periphery was not correlated with the collagen abundance and organisation at the wound centre. These findings confirm that the correlations are region specific (i.e., only indentation stiffness measured at the wound centre, but not periphery, reflects the collagen at the wound centre). Interestingly, such negative correlations between the indentation stiffness at the wound centre (but not the wound periphery) and collagen abundance and organisation were also found significant in non-diabetic wounds of strain-, sex-, and age-matched rats (**Supplementary Figure 2**).

DISCUSSION

This study is the first one to show that the abundance and organisation of collagen in wounds could be reflected by an *in vivo*, non-contact and non-invasive biomechanical measurement. This provides further evidence to support the use of indentation stiffness as a biomechanical assessment of diabetic wounds. As our previous study have shown that the indentation stiffness could reflect the tensile properties of diabetic wounds, we postulated that collagen fibril alignment and fibre orientation should also be factors in the correlation (Choi et al., 2015). The current study demonstrating negative correlations between indentation stiffness, and type I collagen abundance and organisation in diabetic wounds may therefore further explain the negative correlations between the indentation stiffness and tensile properties, which are mainly contributed by type I collagen fibres.

Proteoglycans may absorb compressive stress and resist tissue deformation upon compression, thus contributing to the compressive/indenting property of the skin (Silver et al., 1992). Correlation between indentation stiffness and collagen shown in the current study suggests interesting relationships between indenting property, proteoglycans and collagen in wound healing. Proteoglycans, which is a component of the ground substance, have roles in collagen deposition and maturation. Decorin, regarded as one of the small-sized proteoglycans found in the skin, interacts with various types of collagen (Vogel et al., 1984; Brown and Vogel, 1989; Tenni et al., 2002). It plays an important role in regulating collagen deposition (Reed and Iozzo, 2002) and also the recovery of collagen organisation upon injury (Dunkman et al., 2014). Hence, it potentially affects the tensile properties of the skin wounds (Carrino et al., 2000). It should be noted that the abundance of decorin increases following wound closure (Yeo et al., 1991). In contrast, other proteoglycans such as chondroitin sulphate proteoglycans of large molecular size remain dominant during the wound healing process, when the wound is not completely closed (Yeo et al., 1991). Proteoglycans of large size (e.g., chondroitin sulphate proteoglycans) are interlaced with thin collagen fibrils, vice versa, the smaller-sized (e.g., decorin) are distributed among thicker collagen (Kuwaba et al., 2002). Owing to such characteristic, we speculate that the dynamic changes in molecular size of proteoglycans do not only contribute to the organisation and maturation of collagen fibres, but also the indentation stiffness during wound healing. The predominance of large-sized proteoglycans may contribute to an increased indentation stiffness in the early phase (day 3 to day 7), prior to wound closure. They are then replaced by the smaller-sized proteoglycans following wound closure, which may account for the reduced indentation stiffness in the later phase (day 10 to day 21). This may not only justify the negative correlations between the indentation stiffness and collagen abundance and organisation found in the current study, but also explain the consistently smaller indentation stiffness at the wound periphery, which is presumably uninjured skin, with proteoglycans of smaller size (Kuwaba et al., 2002). Future study is warranted to confirm the relationships between the indentation stiffness, proteoglycans, and collagen deposition and organisation of

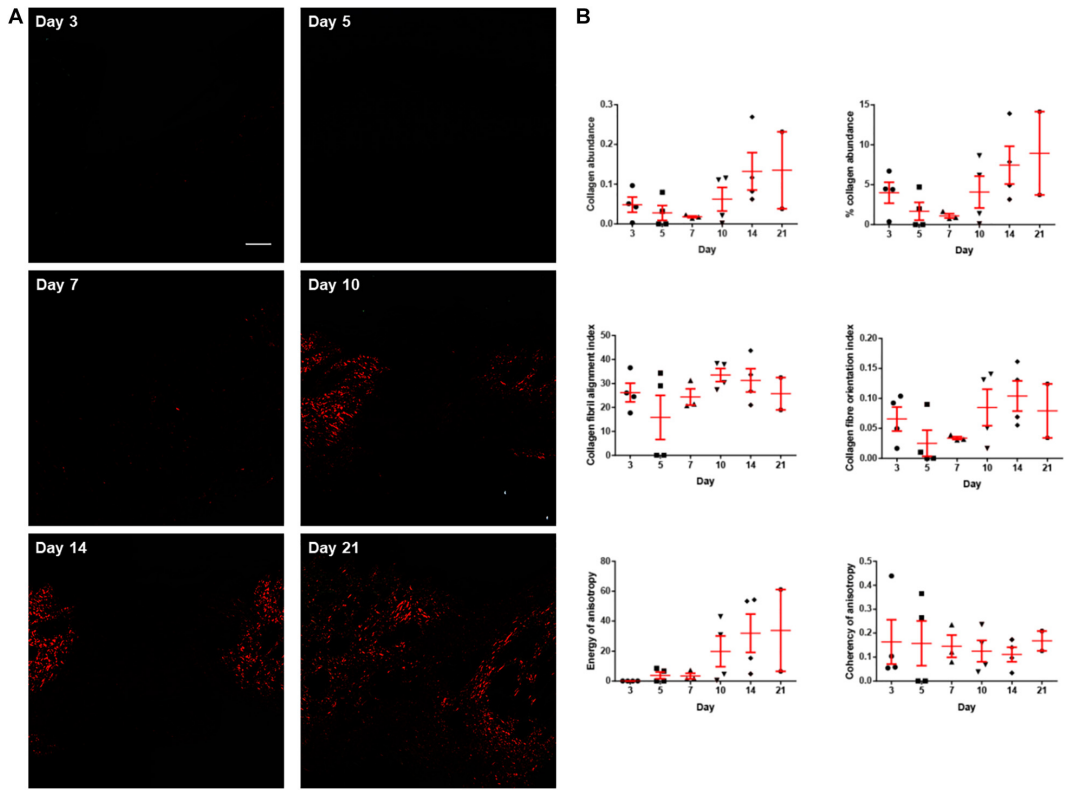

FIGURE 4 | The collagen histology of the diabetic wounds examined over 3 weeks. **(A)** Representative picrosirius red stained sections at the centre of the diabetic wounds examined under polarised light microscope on post-wounding day 3, day 5, day 7, day 10, day 14, and day 21. Type I collagen fibres appear red under polarised light. No collagen was observed to be deposited on days 3 and 5. Very limited collagen was observed on day 7. The abundance of collagen increased as the wounds healed on days 10, 14, and 21. Scale bar = 150 μm. **(B)** The collagen histology including collagen abundance, percentage collagen abundance, collagen fibril alignment, collagen fibre orientation, energy of anisotropy and coherency of anisotropy quantified over 3 weeks. Both abundance of collagen and energy of anisotropy showed obvious increasing trend from post-wounding day 7 to day 21. Data are expressed as individual data points as well as mean ± standard error of mean. Day 3: n = 4 wounds, 4 rats; day 5: n = 4 wounds, 4 rats; day 7: n = 3 wounds, 3 rats; day 10: n = 4 wounds, 4 rats; day 14: n = 4 wounds, 4 rats; and day 21: n = 2 wounds, 2 rats.

diabetic wounds, in order to provide concrete support on the clinical use of the indentation stiffness measurement.

Although the present study focuses on the dermal layer of the skin/wound, wound healing does involve re-epithelialisation. Particularly in the early phase where the dermal layer is still very thin or even absent, the epidermal layer may probably be the main structure contributing to the biomechanical properties of the wound. Indeed, our data show that the thicker epidermal layer in the early phase (**Supplementary Figure 3**) coincides with the greater indentation stiffness in the early phase of diabetic wound healing (days 3, 5, and 7; **Figure 3**). The epidermal thickness at different time points has a significant positive correlation with the indentation stiffness at the wound centre (**Supplementary Figure 3**). Keratinocyte is the major cell type in the epidermal layer, which synthesises protein fibre keratin that can potentially contribute to compressive/indenting biomechanical properties (Wang et al., 2016). The presence of epidermal layer in the early phase of wound centre in the current study suggests the presence of keratin and keratinocytes at the wound centre in the early phase. Other studies conducted with excisional wounds in rats (Sabol et al., 2012) and humans (Usui et al., 2005) have also found the presence of keratin and keratinocytes in the early phase of wound healing. During wound healing, keratinocytes proliferate, migrate, differentiate into different stages and express distinct types of keratins such as K16 in activated proliferating keratinocytes and K10 in terminally differentiated keratinocytes (Freedberg et al., 2001; Santos et al., 2002; Usui et al., 2008). It has been suggested that different types of keratins with different structures and molecular weights could have different biomechanical properties (Bragulla and Homberger, 2009). Therefore, in different phases of wound healing, different compositions and abundance of various types of keratins may possibly contribute to the different indentation stiffness. This may also explain why the indentation stiffness at the wound centre is significantly different from that at the periphery as the compositions of keratins at these sites are probably different. At the wound centre, it is expected that keratinocytes are more activated and proliferative expressing high level of K16. Conversely, keratinocytes in the uninjured area at the wound periphery express less K16 but more K10. Interestingly, keratinocytes expressing different types of keratins release different signalling molecules such as cytokines (e.g.,

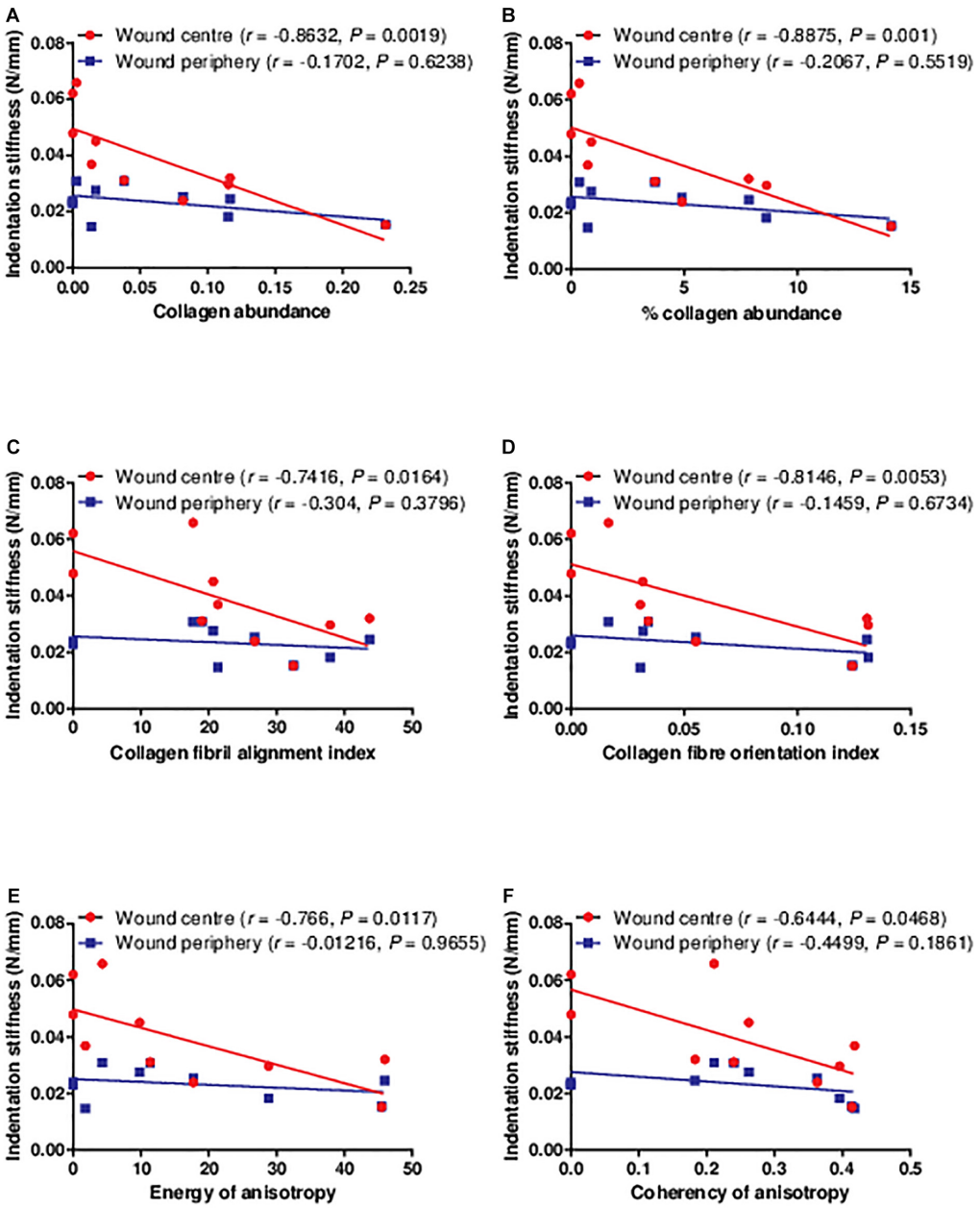

FIGURE 5 | The correlations between the indentation stiffness and collagen histology examined in the diabetic wounds. The indentation stiffness measured at the wound centre was significantly negatively correlated to the **(A,B)** collagen abundance, **(C)** alignment, **(D)** orientation, and **(E,F)** anisotropy on post-wounding day 3 (n = 1 wound, 1 rat), 5 (n = 2 wounds, 2 rats), 7 (n = 2 wounds, 2 rats), 10 (n = 1 wound, 1 rat), 14 (n = 2 wounds, 2 rats), and 21 (n = 2 wounds, 2 rats). Data at different time points were pooled together.

TNF-α) and growth factors (TGF-β) to regulate the signalling and differentiation of fibroblasts. The release of various signalling molecules has potential effects on the collagen deposition and maturation in dermis (Werner et al., 2007; Pastar et al., 2014). Future studies are needed to clarify the indentation stiffness of specific types, compositions and abundance of keratins in *in vivo* wound models and, in addition, to examine the regulation of collagen deposition and maturation in dermal layer by keratinocytes expressing distinct types of keratins in wound healing process. This series of studies will hopefully be able to further elucidate the biomechanical and molecular characteristics of the wounds reflected by the indentation stiffness in different phases of wound healing.

Apart from the possible contribution by proteoglycans and keratins, the consistently high indentation stiffness in the early phase of wound healing could be related to wound oedema. The histological finding in the present study suggests that oedema was present in the wounds on days 3, 5, and 7 but not on days 10, 14,

and 21 (**Supplementary Figure 3**). This observation is consistent with the report by Vexler et al. (1999) who reported skin oedema to be associated with increased stiffness. In addition, it is generally agreed that oedema increases the stiffness of the tissue due to hydrostatic pressure in a confined space. The hypothesis that the high indentation stiffness is related to wound oedema is also partly supported by the present finding that the indentation stiffness at the wound periphery, where no wound oedema was found, was substantially smaller than that at the wound centre.

The main focus of the current study is to evaluate the correlations between the indentation stiffness, and type I collagen abundance and organisation in diabetic wounds. Nevertheless, to the best of our knowledge, this study is the first study to illustrate the quantitative changes in collagen abundance and organisation of diabetic wounds, over a period of time from the early phase (post-wounding day 3) to the later phase (day 21). Existing literature on the collagen histology is lacking the presentation of changes at various time points. Therefore, the present findings may provide insights to the research on optimal time points for specific interventions to diabetic wounds in different phases of wound healing. For the collagen abundance, our data show a non-significant decreasing trend from post-wounding day 3 to day 7 and an increasing trend thereafter. Majority of the studies which investigated the time course changes in collagen using either diabetic (Ponrasu and Suguna, 2012; Ram et al., 2015; Zhang et al., 2016) or non-diabetic wound models (Oxlund et al., 1996; Ponrasu and Suguna, 2012; Almeida et al., 2014) demonstrated an increase in collagen abundance over time and plateau or slightly decreases in the very late phase, which is consistent with the rising trend from day 7 to day 21 concluded in the current study. Therefore, the non-significant decrease from day 3 to day 7 in the collagen abundance shown in the present study could be attributed to individual variation. However, since limited study has focussed on the time course changes of collagen abundance between day 3, or earlier, and day 7 in diabetic wound models, we are unable to rule out the possibility that the decreasing trend of collagen abundance on post-wounding day 7 is as a result of diabetes-related complications in wound healing.

For collagen fibril alignment and fibre orientation indices, as well as the coherency of anisotropy which is also a measurement of collagen fibre orientation estimated by tensor analysis, there was no obvious increase or decrease across the time points. On the other hand, the energy of anisotropy is a function of both area and orientation of fibres. The rising trend of the energy of anisotropy corresponds to the increasing trend of the collagen abundance. In agreement with the unchanged collagen fibril alignment and fibre orientation in the current study, our previous study have also found no significant difference in the collagen fibril alignment and fibre orientation between post-wounding day 7 and day 14 in a diabetic rat excisional wound model (Choi et al., 2016). Broadley et al. (1989) demonstrated that even though the collagen concentration in diabetic wounds approached to the non-diabetic wound level over time, the tensile strength of the diabetic wounds remained impaired. Since tensile strength is contributed by all collagen abundance, alignment and orientation, they extrapolated that wounds in diabetic rat model might have deficits in the recovery of collagen alignment and orientation (Broadley et al., 1989). To date, no other published studies have quantitatively assessed the collagen fibril alignment and fibre orientation in wounds over a period of time. We therefore believe that the recovery of collagen alignment and orientation may not be significant in the current diabetic wound model within the experimental period, which is in agreement with the literature.

In conclusion, we established correlations between the indentation stiffness, type I collagen abundance and organisation of diabetic wounds in a rat model. Our findings provide evidence supporting the potential clinical use of the OCT-based air-jet indentation system for biomechanical assessment of diabetic wounds. In the future, we anticipate investigations using a more clinically relevant wound model involving repetitive stress and chronic inflammation resembling foot ulcers in patients to explore the correlations between the indentation stiffness and more clinically oriented parameters such as the prognosis of the wounds, risk of infections and severity of diabetes.

DATA AVAILABILITY STATEMENT

The raw data supporting the conclusions of this article will be made available by the authors, without undue reservation.

ETHICS STATEMENT

The animal study was reviewed and approved by the Animal Subjects Ethics Sub-Committee of the Hong Kong Polytechnic University.

AUTHOR CONTRIBUTIONS

HC, AC, and GC: conceptualisation. HC: data curation, formal analysis, visualisation, and writing – original draft. GC: funding acquisition and project administration. HC and MN: investigation. YZ: methodology. AC and GC: supervision. HC, AC, YZ, Y-KJ, and GC: writing – review and editing. All authors contributed to the article and approved the submitted version.

FUNDING

This work was supported by the General Research Fund from Research Grants Council of the Hong Kong SAR Government (PolyU 5602/13M and PolyU 151003/14M).

SUPPLEMENTARY MATERIAL

The Supplementary Material for this article can be found online at: https://www.frontiersin.org/articles/10.3389/fbioe.2021.648453/full#supplementary-material

REFERENCES

Almeida, B. M., Nascimento, M. F., Pereira-Filho, R. N., Melo, G. C., Santos, J. C., Oliveira, C. R., et al. (2014). Immunohistochemical profile of stromal constituents and lymphoid cells over the course of wound healing in murine model. *Acta Cir. Bras.* 29, 596–602.

Bjarnsholt, T., Kirketerp-Møller, K., Jensen, P. Ø, Madsen, K. G., Phipps, R., Krogfelt, K., et al. (2008). Why chronic wounds will not heal: a novel hypothesis. *Wound Repair Regen.* 16, 2–10. doi: 10.1111/j.1524-475X.2007.00283.x

Bragulla, H. H., and Homberger, D. G. (2009). Structure and functions of keratin proteins in simple, stratified, keratinized and cornified epithelia. *J. Anat.* 214, 516–559. doi: 10.1111/j.1469-7580.2009.01066.x

Broadley, K. N., Aquino, A. M., Hicks, B., Ditesheim, J. A., McGee, G. S., Demetriou, A. A., et al. (1989). The diabetic rat as an impaired wound healing model: stimulatory effects of transforming growth factor-beta and basic fibroblast growth factor. *Biotechnol. ther.* 1, 55–68.

Brown, D. C., and Vogel, K. G. (1989). Characteristics of the in vitro interaction of a small proteoglycan (PG II) of bovine tendon with type I collagen. *Matrix* 9, 468–478.

Carrino, D. A., Sorrell, J. M., and Caplan, A. I. (2000). Age-related changes in the proteoglycans of human skin. *Arch. Biochem. Biophys.* 373, 91–101. doi: 10.1006/abbi.1999.1545

Chao, C. Y. L., Zheng, Y. P., and Cheing, G. L. Y. (2011). A novel noncontact method to assess the biomechanical properties of wound tissue. *Wound Repair Regen.* 19, 324–329. doi: 10.1111/j.1524-475X.2011.00694.x

Choi, M. C., Cheung, K. K., Li, X., and Cheing, G. L. (2016). Pulsed electromagnetic field (PEMF) promotes collagen fibre deposition associated with increased myofibroblast population in the early healing phase of diabetic wound. *Arch. Dermatol. Res.* 308, 21–29. doi: 10.1007/s00403-015-1604-9

Choi, M. C., Cheung, K. K., Ng, G. Y., Zheng, Y. P., and Cheing, G. L. (2015). Measurement of diabetic wounds with optical coherence tomography-based air-jet indentation system and a material testing system. *J. Wound Care* 24, 519–528. doi: 10.12968/jowc.2015.24.11.519

Dadpay, M., Sharifian, Z., Bayat, M., Bayat, M., and Dabbagh, A. (2012). Effects of pulsed infra-red low level-laser irradiation on open skin wound healing of healthy and streptozotocin-induced diabetic rats by biomechanical evaluation. *J. Photochem. Photobiol. B* 111(Suppl. C), 1–8. doi: 10.1016/j.jphotobiol.2012.03.001

Davidson, J. M., Broadley, K. N., and Quaglino, D. (1997). Reversal of the wound healing deficit in diabetic rats by combined basic fibroblast growth factor and transforming growth factor-β1 therapy. *Wound Repair Regen.* 5, 77–88. doi: 10.1046/j.1524-475X.1997.50115.x

Dogan, S., Demirer, S., Kepenekci, I., Erkek, B., Kiziltay, A., Hasirci, N., et al. (2009). Epidermal growth factor-containing wound closure enhances wound healing in non-diabetic and diabetic rats. *Int. Wound J.* 6, 107–115. doi: 10.1111/j.1742-481X.2009.00584.x

Dunkman, A. A., Buckley, M. R., Mienaltowski, M. J., Adams, S. M., Thomas, S. J., Satchell, L., et al. (2014). The tendon injury response is influenced by decorin and biglycan. *Ann. Biomed. Eng.* 42, 619–630. doi: 10.1007/s10439-013-0915-2

Fonck, E., Feigl, G. G., Fasel, J., Sage, D., Unser, M., Rüfenacht, D. A., et al. (2009). Effect of aging on elastin functionality in human cerebral arteries. *Stroke* 40, 2552–2556. doi: 10.1161/strokeaha.108.528091

Freedberg, I. M., Tomic-Canic, M., Komine, M., and Blumenberg, M. (2001). Keratins and the keratinocyte activation cycle. *J. Invest. Dermatol.* 116, 633–640. doi: 10.1046/j.1523-1747.2001.01327.x

Gul, A., Basit, A., Ali, S. M., Ahmadani, M. Y., and Miyan, Z. (2006). Role of wound classification in predicting the outcome of diabetic foot ulcer. *J. Pak. Med. Assoc.* 56, 444–447.

Howes, E. L., Sooy, J. W., and Harvey, S. C. (1929). The healing of wounds as determined by their tensile strength. *J. Am. Med. Assoc.* 92, 42–45. doi: 10.1001/jama.1929.02700270046011

Huang, Y. P., Zheng, Y. P., Wang, S. Z., Chen, Z. P., Huang, Q. H., and He, Y. H. (2009). An optical coherence tomography (OCT)-based air jet indentation system for measuring the mechanical properties of soft tissues. *Meas. Sci. Technol.* 20, 1–11.

Immonen, J. A., Zagon, I. S., Lewis, G. S., and McLaughlin, P. J. (2013). Topical treatment with the opioid antagonist naltrexone accelerates the remodeling phase of full-thickness wound healing in type 1 diabetic rats. *Exp. Biol. Med.* 238, 1127–1135. doi: 10.1177/1535370213502632

Jeffcoate, W. J., and Harding, K. G. (2003). Diabetic foot ulcers. *Lancet* 361, 1545–1551.

Kiernan, J. A. (2002). Collagen type I staining. *Biotech. Histochem.* 77:31.

King, A. J. (2012). The use of animal models in diabetes research. *Br. J. Pharmacol.* 166, 877–894. doi: 10.1111/j.1476-5381.2012.01911.x

Kuwaba, K., Kobayashi, M., Nomura, Y., Irie, S., and Koyama, Y. (2002). Size control of decorin dermatan sulfate during remodeling of collagen fibrils in healing skin. *J. Dermatol. Sci.* 29, 185–194.

Lau, P. S., Bidin, N., Krishnan, G., Nassir, Z., and Bahktiar, H. (2015). Biophotonic effect of diode laser irradiance on tensile strength of diabetic rats. *J. Cosmet. Laser Ther.* 17, 86–89. doi: 10.3109/14764172.2014.968587

Lei, X., Huo, P., Wang, Y., Xie, Y., Shi, Q., Tu, H., et al. (2020). Lycium barbarum polysaccharides improve testicular spermatogenic function in streptozotocin-induced diabetic rats. *Front. Endocrinol.* 11:164. doi: 10.3389/fendo.2020.00164

Melis, P., Noorlander, M. L., van der Horst, C. M., and van Noorden, C. J. (2002). Rapid alignment of collagen fibers in the dermis of undermined and not undermined skin stretched with a skin-stretching device. *Plast. Reconstr. Surg.* 109, 674–680.

Minossi, J. G., Lima, F. D. O., Caramori, C. A., Hasimoto, C. N., Ortolan, ÉV. P., Rodrigues, P. A., et al. (2014). Alloxan diabetes alters the tensile strength, morphological and morphometric parameters of abdominal wall healing in rats. *Acta Cir. Bras.* 29, 118–124.

Monnier, J., Tognetti, L., Miyamoto, M., Suppa, M., Cinotti, E., Fontaine, M., et al. (2020). In vivo characterization of healthy human skin with a novel, non-invasive imaging technique: line-field confocal optical coherence tomography. *J. Eur. Acad. Dermatol. Venereol.* 34, 2914–2921. doi: 10.1111/jdv.16857

Montes, G., and Junqueira, L. (1991). The use of the Picrosirius-polarization method for the study of the biopathology of collagen. *Mem. Inst. Oswaldo Cruz* 86, 1–11.

Noorlander, M. L., Melis, P., Jonker, A., and Van Noorden, C. J. (2002). A quantitative method to determine the orientation of collagen fibers in the dermis. *J..Histochem. Cytochem.* 50, 1469–1474.

Oxlund, H., Christensen, H., Seyer-Hansen, M., and Andreassen, T. T. (1996). Collagen deposition and mechanical strength of colon anastomoses and skin incisional wounds of rats. *J. Surg. Res.* 66, 25–30. doi: 10.1006/jsre.1996.0367

Oyibo, S. O., Jude, E. B., Tarawneh, I., Nguyen, H. C., Harkless, L. B., and Boulton, A. J. (2001). A comparison of two diabetic foot ulcer classification systems: the Wagner and the University of Texas wound classification systems. *Diabetes Care* 24, 84–88.

Pastar, I., Stojadinovic, O., Yin, N. C., Ramirez, H., Nusbaum, A. G., Sawaya, A., et al. (2014). Epithelialization in wound healing: a comprehensive review. *Adv. wound care* 3, 445–464. doi: 10.1089/wound.2013.0473

Ponrasu, T., and Suguna, L. (2012). Efficacy of *Annona squamosa* on wound healing in streptozotocin-induced diabetic rats. *Int. Wound J.* 9, 613–623. doi: 10.1111/j.1742-481X.2011.00924.x

Raghow, R. (1994). The role of extracellular matrix in postinflammatory wound healing and fibrosis. *FASEB J.* 8, 823–831.

Ram, M., Singh, V., Kumawat, S., Kumar, D., Lingaraju, M. C., Uttam Singh, T., et al. (2015). Deferoxamine modulates cytokines and growth factors to accelerate cutaneous wound healing in diabetic rats. *Eur. J. Pharmacol.* 764, 9–21. doi: 10.1016/j.ejphar.2015.06.029

Reddy, G. K., Stehno-Bittel, L., and Enwemeka, C. S. (2001). Laser photostimulation accelerates wound healing in diabetic rats. *Wound Repair Regen.* 9, 248–255.

Reed, C. C., and Iozzo, R. V. (2002). The role of decorin in collagen fibrillogenesis and skin homeostasis. *Glycoconj. J.* 19, 249–255. doi: 10.1023/a:1025383913444

Rezakhaniha, R., Agianniotis, A., Schrauwen, J. T., Griffa, A., Sage, D., Bouten, C. V., et al. (2012). Experimental investigation of collagen waviness and orientation in the arterial adventitia using confocal laser scanning microscopy. *Biomech. Model. Mechanobiol.* 11, 461–473. doi: 10.1007/s10237-011-0325-z

Sabol, F., Dancakova, L., Gal, P., Vasilenko, T., Novotny, M., Smetana, K., et al. (2012). Immunohistological changes in skin wounds during the early periods of healing in a rat model. *Vet. Med.* 57, 77–82. doi: 10.17221/5253-vetmed

Santos, M., Paramio, J. M., Bravo, A., Ramirez, A., and Jorcano, J. L. (2002). The expression of keratin K10 in the basal layer of the epidermis inhibits cell

proliferation and prevents skin tumorigenesis. *J. Biol. Chem.* 277, 19122–19130. doi: 10.1074/jbc.M201001200

Schäffer, M. R., Tantry, U., Efron, P. A., Ahrendt, G. M., Thornton, F. J., and Barbul, A. (1997). Diabetes-impaired healing and reduced wound nitric oxide synthesis: a possible pathophysiologic correlation. *Surgery* 121, 513–519. doi: 10.1016/S0039-6060(97)90105-7

Schindelin, J., Arganda-Carreras, I., Frise, E., Kaynig, V., Longair, M., Pietzsch, T., et al. (2012). Fiji: an open-source platform for biological-image analysis. *Nat. Methods* 9, 676–682. doi: 10.1038/nmeth.2019

Schultz, G. S., and Wysocki, A. (2009). Interactions between extracellular matrix and growth factors in wound healing. *Wound Repair Regen.* 17, 153–162. doi: 10.1111/j.1524-475X.2009.00466.x

Silver, F. H., Kato, Y. P., Ohno, M., and Wasserman, A. J. (1992). Analysis of mammalian connective tissue: relationship between hierarchical structures and mechanical properties. *J. Long Term Eff. Med. Implants* 2, 165–198.

Tenni, R., Viola, M., Welser, F., Sini, P., Giudici, C., Rossi, A., et al. (2002). Interaction of decorin with CNBr peptides from collagens I and II. evidence for multiple binding sites and essential lysyl residues in collagen. *Eur. J. Biochem.* 269, 1428–1437.

Usui, M. L., Mansbridge, J. N., Carter, W. G., Fujita, M., and Olerud, J. E. (2008). Keratinocyte migration, proliferation, and differentiation in chronic ulcers from patients with diabetes and normal wounds. *J. Histochem. Cytochem.* 56, 687–696. doi: 10.1369/jhc.2008.951194

Usui, M. L., Underwood, R. A., Mansbridge, J. N., Muffley, L. A., Carter, W. G., and Olerud, J. E. (2005). Morphological evidence for the role of suprabasal keratinocytes in wound reepithelialization. *Wound Repair Regen.* 13, 468–479. doi: 10.1111/j.1067-1927.2005.00067.x

Vexler, A., Polyansky, I., and Gorodetsky, R. (1999). Evaluation of skin viscoelasticity and anisotropy by measurement of speed of shear wave propagation with viscoelasticity skin analyzer. *J. Invest. Dermatol.* 113, 732–739. doi: 10.1046/j.1523-1747.1999.00751.x

Vogel, K. G., Paulsson, M., and Heinegård, D. (1984). Specific inhibition of type I and type II collagen fibrillogenesis by the small proteoglycan of tendon. *Biochem. J.* 223, 587–597.

Wang, B., Yang, W., McKittrick, J., and Meyers, M. A. (2016). Keratin: structure, mechanical properties, occurrence in biological organisms, and efforts at bioinspiration. *Prog. Mat. Sci.* 76, 229–318. doi: 10.1016/j.pmatsci.2015.06.001

Werner, S., and Grose, R. (2003). Regulation of wound healing by growth factors and cytokines. *Physiol. Rev.* 83, 835–870.

Werner, S., Krieg, T., and Smola, H. (2007). Keratinocyte–fibroblast interactions in wound healing. *J. Investig. Dermatol.* 127, 998–1008. doi: 10.1038/sj.jid.5700786

Yeo, T. K., Brown, L., and Dvorak, H. F. (1991). Alterations in proteoglycan synthesis common to healing wounds and tumors. *Am. J. Pathol.* 138, 1437–1450.

Yue, D. K., McLennan, S., Marsh, M., Mai, Y. W., Spaliviero, J., Delbridge, L., et al. (1987). Effects of experimental diabetes, uremia, and malnutrition on wound healing. *Diabetes* 36, 295–299. doi: 10.2337/diab.36.3.295

Zhang, Y., McClain, S. A., Lee, H.-M., Elburki, M. S., Yu, H., Gu, Y., et al. (2016). A novel chemically modified curcumin "normalizes" wound-healing in rats with experimentally induced type I diabetes: initial studies. *J. Diabetes Res.* 2016:5782904. doi: 10.1155/2016/5782904

Conflict of Interest: The authors declare that the research was conducted in the absence of any commercial or financial relationships that could be construed as a potential conflict of interest.

frontiers in Bioengineering and Biotechnology

BRIEF RESEARCH REPORT
published: 09 March 2021
doi: 10.3389/fbioe.2021.654920

Parameter-Dependency of Low-Intensity Vibration for Wound Healing in Diabetic Mice

*Rita E. Roberts[1,2,3], Onur Bilgen[4], Rhonda D. Kineman[3,5] and Timothy J. Koh[1,2,3]**

[1] Department of Kinesiology and Nutrition, University of Illinois at Chicago, Chicago, IL, United States, [2] Center for Tissue Repair and Regeneration, University of Illinois at Chicago, Chicago, IL, United States, [3] Jesse Brown VA Medical Center, Chicago, IL, United States, [4] Department of Mechanical and Aerospace Engineering, Rutgers University, Piscataway, NJ, United States, [5] Department of Medicine, Section of Endocrinology, Diabetes and Metabolism, University of Illinois at Chicago, Chicago, IL, United States

OPEN ACCESS

Edited by:
Yih-Kuen Jan, University of Illinois at Urbana-Champaign, United States

Reviewed by:
Laisa Liane Paineiras-Domingos, Federal University of Bahia, Brazil
Gabriele Ceccarelli, University of Pavia, Italy
Taiar Redha, Université de Reims Champagne-Ardenne, France

***Correspondence:**
Timothy J. Koh
tjkoh@uic.edu

Specialty section:
This article was submitted to Biomechanics, a section of the journal Frontiers in Bioengineering and Biotechnology

Received: *17 January 2021*
Accepted: *12 February 2021*
Published: *09 March 2021*

Citation:
Roberts RE, Bilgen O, Kineman RD and Koh TJ (2021) Parameter-Dependency of Low-Intensity Vibration for Wound Healing in Diabetic Mice. Front. Bioeng. Biotechnol. 9:654920. doi: 10.3389/fbioe.2021.654920

Chronic wounds in diabetic patients represent an escalating health problem, leading to significant morbidity and mortality. Our group previously reported that whole body low-intensity vibration (LIV) can improve angiogenesis and wound healing in diabetic mice. The purpose of the current study was to determine whether effects of LIV on wound healing are frequency and/or amplitude dependent. Wound healing was assessed in diabetic (db/db) mice exposed to one of four LIV protocols with different combinations of two acceleration magnitudes (0.3 and 0.6 g) and two frequencies (45 and 90 Hz) or in non-vibration sham controls. The low acceleration, low frequency protocol (0.3 g and 45 Hz) was the only one that improved wound healing, increasing angiogenesis and granulation tissue formation, leading to accelerated re-epithelialization and wound closure. Other protocols had little to no impact on healing with some evidence that 0.6 g accelerations negatively affected wound closure. The 0.3 g, 45 Hz protocol also increased levels of insulin-like growth factor-1 and tended to increase levels of vascular endothelial growth factor in wounds, but had no effect on levels of basic fibroblast growth factor or platelet derived growth factor-bb, indicating that this LIV protocol induces specific growth factors during wound healing. Our findings demonstrate parameter-dependent effects of LIV for improving wound healing that can be exploited for future mechanistic and therapeutic studies.

Keywords: low-intensity vibration, wound healing, angiogenesis, growth factors, diabetes

INTRODUCTION

Chronic wounds represent an escalating health problem around the world, especially in diabetic patients. Over 415 million people (8.3% of the world's adult population) are afflicted with diabetes and associated complications, including chronic wounds (Chatterjee et al., 2017). People with diabetes incur a 25% lifetime risk of developing chronic wounds, which often lead to amputation, resulting in decreased quality of life, high morbidity and mortality (Ramsey et al., 1999; Jeffcoate and Harding, 2003; Hoffstad et al., 2015). Wound healing typically occurs through overlapping

phases of inflammation, proliferation and remodeling (Koh and DiPietro, 2011; Eming et al., 2014). Although chronic wounds are known to exhibit defects in each phase of healing, including dysregulated inflammation, impaired perfusion and neovascularization, and poor tissue maturation (Blakytny and Jude, 2006), few therapies are available to improve healing of diabetic wounds.

Energy-based modalities are often used in conjunction with standard treatments for hard to heal chronic wounds. These treatments use laser, electrical, or mechanical stimulation, in an attempt to modify the cellular and biochemical environment to improve angiogenesis and healing (Ennis et al., 2016; Game et al., 2016; Sousa and Batista Kde, 2016). Recently, our group demonstrated that whole body low-intensity vibration (LIV) can improve angiogenesis and wound healing in diabetic mice, potentially by increasing growth factors such as insulin-like growth factor (IGF)-1 and vascular endothelial growth factor (VEGF) in the wound (Weinheimer-Haus et al., 2014). In addition, we and others have demonstrated that LIV can rapidly increase systemic and regional (i.e., skin) blood flow (Nakagami et al., 2007; Maloney-Hinds et al., 2008; Tzen et al., 2018; Zhu et al., 2020) and can inhibit progression of pressure ulcers (Arashi et al., 2010; Sari et al., 2015). However, much remains to be learned about how LIV signals influence different aspects of wound healing.

The purpose of the current study was to identify LIV amplitudes and frequencies that promote healing in diabetic mice. The hypothesis of this study was that effects of LIV on wound healing are frequency and amplitude dependent.

MATERIALS AND METHODS

Animals

Diabetic db/db mice (BKS.Cg-Dock7m+/+Leprdb/J) were obtained from the Jackson Laboratory. Experiments were performed on 12–16 weeks-old male mice. Only mice with fasting blood glucose >250 mg/dl were included in the study. Mice were housed in environmentally controlled conditions with a 12-h light/dark cycle. Water and food were available *ad libitum*. Two wounds from each of four mice were analyzed for each assay ($N = 8$ total for each assay). To minimize bias, mice were randomly assigned to experimental groups and resulting samples were coded and analyzed in a blinded fashion. All procedures involving animals were approved by the Animal Care Committee at the Jesse Brown Veterans' Affairs Medical Center [OLAW Assurance number D16-00722 (A4456-01)].

Excisional Wounding

Mice were subjected to excisional wounding as described previously (Weinheimer-Haus et al., 2014). Briefly, mice were anesthetized with isoflurane and their dorsum was shaved and cleaned with alcohol. Four 8 mm wounds were made on the back of each mouse with a dermal biopsy punch and covered with Tegaderm (3M, Minneapolis, MN, United States) to keep the wounds moist and maintain consistency with treatment of human wounds.

Low-Intensity Vibration

Following wounding, mice were randomly assigned to one of four whole-body LIV treatment groups or to a non-vibration sham (control) group. LIV treatment groups utilized different combinations of low (45 Hz) and high (90 Hz) frequencies and low (0.3 g) and high (0.6 g) peak accelerations. Harmonic LIV signals were calibrated using an accelerometer attached directly to top surface of the vibrating plate (Weinheimer-Haus et al., 2014). For LIV treatment, mice were placed in an empty cage directly on a vibrating plate, and LIV was applied for 30 min per day for 7 days/week starting on the day of wounding [cf (Weinheimer-Haus et al., 2014) for image of set-up]. Non-vibrated sham controls were similarly placed in a separate empty cage but were not subjected to LIV.

Wound Closure

Wound closure was assessed in digital images of the external wound surface taken immediately after injury and on days 3, 6, and 10 post-injury. Wound area was measured using Fiji Image J and expressed as a percentage of the area immediately after injury.

Wound Histology

Skin wounds were collected from the pelt of each animal on day 10 post-injury, followed by embedding in tissue freezing medium and freezing in isopentane cooled with dry ice. Each wound was cryosectioned from one edge to well past the center and 10-μm sections were selected from the center of the wound for staining and analysis of re-epithelialization, granulation tissue formation, angiogenesis and collagen deposition (Weinheimer-Haus et al., 2014). For all wound healing analyses, digital images were obtained using a Keyence BZ-X710 microscope with 2×/0.10 or 20×/0.75 Nikon objectives and BZ-X Analyzer software.

Re-Epithelialization and Granulation Tissue Area

Wound re-epithelialization and granulation tissue area were assessed by morphometric analysis of hematoxylin and eosin stained cryosections from the wound center (Weinheimer-Haus et al., 2014). The distance between the wound edges, defined by the distance between the first hair follicle encountered at each end of the wound, and the distance that the epithelium had traversed into the wound, were measured using image analysis software. Re-epithelialization was then calculated as: [(distance traversed by epithelium)/(distance between wound edges) × 100]. Granulation tissue area was measured as the area of new tissue formation between wound edges. Re-epithelialization and granulation tissue area were measured in three sections per wound and was averaged over sections to provide a representative value for each wound.

Angiogenesis and Collagen Deposition

Dermal healing was assessed using immunohistochemical staining for platelet-derived endothelial cell adhesion molecule-1 (also called CD31) for angiogenesis and Masson's trichrome stain for collagen deposition (Weinheimer-Haus et al., 2014). For angiogenesis assessment, sections were first air-dried, fixed in cold acetone, washed with PBS, quenched with 0.3% hydrogen peroxide, then washed again with PBS. Sections were blocked

with buffer containing 3% bovine serum albumin and then incubated overnight with CD31 antibody (1:100, Biolegend, San Diego, CA, United States). Sections were then washed with PBS and incubated with biotinylated anti-rat secondary antibody (1:200, Vector Laboratories, Burlingame, CA, United States). After a wash with PBS, sections were incubated with avidin D-horseradish peroxidase (1:1000) and developed with a 3-amino-9-ethylcarbazole kit (Vector Laboratories). Image J was used to quantify the percentage of CD31-stained area relative to the total area of the wound bed. For each assay, digital images covering the majority of the wound bed (usually three images at $\times 20$ magnification) were first obtained. The percent area stained in each image was then quantified by counting the number of pixels staining above a threshold intensity and normalizing to the total number of pixels. Threshold intensity was set such that only clearly stained pixels were counted. The software allowed the observer to exclude staining identified as artifact, large vessels, and areas deemed to be outside the wound bed. For trichrome analysis, staining was performed according to the manufacturer's directions (IMEB, San Marcos, CA, United States), and Image J was used to quantify the percentage of blue collagen-stained area relative to the total area of the wound bed. For both trichrome and CD31 staining, three sections per wound were analyzed, and data were averaged over sections to provide a representative value for each wound.

ELISA

Wounds were snap frozen and stored in LN2 and then homogenized in cold PBS (10 μl of PBS per mg wound tissue) supplemented with protease inhibitor cocktail (Sigma Aldrich, St. Louis, MO, United States) using a dounce homogenizer and then centrifuged. Supernatants were used for enzyme-linked immunoassay of IGF-1, VEGF, basic fibroblast growth factor (bFGF) and platelet derived growth factor (PDGF)-bb (R&D Systems, Minneapolis, MN, United States).

Statistics

Values are reported as means $\pm$ standard deviation. Measurements of wound healing or wound growth factors were compared between treatment groups using one-way ANOVA. Dunnett's multiple comparisons test was used when ANOVAs demonstrated significance. Differences between groups were considered significant if $P \leq 0.05$.

RESULTS

LIV Promotes Wound Closure in a Parameter Dependent Fashion

Mice were treated with one of four LIV protocols: low (45 Hz) frequency, low (0.3 g) acceleration (LL), high (90 Hz) frequency, high (0.6 g) acceleration (HH), low frequency, high acceleration (LH) or high frequency, low acceleration (HL) (**Table 1**). Consistent with our previous study (Weinheimer-Haus et al., 2014), none of the protocols in the current study altered blood glucose levels of the diabetic db/db mice (data not shown). The LL protocol was the only one to increase external measurements of wound closure on days 6 and 10 post-injury compared to sham control, whereas the LH and HH protocols decreased wound closure at all time points (**Figure 1**). Similarly, the LL protocol was the only one to increase histological measurements of re-epithelialization on day 10 post-injury compared to sham control, whereas the LH and HH protocols decreased re-epithelialization (**Figure 1**). In short, the LL protocol improved wound closure in diabetic mice, whereas the LH and HH protocols impaired wound closure.

TABLE 1 | LIV protocols.

	LL	LH	HL	HH
Acceleration (g)	0.3	0.6	0.3	0.6
Frequency (Hz)	45	45	90	90

LL, low acceleration, low frequency; LH, low acceleration, high frequency; HL, high acceleration, low frequency; HH, high acceleration, high frequency.

LIV Promotes Wound Angiogenesis and Granulation Tissue Formation in a Parameter Dependent Fashion

Similar to the wound closure measurements, the LL protocol was the only LIV protocol to increase granulation tissue area on day 10 post-injury compared to sham controls (bar graph in **Figure 2**, example images in **Figure 1**). The other protocols produced no significant change in granulation tissue area. In addition, only the LL protocol induced a robust increase in angiogenesis on day 10 as assessed by CD31 staining compared to sham controls (**Figure 2**). The other protocols produced no significant change in angiogenesis. In short, the LL protocol improved angiogenesis and granulation tissue formation in diabetic mice, whereas the other protocols had no effect.

LIV Enhances Wound IGF-1 Levels in a Parameter Dependent Fashion

Associated with the accelerated re-epithelialization and dermal healing, the LL protocol significantly increased levels of IGF-1 and tended to increase levels of VEGF in wounds on day 10 post-injury compared to sham controls (**Figure 3**). The other protocols did not alter wound levels of IGF-1 or VEGF. In addition, none of the LIV protocols altered wound levels of either bFGF or PDGF-bb. Thus, LIV induces specific growth factors during wound healing in a parameter dependent fashion.

DISCUSSION

Despite the escalating socioeconomic impact of diabetic wounds, effective treatments remain elusive. In this study, we sought to determine the parameter dependency of a novel therapeutic approach to improve diabetic wound healing using whole-body LIV. The major finding of this study is that only LIV with relatively low frequency (45 Hz) and low acceleration levels (0.3 g) improve wound healing in diabetic mice. Compared to non-vibrated control mice, such LIV treatment increased

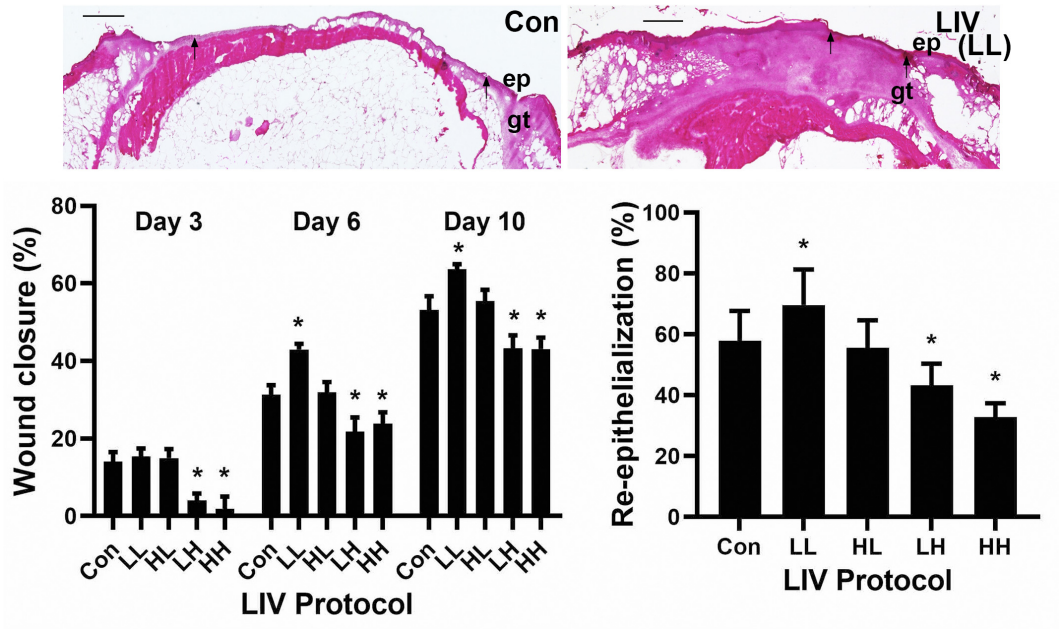

FIGURE 1 | Parameter dependency of low-intensity vibration (LIV) for improving wound closure. Mice either received one of four protocols of whole-body LIV: 0.3 g at 45 Hz (LL), 0.3 g at 90 Hz (LH), 1.0 g at 45 Hz (HL), 1.0 g at 90 Hz (HH) or sham control treatment (Con) for 30 min per day, starting the day of wounding for 5 days per week. Left: Wound closure was measured in digital images of wound surface on days 3, 6, and 10 post-injury. Right: Re-epithelialization was measured in hematoxylin and eosin stained sections from center of day 10 wounds. Top: Representative images of hematoxylin and eosin stained sections; arrows mark ends of epithelial tongues growing into wound, ep = epithelium, gt = granulation tissue, scale bar = 500 μm. Two wounds from each of four mice were analyzed for each assay (N = 8 total for each assay). *Mean value significantly different from that of Con for same time point, $P \leq 0.05$.

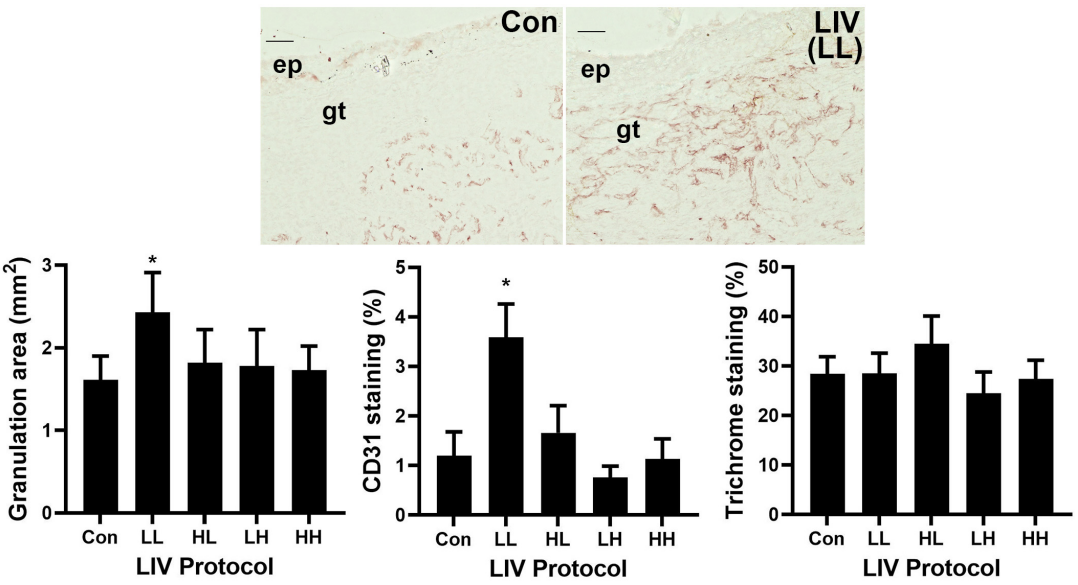

FIGURE 2 | Parameter dependency of low-intensity vibration (LIV) for improving granulation and angiogenesis. Mice either received one of four protocols of whole-body LIV: 0.3 g at 45 Hz (LL), 0.3 g at 90 Hz (LH), 1.0 g at 45 Hz (HL), 1.0 g at 90 Hz (HH) or sham control treatment (Con) for 30 min per day, starting the day of wounding for 5 days per week. Left: Granulation tissue thickness was measured as the area of granulation tissue divided by the distance between wound edges in hematoxylin and eosin stained sections from center of day 10 wounds. Center: Angiogenesis was measured as percent area stained with antibody against CD31 in sections from center of day 10 wounds. Top: Representative images of CD31 stained sections; ep, epithelium; gt, granulation tissue; scale bar = 50 μm. Right: Collagen deposition assessed as percent area stained blue in Trichrome stained sections of center of day 10 wounds. Two wounds from each of four mice were analyzed for each assay (N = 8 total for each assay). *Mean value significantly different from that of Con, $P \leq 0.05$.

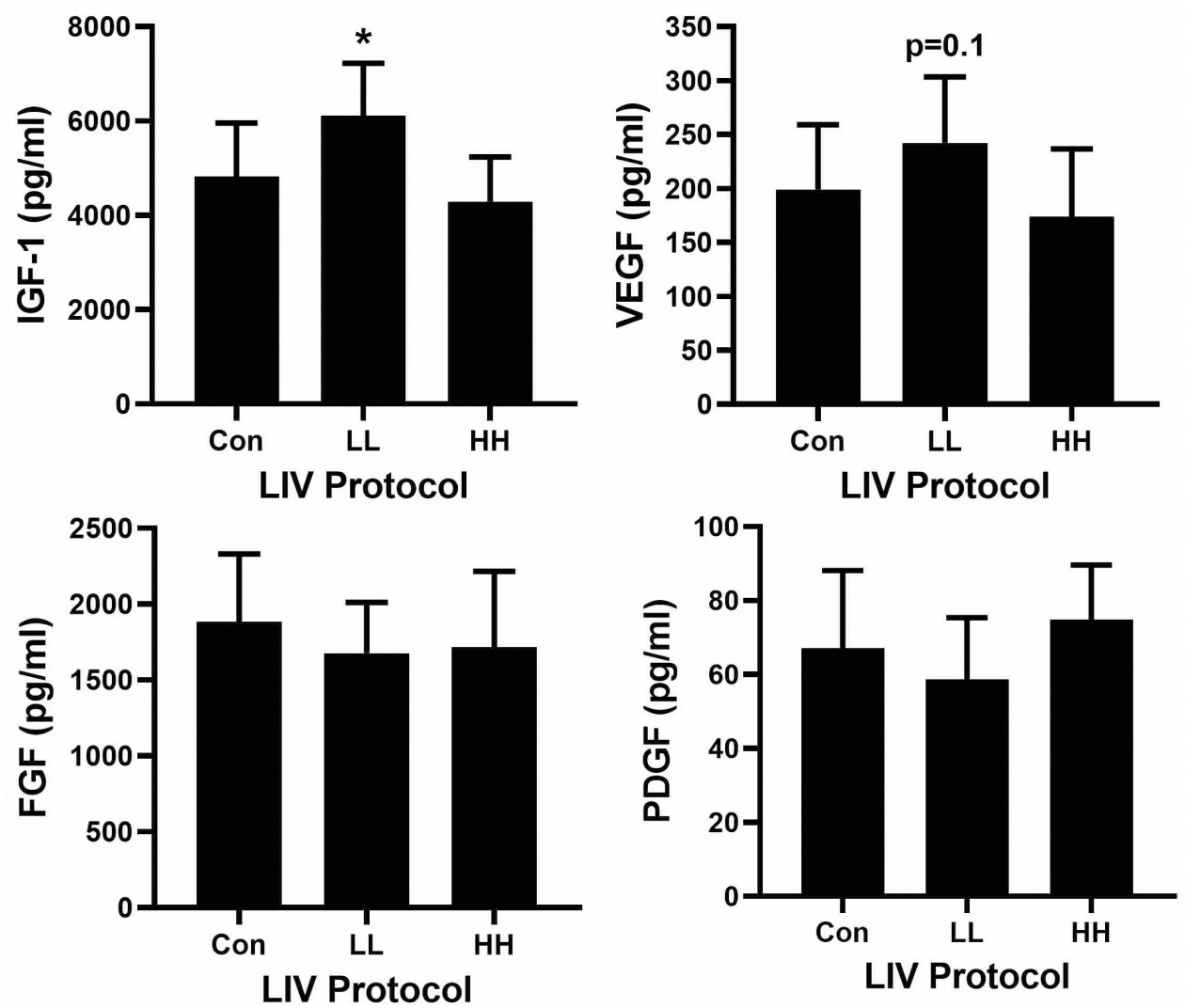

FIGURE 3 | Parameter dependency of low-intensity vibration (LIV) for increasing IGF-1 in wounds. Mice either received one of two protocols of whole-body LIV: 0.3 *g* at 45 Hz (LL), 1.0 g at 90 Hz (HH) or sham control treatment (Con) for 30 min per day, starting the day of wounding for 5 days per week. Protein levels of IGF-1, VEGF, FGF-b, and PDGF-bb measured in homogenates of day 10 wounds using ELISA. Two wounds from each of four mice were analyzed for each assay ($N = 8$ total for each assay). *Mean value significantly different from that of Con, $P \leq 0.05$.

granulation tissue formation and angiogenesis, and accelerated closure and re-epithelialization. In contrast, LIV with higher frequency (90 Hz) and/or higher acceleration levels (0.6 g) tended to impair wound closure and had little to no effect on angiogenesis or granulation tissue formation. Thus, LIV does indeed exhibit parameter-dependent effects on wound healing.

The results of the current study are consistent with our previous study, in which we reported that LIV with 45 Hz frequency and 0.4 g acceleration increased angiogenesis, granulation tissue formation, and re-epithelialization (Weinheimer-Haus et al., 2014). This protocol was similar to our LL protocol (45 Hz frequency, 0.3 g acceleration). In addition, data in the present study demonstrates that protocols with higher frequency and/or acceleration do not improve skin healing. Related studies on the effect of LIV with similar frequency (47 Hz) and acceleration (0.2 g) on pressure ulcers (3.15 min treatments per day) demonstrated that LIV can improve healing of stage I pressure ulcers in elderly patients compared to standard care (Arashi et al., 2010). Similar LIV treatment for 15 min per day also reduced progression of pressure induced deep tissue injury associated with downregulation of matrix metalloproteinase-2 and -9 activity in rats (Sari et al., 2015).

A number of studies have focused on the effects of vibrations on skin blood flow in both rodents and humans, which could influence wound healing along with other physiological processes. LIV with frequency of 47 Hz and unknown acceleration increased skin blood flow measured by intravital microscopy of the mouse ear in what appears to be a nitric oxide dependent manner (Nakagami et al., 2007;

Ichioka et al., 2011). A series of studies has also shown that vibrations can increase skin blood flow as measured by laser Doppler flowmetry when vibrations were applied to the forearm or lower leg in healthy human participants or diabetic patients (Lohman et al., 2007; Maloney-Hinds et al., 2009; Johnson et al., 2014). These latter studies used frequencies between 30 and 50 Hz and accelerations between 6 and 7 g, and found no difference in skin blood flow response between 30 and 50 Hz protocols (Maloney-Hinds et al., 2008). These protocols may be considered high-intensity vibration, since LIV is typically considered to utilize accelerations <1.0 g. We performed a similar experiment using LIV with frequency of 30 Hz and accelerations of 0.4 g and found that LIV signals also increase lower leg skin blood flow in healthy human participants but this effect only lasts while LIV is applied (Tzen et al., 2018). A recent study compared LIV protocols with frequencies of 35 and 100 Hz and an amplitude of 1 mm and found that the 100 Hz protocol produced larger increase in skin blood flow over the first metatarsal head (Zhu et al., 2020). Finally, recent systematic reviews have provided additional evidence that vibration can increase blood flow in the lower extremities in diabetic patients (Sa-Caputo et al., 2017; Gomes-Neto et al., 2019). These studies support the translation of LIV into a treatment that can improve wound healing in human patients.

Limitations of this study include the small number of parameters tested; two frequencies and two accelerations. However, our finding that only the 45 Hz, 0.3 g protocol improved wound healing narrows the solution space for pro-healing parameters. The parameters were measured at the surface of the vibrating plate; the actual vibrations experienced by the wound could be different and would be extremely difficult to measure. In addition, although we have identified growth factors that are increased by LIV and are associated with angiogenesis, granulation tissue formation and closure, the precise mechanisms involved remain to be elucidated. Along the same lines, although we assessed effects of LIV on re-epithelialization, granulation and angiogenesis, more detailed analysis of the effects of LIV on wound cells, including keratinocytes, fibroblasts, endothelial cells and inflammatory cells awaits further study.

In summary, our findings demonstrate parameter-dependent effects of LIV for improving wound healing and only LIV with 45 Hz frequency and 0.3 g acceleration levels increased angiogenesis, granulation tissue formation and re-epithelialization associated with increased wound levels of IGF-1. Importantly, the LIV protocol could easily be translated to clinical trials for diabetic patients with chronic wounds.

DATA AVAILABILITY STATEMENT

The raw data supporting the conclusions of this article will be made available by the authors, without undue reservation.

ETHICS STATEMENT

All procedures involving animals were approved by the Animal Care Committee at the Jesse Brown Veterans' Affairs Medical Center.

AUTHOR CONTRIBUTIONS

RR helped design the study, performed experiments, and wrote the manuscript. OB, RK, and TK helped design the study and write the manuscript. All authors contributed to the article and approved the submitted version.

FUNDING

This study was supported by VA grant I01 RX002636 to RK, OB, and TK, and NIGMS grant R35 GM136228 to TK.

REFERENCES

Arashi, M., Sugama, J., Sanada, H., Konya, C., Okuwa, M., Nakagami, G., et al. (2010). Vibration therapy accelerates healing of Stage I pressure ulcers in older adult patients. *Adv. Skin Wound Care* 23, 321–327. doi: 10.1097/01.ASW.0000383752.39220.fb

Blakytny, R., and Jude, E. (2006). The molecular biology of chronic wounds and delayed healing in diabetes. *Diabet Med.* 23, 594–608. doi: 10.1111/j.1464-5491.2006.01773.x

Chatterjee, S., Khunti, K., and Davies, M. J. (2017). Type 2 diabetes. *Lancet* 389, 2239–2251. doi: 10.1016/S0140-6736(17)30058-2

Eming, S. A., Martin, P., and Tomic-Canic, M. (2014). Wound repair and regeneration: mechanisms, signaling, and translation. *Sci. Transl. Med.* 6:265sr6. doi: 10.1126/scitranslmed.3009337

Ennis, W. J., Lee, C., Gellada, K., Corbiere, T. F., and Koh, T. J. (2016). Advanced Technologies to Improve Wound Healing: Electrical Stimulation, Vibration Therapy, and Ultrasound-What Is the Evidence? *Plast Reconstr. Surg.* 138(3 Suppl.), 94S–104S. doi: 10.1097/PRS.0000000000002680

Game, F. L., Apelqvist, J., Attinger, C., Hartemann, A., Hinchliffe, R. J., Londahl, M., et al. (2016). Effectiveness of interventions to enhance healing of chronic ulcers of the foot in diabetes: a systematic review. *Diabetes Metab. Res. Rev.* 32(Suppl. 1), 154–168. doi: 10.1002/dmrr.2707

Gomes-Neto, M., de Sa-Caputo, D. D. C., Paineiras-Domingos, L. L., Brandao, A. A., Neves, M. F., Marin, P. J., et al. (2019). Effects of Whole-Body Vibration in Older Adult Patients With Type 2 Diabetes Mellitus: A Systematic Review and Meta-Analysis. *Can. J. Diabetes* 43, 524–529e2. doi: 10.1016/j.jcjd.2019.03.008

Hoffstad, O., Mitra, N., Walsh, J., and Margolis, D. J. (2015). Diabetes, lower-extremity amputation, and death. *Diabetes Care* 38, 1852–1857. doi: 10.2337/dc15-0536

Ichioka, S., Yokogawa, H., Nakagami, G., Sekiya, N., and Sanada, H. (2011). In vivo analysis of skin microcirculation and the role of nitric oxide during vibration. *Ostomy Wound Manag.* 57, 40–47.

Jeffcoate, W. J., and Harding, K. G. (2003). Diabetic foot ulcers. *Lancet* 361, 1545–1551. doi: 10.1016/S0140-6736(03)13169-8

Johnson, P. K., Feland, J. B., Johnson, A. W., Mack, G. W., and Mitchell, U. H. (2014). Effect of whole body vibration on skin blood flow and nitric oxide production. *J. Diabetes. Sci. Technol.* 8, 889–894. doi: 10.1177/1932296814536289

Koh, T. J., and DiPietro, L. A. (2011). Inflammation and wound healing: the role of the macrophage. *Exp. Rev. Mol. Med.* 13:e23. doi: 10.1017/S1462399411001943

Lohman, E. B. III, Petrofsky, J. S., Maloney-Hinds, C., Betts-Schwab, H., and Thorpe, D. (2007). The effect of whole body vibration on lower extremity skin blood flow in normal subjects. *Med. Sci. Monit.* 13, CR71–CR76.

Maloney-Hinds, C., Petrofsky, J. S., and Zimmerman, G. (2008). The effect of 30 Hz vs. 50 Hz passive vibration and duration of vibration on skin blood flow in the arm. *Med. Sci. Monit* 14, CR112–CR116.

Maloney-Hinds, C., Petrofsky, J. S., Zimmerman, G., and Hessinger, D. A. (2009). The role of nitric oxide in skin blood flow increases due to vibration in healthy adults and adults with type 2 diabetes. *Diabetes Technol. Ther.* 11, 39–43. doi: 10.1089/dia.2008.0011

Nakagami, G., Sanada, H., Matsui, N., Kitagawa, A., Yokogawa, H., Sekiya, N., et al. (2007). Effect of vibration on skin blood flow in an in vivo microcirculatory model. *Biosci. Trends* 1, 161–166.

Ramsey, S. D., Newton, K., Blough, D., McCulloch, D. K., Sandhu, N., Reiber, G. E., et al. (1999). Incidence, outcomes, and cost of foot ulcers in patients with diabetes. *Diabetes Care* 22, 382–387.

Sa-Caputo, D., Paineiras-Domingos, L., Carvalho-Lima, R., Dias-Costa, G., de Paiva, P. C., de Azeredo, C. F., et al. (2017). Potential Effects of Whole-Body Vibration Exercises on Blood Flow Kinetics of Different Populations: A Systematic Review with a Suitable Approach. *Afr. J. Tradit Complement Altern Med.* 14(4 Suppl.), 41–51. doi: 10.21010/ajtcam.v14i4S.6

Sari, Y., Sanada, H., Minematsu, T., Nakagami, G., Nagase, T., Huang, L., et al. (2015). Vibration inhibits deterioration in rat deep-tissue injury through HIF1-MMP axis. *Wound Repair Regen* 23, 386–393. doi: 10.1111/wrr.12286

Sousa, R. G., and Batista Kde, N. (2016). Laser therapy in wound healing associated with diabetes mellitus - Review. *An Bras. Dermatol.* 91, 489–493. doi: 10.1590/abd1806-4841.20163778

Tzen, Y. T., Weinheimer-Haus, E. M., Corbiere, T. F., and Koh, T. J. (2018). Increased skin blood flow during low intensity vibration in human participants: Analysis of control mechanisms using short-time Fourier transform. *PLoS One* 13:e0200247. doi: 10.1371/journal.pone.0200247

Weinheimer-Haus, E. M., Judex, S., Ennis, W. J., and Koh, T. J. (2014). Low-intensity vibration improves angiogenesis and wound healing in diabetic mice. *PLoS One* 9:e91355. doi: 10.1371/journal.pone.0091355

Zhu, T., Wang, Y., Yang, J., Liao, F., Wang, S., and Jan, Y. K. (2020). Wavelet-based analysis of plantar skin blood flow response to different frequencies of local vibration. *Physiol. Meas* 41, 025004. doi: 10.1088/1361-6579/ab6e56

Conflict of Interest: TK has a patent pending on the application of vibration for therapeutic treatment for tissue repair "Method and system for physical stimulation of tissue" (#2013/0165,824).

The remaining authors declare that the research was conducted in the absence of any commercial or financial relationships that could be construed as a potential conflict of interest.

frontiers in Bioengineering and Biotechnology

ORIGINAL RESEARCH
published: 15 April 2021
doi: 10.3389/fbioe.2021.665248

The Injury Mechanism of Traumatic Amputation

*Iain A. Rankin[1], Thuy-Tien Nguyen[1], Louise McMenemy[1,2], Jonathan C. Clasper[1,3] and Spyros D. Masouros[1]**

[1] Department of Bioengineering, Imperial College London, London, United Kingdom, [2] Academic Department of Military Surgery and Trauma, Royal Centre for Defence Medicine, ICT Centre, Birmingham Research Park, Birmingham, United Kingdom, [3] Department of Trauma and Orthopaedic Surgery, Frimley Park Hospital, Surrey, United Kingdom

Traumatic amputation has been one of the most defining injuries associated with explosive devices. An understanding of the mechanism of injury is essential in order to reduce its incidence and devastating consequences to the individual and their support network. In this study, traumatic amputation is reproduced using high-velocity environmental debris in an animal cadaveric model. The study findings are combined with previous work to describe fully the mechanism of injury as follows. The shock wave impacts with the casualty, followed by energised projectiles (environmental debris or fragmentation) carried by the blast. These cause skin and soft tissue injury, followed by skeletal trauma which compounds to produce segmental and multifragmental fractures. A critical injury point is reached, whereby the underlying integrity of both skeletal and soft tissues of the limb has been compromised. The blast wind that follows these energised projectiles completes the amputation at the level of the disruption, and traumatic amputation occurs. These findings produce a shift in the understanding of traumatic amputation due to blast from a mechanism predominately thought mediated by primary and tertiary blast, to now include secondary blast mechanisms, and inform change for mitigative strategies.

Keywords: biomechanics, traumatic amputation, fracture, blast injury, military, mouse, soil, sand

OPEN ACCESS

Edited by:
Matthew J. Major, Northwestern University, United States

Reviewed by:
Kenneth L. Monson, The University of Utah, United States
Panagiotis Chatzistergos, Staffordshire University, United Kingdom

***Correspondence:**
Spyros D. Masouros
s.masouros04@imperial.ac.uk

Specialty section:
This article was submitted to Biomechanics, a section of the journal Frontiers in Bioengineering and Biotechnology

Received: *07 February 2021*
Accepted: *30 March 2021*
Published: *15 April 2021*

Citation:
Rankin IA, Nguyen T-T, McMenemy L, Clasper JC and Masouros SD (2021) The Injury Mechanism of Traumatic Amputation. Front. Bioeng. Biotechnol. 9:665248. doi: 10.3389/fbioe.2021.665248

INTRODUCTION

Recent conflicts have seen improvised explosive devices (IEDs) rise as the insurgents' weapon of choice, where they have been the primary cause of military deaths (Clasper and Ramasamy, 2013). Outside of the military setting, use of IEDs by terrorist organisations has increased steadily over the last 40 years (Edwards et al., 2016). One of the most common and defining injuries of an IED explosion is of blast-mediated traumatic amputation (Ramasamy et al., 2009a). This injury represents a significant cause of morbidity and mortality. It is associated with fatality either directly through haemorrhage, or indirectly as a marker of other severe blast trauma (Mellor and Cooper, 1989). With regards to morbidity, a US-Army study showed only a 2.3% return-to-duty rate for soldiers who had sustained a traumatic amputation (of whom most had suffered only partial hand or foot loss) (Kishbaugh et al., 1995). The 2013 Boston Marathon bombing caused 17 lower limb traumatic amputations and a further 10 severe soft tissue extremity injuries (King et al., 2015); the morbidity in these civilian injuries is likewise extensive with reduced mobility, phantom limb pain, and an overall reduced quality of life reported (Sinha et al., 2011;

Azocar et al., 2020). To limit future morbidity and mortality through mitigative strategies, an accurate understanding of the mechanism of injury is essential.

The mechanisms of injury due to an explosion in general can be separated into five distinct categories: primary (direct effects of the shock front over-pressurisation), secondary (injury caused by energised projectiles propagated by the blast), tertiary (bodily displacement, either directly or indirectly as a result of the blast wind), quaternary (a miscellaneous category of injuries, including burns), and quinary (non-explosion related effects resulting in a hyper-inflammatory state, including through the use of biological, chemical or nuclear products). The mechanism of injury by which blast results in traumatic amputation is not clearly understood. Several mechanisms of injury have been proposed. The first proposed mechanism was hypothesised to occur due to a combination of primary and tertiary blast mechanisms, whereby the shock front over-pressurisation causes diaphyseal fracture through shear and axial stress, followed by the blast wind completing the amputation (Hull and Cooper, 1996). Other proposed mechanisms of injury include tertiary blast injury in isolation, as rapid lower limb movement propagated by the blast wind results in traumatic amputation (Singleton et al., 2014). Secondary blast injury has also been linked to traumatic amputation, where single large fragments propagated by the blast have resulted in "guillotine type" injuries (Hull and Cooper, 1996). More recently, we have shown secondary blast injury as a result of energised environmental debris to be linked to causing traumatic amputation in an animal model (Rankin et al., 2020a). Whilst we showed that high velocity environmental debris (sandy gravel soil) can cause a cohort of injuries, including traumatic amputation, the exact mechanism by which the traumatic amputation had occurred was not examined specifically.

With regards to the type of environmental debris, North Atlantic Treaty Organization (NATO) standards for testing protection against a buried explosive device defines the testing conditions as utilising a soil type which is of a sandy gravel composition (Nato/PfP Unclassified, 2006). Whilst the mechanism by which energised sandy gravel soil causes traumatic amputation is not clear, the process by which it propagates following an explosion is known. When a buried explosive is detonated, the resultant shockwave compresses this surrounding sandy gravel soil. Immediately following this, gas from the explosion is released at high velocity and acts to eject this compressed soil at supersonic speeds, which rapidly decelerate to below 600 m/s before impacting with casualties (Bowyer, 1996; Tremblay et al., 1998). The soil is carried upwards from the ground by the gas flow to project, dependent upon the soil's characteristics, at an angle of between 45 and 120 degrees, in a cone shape. With dry soil, easier venting of gaseous detonation products results in a wider spread. In contrast, water saturated soil resists gaseous venting to a greater degree; this results in a tunnelling effect and concentration of the soil in a vertical direction, which may result in increased injury at the point of impact (Grujicic et al., 2008; Ramasamy et al., 2009b). This injury mechanism has previously been referred to as "sand blast" (Webster et al., 2018).

A further variable which may affect injury risk is the size of the propagated soil. Typical sandy gravel soil granulometry has been described, with ideally distributed particle sizes ranging from 0.1 to 40 mm (Nato/PfP Unclassified, 2006). The effect that variations in soil size or moisture content may have on the injury risk of traumatic amputation is not known.

The aims of this study were (1) to replicate isolated traumatic amputation in a cadaveric small animal mouse model, caused by propagated high velocity sandy gravel soil (subsequently referred to as "sand blast"), (2) to investigate and describe the mechanism of injury of sand blast mediated traumatic amputation, through high-speed video recording and injury documentation, and (3) to investigate the effect of changes in sandy gravel soil size and moisture content on the risk for sustaining traumatic amputation.

MATERIALS AND METHODS

The experimental design and procedures were carried out in compliance with the UK Animal (Scientific Procedures) Act 1986. Testing was conducted using an established model on fresh-frozen cadaveric male MF-1 (out-bred, ex-breeder, wild type) murine specimens (8–9 weeks of age, Charles River Ltd., United Kingdom) (Rankin et al., 2019). Specimens were stored at −20°C and thawed at room temperature (21 ± 2°C) prior to testing.

Sandy gravel soil sizes were chosen based upon NATO unclassified AEP-55 recommendations for typical sandy gravel soil granulometry (Nato/PfP Unclassified, 2006). This was subsequently scaled to the murine model based upon recommended animal scaling parameters in blast, where the scale is equal to the length of a parameter of the human species divided by that of the animal species used ($\lambda_L = L_1/L_2$) (Panzer et al., 2014). The thigh circumference of each species was taken as the representative parameter for scaling, in view of traumatic amputation of the lower limb as the primary outcome. Median mouse thigh circumference was calculated as 2.7 cm (range 2.4–3.2 cm) from specimens (n = 59), whilst human thigh circumference was taken from literature as 55 cm (White and Churchill, 1971). From this, a downscaling of 20× for sandy gravel size was utilized (λ_L = 55 / 2.7 = 20). A minimum sandy gravel size cut-off of 0.1 mm was taken to avoid sublimation of sandy gravel particles smaller than this at high velocity.

Testing with different sandy gravel soil size and moisture content was performed to ascertain for any difference seen in injury risk. Three sandy gravel soil size ranges were tested, consisting of (1) ideally distributed, (2) minimum, and (3) maximum sandy gravel soil size range. These groups were further subdivided into dry, or saturated with water prior to testing. Sand saturated with water was formed by first submerging a sample of dry sand into a beaker of shallow water (with sufficient quantity to cover the total sand mass). The sand was then removed from the beaker by means of a laboratory micro spatula and transferred to absorbent tissue paper, to remove excess water. The sand was subsequently transferred from the tissue paper via micro

spatula to the hollow polycarbonate sabot, for use immediately in an experiment.

This gave a total of six different sandy gravel soil test groups. The ideally distributed sandy gravel soil size range chosen consisted of sandy gravel as closely representative to human scaled values, ranging from the human ideal particle size median value to the 85th centile value, consisting of 60% sandy gravel sized 0.1 to 0.3 mm, 20% sized 0.3 to 0.5 mm, and 20% sized 0.5 to 1 mm. The minimum sandy gravel soil size group consisted of 100% sandy gravel sized 0.1 to 0.3 mm. The maximum sandy gravel soil size group consisted of 100% sandy gravel sized 0.5 to 1 mm. The experimental sand sizes and distribution used (scaled to human values) are shown alongside those recommended in NATO AEP-55, ideally distributed particle sizes in **Figure 1** (Nato/PfP Unclassified, 2006).

The sandy gravel was housed within a hollow polycarbonate sabot which was loaded into the firing chamber of a double-reservoir gas-gun system (Nguyen et al., 2018). Within this system, a 2-litre reservoir charged with air or helium and a Mylar® diaphragm firing mechanism was used to accelerate the sabot-sand unit down a 3-m-long, 32-mm-bore barrel. The output velocity was controlled by the thickness of the Mylar® diaphragm. The reservoir section of the gas gun was charged to a predetermined firing pressure, to accelerate the sabot-sand unit to the desired velocity. The pressure was maintained within the reservoir section by a Mylar® diaphragm of appropriate thickness (ranging from 50 to 150 μm). The system utilises a priming section, which is charged to a pressure below the rupture pressure of the diaphragm. This reduces the pressure gradient across the mylar diaphragm (containing the reservoir system) and prevents it from rupturing early, as the reservoir is filled. The pressure in the prime section is vented at the point of initiating firing of the gas gun, resulting in rupture of the diaphragm, with release of the pressurised gas. The gas-gun system accelerates the sabot-sandy-gravel unit down a barrel to exit into a target chamber, where the sabot is separated from the sandy gravel by a sabot stripper. The sabot is halted at this point, while the sandy gravel continues to travel toward the mouse specimen at the intended terminal velocity.

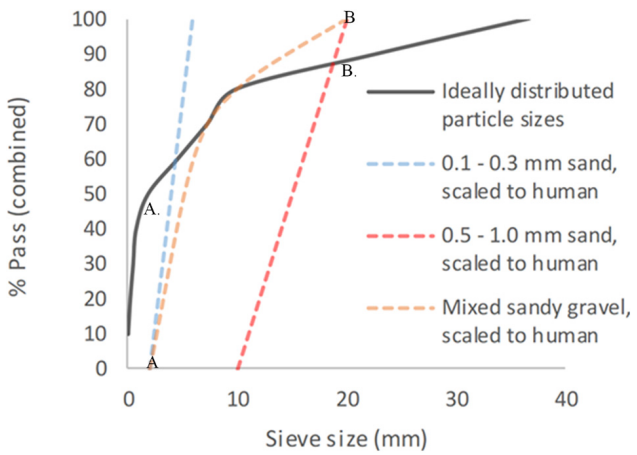

FIGURE 1 | Experimental sandy gravel sizes used, scaled to human values, shown alongside ideally distributed particle sizes. (A) = human median value. (B) = human 85th centile. (A) = lower limit of experimental sandy gravel range. (B) = upper limit of experimental sandy gravel range. % pass (combined) describes the percentage of total volume of sandy gravel passing a specific sieve size; sieve size (mm) relates to the diameter of each hole within the sieve.

Mice were secured in an upright posture on a steel mount of 10 mm diameter fixed within the target chamber, 50 mm distal to the gas-gun outlet. A single cable tie across the thorax was applied to secure the specimens in position on the mount, whilst leaving the lower limbs exposed and freely mobile (**Figure 2**). The right lower limb was centred in the midpoint of the path of the focused sand blast. Experiments were then repeated with re-positioning of the mount to target the contralateral limb.

The speed of the sandy gravel particles at the point of impact with the specimen was estimated using high-speed photography (Phantom VEO710L, AMETEK, United States) at 68,000-fps. An average velocity for the sand blast was determined based upon identifying and tracking four unique points evenly distributed across the sandy gravel. From this, the mean with standard deviation of the velocity of the sand blast as a whole was calculated.

A single control test was performed utilising the maximum gas-gun pressure used previously with the absence of any sandy gravel ejecta. This was performed in order to ascertain whether any injurious effects are caused by the pressurised air alone. This control test was performed on a single mouse specimen.

Prior to and following each test, mouse specimens underwent radiographic imaging using a mini C-arm (Fluoroscan® InSight™ FD system, United States) to identify any lower limb fractures. Following this, the specimens were reviewed to identify lower limb traumatic amputation. Where a lower limb open fracture was present with extensive soft tissue loss, the injury was classified as a traumatic amputation.

Statistical Analysis and Development of the Risk Function

The NCSS statistical software was used for statistical analysis (version 12, UT, United States). A likelihood-criteria best-fit analysis, with the aid of probability plots, was performed to choose the distribution that best fit the data for each injury type. The Weibull distribution was shown to be the best fit in the majority of cases; hence, it was chosen as the probability distribution to represent the risk for all injury types observed in this study. Weibull survival analysis was used to examine the association between sandy gravel velocity and traumatic amputation. The Weibull regression model is $P(v) = 1 - e^{-(v/\lambda)^{\kappa}}$, where P is the probability of injury, v (the average velocity of the sandy gravel) is the predictor variable, and λ and κ are the corresponding coefficients associated with the predictor variable. To derive the injury-risk curves, data were classified as left censored where injury was present and right censored where there was no injury. A *post hoc* two-sample Kolmogorov-Smirnov test was performed to assess

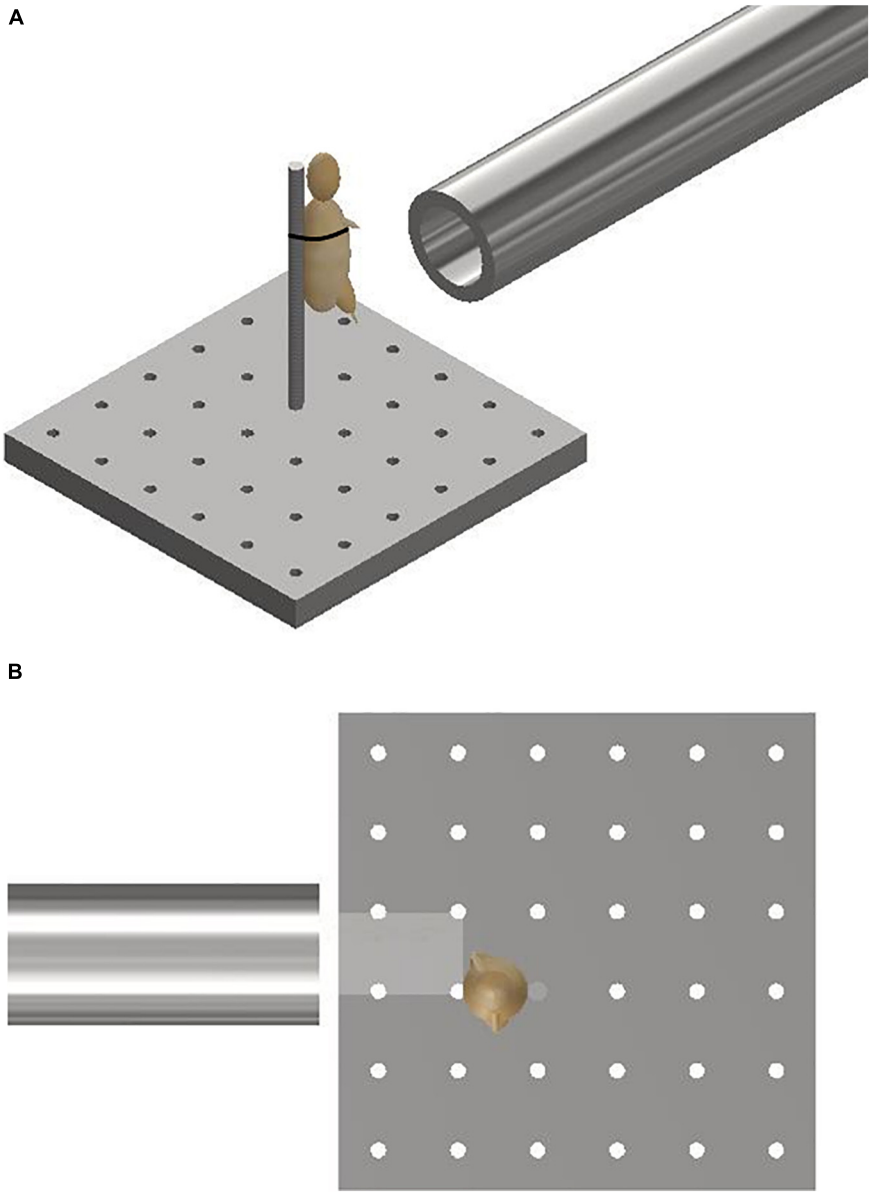

FIGURE 2 | (A) Schematic illustrating the experimental setup showing the gas-gun outlet with mounting platform and mouse. The mouse represented with a model. **(B)** Aerial view of schematic illustrating initial sandy gravel stream passing through distal outlet to impact with offset lower limb of mouse. The mouse is represented with a model.

for significant differences between the distribution of injury-risk curves across groups. A Bonferroni corrected α value of 0.0083 was used to compensate for multiple comparisons (0.0083 = 0.05/6).

RESULTS

Fifty-nine cadaveric mice were used across experiments, comprising of a total of 117 lower limbs impacted by high-velocity sandy gravel soil, and one lower limb control specimen. No injuries were seen in the control specimen. A gas-gun system was used to accelerate the sandy gravel; the average sand blast velocity at the exit of the gun's barrel ranged from 20 ± 5 to 136 ± 5 m/s. A radiograph showing a mouse which sustained a traumatic amputation due to high velocity sand blast is shown in **Figure 3**. **Supplementary Material Video 1** shows a 68,000 frames per second (fps) recorded video with an aerial viewpoint, played at 30 fps, capturing sandy gravel soil travelling at 64 m/s as it impacts a specimen. **Supplementary Material Video 2** shows a 68,000-fps recorded video with a side-on viewpoint, played at 30 fps, capturing sandy gravel impact at 130 m/s. Images from **Supplementary Material Video 2**, showing the sequential stages of sand blast impact, can be seen in **Figure 4**.

FIGURE 3 | Radiograph of mouse injured with high velocity sand blast, sustaining a right sided lower limb traumatic amputation.

Images showing exemplar injuries sustained are shown in **Figure 5**. These images show increasing severity of injury: initial skin lacerations and superficial wounding only (A), skin and underlying soft tissue injury (B), associated open fracture with extensive tissue loss (C), and complete limb avulsion (D).

Risk of traumatic amputation increased with increasing sand blast velocity across all groups. The 50% risk of traumatic amputation ranged from 70 m/s (95% CI 63–77 m/s) in the 0.1–0.3 mm wet sandy gravel group to 77 m/s (95% CI 69–86 m/s) in the 0.5–1.0 mm dry sandy gravel group. No significant differences between the distribution of injury-risk curves for sandy gravel soil groups were seen, including across size ranges and moisture content (**Table 1**). Full injury risk curves with 95% CIs are shown in **Figure 6**, with the 25, 50, and 75% risks of injury presented in **Table 2**.

DISCUSSION

The first aim of this study was to reproduce isolated traumatic amputation due to sand blast in a cadaveric mouse model, utilising a gas-gun system. We showed that high velocity sand blast is an independent mechanism of injury causing traumatic amputation, with extensive soft tissue and skeletal disruption seen at high velocities. The injury curves presented (**Figure 4**) show a clear link between increasing sandy gravel velocity and likelihood of injury. For example, ideally distributed dry sandy gravel showed a 25, 50, and 75% risk of traumatic amputation at sand blast velocities of 62, 71, and 79 m/s, respectively.

We have previously demonstrated traumatic amputation in conjunction with pelvic fractures, perineal injury and open abdominal trauma, due to impact with a widely dispersed cloud of high velocity sandy gravel, from an under-body blast position (Rankin et al., 2020a). High velocity sand blast was implicated in the mechanism of injury for traumatic amputation, however, from the injury outcome data alone a characterisation of the process was not possible. In the present study, we have utilised a focused sand blast to impact the lower limb in isolation. This has allowed us to characterise the pattern and development of injury and provide a detailed account of the underlying mechanism of injury. Based on these findings, we describe in detail and characterise the process of traumatic amputation due to high velocity sand blast: an initial bolus of compressed sandy gravel soil is propagated at high velocity toward the

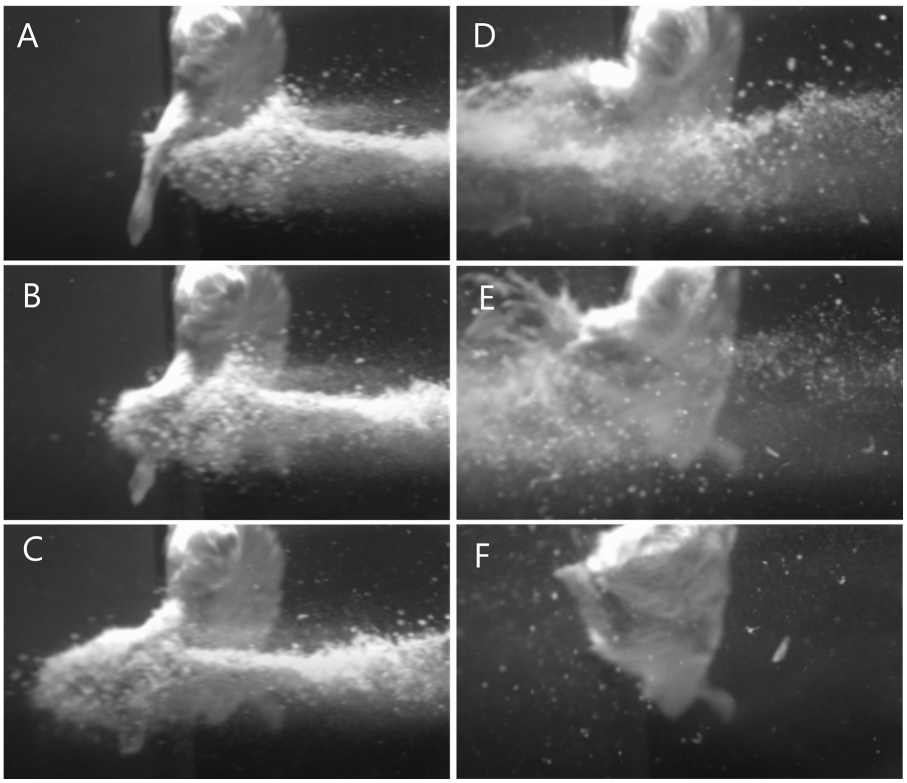

FIGURE 4 | Images illustrating the stages of traumatic amputation secondary to high velocity sand blast. **(A)** Immediately pre-impact. **(B)** Point of initial impact. The sandy gravel has begun to move through and around the tissues of the lower limb at high velocity. Due to the experimental setup the foot has evaded the trajectory of the sandy gravel, whilst the limb above has begun to fragment and displace relative to the foot below. **(C)** The foot has been pulled upward into the trajectory of the sandy gravel, whilst the skeletal and soft tissue above are now significantly fragmented and displaced. **(D)** The lower limb has now been entirely shattered and displaced, with soft tissue stripping on the periphery of the blast now evident as the muscle is seen moving outwards. **(E)** As the sand blast dissipates, the remaining surrounding soft tissues can be seen more clearly to be stripped and displaced. **(F)** Completed traumatic amputation. (A schematic to provide context of the animal's position and orientation is provided in **Figures 2A,B**).

casualty (**Figure 4A**). The initial impact results in superficial burst lacerations and tears to the skin of impacted limbs (**Figure 5A**). As the soil continues to propagate (**Figure 4B**), it progresses to infiltrate deep to the skin, spreading out both within and through tissue planes; this occurs through a series of multiple microtraumas to the underlying fascia and muscular tissue, where the sand blast damages and displaces these soft tissues (**Figure 5B**). With sufficient velocity, the soil progresses to cause a series of microfractures to the underlying skeletal structures which compound to cause segmented or multifragmentary fractures to the long bones of the lower limb; the ongoing impact of soil to the soft tissues of the limb has at this stage resulted in extensive soft tissue loss in association with long bone fractures (**Figure 5C**). The skeletal and soft tissue are now seen to be fragmented and displaced (**Figure 4C**). A critical injury point is reached, whereby the underlying integrity of both skeletal and soft tissues of the limb has been compromised (**Figure 4D**). These tissues progress to be avulsed, whilst tissues in the periphery are injured and propagated outward from the point of maximal impact (**Figure 4E**). At this stage, a completed traumatic amputation of the limb has occurred (**Figures 4F**, **5D**).

Multiple mechanisms of injury for blast-related traumatic amputation have been described. The initial accepted mechanism of injury was hypothesised to be due to the initial blast shock front causing a diaphyseal fracture of the limb, with the subsequent blast wind separating and amputating the limb at the point of fracture. This theory was based on laboratory work with a goat hind limb model, which showed that a diaphyseal fracture occurred when a long bone was impacted with a shock front but shielded from the subsequent blast wind or any associated secondary blast injury (Hull and Cooper, 1996). Of note, diaphyseal fracture occurred at distances of 0.5 m proximity to the explosive, but not at 1 m, suggesting the requirement for the casualty to be in close proximity to the explosive for this mechanism of injury to occur (Hull and Cooper, 1996). Further underpinning this mechanism was the clinical association at the time of traumatic amputation to fatal traumatic blast-lung injury, and a lack of through-joint traumatic amputations (Mellor and Cooper, 1989; Hull et al., 1994). More recent military data have questioned this theory. Data from the recent conflicts in Iraq and Afghanistan showed no link between traumatic amputation and primary blast-lung injury, with a high proportion of amputees surviving their injuries;

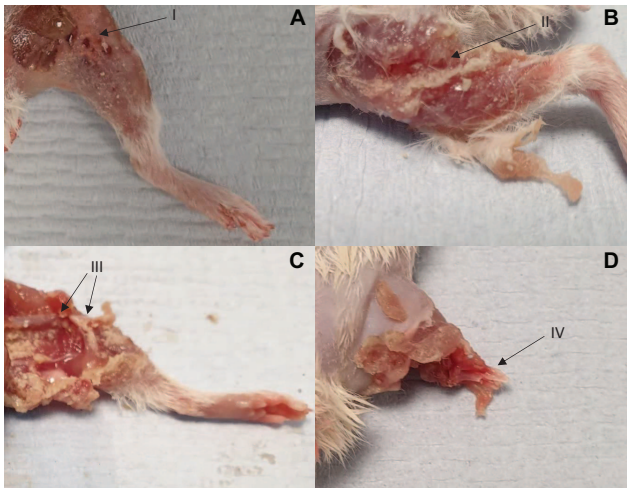

FIGURE 5 | Four separate injuries of worsening severity sustained following impact with high velocity sand blast. **(A)** Burst lacerations and skin tears seen at I. **(B)** Involvement of the underlying subcutaneous and muscular layers, with muscle tears and stripping seen at II. **(C)** Associated open segmental femoral fracture seen at III, with extensive surrounding soft tissue damage and loss. **(D)** Complete limb avulsion with traumatic amputation seen at IV.

TABLE 1 | Two sample Kolmogorov-Smirnov test to assess for significant differences between the distribution of injury risk curves.

	0.1–0.3 dry	0.5–1.0 dry	Mix dry	0.1–0.3 wet	0.5–1.0 wet
0.1–0.3 dry					
0.5–1.0 dry	0.591				
Mix dry	1.000	0.358			
0.1–0.3 wet	0.841	0.095	0.841		
0.5–1.0 wet	0.591	0.841	0.358	0.194	
Mix wet	0.591	0.841	0.358	1.000	0.194

P values shown.

furthermore, a substantially higher incidence of through-joint traumatic amputation was seen, again questioning the shockwave mediated diaphyseal fracture mechanism of injury (Singleton et al., 2014). In that study, we hypothesised that the blast wind played a far more substantial role in the mechanism of injury for traumatic amputation and could itself be a mechanism of injury independent of other factors (Singleton et al., 2014).

Our previous work investigating pelvic fracture and vascular injury due to a shock-tube mediated blast wave (consisting of both a shock front and subsequent blast wind) using a cadaveric mouse model, showed traumatic amputation rates following blast far lower than what would be expected to be present in association with the pelvic fractures and vascular injury seen, as compared to battlefield data (Rankin et al., 2019, 2020b). We subsequently showed that when an initial injuring force to the lower limb occurred prior to impact with the blast wind, traumatic amputation occurred. We concluded that the lower-than-expected traumatic amputation rates were likely due to the absence of any secondary blast injury from the experimental model, to cause this initial injury (Rankin et al., 2019). The current study has shown that high velocity sand blast (a secondary blast-injury mechanism) can be in and of itself, an independent mechanism of injury causing traumatic amputation. Both shock tube and gas-gun experimental models are surrogates of the blast environment. Both platforms provide parts of the blast injury in isolation: a shock-tube system allows focused study of the shock front and blast wind (primary and tertiary blast injury) whilst the gas-gun system allows focused study of energised environmental debris (secondary blast injury). Both platforms have produced traumatic amputation, of varying incidence rates, in a cadaveric animal model. In a blast environment, all of these mechanisms (the primary shock front, the secondary energised environmental debris, and the tertiary blast wind causing bodily displacement) occur together. As such, whilst each is possible of causing traumatic amputation in isolation, the reality likely is that traumatic amputation is caused by all three of these described mechanisms synergistically, to varying degrees of each, dependent upon the blast conditions. These mechanisms acting synergistically are thought to be the causative factors for both military and civilian blast-mediated traumatic amputation, where in the civilian setting the sand blast effect is replaced by explosive fragmentation and any surrounding environmental debris. Whilst other authors have linked energised environmental debris following blast to infection and delayed amputation, we are the first to implicate it as a causative mechanism of injury for traumatic amputation, either independently or in association with the shock front and blast wind (Khatod et al., 2003; Covey and Ficke, 2016; Rankin et al., 2020a).

The second aim of the study was to ascertain differences to the risk of injury from different loading conditions of the energised environmental debris, with reference to size and moisture content. No significant differences were seen across groups when comparing sandy gravel size (ideally distributed, small, large), moisture content (dry or saturated with water), or both. Whilst a type II error of non-significance is possible, the *P* values obtained were far from reaching significance, with values ranging from 0.194 to 1.0. As such, the data leads us to accept the null hypothesis that neither sandy gravel size nor moisture content increase the risk of traumatic amputation as occurs following high velocity sand blast in this model. Of note, the mass of sandy gravel was standardised across all experiments, irrespective of sandy gravel size. As such, it could be concluded that failure to reject the null hypothesis highlights that the total mass and dissipation of energy is the determinant factor in causing injury, as opposed to the individual size of any one piece of environmental debris.

In the present study, the 50% risk of traumatic amputation ranged from 70 m/s (95% CI 63–77 m/s) in the 0.1–0.3 mm wet sandy gravel group to 77 m/s (95% CI 69–86 m/s) in the 0.5–1.0 mm dry sandy gravel group. This compares to our previous work which showed the 50% risk of traumatic amputation in the mouse model to occur, following impact with a widely dispersed high velocity sand blast cloud, at 247 m/s (95% CI: 222–274 m/s). The same gas-gun system and standardised mass of sandy gravel was used in both experiments. In our previous work, the sandy gravel ejecta was widely dispersed to encompass a whole-body

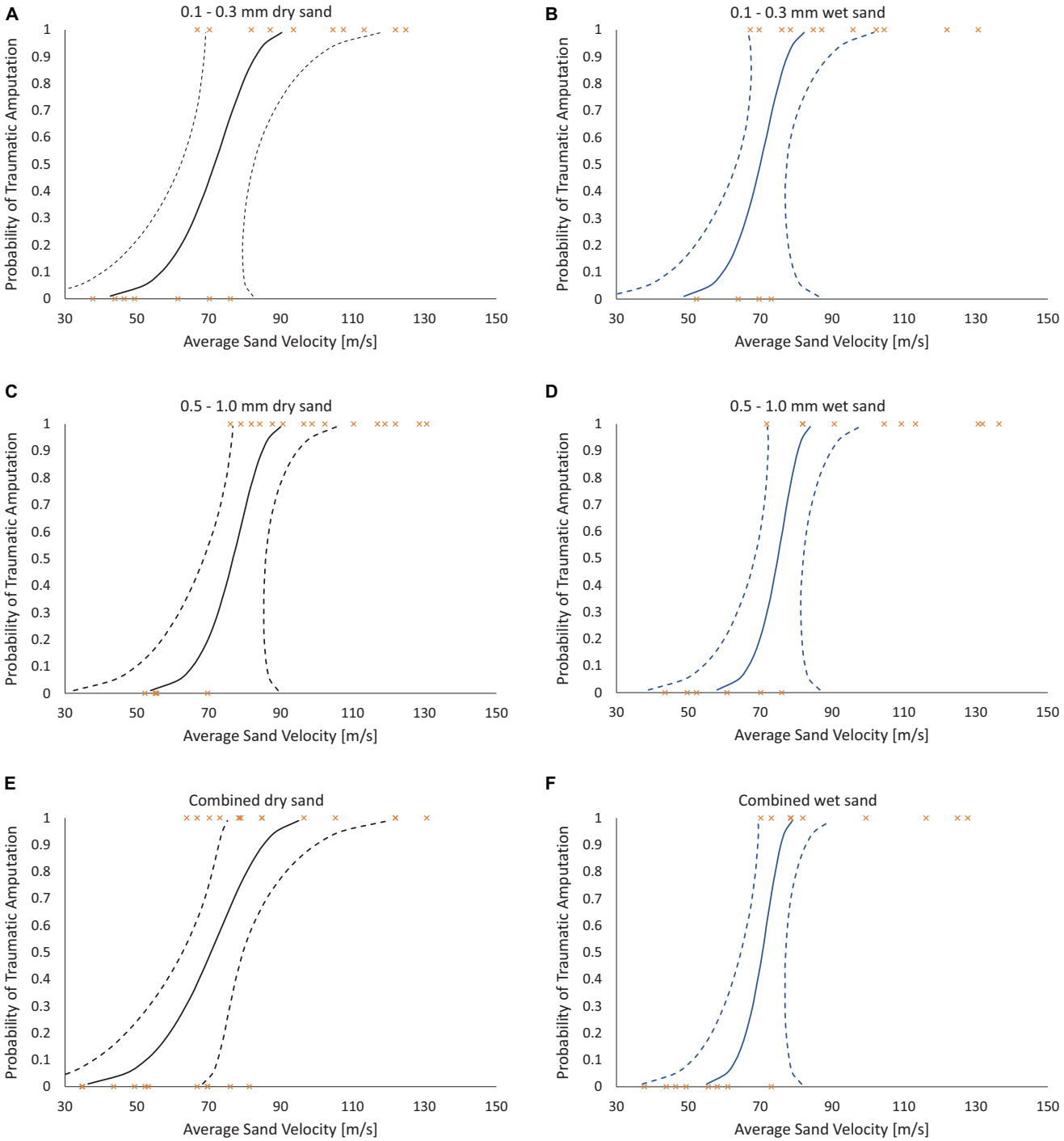

FIGURE 6 | Traumatic amputation (as per **Figures 5C,D**) risk curves as a function of average sandy gravel velocity. **(A)** 0.1–0.3 mm dry sandy gravel. **(B)** 0.1–0.3 mm wet sandy gravel. **(C)** 0.5–1.0 mm dry sandy gravel. **(D)** 0.5–0.1 mm wet sandy gravel. **(E)** Combined (ideally distributed) dry sandy gravel. **(F)** Combined (ideally distributed) wet sandy gravel. 95% CI represented with dashed lines.

field of impact, as occurs following blast, to best recreate the boundary conditions of a blast scenario. As the present work focused on traumatic amputation in isolation, a proportionately greater mass of sandy gravel impacted with the lower limb of the specimen. As such, a greater amount of kinetic energy is expected to be imparted upon the lower limb, where kinetic energy is equal to half of an object's mass multiplied by the velocity squared. It is therefore not unexpected that traumatic amputation was

TABLE 2 | The velocities (m/s) at 25, 50, and 75% risk of injury (V_{25}, V_{50}, and V_{75}, respectively) for traumatic amputation across all group.

	V_{25} (95% CI) m/s	V_{50} (95% CI) m/s	V_{75} (95% CI) m/s
0.1–0.3 mm, dry	64 (52–80)	72 (63–83)	78 (67–90)
0.5–1.0 mm, dry	71 (60–85)	77 (69–86)	81 (74–89)
Ideally distributed, dry	62 (50–75)	71 (63–80)	79 (70–89)
0.1–0.3 mm, wet	65 (55–77)	70 (63–77)	74 (67–82)
0.5–1.0, wet	71 (62–81)	75 (68–82)	78 (72–85)
Ideally distributed, wet	67 (58–77)	71 (65–77)	74 (68–79)

95% confidence intervals (CI) in parenthesis.

seen to occur at a lower velocity than our previous work, nor that any difference in injury risk curve distribution across groups was seen, where the sandy gravel mass across these experiments was standardised.

The current study used a focused sand blast impacting specimens from the front. This experimental setup was utilised as it most accurately allowed for traumatic amputation secondary to high velocity sand blast to occur in a reproducible manner and allowed for accurate characterisation of the injury process. It is more likely in the combat environment, however, that sand blast is encountered below the casualty and that the sand blast projectiles scatter outwards, rather than to focus on a specific target (the lower extremity as in this study). As such, the velocity values obtained from our previous work, utilising an under-body dispersing blast wave, are thought to more accurately represent the velocities required to cause traumatic amputation secondary to high velocity sand blast.

A limitation of the present study is that it was not possible to alter the standardised mass of sandy gravel, due to the experimental setup and customised sabots used in the delivery of the sand. Future work could address this limitation with further customised sabots, of differing sizes and geometry, to accommodate varying sand masses.

Whilst the current study's findings have shown sand blast to be a mechanism of injury for traumatic amputation, scaled animal models cannot be expected to be exact replicates of what occurs in humans (Bowen et al., 1968; Bowyer, 1996; Panzer et al., 2014). Irrespective of scaling, however, this study has shown that sand blast causes significant and progressively worsening injury at high and increasing velocities, resulting in extensive soft tissue and skeletal disruption in the mouse model, and a similar effect therefore should be expected in the human. Future work reproducing high velocity sand blast could utilise human cadaveric tissue, with a focus on protective equipment which may mitigate this mechanism of injury.

This work has now allowed us to describe in detail the complete injury mechanism of traumatic amputation. Following the energy imparted by the initial shock wave (which itself may cause skeletal trauma, if the casualty is sufficiently close to the explosive), energised projectiles (sand blast; or fragmentation and other environmental debris in an urban setting) are propagated at high velocity toward the casualty. This causes initial lacerations to the skin followed by continued progression through tissue planes, as a series of microtraumas to the underlying fascia and muscular tissue occurs. With sufficient velocity the energised projectiles cause multiple fractures to the underlying skeletal structures, which compound to cause segmental and multifragmental fractures to the long bones of the limb. A critical injury point is reached, whereby the underlying integrity of both skeletal and soft tissues of the limb has been compromised. The blast wind that follows these energised projectiles completes the amputation at the level of the disruption, and traumatic amputation occurs. In cases of through-joint amputations, the energised projectiles and subsequent blast wind results in failure of the supportive soft tissues (including the ligamentous structures, but with integrity of the skeletal structures intact) to result in limb avulsion and through-joint amputation.

DATA AVAILABILITY STATEMENT

The original contributions presented in the study are included in the article/**Supplementary Material**, further inquiries can be directed to the corresponding author.

ETHICS STATEMENT

Ethical review and approval was not required for the animal study because cadaveric mice were purchased as a by-product from Charles River UK. Male ex-breeder mice that had been already euthanized as per CRUK standard operating protocol, killed with a Schedule 1 procedure (CO2 asphyxiation), were subsequently used in the tests of this manuscript. These mice were accounted for under Charles River UK's Return of Procedures Animal Use Data to the UK Home Office. As such, all animal by-product material and its use are in compliance with the UK Animal (Scientific Procedures) Act 1986.

AUTHOR CONTRIBUTIONS

IR, SM, and JC were involved in the conception of the study. IR and T-TN were involved in the preparation of tests, data acquisition, and in conducting the tests. IR, T-TN, and LM were involved in the data analysis. IR drafted the manuscript. All authors revised it and involved in the interpretation of the data.

ACKNOWLEDGMENTS

This study was conducted in the Royal British Legion Centre for Blast Injury Studies. We would like to thank the Royal British Legion for their ongoing funding and support.

SUPPLEMENTARY MATERIAL

The Supplementary Material for this article can be found online at: https://www.frontiersin.org/articles/10.3389/fbioe.2021.665248/full#supplementary-material

REFERENCES

Azocar, A. F., Mooney, L. M., Duval, J. F., Simon, A. M., Hargrove, L. J., and Rouse, E. J. (2020). Design and clinical implementation of an open-source bionic leg. *Nat. Biomed. Eng.* 4, 941–953. doi: 10.1038/s41551-020-00619-3

Bowen, I., Fletcher, E., and Richmond, D. (1968). *Estimate of man's tolerance to the direct effects of air blast. TIechniCal Progress Report,. DASA-2113*. Washington, DC: Defense Atomic Support Agency.

Bowyer, G. W. (1996). Management of small fragment wounds: experience from the Afghan border. *J. Trauma Inj. Infect. Crit. Care* 40(Suppl. 3), S170–S172. doi: 10.1097/00005373-199603001-00037

Clasper, J., and Ramasamy, A. (2013). Traumatic amputations. *Br. J. Pain* 7, 67–73. doi: 10.1177/2049463713487324

Covey, D. C., and Ficke, J. (2016). "Blast and fragment injuries of the musculoskeletal system," in *Orthopedics in Disasters*, eds N. Wolfson, A. Lerner, and L. Roshal (Heidelberg: Springer), 269–280.

Edwards, D. S., McMenemy, L., Stapley, S. A., Patel, H. D. L., and Clasper, J. C. (2016). 40 years of terrorist bombings–a meta-analysis of the casualty and injury profile. *Injury* 47, 646–652. doi: 10.1016/j.injury.2015.12.021

Grujicic, M., Pandurangan, B., Qiao, R., Cheeseman, B. A., Roy, W. N., Skaggs, R. R., et al. (2008). Parameterization of the porous-material model for sand with different levels of water saturation. *Soil Dyn. Earthq. Eng.* 28, 20–35. doi: 10.1016/j.soildyn.2007.05.001

Hull, J. B., and Cooper, G. J. (1996). Pattern and mechanism of traumatic amputation by explosive blast. *J. Trauma* 40, S198–S205.

Hull, J. B., Bowyer, G. W., Cooper, G. J., and Crane, J. (1994). Pattern of injury in those dying from traumatic amputation caused by bomb blast. *Br. J. Surg.* 81, 1132–1135.

Khatod, M., Botte, M. J., Hoyt, D. B., Meyer, R. S., Smith, J. M., and Akeson, W. H. (2003). Outcomes in open tibia fractures: Relationship between delay in treatment and infection. *J. Trauma* 55, 949–954. doi: 10.1097/01.TA.0000092685.80435.63

King, D. R., Larentzakis, A., and Ramly, E. P. (2015). Tourniquet use at the Boston Marathon bombing. *J. Trauma Acute Care Surg.* 78, 594–599. doi: 10.1097/TA.0000000000000561

Kishbaugh, D., Dillingham, T. R., Howard, R. S., Sinnott, M. W., and Belandres, P. V. (1995). Amputee soldiers and their return to active duty. *Mil. Med.* 160, 82–84. doi: 10.1093/milmed/160.2.82

Mellor, S. G., and Cooper, G. J. (1989). Analysis of 828 servicemen killed or injured by explosion in Northern Ireland 1970–84: the hostile action casualty system. *Br. J. Surg.* 76, 1006–1010. doi: 10.1002/bjs.1800761006

Nato/PfP Unclassified. (2006). Procedures for Evaluating the Protection Level of Logistic and Light Armoured Vehicles Volume 2 For Mine Threat. AEP-55 2, Annex C. NATO/PfP Unclassified, Brussels.

Nguyen, T. T. N., Tear, G. R., Masouros, S. D., and Proud, W. G. (2018). Fragment penetrating injury to long bones. *AIP Conf. Proc.* 1979, 90011–90011. doi: 10.1063/1.5044868

Panzer, M. B., Wood, G. W., and Bass, C. R. (2014). Scaling in neurotrauma: how do we apply animal experiments to people? *Exp. Neurol.* 261, 120–126. doi: 10.1016/j.expneurol.2014.07.002

Ramasamy, A., Hill, A. M., and Clasper, J. C. (2009a). Improvised explosive devices: pathophysiology, injury profiles and current medical management. *J. R. Army Med. Corps* 155, 265–272. doi: 10.1136/jramc-155-04-05

Ramasamy, A., Hill, A. M., Hepper, A. E., Bull, A. M., and Clasper, J. C. (2009b). Blast mines: physics, injury mechanisms and vehicle protection. *J. R. Army Med. Corps* 155, 258–264. doi: 10.1136/jramc-155-04-06

Rankin, I. A., Nguyen, T. T., Carpanen, D., Clasper, J. C., and Masouros, S. D. (2019). Restricting lower limb flail is key to preventing fatal pelvic blast injury. *Ann. Biomed. Eng.* 47, 2232–2240. doi: 10.1007/s10439-019-02296-z

Rankin, I. A., Nguyen, T.-T., Carpanen, D., Clasper, J. C., and Masouros, S. D. (2020a). A new understanding of the mechanism of injury to the pelvis and lower limbs in blast. *Front. Bioeng. Biotechnol.* 8:960. doi: 10.3389/fbioe.2020.00960

Rankin, I. A., Webster, C. E., Gibb, I., Clasper, J. C., and Masouros, S. D. (2020b). Pelvic injury patterns in blast. *J. Trauma Acute Care Surg.* 88, 832–838. doi: 10.1097/ta.0000000000002659

Singleton, J. A. G., Gibb, I. E., Bull, A. M. J., and Clasper, J. C. (2014). Blast-mediated traumatic amputation: evidence for a revised, multiple injury mechanism theory. *J. R. Army Med. Corps* 160, 175–179. doi: 10.1136/jramc-2013-000217

Sinha, R., Van Den Heuvel, W. J. A., and Arokiasamy, P. (2011). Factors affecting quality of life in lower limb amputees. *Prosthet. Orthot. Int.* 35, 90–96. doi: 10.1177/0309364610397087

Tremblay, J., Bergeron, D., and Gonzalez, R. (1998). "KTA1-29: protection of soft-skinned vehicle occupants from landmine effects," in *Val-Belair, Canada, Defence Research Establishment*, ed. T. T. C. P. Program (Quebec: Valcartier).

Webster, C. E., Clasper, J., Stinner, D. J., Eliahoo, J., and Masouros, S. D. (2018). Characterization of lower extremity blast injury. *Mil. Med.* 183, e448–e453. doi: 10.1093/milmed/usx126

White, R., and Churchill, E. (1971). *The Body Size of Soldiers U.S. Army Anhropometry. Report Number 72-51-CE (CPLSEL-94)*. Natick, MA: U.S. Army Natick Laboratories.

Conflict of Interest: The authors declare that the research was conducted in the absence of any commercial or financial relationships that could be construed as a potential conflict of interest.

frontiers in Bioengineering and Biotechnology

REVIEW
published: 14 September 2021
doi: 10.3389/fbioe.2021.732753

The Role of Cutaneous Microcirculatory Responses in Tissue Injury, Inflammation and Repair at the Foot in Diabetes

*Gayathri Victoria Balasubramanian, Nachiappan Chockalingam and Roozbeh Naemi**

Centre for Biomechanics and Rehabilitation Technologies, Staffordshire University, Stoke-on-Trent, United Kingdom

Diabetic foot syndrome is one of the most costly complications of diabetes. Damage to the soft tissue structure is one of the primary causes of diabetic foot ulcers and most of the current literature focuses on factors such as neuropathy and excessive load. Although the role of blood supply has been reported in the context of macro-circulation, soft tissue damage and its healing in the context of skin microcirculation have not been adequately investigated. Previous research suggested that certain microcirculatory responses protect the skin and their impairment may contribute to increased risk for occlusive and ischemic injuries to the foot. The purpose of this narrative review was to explore and establish the possible link between impairment in skin perfusion and the chain of events that leads to ulceration, considering the interaction with other more established ulceration factors. This review highlights some of the key skin microcirculatory functions in response to various stimuli. The microcirculatory responses observed in the form of altered skin blood flow are divided into three categories based on the type of stimuli including occlusion, pressure and temperature. Studies on the three categories were reviewed including: the microcirculatory response to occlusive ischemia or Post-Occlusive Reactive Hyperaemia (PORH); the microcirculatory response to locally applied pressure such as Pressure-Induced Vasodilation (PIV); and the interplay between microcirculation and skin temperature and the microcirculatory responses to thermal stimuli such as reduced/increased blood flow due to cooling/heating. This review highlights how microcirculatory responses protect the skin and the plantar soft tissues and their plausible dysfunction in people with diabetes. Whilst discussing the link between impairment in skin perfusion as a result of altered microcirculatory response, the review describes the chain of events that leads to ulceration. A thorough understanding of the microcirculatory function and its impaired reactive mechanisms is provided, which allows an understanding of the interaction between functional disturbances of microcirculation and other more established factors for foot ulceration.

Keywords: diabetic foot, foot ulcer, microvessels, post-occlusive reactive hyperaemia, pressure-induced vasodilation, LDI flare, plantar soft tissues

Abbreviations: PORH, Post-Occlusive reactive hyperaemia; PIV, Pressure-Induced Vasodilation; LDI, Laser Doppler Imager; GDP, Gross Domestic Product.

OPEN ACCESS

Edited by:
Matthew J. Major, Northwestern University, United States

Reviewed by:
Chi-Wen Lung, Asia University, Taiwan
Fu-Lien Wu, University of Illinois at Urbana-Champaign, United States

****Correspondence:***
Roozbeh Naemi
r.naemi@staffs.ac.uk

Specialty section:
This article was submitted to Biomechanics, a section of the journal Frontiers in Bioengineering and Biotechnology

Received: *29 June 2021*
Accepted: *26 August 2021*
Published: *14 September 2021*

Citation:
Balasubramanian GV, Chockalingam N and Naemi R (2021) The Role of Cutaneous Microcirculatory Responses in Tissue Injury, Inflammation and Repair at the Foot in Diabetes. Front. Bioeng. Biotechnol. 9:732753. doi: 10.3389/fbioe.2021.732753

DIABETES IS A GLOBAL HEALTH ISSUE

Diabetes is a common condition which has a considerable impact on the health and economy of nations around the world. There is an annual upsurge in the number of patients being diagnosed with diabetes. The International Diabetes Federation estimates that total global health-care spending on diabetes more than tripled over the period 2003 to 2013 (World Health Organization, 2016). The estimated direct annual cost of diabetes to the world is more than US$ 827 billion and the projected losses in gross domestic product (GDP) for the period 2011 to 2030 is a total of US$ 1.7 trillion worldwide incurred by both the direct and indirect costs (World Health Organization, 2016). This indicates that diabetes imposes a large economic burden on the global health-care system and the wider global economy. As diabetes is a chronic condition, many complications arise as the disease progresses.

DIABETES COMPLICATIONS AND THE ROLE OF MICROCIRCULATION

Microcirculation is vital for the efficient exchange of gases and nutrients and the removal of the waste products of metabolism. In addition, the cutaneous microcirculation plays an important role in thermoregulation (Flynn and Tooke, 1992). Some of the common complications of diabetes are retinopathy, neuropathy, nephropathy, peripheral vascular diseases, and diabetic foot syndrome. One of the important aspects that resonate with all these complications is microcirculation. Endothelial damage and dysfunction of the microvasculature have been observed in various parts of the body such as the eyes, kidneys and the foot in people with diabetes (Goldenberg et al., 1959; Flynn and Tooke, 1992; Hile and Veves, 2003; Williams et al., 2004; Boulton et al., 2006; Schramm et al., 2006; Körei et al., 2016). Both structural and functional microvascular disturbances (known as microangiopathy or disease to small blood vessels) are commonly observed in people with diabetes as a result of glycation related changes that occur due to the prolonged hyperglycaemic state (Boulton et al., 2006; Singh et al., 2014; Stirban et al., 2014). Besides, glycation related direct changes in the microvessels, both sensory and autonomic neuropathies contribute to the functional changes of the microvasculature (Schramm et al., 2006). As early as in 1983 Parving et al. introduced the "haemodynamic theory" to explain microangiopathy in diabetes (Flynn and Tooke, 1992; Veves et al., 2006; Chao and Cheing, 2009). The theory proposes that the increased microvascular blood flow triggers endothelial injury response, followed by microvascular sclerosis (Flynn and Tooke, 1992; Veves et al., 2006). This, in turn, may lead to functional abnormalities such as impaired maximum hyperaemic response, reduced tissue response to injury or trauma, autoregulation of blood flow and changes to vascular tone (Flynn and Tooke, 1992; Boulton et al., 2006; Veves et al., 2006).

DIABETIC FOOT DISEASE AS A SIGNIFICANT COMPLICATION AND THE ROLE OF MICROCIRCULATION

In the foot, the adverse complications of diabetes are ulceration and amputation. The annual population-based incidence of diabetic foot ulcers is estimated to be 1.9–2.2% (Levin et al., 2008). Once the skin on the foot is ulcerated, it is susceptible to infections leading to an urgent medical problem (Bakker et al., 2016). It is estimated that only two-thirds of diabetic foot ulcers will eventually heal, but approximately 28% may result in some form of lower extremity amputation (Bakker et al., 2016). Hence, understanding the risks associated with foot ulcer development and its course is crucial. While the role of peripheral vascular disease and neuropathy resulting in diabetic foot ulcers is well-established, more research is needed to understand the contribution of microcirculation (Schaper et al., 2016).

The role of microcirculation in diabetic foot ulcers is a continuing area of research, where there are many theories put forth by several studies on microcirculation and the concept of "small vessel disease" was proposed (Goldenberg et al., 1959). Although this theory of an exclusive microvascular disease is widely debated, historical evidence for structural and functional microcirculation and related disturbances exist (Boulton et al., 2006). Also, studies have shown that capillary pressure is increased in the foot of people with diabetes due to arteriovenous shunting caused by sympathetic denervation (Deanfield et al., 1980; Flynn and Tooke, 1992; Boulton, 2000; Korzon-Burakowska & Edmonds, 2006). Collectively, these studies outline a critical role for microcirculation in ulceration.

With respect to diabetic foot ulcers, it is proposed that the impaired microcirculatory response may induce microcirculatory failure, resulting in tissue necrosis and ulceration (Flynn and Tooke, 1992; Korzon-Burakowska & Edmonds, 2006). Although microvascular disease may not be the single cause of pathogenesis of diabetic foot ulcers, the co-existence of abnormal microcirculatory function with both peripheral arterial disease and neuropathy may be associated with tissue damage (Flynn and Tooke, 1990; Boulton et al., 2006). This is supported by the evidence from studies that demonstrate the role of microcirculation in the development of ulceration, gangrene, necrosis and wound healing (Flynn and Tooke, 1992; Boulton et al., 2006; Levin et al., 2008; Lanting et al., 2017). Therefore, understanding functional abnormalities is of importance when studying diabetic foot ulcers.

INJURY, INFLAMMATION AND SOFT-TISSUES

To gain a better understanding of microcirculatory function and recognise appropriate methods to evaluate it, it is important to look at the bigger picture of the body's defence, injury, inflammation and repair mechanisms. In the host defence mechanism, both lymphatic and blood vessels play an important role in an inflammatory response (Granger and Rodrigues, 2016; Parnham, 2016). Changes in the

inflammatory mediators are known to correlate with the risk of developing a diabetic foot ulcer and inflammation is one of the earliest signs of ulcer (Lanys et al., 2021). Inflammation is a microcirculation-dependent tissue response to extrinsic and intrinsic stimuli (Granger and Rodrigues, 2016). During such an inflammatory response, the cardinal signs of inflammation that can be observed are heat (calor), pain (dolor), redness (rubor), and swelling (tumor), which may eventually lead to the loss of tissue function. In general, microcirculation is highly reactive to inflammatory response and plays a pivotal role in it as all components of the microvasculature such as the arterioles, capillaries, and venules respond and work towards the delivery of inflammatory cells to the injured or infected tissue/site (Granger and Senchenkova, 2010). The microvasculature isolates the infected or injured region from the healthy tissue and the systemic circulation, to facilitate tissue repair and regeneration (Johnson, 1973; Granger and Senchenkova, 2010; Bentov and Reed, 2014). The inflammatory responses of microcirculation include impaired vasomotor function, reduced capillary perfusion, leukocytes and platelets adhesion, activation of the coagulation cascade, enhanced thrombosis, increased vascular permeability, and an increased proliferation rate of blood and lymphatic vessels (Granger and Senchenkova, 2010). Other common microcirculatory changes result in shunting and hypoxia (reduced oxygen capacity of the tissues) caused by endothelial cell injury induced by a severe form of infection like sepsis, stasis of red blood cells due to vascular resistance, increased distances in oxygen diffusion in case of oedema owing to capillary leak syndrome (Guven et al., 2020).

In the foot, defence mechanisms (stimulation–response) plays a vital role. The role of microcirculation in wound repair and healing is well-realised (Shapiro and Nouvong, 2011; Ambrózy et al., 2013). Evidence suggests that despite the reasons behind an ulcer incident, the microcirculatory role in the process of healing remains the same and that the subpapillary perfusion plays a major role in the formation of granulation tissue, which was studied through the use of Laser Doppler Flowmetry system in patients with venous ulcers (Ambrózy et al., 2013). Microvasculature aids with tissue perfusion, fluid homeostasis, cutaneous oxygen delivery and recruiting collateral vessels to facilitate healing process (Bentov and Reed, 2014). Transcutaneous Oxygen Pressure (TcPo2) technique allows the measurement of cutaneous oxygen supply, which is found to be reduced in type 2 diabetic patients with the foot at risk of ulceration (Zimny et al., 2001). This was related to an impaired neurogenic blood flow regulation, which may contribute to capillary hypertension, endothelial dysfunction leading to oedema and skin damage (Zimny et al., 2001). Other non-invasive methods such as the measurement of skin perfusion pressure allow to assess healing (wound is likely to heal if pressure is above 30 mmHg) and to determine amputation levels (Sarin et al., 1991; Shapiro and Nouvong, 2011). Newer technology such as Laser Speckle Perfusion Imaging allows visualising the blood in the microvaculatore in and around the ulcer area, which may indicate the ability to heal (Shapiro and Nouvong, 2011). However, this device images cutaneous circulation to a depth no greater than 1 mm (Shapiro and Nouvong, 2011). While recent research focuses on assessing microcirculation to predict ulcer outcomes, further studies are needed to gain a deeper understanding of the microcirculatory changes in the ulcers with respect to the stages of healing for better prediction of wound healing.

Although the responses of the inflammatory system are regarded as defence mechanisms (stimulation–response) it may also be considered as a homeostatic system that operates continually to maintain organ and organism function (Tracy, 2006). Based on the dual nature of inflammation, stimulation–response and homeostatic, research suggest the use of biomarkers such as C-reactive protein or interleukin-6 to assess the activity level of the inflammatory process (Tracy, 2006). These biomarkers may represent normal homeostatic function, a response to a pathological condition or to both, which can take place to varying degrees depending on the differences in the person, time and condition (Tracy, 2006). Whilst in younger, healthier people, the biomarkers may likely represent the ongoing homeostatic activity, with increasing age and in the presence of underlying pathology such as chronic inflammatory changes due to diabetes or triggered atherosclerotic changes in cardiovascular conditions, these biomarkers may indicate a stimulation–response type inflammation (Payne, 2006; Tracy, 2006; Pahwa et al., 2020). Overall, there is consensus that inflammation biomarkers are independent predictors of the future occurrence of chronic disease outcomes and events (Tracy, 2006). Similarly, physiological markers such as skin temperature, galvanic skin response and perfusion measurements that indicate homeostatic and stimulation-response in relation to microcirculation may be pertinent to predict the future occurrences of chronic disease outcomes or events such as ulcers.

ASSESSMENT OF MICROCIRCULATION

Diabetic foot ulcers are multifactorial and there are new and emerging technologies that enable the assessment of these factors to aid prevention and management. Some of the methods are various nerve function tests (quantitative sensory testing, vibration perception, galvanic skin response and sudomotor activity testing), temperature measurement (infrared thermography), biomechanical properties measurements (plantar pressure and ultrasound indentation tests/ elastography), macrovascular assessments (ankle-brachial index and toe brachial index) and microvascular assessments (TCPO2, laser doppler flowmetry, hyperspectral imaging and laser speckle contrast imager) and such (Pham et al., 2000; Naemi et al., 2017; Balasubramanian et al., 2020; Lung et al., 2020). However, in this review the main focus would be to discuss the assessment of microcirculation in tissue injury and inflammation to better understand its role in ulceration.

In the past, the key signs of inflammation were predominantly detected through mere observation. However, nowadays contactless and pain-free non-invasive techniques have facilitated objective assessment of inflammatory signs, tissue injury responses, repairs

and healing. Laser Doppler flowmetry (LDF) technique is one such non-invasive technique, which allows assessment of microvascular blood flow when reflection and scattering of the laser light occurs due to the movement of the red blood cells (Nakamoto et al., 2012; Balasubramanian et al., 2020). Although the depth the laser penetrates is relatively low (~1 mm), it is a useful device for the evaluation of cutaneous microcirculation. This device is gaining popularity in the field of research in diabetes, cerebrovascular conditions, Raynaud's phenomenon and others. The use of LDF is being explored in dentistry as well, especially for perioperative procedures to gain a better understanding of soft tissue diagnosis. Apart from LDF, other non-invasive methods used to evaluate microcirculation are Laser Speckle Contrast Imager (LSCI) and photo-plethysmography. At times, since small fibre nerve functions and thermal changes influence microcirculation, methods such as quantitative sensory testing, skin electrodermal activity assessment and thermography are also used in conjunction with microvascular testing.

SCOPE OF THIS REVIEW

This narrative review of literature focuses on key microcirculatory responses in relation to diabetic foot in order to understand some of the functional aspects of microcirculation. Firstly, search terms such as "Post-Occlusive Reactive Hyperaemia", "PORH" "pressure-induced vasodilation", "PIV" and "skin blood flow" "local application of pressure", "LDI flare" and "axon-mediated flare" were listed and used to identify articles (the search was not limited to these terms only). PubMed and Medline databases were searched to identify relevant publications in journals. Secondly, the reference lists of the selected articles were scrutinised to find additional studies. However, the data sources were not limited to articles published in journals, but also included grey literature. The sources for grey literature included: 1) Reports from International Diabetes Federation and Diabete UK 2) Websites of equipment manufacturers (Perimed AB, Moor Instruments, FLIR and Impeto Medical Solutions) 3) OpenGrey, and 4) Google. The articles of interest from MEDLINE, PubMed, and PubMed Central (PMC) included in the review were identified through the initial phase of title and abstract sifting. Subsequently, after the title and abstract sifting, relevant articles that adequately described cutaneous microcirculatory responses were retrieved for further study. Later, the data were extracted from relevant articles. Specific insights generated from the literature are presented and discussed below.

VARIOUS MICROCIRCULATORY RESPONSES AND THEIR ASSOCIATION IN DIABETES FOOT-RELATED COMPLICATIONS

The foot is continuously under mechanical stress due to weight-bearing activities of daily living such as walking, exercise, and standing. It is exposed to various trauma, physical injury due to sudden or violent action, exposure to dangerous toxins or repetitive mechanical stress. Some of the extrinsic factors for trauma are thermal (Example: hot surfaces), mechanical (Example: repetitive damage from ill-fitted shoes), and chemical (Example: corn treatments) (Boulton, 2000; Armstrong and Lavery, 2005; Boulton et al., 2006; Vanderah, 2007; Hawke and Burns, 2009). On the other hand, some of the intrinsic factors that contribute to the risk of trauma are foot deformity and glycation related changes in case of diabetes.

Both neuro and vascular aspects are essential for healthy foot function. The nerves of the feet can respond to the thermal, mechanical and chemical stimuli, provoking a reflex withdrawal from the respective harmful stimulus (Hawke and Burns, 2009). For instance, jerking the foot away from a sharp object. This protective mechanism may be absent due to neuropathy in people with diabetes (Boulton et al., 2006; Hawke and Burns, 2009). On the other hand, microcirculation is important for tissue injury response to stimuli such as local heat or pressure (Abraham et al., 2001; Korzon-Burakowska & Edmonds, 2006). Such neurovascular mechanisms of the foot appear to play a vital role to prevent tissue injuries.

Previous research shows that there are certain protective microcirculatory responses to stimuli, which are controlled by neural mechanisms, metabolic aspects, hormones and chemicals (Guyton, 1991). A microcirculatory hyperaemic response is induced on the application of a stimulus. This transient hyperaemic response to various stimuli, witnessed by an increase in blood perfusion is one of the measures to assess microcirculatory function known as reactive hyperaemia. Reactive hyperaemia is an indicator of the intrinsic ability of an organ or tissue to locally autoregulate its blood supply, which is found to be impaired in people with diabetes (Flynn and Tooke, 1992; Korzon-Burakowska & Edmonds, 2006; Merrill, 2008; Klabunde, 2012). For the purpose of this review, based on the select stimuli, the microcirculatory responses observed are stratified into:

1) Vasodilation in response to occlusive ischemia or Post-Occlusive Reactive Hyperaemia (PORH)
2) Microcirculatory response to locally applied pressure;
   (a) Pressure-induced vasodilation (PIV);
   (b) Reduced skin blood flow;
3) Interplay between microcirculation and temperature -vasodilation in response to local heating

The reviewed studies demonstrate the inability of cutaneous microcirculation to respond normally to non-painful stimulation, such as the application of pneumatic pressure, local pressure and local heating in people with diabetes (Fromy et al., 2002). This may be significant in understanding tissue response to injuries. During incidents of prolonged pressure, injury or infection, more demands are made upon the capillary circulation (Flynn and Tooke, 1992; Abraham et al., 2001). Owing to the microcirculatory dysfunction, the hyperaemic response may be impaired and tissue demands are not met (Flynn and Tooke, 1992). Vascular insufficiency to the tissues that leads to breakdown may contribute to adverse complications and increase the risk of ulceration (Flynn and Tooke, 1992).

Nevertheless, there are very limited studies that evaluate the vasodilatory responses to stimuli in subjects with diabetes. Furthermore, only a handful number of research articles address these vasodilatory responses in diabetic foot syndrome, including ulcerated and non-ulcerated cohorts. Key articles on this subject were appraised and discussed in this review.

Vasodilation in Response to Occlusion or Post Occlusive Reactive Hyperaemia (PORH)

Reactive hyperaemia to occlusion is the transient increase in blood flow in the organ or tissue that occurs following a brief period of arterial occlusion. During the process of occlusion, the blood flow goes to a biological zero that is defined as the "no flow" Laser Doppler signal during a PORH test. Following the release of the occlusion, blood flow rapidly increases, which is reactive hyperaemia (Klabunde, 2012). This process is known as post-occlusive reactive hyperaemia (PORH). During the hyperaemia, the tissue becomes re-oxygenated and reperfusion occurs. Simultaneously, the vasodilator metabolites are removed from the tissue, which restores the vascular tone of the resistant vessels causing the blood flow to return to normal (Klabunde, 2012). The longer the period of occlusion, the greater the metabolic stimulus for vasodilation leading to an increase in peak reactive hyperaemia and duration of hyperaemia (Guyton, 1991; Larkin and Williams, 1993; Klabunde, 2012). Based on the time taken to occlude the blood supply to the tissue from few seconds to several hours, the blood flow post-occlusion increases four to seven times in the tissue than normal and lasts from few seconds to hours in relation to the initial occlusion time (Guyton, 1991). Additionally, depending upon the organ or tissue, maximal vasodilation as indicated by peak flow varies (Klabunde, 2012).

PORH is predominantly an endothelial-dependent process, however, it also aids combined assessment of both endothelial-dependent and independent function (Maniewski et al., 2014; Lanting et al., 2017). Hyperaemia occurs because of the shear stress, the tangential frictional force-acting at the endothelial cell surface caused by arterial occlusion (Maniewski et al., 2014). A mechanical stimulation occurs when the shear stress vector is directed perpendicular to the long axis of the arterial vessel (Maniewski et al., 2014). The endothelium responds to this mechanical stimuli, thereby, releasing vasodilatory substances (Maniewski et al., 2014). The factors that are known to contribute to vasodilation are myogenic, neurogenic, and other local factors, such as potassium ions, hydrogen ions, carbon dioxide, catecholamines, prostaglandins, and adenosine (Maniewski et al., 2014; Lanting et al., 2017). Few studies mention that endothelial nitric oxide and other endothelium-derived agents, such as prostaglandins and endothelium-derived hyperpolarizing factors are known to be involved in the mechanism of PORH (Maniewski et al., 2014; Carasca et al., 2017; Marche et al., 2017). However, some researchers contend that nitric oxide and prostaglandins may not be contributing to the mechanism (Cracowski et al., 2011; Maniewski et al., 2014). It is argued that whilst nitric oxide is known to play a major role in the vasodilation of macrovessels, endothelium-derived hyperpolarizing factors are found to play a substantial role in the dilation of microvessels (Quyyumi and Ozkor, 2006; Cracowski et al., 2011). Apart from these substances, the sensory nerves make a vital contribution to the PORH mechanism (Larkin and Williams, 1993; Lorenzo and Minson, 2007; Cracowski et al., 2011; Lanting et al., 2017; Marche et al., 2017). To summarise, various studies have shown that PORH response is elicited with temporary tissue hypoxia upon occlusion through the accumulation of vasodilators (substances that cause the blood vessels to dilate or expand) and other complex factors that are myogenic, endothelial, neurogenic and metabolic (Guyton, 1991; Klabunde, 2012; Lanting et al., 2017).

The PORH test has a wide range of applications. Previously, PORH has been used to assess microcirculatory function in people with arterial diseases, certain ophthalmologic conditions and cardiovascular disorders (Morales et al., 2005; Maniewski et al., 2014; Carasca et al., 2017). It is impaired in people with peripheral arterial disease and has been associated with increased cardiovascular risk (Morales et al., 2005). The test was observed to be useful as an early marker of cardiovascular damage (Busila et al., 2015). PORH test is also used to assess the altered microvascular reactivity in patients with advanced renal dysfunction (Busila et al., 2015). Besides, the use of the PORH test has also been explored in the area of diabetes.

A limited amount of research has been conducted in people with diabetes using PORH measures, both in type 1 and 2. PORH vasodilation is significantly decreased in patients with type 1 diabetes (Marche et al., 2017). In 1986, Rayman et al. demonstrated the impaired hyperaemic response to injury in people with diabetes for the first time (Rayman et al., 1986). Prolongation of the hyperaemic reaction and decrease in response was observed in patients with insulin-dependent diabetes and peripheral occlusive arterial disease (Maniewski et al., 2014). PORH is known to be impaired not only in adults but also in children with type 1 diabetes (Schlager et al., 2012). The results from children in terms of diabetic foot complications is as important as the studies conducted in adults because of two main reasons. Firstly, although this segment of the population is less likely to be vulnerable to foot complications at a younger age, but they are likely to develop complications as they advance in age. Therefore, understanding the microvascular reactivity from an earlier period may prove to be useful. Secondly, this particular study explored other less commonly assessed variables such as biological zero and reperfusion time, which can shed more light on understanding PORH. It was identified that peak perfusion was higher and biological zero was lower in children with type 1 diabetes in comparison to the controls. A key implication from this study was that higher peak perfusion might reflect a decline in the vasoconstrictive ability of arteriolar smooth muscle cells upstream of capillary beds in children with type 1 diabetes (Schlager et al., 2012).

Few studies have explored PORH more specifically in diabetic foot complications (Cheng et al., 2004; Barwick et al., 2016; Lanting et al., 2017). The presence of peripheral sensory neuropathy in people with type 2 diabetes is found to be associated with altered PORH in the foot (Barwick et al.,

2016). A study on the relationship between active or previous foot complication and PORH measured by LDF in people with type 2 diabetes revealed that the increase in time to Peak, which is a variable that shows the time taken for a maximum flux post occlusion, increased the likelihood of a participant having a history of foot complication by 2% (Lanting et al., 2017). This association was not reflected in people with an active foot ulcer (Lanting et al., 2017). These findings in a cohort with type 2 diabetes with a previous history or existing foot-related complications support the need for further investigation into the relationship between measures of microvascular function and development of diabetic foot complications, prospectively (Lanting et al., 2017). Considering this evidence, it seems that PORH is an interesting microcirculatory mechanism that may be useful to assess a foot at risk. In future, their application may be a useful indicator for determining the future risk of diabetic foot complications, especially with ulcer prediction and prevention of amputation.

Microcirculation in Response to Local Application of Pressure

In the foot, the areas prone to high pressure such as the heel, the great toe and areas under the metatarsal heads are at risk of ulceration (Veves et al., 1992; Ledoux et al., 2013). Based on this, many weight-bearing activities were considered to be a contraindication to people with neuropathy (Kluding et al., 2017). However, this has recently changed as there is emerging evidence of positive adaptations of the musculoskeletal and integumentry system to overload stress (Kluding et al., 2017). Literature suggests that peripheral neuropathy may no longer be a hindrance to promoting weight-bearing activity as it did not lead to significant increases in foot ulcers (LeMaster et al., 2008). However, in people with diabetes various other factors may interplay with pressure such as increased stiffness of tissues, aging related changes, presence of other comorbidities, mobility and vascular issues. Studies show that the accumulated mechanical stimulus affected blood perfusion in the foot and should be considered when assessing the risk of developing ulcers (Ledoux et al., 2013; Pu et al., 2018). However, more understanding on the relationship between pressure stimulus and microvascular responses could shed more light on the effect of different levels of accumulated mechanical stimulus on microvascular response and their significance in an ulcer incident.

Responses to local mechanical stresses are mediated through a considerable number and variety of cutaneous receptors and some of these receptors are connected to the small fibres (Abraham et al., 2001). The vasodilation to pressure strains not only occur for noxious stimuli but also non-noxious stimuli applied over a period (Abraham et al., 2001). Local pressure strain to the skin is recognised to play a vital role in cutaneous microcirculatory impairment (Fromy et al., 2000; Abraham et al., 2001). It is presumed that this may be linked to the development of cutaneous lesions such as pressure sores and diabetic foot ulcers (Abraham et al., 2001; Fromy et al., 2002). Two important microcirculatory responses to locally applied pressure identified through the literature review are discussed below.

Pressure-induced Vasodilation

The transient increase in cutaneous blood flow initially before it decreases in response to a progressive locally applied pressure strain is known as pressure-induced vasodilation (PIV). This microcirculatory response appears to be a protective cutaneous response that relies on the excitation of unmyelinated afferent nerve fibres (Fromy et al., 2002; Koïtka et al., 2004; Körei et al., 2016). PIV is considered to be more than a transient phenomenon and an important physiological response allowing the skin to respond adequately to mechanical stimuli (Abraham et al., 2001). Cutaneous receptors in the skin respond to local mechanical stresses such as local pressure strain and these receptors are found to be of mechanothermal nature (Fromy et al., 2002). This response is noted to be compromised in the aging population (Fromy et al., 2010; Fouchard et al., 2019). Furthermore, the impairment of PIV is postulated to contribute to the development of lesions such as pressure ulcers and diabetic foot ulcers (Abraham et al., 2001; Saumet, 2005; Vouillarmet et al., 2019).

The interplay between biomechanical factors and physiological responses is well-realised in the development of pressure ulcers, including in people with diabetes. Current studies highlight PIV in relation to the development of pressure ulcers or decubitus ulcers in the sacral region. As discussed above, one of the key implications from the studies on PIV is that it is a protective mechanism without which certain pressure-associated lesions may develop and plausibly this could explain the high risk of decubitus and plantar ulcers in people with diabetes (Abraham et al., 2001; Fromy et al., 2002; Bergstrand, 2014). Although pressure ulcers and plantar ulcers may differ in many ways, one of the key causal pathways to foot ulceration is somatic motor neuropathy that leads to small muscle wasting, foot deformities, loss of sensation, increased plantar pressure and repetitive trauma resulting in neuropathic foot ulcer (Armstrong and Lavery, 2005). This suggests that local pressure strain increases the vulnerability of the foot to ulcerate. Similar to pressure ulcer development, reduced physiological responses may induce local ischaemia and reperfusion injury in the foot (Flynn and Tooke, 1992; Coleman et al., 2014). A similar role of reduced microcirculatory responses in foot ulcer development is widely discussed in the literature (Flynn and Tooke, 1992; Boulton et al., 2006; Korzon-Burakowska & Edmonds, 2006). This knowledge can potentially be translated to diabetic foot ulcer prediction to see if the microcirculatory response to local pressure and plantar pressure have any association. This also accords with other observations, which showed that people with impaired or absent PIV are known to be at a higher risk to develop pressure ulcers (Fromy et al., 2002; Braden and Blanchard, 2007; Bergstrand, 2014). Evidence shows that decreased hyperaemic response and absence of PIV is known to increase the risk of pressure ulcers (Bergstrand et al., 2014). However, very limited research is available on PIV in human hand and feet in relation to diabetes (Abraham et al., 2001; Koïtka et al., 2004).

A particular study by Koitka et al. (2004) observed PIV at the foot level in people type 1 diabetes (Koïtka et al., 2004). Since low skin temperature in people with diabetes is known to interfere with microcirculation, this research was performed in warm conditions of 29.5± 0.2°C (Koïtka et al., 2004). The cutaneous blood flow was studied at warm conditions using laser Doppler flowmetry on the first metatarsal head in response to applied pressure at 5.0 mmHg/min and PIV was found to be absent at foot level in people with type 1 diabetes whereas it existed in healthy subjects at 29.5±0.2°C (Koïtka et al., 2004). These findings were attributed to an interaction between functional changes in C-fibres and the endothelium in people with diabetes (Koïtka et al., 2004). A similar study found PIV to be absent at low skin temperature even in healthy subjects (28.7±0.4°C) (Fromy et al., 2002). It was explained that a skin temperature close to 34°C was optimal for the evaluation of skin vasomotor reflexes in the lower limb and the nervous receptors involved in the PIV development are mechanothermal, and not only mechanical (Fromy et al., 2002). The results from Koitka et al. (2004) revealed that in the same subjects the non-endothelial-mediated response to sodium nitroprusside was preserved, whereas the endothelial-mediated response to acetylcholine was impaired (Koïtka et al., 2004). Therefore, suggesting the relevance of endothelial dysfunction to PIV. Also, a previous study on PIV found that the absence of vasodilatory axon reflex response to local pressure strain when the capsaicin-sensitive nerve terminals were pre-treated with local anaesthetic or chronically applied capsaicin (Fromy et al., 1998). The capsaicin-sensitive nerve fibres are the small nerve fibres and their role in neuropathic pain and related complications, especially in people with diabetes is well-established (Boulton et al., 2006). Thus, the researchers speculated that the PIV, which is associated with the stimulation of small fibre nerves, could be a missing link between neuropathy and foot ulcers in diabetes (Koïtka et al., 2004). In support of this, several studies have demonstrated that damage to C-fibres have a great impact on skin, with disrupted blood flow predisposing to foot ulcers (Vinik et al., 2001; Caselli et al., 2003; Boulton et al., 2006; Themistocleous et al., 2014). As previously discussed, impaired microcirculatory response to local pressure strain may potentially make people with diabetes more vulnerable to pressure strains and explain the high prevalence of foot ulcer that occurs in diabetic patients (Koïtka et al., 2004).

The insights from the above-discussed studies suggest that PIV is absent at the foot level in people with diabetes. Identifying the point or stage of the disappearance of PIV in the foot, during the disease progression through prospective studies, may help in understanding the progression of neurovascular dysfunction in the foot. On the other hand, since PIV may be absent from an earlier stage, its capability to indicate risk for ulceration is disputable and needs further research. Also, the current study has observed PIV only at two sites, which was the head of the first metatarsus and the area over the internal ankle bone in a small sample size. More research is required to explore various regions of the plantar aspect of the foot, especially in areas subject to increased plantar pressure. The findings from such research can aid to comprehend the association between PIV and plantar ulcers and help identify foot at risk. Furthermore, it may aid to bridge the research gap to understand the role of microcirculation in the development of diabetic foot ulcers.

Reduced Skin Blood Flow to Locally Applied Pressure

As discussed earlier, PIV allows the skin blood flow to increase in response to locally applied pressure. In the absence of the transient PIV response, the cutaneous blood flow is observed to progressively decrease with the application of increasing local pressure (Fromy et al., 2002). The observed cutaneous blood flow in response to locally applied pressure is found to be impaired in people with diabetes owing to the combined effects of low cutaneous temperature and alterations in microcirculatory function (Fromy et al., 2002). Additionally, the presence of neuropathy may aggravate the condition (Fromy et al., 2002). This study used a laser Doppler flowmetry system and applied local pressure using a specially designed apparatus at the internal anklebone allowing for a 5.0 mmHg/min rate of pressure increase (Fromy et al., 2000; Fromy et al., 2002). The skin blood flow decreased significantly from baseline at much lower applied pressure of 7.5 mmHg in people with diabetes in groups without neuropathy and with subclinical or clinical neuropathy at 6.3 mmHg in comparison to the healthy controls at 48.8 mmHg (Fromy et al., 2002). The large difference between these pressures reported within this study indicate a plausible association between decreased skin blood flow to local pressure and the development of decubitus and plantar ulcers (Fromy et al., 2002). This hypothesis is consistent with the one proposed by Koitka et al. (2004) who suggested an association between microcirculatory dysfunction and the high prevalence of foot ulcer (Koïtka et al., 2004). They also postulate that the arterial wall and surrounding tissues are very compressible in people with diabetes making them vulnerable to the development of pressure ulcers (Fromy et al., 2002; Coleman et al., 2014). The application of this knowledge to understand the role of microcirculation in foot ulceration may potentially be useful.

Although the collated findings reveal the possibility of decreased skin blood flow and PIV to be associated with pressure ulcer development, more research is needed to understand the mechanism in relation to diabetic foot complications. The aetiology for decubitus ulcer and plantar ulcers may vary, nevertheless, pressure remains as a common contributing factor in both the incidents. Studies suggest pressure-induced local ischaemia and reperfusion injuries in relation to both pressure ulcers and diabetic foot ulcers (Flynn and Tooke, 1992; Korzon-Burakowska & Edmonds, 2006; Coleman et al., 2014; Shahwan, 2015). Understanding PIV, reduced skin flow and other microcirculatory responses in various regions prone to diabetic foot ulcers and in relation to plantar pressure during standing or walking are important. The need for such a study is further supported by the evidence from a study that identified subjects who lacked PIV and reactive hyperaemia in response to locally applied pressure, to be particularly vulnerable to pressure exposure (Bergstrand, 2014; Bergstrand et al., 2014). These subjects were stratified to be at a higher risk for pressure ulcer development (Bergstrand, 2014; Bergstrand et al., 2014). Thereby, translating the knowledge generated from the studies on microcirculatory responses in

the development of pressure ulcers to diabetic foot ulcers can prove to be useful.

Interplay Between Microcirculation and Temperature - Vasodilation in Response to Local Heating

While specific literature on the microcirculatory responses and temperature changes in response to plantar skin tissue injuries and healing are limited, previous studies reviewed microcirculatory assessments in various organs in people with diabetes. The knowledge of microcirculatory responses to temperature changes in other organs, can reveal that external stimuli causes an increased microvascular demand. This showcases the role of cutaneous microcirculatory response in tissue injuries and healing.

When injuries and repair occur, monitoring the conditions between the skin, soft tissues or even after skin grafts can aid better prognosis. A study explored the proposed theory that conducive interface conditions between soft tissue and prostheses are necessary for a better outcome with prosthodontic treatment. This study by Nakamoto et al. (2012) focused on the gingiva and mucosa surrounding anterior implants and both LDF and thermographs were concurrently used to elucidate the relationship between temperature and blood flow as peri-implant soft tissues are often portrayed to have decreased blood flow because of the lack of blood supply from the periodontal ligament. The study also analysed the morphological changes of the cutaneous microvasculature and temperature changes between participants with and without bone grafting associated with implant placement. The findings suggested that soft tissue around implants showed decreased blood flow compared with periodontal tissue in adjacent natural teeth, despite the absence of clinical signs such as chronic inflammation. The study also highlighted the significance of bone quality to maintain blood flow in the soft as the area around implants with bone grafting showed significantly reduced blood flow. Many research studies suggest that microcirculatory blood flow is influenced by thermal changes and reportedly increases in proportion to temperature to an extent, which is not limited to dentistry but also in studies on other cutaneous microcirculation (Molnár et al., 2015). However, the observed results by Nakamoto et al. (2012) were contrary to this popular idea. The suggested explanation for this was the involvement of deeper structures that modified the thermal properties and the usually observed increase in temperature was often associated with inflammation due to infection such as periodontitis but not in case of tissue surrounding implants (Baab et al., 1990).

Although the skin and the oral mucosa have certain similarities and differences anatomically, they have some comparable physiological properties. For instance, they play a crucial role in the prevention of infections and act as a barrier against exogenous or endogenous substances, pathogens, and mechanical stresses (Liu et al., 2010). The dysfunction of these barriers can compromise the integrity of the underlying tissue as well. The combination of findings from the study provides some support for the conceptual premise that the simultaneous measurements of blood flow and temperature are useful to evaluate the microcirculation of soft tissue behaviour in injury and healing, and its significane even in the absence of noticeable signs chronic inflammation. A similar study compared the peripheral blood flow in the lower limbs during the local heating tests with different temperature protocols in people with diabetes mellitus and healthy participants (Filina et al., 2017). The LDF was used to evaluate the adaptive changes of the microvascular bed during thermal tests and the detection of the preclinical stage of trophic disorders owing to disruption in nutritional or nerve supply (Filina et al., 2017). Research suggest that in the feet of patients with diabetic neuropathy, total skin blood flow is increased due to an increased shunt flow due to denervation (Harpuder et al., 1940; Schaper et al., 2008). Further study in the area has shown that the increased anastomotic shunt flow lead to either under- or over perfused nutritive capillaries (Netten et al., 1996). Skin temperature measurements and LDF were performed to record mainly shunt flow and capillaroscopy to study nailfold capillary blood flow (Netten et al., 1996). The study showed that in insulin-dependent diabetic patients with neuropathy, the baseline skin temperature and capillary blood-cell velocity was higher in comparison to those without neuropathy and healthy control subjects (Netten et al., 1996). The findings from the study highlighted the presence of hyperperfused nutritive capillary circulation in the feet of patients with diabetic neuropathy favouring the previously discussed hyperdynamic hypothesis and in contradiction to the capillary steal phenomenon to explain the decreased healing potential in diabetic neuropathic foot ulceration.

As suggested by previous research, microcirculatory and temperature measurements might become useful techniques to evaluate healthy, infected, injured, inflamed and treated skin and soft tissues of the foot (Netten et al., 1996; Gatt et al., 2018; Gatt et al., 2020). But, there is abundant room for further progress in determining if these two measurements may be useful for the diagnosis or prognosis of foot ulcers. Such research may aid to draw a margin between the compromised tissue and the surrounding healthy tissue when determining the course of treatment, surgery or even amputation. Furthermore, comparative studies conducted on healthy vs inflamed/injured tissue in the foot can help to identify early signs of dysfunction, inflammation and injury in a foot in order to effectively manage the condition. For instance, Ren et al. (2021) explored the stimulation of microcirculation using simple thermal stimuli such as infrared and warm bath in healthy adults to explore the options in hope to design interventions to promote better circulation in the lower extremities of the body in the geriatric population and those suffering from diabetes who are likely to have impaired microcirculation (Ren et al., 2021).

The vasodilation in response to local heating and the neurogenic flare response to nociceptive stimuli is mediated by an axon reflex involving C-fibres. This is studied using the laser Doppler imager (LDI) and the induced flare response is known as the LDI flare. The LDI flare area which is the area with the hyperaemic response is known to be reflective of the small fibre

function. Therefore, the size of the LDI flare is known to be dependent on the C-fibre function and the underlying skin small fibre neural network and its extent (Green et al., 2010; Vas et al., 2012). Whereas, the LDI max (perfusion) in the skin immediately beneath the heating probe is shown to be mediated by non-neurogenic means and to reflect the endothelial function (Green et al., 2010; Vas et al., 2012). Therefore, the intensity of the hyperaemic response depends on the microvascular ability to vasodilate. The site commonly studied is the dorsum of the feet because the underlying skin is less influenced by the thermoregulatory blood flow due to the absence of arteriovenous anastomoses (Braverman, 2000). The method used to assess this reflex involves local skin heating to 44°C for 20 min or 6 min in a stepwise fashion: 44°C for 2 min, 46°C for 1 min and finally 47°C for 3 min in a temperature-controlled room to evoke the flare followed by scanning the site using an LDI to measure the area (Krishnan and Rayman, 2004; Green et al., 2010; Vas et al., 2012). Another technique is also known to be used to observe the hyperaemic response to local heating. This involves the use of a skin-heating probe filled with deionized water and heating to 44 °C to assess heat-induced vasodilation. In summary, the LDI flare test in subjects shows reduced microcirculatory response as well as a neurogenic flare in people with either type 1 or two diabetes (Krishnan and Rayman, 2004; Vas et al., 2012). It facilitates early diagnosis of C-fibre dysfunction even before its detection by other available methods such as the quantitative sensory testing, which focuses on the testing of sensory abnormalities in the areas of temperature change sensation, vibration, and pain threshold testing (Example: Using equipment named Computer Aided Sensory Evaluator–IV - case IV) (Krishnan and Rayman, 2004). Therefore, the heat provocation or LDI flare test is commonly used with a focus on LDI flare for the assessment of C-fibre function than with a concentration on the LDI max for evaluating the microcirculatory function. However, the test can be used to assess not only C-fibre function but also microcirculation, and additionally investigate their association in neuropathy (Vas et al., 2012; Marche et al., 2017). This can further clarify the link between microcirculation impairment and tissue damage in light of impaired sensation.

CONCLUSION

Microcirculation plays a vital role in homeostatic and defence states during tissue injury and inflammation. Firstly, the most obvious finding to emerge from this review is the protective role of microcirculation. Secondly, the impairment of microcirculation and the possibility of it being the missing link in the chain of events that leads to foot ulceration in people with diabetes is clearly supported by the current findings. Thirdly, assessment of microcirculatory structural damages might be complex, however, the insights emerged from this review has shown that there are responses such as post-occlusive reactive hyperaemia, pressure-induced vasodilation and vasodilation to local heating (LDI flare) that are simple to assess. In conclusion, a thorough understanding of the microcirculatory function and its impaired reactive mechanisms is imperative and will contribute extensively to understanding the soft tissue biomechanics and aid to devise strategies for comprehensive assessment of the diabetic foot. This, in turn, will aid in prevention and early diagnosis of ulcers, thereby, reducing amputations.

AUTHOR CONTRIBUTIONS

GB: Conducted the literature review and wrote the first draft of the manuscript. NC: Reviewed the manuscript draft and provided comments. RN: Developed the concept and contributed to revising the draft and shaping the manuscript.

REFERENCES

Abraham, P., Fromy, B., Merzeau, S., Jardel, A., and Saumet, J.-L. (2001). Dynamics of Local Pressure-Induced Cutaneous Vasodilation in the Human Hand. *Microvasc. Res.* 61 (1), 122–129. doi:10.1006/MVRE.2000.2290

Ambrózy, E., Waczulíková, I., Willfort, A., Böhler, K., Cauza, K., Ehringer, H., et al. (2013). Healing Process of Venous Ulcers: The Role of Microcirculation. *Int. Wound J.* 10 (1), 57–64. doi:10.1111/j.1742-481X.2012.00943.x

Armstrong, D. G., and Lavery, L. A. (2005). *Clinical Care of the Diabetic Foot*. American Diabetes Association.

Baab, D. A., Öberg, Å., and Lundström, Å. (1990). Gingival Blood Flow and Temperature Changes in Young Humans with a History of Periodontitis. *Arch. Oral Biol.* 35 (2), 95–101. doi:10.1016/0003-9969(90)90169-B

Bakker, K., Apelqvist, J., Lipsky, B. A., Van Netten, J. J., and Schaper, N. C. (2016). The 2015 IWGDF Guidance Documents on Prevention and Management of Foot Problems in Diabetes: Development of an Evidence-Based Global Consensus. *Diabetes Metab. Res. Rev.* 32, 2–6. doi:10.1002/dmrr.2694

Balasubramanian, G., Vas, P., Chockalingam, N., and Naemi, R. (2020). A Synoptic Overview of Neurovascular Interactions in the Foot. *Front. Endocrinol.* 11, 308. doi:10.3389/fendo.2020.00308

Barwick, A. L., Tessier, J. W., Janse de Jonge, X., Ivers, J. R., and Chuter, V. H. (2016). Peripheral Sensory Neuropathy Is Associated with Altered Postocclusive Reactive Hyperemia in the Diabetic Foot. *BMJ Open Diab Res. Care* 4, e000235. doi:10.1136/bmjdrc-2016-000235

Bentov, I., and Reed, M. J. (2014). Anesthesia, Microcirculation, and Wound Repair in Aging. *Anesthesiology* 120 (3), 760–772. doi:10.1097/ALN.0000000000000036

Bergstrand, S., Källman, U., Ek, A.-C., Lindberg, L.-G., Engström, M., Sjöberg, F., et al. (2014). Pressure-induced Vasodilation and Reactive Hyperemia at Different Depths in Sacral Tissue under Clinically Relevant Conditions. *Microcirculation* 21 (8), 761–771. doi:10.1111/micc.12160

Bergstrand, S. (2014). *Preventing Pressure Ulcers by Assessment of the Microcirculation in Tissue Exposed to Pressure*. Doctoral dissertation, (Linköping, Sweden): Linköping University Electronic Press. doi:10.3384/diss.diva-109960

Boulton, A. J. (2000). *The Diabetic Foot*. South Dartmouth: MDText.com, Inc. Available at: http://www.ncbi.nlm.nih.gov/pubmed/28121117 (Accessed February 18, 2018).

Boulton, A. J. M., Cavanagh, P. R., and Rayman, G. (2006). *The Foot in Diabetes*. Wiley.

Braden, B., and Blanchard, S. (2007). "Risk Assessment in Pressure Ulcer Prevention," in *Chronic Wound Care A Clin Source B Healthc Prof*, 593–608.

Braverman, I. M. (2000). The Cutaneous Microcirculation. *J. Invest. Dermatol. Symp. Proc.* 5 (1), 3–9. doi:10.1046/j.1087-0024.2000.00010.x

Busila, I., Onofriescu, M., Gramaticu, A., Hogas, S., Covic, A., and Florea, L. (2015). ENDOTHELIAL DYSFUNCTION ASSESSED BY LASER DOPPLER POST-OCCLUSIVE HYPEREMIA IN CHRONIC KIDNEY DISEASE PATIENTS. *Rev. Med. Chir Soc. Med. Nat. Iasi* 119 (4), 1001–1009.

Carasca, C., Magdas, A., Tilea, I., and Incze, A. (2017). Assessment of Post-Occlusive Reactive Hyperaemia in the Evaluation of Endothelial Function in Patients with Lower Extremity Artery Disease. *Acta Med. Marisiensis* 63 (3), 129–132. doi:10.1515/amma-2017-0024

Caselli, A., Rich, J., Hanane, T., Uccioli, L., and Veves, A. (2003). Role of C-Nociceptive Fibers in the Nerve Axon Reflex-Related Vasodilation in Diabetes. *Neurology* 60, 297–300. doi:10.1212/01.wnl.0000040250.31755.f9

Chao, C. Y. L., and Cheing, G. L. Y. (2009). Microvascular Dysfunction in Diabetic Foot Disease and Ulceration. *Diabetes Metab. Res. Rev.* 25 (7), 604–614. doi:10.1002/dmrr.1004

Cheng, X., Mao, J. M., Xu, X., Elmandjra, M., Bush, R., Christenson, L., et al. (2004). Post-occlusive Reactive Hyperemia in Patients with Peripheral Vascular Disease. *Clin. Hemorheol. Microcirc.* 31 (1), 11–21. Available at: http://www.ncbi.nlm.nih.gov/pubmed/18644817.

Coleman, S., Nixon, J., Keen, J., Wilson, L., McGinnis, E., Dealey, C., et al. (2014). A New Pressure Ulcer Conceptual Framework. *J. Adv. Nurs.* 70 (10), 2222–2234. doi:10.1111/jan.12405

Cracowski, J. L., Gaillard-Bigot, F., Cracowski, C., Roustit, M., and Millet, C. (2011). Skin Microdialysis Coupled with Laser Speckle Contrast Imaging to Assess Microvascular Reactivity. *Microvasc. Res.* 82 (3), 333–338. doi:10.1016/j.mvr.2011.09.009

Deanfield, J. E., Daggett, P. R., and Harrison, M. J. G. (1980). The Role of Autonomic Neuropathy in Diabetic Foot Ulceration. *J. Neurol. Sci.* 47 (2), 203–210. doi:10.1016/0022-510X(80)90004-0

Filina, M. A., Potapova, E. V., Makovik, I. N., Zharkih, E. V., Dremin, V. V., Zherebtsov, E. A., et al. (2017). Functional Changes in Blood Microcirculation in the Skin of the Foot during Heating Tests in Patients with Diabetes Mellitus. *Hum. Physiol.* 43 (6), 693–699. doi:10.1134/S0362119717060020

Flynn, M. D., and Tooke, J. E. (1992). Aetiology of Diabetic Foot Ulceration: a Role for the Microcirculation? *Diabet Med. A. J. Br. Diabet Assoc.* 9 (4), 320–329. doi:10.1111/j.1464-5491.1992.tb01790.x

Flynn, M. D., and Tooke, J. E. (1990). Microcirculation and the Diabetic Foot. *Vasc. Med. Rev.* 1 (2), 121–138. doi:10.1177/1358836X9000100204

Fouchard, M., Misery, L., Le Garrec, R., Sigaudo-Roussel, D., and Fromy, B. (2019). Alteration of Pressure-Induced Vasodilation in Aging and Diabetes, a Neuro-Vascular Damage. *Front. Physiol.* 10, 862. doi:10.3389/fphys.2019.00862

Fromy, B., Abraham, P., and Saumet, J. L. (1998). Non-nociceptive Capsaicin-Sensitive Nerve Terminal Stimulation Allows for an Original Vasodilatory Reflex in the Human Skin. *Brain Res.* 811 166 doi:10.1016/S0006-8993(98)00973-1

Fromy, B., Abraham, P., Bouvet, C., Bouhanick, B., Fressinaud, P., and Saumet, J. L. (2002). Early Decrease of Skin Blood Flow in Response to Locally Applied Pressure in Diabetic Subjects. *Diabetes* 51 (4), 1214–1217. doi:10.2337/DIABETES.51.4.1214

Fromy, B., Abraham, P., and Saumet, J.-L. (2000). Progressive Calibrated Pressure Device to Measure Cutaneous Blood Flow Changes to External Pressure Strain. *Brain Res. Protoc.* 5 (2), 198–203. doi:10.1016/S1385-299X(00)00013-1

Fromy, B., Sigaudo-Roussel, D., Gaubert-Dahan, M.-L., Rousseau, P., Abraham, P., Benzoni, D., et al. (2010). Aging-associated Sensory Neuropathy Alters Pressure-Induced Vasodilation in Humans. *J. Invest. Dermatol.* 130 (3), 849–855. doi:10.1038/jid.2009.279

Gatt, A., Falzon, O., Cassar, K., Ellul, C., Camilleri, K. P., Gauci, J., et al. (2018). Establishing Differences in Thermographic Patterns between the Various Complications in Diabetic Foot Disease. *Int. J. Endocrinol.* 2018, 1–7. doi:10.1155/2018/9808295

Gatt, A., Mercieca, C., Borg, A., Grech, A., Camilleri, L., Gatt, C., et al. (2020). Thermal Characteristics of Rheumatoid Feet in Remission: Baseline Data. *PLoS One* 15, e0243078. doi:10.1371/journal.pone.0243078

Goldenberg, S., Alex, M., Joshi, R. A., and Blumenthal, H. T. (1959). Nonatheromatous Peripheral Vascular Disease of the Lower Extremity in Diabetes Mellitus. *Diabetes* 8 (4), 261–273. doi:10.2337/diab.8.4.261

Granger, D. N., and Senchenkova, E. (2010). "Inflammation and the Microcirculation," in *Colloquium Series On Integrated Systems Physiology: From Molecule To Function* (Morgan & Claypool Life Sciences) Vol. 2, 1–87. Available at: https://www.ncbi.nlm.nih.gov/books/NBK53373/ (Accessed June 27, 2021).

Granger, D. N., and Rodrigues, S. F. (2016). "Microvascular Responses to Inflammation," in *Compendium of Inflammatory Diseases* (Springer Basel), 942–948. doi:10.1007/978-3-7643-8550-7_178

Green, A. Q., Krishnan, S., Finucane, F. M., and Rayman, G. (2010). Altered C-Fiber Function as an Indicator of Early Peripheral Neuropathy in Individuals with Impaired Glucose Tolerance. *Diabetes Care* 33 (1), 174–176. doi:10.2337/dc09-0101

Guven, G., Hilty, M. P., and Ince, C. (2020). Microcirculation: Physiology, Pathophysiology, and Clinical Application. *Blood Purif.* 49 (1-2), 143–150. doi:10.1159/000503775

Guyton, A. C. (1991). *Textbook of Medical Physiology*. Philadelphia: Saunders.

Harpuder, K., Stein, I. D., and Byer, J. (1940). The Role of the Arteriovenous Anastomosis in Peripheral Vascular Disease. *Am. Heart J.* 20 (5), 539–545. doi:10.1016/S0002-8703(40)90932-2

Hawke, F., and Burns, J. (2009). Understanding the Nature and Mechanism of Foot Pain. *J. Foot Ankle Res.* 2, 1. doi:10.1186/1757-1146-2-1

Hile, C., and Veves, A. (2003). Diabetic Neuropathy and Microcirculation. *Curr. Diab Rep.* 3 (6), 446–451. doi:10.1007/s11892-003-0006-0

Johnson, P. C. (1973). The Microcirculation of normal and Injured Tissue. *Adv. Exp. Med. Biol.* 33 (0), 45–51. doi:10.1007/978-1-4684-3228-2_5

Klabunde, R. E. (2012). *Cardiovascular Physiology Concepts*. Lippincott Williams & Wilkins/Wolters Kluwer. Available at: https://books.google.co.uk/books/about/Cardiovascular_Physiology_Concepts.html?id=27ExgvGnOagC&redir_esc=y (Accessed July 24, 2018).

Kluding, P. M., Bareiss, S. K., Hastings, M., Marcus, R. L., Sinacore, D. R., and Mueller, M. J. (2017). Physical Training and Activity in People with Diabetic Peripheral Neuropathy: Paradigm Shift. *Phys. Ther.* 97 (1), 31. doi:10.2522/PTJ.20160124

Koïtka, A., Abraham, P., Bouhanick, B., Sigaudo-Roussel, D., Demiot, C., and Saumet, J. L. (2004). Impaired Pressure-Induced Vasodilation at the Foot in Young Adults with Type 1 Diabetes. *Diabetes* 53 (3), 721–725. doi:10.2337/DIABETES.53.3.721

Körei, A. E., Istenes, I., Papanas, N., and Kempler, P. (2016). Small-Fiber Neuropathy. *Angiology* 67 (1), 49–57. doi:10.1177/0003319715583595

Korzon-Burakowska, A., and Edmonds, M. (2006). Role of the Microcirculation in Diabetic Foot Ulceration. *The Int. J. Lower Extremity Wounds* 5 (3), 144–148. doi:10.1177/1534734606292037

Krishnan, S. T. M., and Rayman, G. (2004). The LDIflare: a Novel Test of C-Fiber Function Demonstrates Early Neuropathy in Type 2 Diabetes. *Diabetes Care* 27 (12), 2930–2935. Available at: http://www.ncbi.nlm.nih.gov/pubmed/15562209 (Accessed May 10, 2018).

Lanting, S. M., Barwick, A. L., Twigg, S. M., Johnson, N. A., Baker, M. K., Chiu, S. K., et al. (2017). Post-occlusive Reactive Hyperaemia of Skin Microvasculature and Foot Complications in Type 2 Diabetes. *J. Diabetes its Complications* 31 (8), 1305–1310. doi:10.1016/j.jdiacomp.2017.05.005

Lanys, A., Moore, Z., and Avsar, P. (2021). What Is the Role of Local Inflammation in the Development of Diabetic Foot Ulcers? A Systematic Review - DiabetesontheNet. DiabetesontheNet. Available at: https://diabetesonthenet.com/diabetic-foot-journal/what-is-the-role-of-local-inflammation-in-the-development-of-diabetic-foot-ulcers-a-systematic-review/(Accessed August 15, 2021).

Larkin, S. W., and Williams, T. J. (1993). Evidence for Sensory Nerve Involvement in Cutaneous Reactive Hyperemia in Humans. *Circ. Res.* 73 (1), 147–154. doi:10.1161/01.RES.73.1.147

Ledoux, W. R., Shofer, J. B., Cowley, M. S., Ahroni, J. H., Cohen, V., and Boyko, E. J. (2013). Diabetic Foot Ulcer Incidence in Relation to Plantar Pressure Magnitude and Measurement Location. *J. Diabetes its Complications* 27 (6), 621–626. doi:10.1016/J.JDIACOMP.2013.07.004

LeMaster, J. W., Mueller, M. J., Reiber, G. E., Mehr, D. R., Madsen, R. W., and Conn, V. S. (2008). Effect of Weight-Bearing Activity on Foot Ulcer Incidence in People with Diabetic Peripheral Neuropathy: Feet First Randomized Controlled Trial. *Phys. Ther.* 88 (11), 1385–1398. doi:10.2522/ptj.20080019

Levin, M. E., O'Neal, L. W., Bowker, J. H., and Pfeifer, M. A. (2008). *Levin and O'Neal's the Diabetic Foot*. St. Louis: Mosby/Elsevier.

Liu, J., Bian, Z., Kuijpers-Jagtman, A. M., and Von den Hoff, J. W. (2010). Skin and Oral Mucosa Equivalents: Construction and Performance, *Orthod. Craniofac. Res.*, 13, 11–20. doi:10.1111/j.1601-6343.2009.01475.x

Lorenzo, S., and Minson, C. T. (2007). Human Cutaneous Reactive Hyperaemia: Role of BKCachannels and Sensory Nerves. *J. Physiol.* 585 (Pt 1), 295–303. doi:10.1113/jphysiol.2007.143867

Lung, C.-W., Wu, F.-L., Liao, F., Pu, F., Fan, Y., and Jan, Y.-K. (2020). Emerging Technologies for the Prevention and Management of Diabetic Foot Ulcers. *J. Tissue Viability* 29 (2), 61–68. doi:10.1016/j.jtv.2020.03.003

Maniewski, R., Wojtkiewicz, S., Zbieć, A., Wierzbowski, R., Liebert, A., and Maniewski, R. (2014). Prolonged Postocclusive Hyperemia Response in Patients with normal-tension Glaucoma. *Med. Sci. Monit.* 20, 2607–2616. doi:10.12659/MSM.891069

Marche, P., Dubois, S., Abraham, P., Parot-Schinkel, E., Gascoin, L., Humeau-Heurtier, A., et al. (2017). Neurovascular Microcirculatory Vasodilation Mediated by C-Fibers and Transient Receptor Potential Vanilloid-Type-1 Channels (TRPV 1) Is Impaired in Type 1 Diabetes. *Sci. Rep.* 7 (1). 44322 doi:10.1038/srep44322

Merrill, G. F. (2008). *Our Marvelous Bodies : An Introduction to the Physiology of Human Health*. Rutgers University Press.

M. J. Parnham (2016). *Compendium of Inflammatory Diseases* Springer Basel. doi:10.1007/978-3-7643-8550-7

Molnár, E., Lohinai, Z., Demeter, A., Mikecs, B., Tóth, Z., and Vág, J. (2015). Assessment of Heat Provocation Tests on the Human Gingiva: The Effect of Periodontal Disease and Smoking. *Acta Physiol. Hungarica* 102 (2), 176–188. doi:10.1556/036.102.2015.2.8

Morales, F., Graaff, R., Smit, A. J., Bertuglia, S., Petoukhova, A. L., Steenbergen, W., et al. (2005). How to Assess post-occlusive Reactive Hyperaemia by Means of Laser Doppler Perfusion Monitoring: Application of a Standardised Protocol to Patients with Peripheral Arterial Obstructive Disease. *Microvasc. Res.* 69 (1-2), 17–23. doi:10.1016/j.mvr.2005.01.006

Naemi, R., Chatzistergos, P., Suresh, S., Sundar, L., Chockalingam, N., and Ramachandran, A. (2017). Can Plantar Soft Tissue Mechanics Enhance Prognosis of Diabetic Foot Ulcer? *Diabetes Res. Clin. Pract.* 126, 182–191. doi:10.1016/j.diabres.2017.02.002

Nakamoto, T., Kanao, M., Kondo, Y., Kajiwara, N., Masaki, C., Takahashi, T., et al. (2012). Two-dimensional Real-Time Blood Flow and Temperature of Soft Tissue Around Maxillary Anterior Implants. *Implant Dent* 21 (6), 522–527. doi:10.1097/ID.0b013e318272fe81

Netten, P. M., Wollersheim, H., Thien, T., and Lutterman, J. A. (1996). Skin Microcirculation of the Foot in Diabetic Neuropathy. *Clin. Sci. (Lond).* 91 (5), 559–565. doi:10.1042/CS0910559

Pahwa, R., Goyal, A., Bansal, P., and Jialal, I. (2020). "Chronic Inflammation," in *StatPearls* Treasure Island: StatPearls. Available at: https://www.ncbi.nlm.nih.gov/books/NBK493173/(Accessed June 27, 2021).

Payne, G. W. (2006). Effect of Inflammation on the Aging Microcirculation: Impact on Skeletal Muscle Blood Flow Control. *Microcirculation* 13 (4), 343–352. doi:10.1080/10739680600618918

Pham, H., Armstrong, D. G., Harvey, C., Harkless, L. B., Giurini, J. M., and Veves, A. (2000). Screening Techniques to Identify People at High Risk for Diabetic Foot Ulceration: a Prospective Multicenter Trial. *Diabetes Care* 23 (5), 606–611. doi:10.2337/diacare.23.5.606

Pu, F., Ren, W., Fu, H., Zheng, X., Yang, M., Jan, Y.-K., et al. (2018). Plantar Blood Flow Response to Accumulated Pressure Stimulus in Diabetic People with Different Peak Plantar Pressure: a Non-randomized Clinical Trial. *Med. Biol. Eng. Comput.* 56 (7), 1127–1134. doi:10.1007/s11517-018-1836-x

Quyyumi, A. A., and Ozkor, M. (2006). Vasodilation by Hyperpolarization. *Hypertension* 48 (6), 1023–1025. doi:10.1161/01.HYP.0000250965.03934.15

Rayman, G., Williams, S. A., Spencer, P. D., Smaje, L. H., Wise, P. H., and Tooke, J. E. (1986). Impaired Microvascular Hyperaemic Response to Minor Skin Trauma in Type I Diabetes. *Bmj* 292 (6531), 1295–1298. Available at: http://www.ncbi.nlm.nih.gov/pubmed/2939920 (Accessed August 8, 2018).

Ren, W., Xu, L., Zheng, X., Pu, F., Li, D., and Fan, Y. (2021). Effect of Different thermal Stimuli on Improving Microcirculation in the Contralateral Foot. *Biomed. Eng. Online* 20 (1), 1–10. doi:10.1186/s12938-021-00849-9

Sarin, S., Shami, S., Shields, D. A., Scurr, J. H., and Coleridge Smith, P. D. (1991). Selection of Amputation Level: a Review. *Eur. J. Vasc. Surg.* 5 (6), 611–620. doi:10.1016/s0950-821x(05)80894-1

Saumet, J. L. (2005). [Cutaneous Vasodilation Induced by Local Pressure Application: Modifications in Diabetes]. *Bull. Acad. Natl. Med.* 189 (1), 99–105. Available at: http://ezproxy.staffs.ac.uk/login?url=http://search.ebscohost.com/login.aspx? direct=true&db=cmedm&AN=16119883&site=ehost-live.

Schaper, N. C., Huijberts, M., and Pickwell, K. (2008). Neurovascular Control and Neurogenic Inflammation in Diabetes. *Diabetes Metab. Res. Rev.* 24 (Suppl. 1), S40–S44. doi:10.1002/dmrr.862

Schaper, N. C., Van Netten, J. J., Apelqvist, J., Lipsky, B. A., and Bakker, K. (2016). Prevention and Management of Foot Problems in Diabetes: A Summary Guidance for Daily Practice 2015, Based on the IWGDF Guidance Documents. *Diabetes Metab. Res. Rev.* 32, 7–15. doi:10.1002/dmrr.2695

Schlager, O., Hammer, A., Willfort-Ehringer, A., Fritsch, M., Rami-Merhar, B., Schober, E., et al. (2012). Microvascular Autoregulation in Children and Adolescents with Type 1 Diabetes Mellitus. *Diabetologia* 55 (6), 1633–1640. doi:10.1007/s00125-012-2502-8

Schramm, J. C., Dinh, T., and Veves, A. (2006). Microvascular Changes in the Diabetic Foot. *Int. J. Lower Extremity Wounds* 5 (3), 149–159. doi:10.1177/1534734606292281

Shahwan, S. (2015). Factors Related to Pressure Ulcer Development with Diabetic Neuropathy. *Clin. Res. Trial* 1 (4). 102–105. doi:10.15761/CRT.1000124

Shapiro, J., and Nouvong, A. (2011). "Assessment of Microcirculation and the Prediction of Healing in Diabetic Foot Ulcers," in *Topics in the Prevention, Treatment and Complications of Type 2 Diabetes* (Riijeka, Croatia: IntechOpen), 215–226. doi:10.5772/21967

Singh, V. P., Bali, A., Singh, N., and Jaggi, A. S. (2014). Advanced Glycation End Products and Diabetic Complications. *Korean J. Physiol. Pharmacol.* 18 (1), 1–14. doi:10.4196/kjpp.2014.18.1.1

Stirban, A., Gawlowski, T., and Roden, M. (2014). Vascular Effects of Advanced Glycation Endproducts: Clinical Effects and Molecular Mechanisms. *Mol. Metab.* 3 (2), 94–108. doi:10.1016/j.molmet.2013.11.006

Themistocleous, A. C., Ramirez, J. D., Serra, J., and Bennett, D. L. H. (2014). The Clinical Approach to Small Fibre Neuropathy and Painful Channelopathy. *Pract. Neurol.* 14 (6), 368–379. doi:10.1136/practneurol-2013-000758

Tracy, R. P. (2006). The Five Cardinal Signs of Inflammation: Calor, Dolor, Rubor, Tumor And Penuria (Apologies to Aulus Cornelius Celsus, De Medicina, C. A.D. 25). *Journals Gerontol. Ser. A: Biol. Sci. Med. Sci.* 61 (10), 1051–1052. doi:10.1093/gerona/61.10.1051

Vanderah, T. W. (2007). Pathophysiology of Pain. *Med. Clin. North America* 91 (1), 1–12. doi:10.1016/j.mcna.2006.10.006

Vas, P. R. J., Green, A. Q., and Rayman, G. (2012). Small Fibre Dysfunction, Microvascular Complications and Glycaemic Control in Type 1 Diabetes: a Case-Control Study. *Diabetologia* 55 (3), 795–800. doi:10.1007/s00125-011-2417-9

Veves, A., Giurini, J. M., and LoGerfo, F. W. (2006). *The Diabetic Foot*. Totowa: Humana Press.

Veves, A., Murray, H. J., Young, M. J., and Boulton, A. J. M. (1992). The Risk of Foot Ulceration in Diabetic Patients with High Foot Pressure: a Prospective Study. *Diabetologia* 35 (7), 660–663. doi:10.1007/bf00400259

Vinik, A. I., Erbas, T., Stansberry, K. B., and Pittenger, G. L. (2001). Small Fiber Neuropathy and Neurovascular Disturbances in Diabetes Mellitus. *Exp. Clin. Endocrinol. Diabetes* 109, S451–S473. doi:10.1055/s-2001-18602

Vouillarmet, J., Josset-Lamaugarny, A., Michon, P., Saumet, J. L., Koitka-Weber, A., Henni, S., et al. (2019). Neurovascular Response to Pressure in Patients with Diabetic Foot Ulcer. *Diabetes*, 68 832. doi:10.2337/DB18-0694

Williams, D. T., Norman, P. E., and Stacey, M. C. (2004). Comparative roles of microvascular and nerve function in poof ulceration in type 2 diabetes: Response to Krishnan et al. [9] (multiple letters). *Diabetes Care* 27 (12), 1343–1348. doi:10.2337/diacare.27.12.3026

World Health Organization (2016). *Global Report on Diabetes*. Geneva: WHO, 83.

Zimny, S., Dessel, F., Ehren, M., Pfohl, M., and Schatz, H. (2001). Early Detection of Microcirculatory Impairment in Diabetic Patients with Foot at Risk. *Diabetes Care* 24 (10), 1810–1814. doi:10.2337/diacare.24.10.1810

Conflict of Interest: The authors declare that the research was conducted in the absence of any commercial or financial relationships that could be construed as a potential conflict of interest.

Publisher's Note: All claims expressed in this article are solely those of the authors and do not necessarily represent those of their affiliated organizations, or those of the publisher, the editors and the reviewers. Any product that may be evaluated in this article, or claim that may be made by its manufacturer, is not guaranteed or endorsed by the publisher.

frontiers in Bioengineering and Biotechnology

ORIGINAL RESEARCH
published: 15 September 2021
doi: 10.3389/fbioe.2021.727940

Morphology and Mechanical Properties of Plantar Fascia in Flexible Flatfoot: A Noninvasive *In Vivo* Study

Zhihui Qian[1], Zhende Jiang[1], Jianan Wu[1], Fei Chang[2], Jing Liu[1], Lei Ren[1,3]* and Luquan Ren[1]*

[1]Key Laboratory of Bionic Engineering, Jilin University, Changchun, China, [2]Orthopaedic Medical Center, The Second Hospital of Jilin University, Changchun, China, [3]School of Mechanical, Aerospace and Civil Engineering, University of Manchester, Manchester, United Kingdom

Plantar fascia plays an important role in human foot biomechanics; however, the morphology and mechanical properties of plantar fascia in patients with flexible flatfoot are unknown. In this study, 15 flexible flatfeet were studied, each plantar fascia was divided into 12 positions, and the morphologies and mechanical properties in the 12 positions were measured *in vivo* with B-mode ultrasound and shear wave elastography (SWE). Peak pressures under the first to fifth metatarsal heads (MH) were measured with FreeStep. Statistical analysis included 95% confidence interval, intragroup correlation coefficient ($ICC_{1,1}$), one-way analysis of variance (one-way ANOVA), and least significant difference. The results showed that thickness and Young's modulus of plantar fascia were the largest at the proximal fascia (PF) and decreased gradually from the proximal end to the distal end. Among the five distal branches (DB) of the fascia, the thickness and Young's modulus of the second and third DB were larger. The peak pressures were also higher under the second and third MH. This study found a gradient distribution in that the thickness and Young's modulus gradient decreased from the proximal end to the distal end of plantar fascia in the longitudinal arch of flexible flatfeet. In the transverse arch, the thickness and Young's modulus under the second and third DB were larger than those under the other three DB in flexible flatfoot, and the peak pressures under the second and third MH were also larger than those under the other three MH in patients with flexible flatfoot. These findings deepen our understanding of the changes of biomechanical properties and may be meaningful for the study of pathological mechanisms and therapy for flexible flatfoot.

Keywords: flexible flatfoot, plantar fascia, shear wave elastography, morphology properties, mechanical properties

OPEN ACCESS

Edited by:
Fang Pu,
Beihang University, China

Reviewed by:
Wenxin Niu,
Tongji University, China
LianWen Sun,
Beihang University, China

****Correspondence:***
Lei Ren
lei.ren@manchester.ac.uk
Jing Liu
jingliu@jlu.edu.cn

Specialty section:
This article was submitted to Biomechanics, a section of the journal Frontiers in Bioengineering and Biotechnology

Received: *20 June 2021*
Accepted: *16 August 2021*
Published: *15 September 2021*

Citation:
Qian Z, Jiang Z, Wu J, Chang F, Liu J, Ren L and Ren L (2021) Morphology and Mechanical Properties of Plantar Fascia in Flexible Flatfoot: A Noninvasive In Vivo *Study. Front. Bioeng. Biotechnol. 9:727940. doi: 10.3389/fbioe.2021.727940*

INTRODUCTION

Plantar fascia is a ligament that attaches the calcaneus to metatarsals (Orchard, 2012). It plays an important role in passive force transmission (Stecco et al., 2013). Its main task is to stabilize the arch of the foot and reduce the influence of ground reaction force on metatarsal heads (MH) and the longitudinal foot arch (Hicks, 1954; Ker et al., 1987; McKeon et al., 2015). There is a close

Abbreviations: SWE, shear wave elastography; PF, proximal fascia; MF, middle fascia; BF, branches of fascia; DB, distal branches; ROI, region of interest; 95% CI, 95% confidence interval; ICC1,1, intragroup correlation coefficient; one-way ANOVA, one-way analysis of variance; MH, metatarsal head; COP, center of pressure.

relationship between plantar fascia and foot function, and studies have shown that when plantar fascia changes, it will produce clinical problems, for example, heel pain (Wearing et al., 2006). Thus, research on plantar fascia has a broad interest.

During the past decades, numerous studies on plantar fascia have been conducted. Guo et al. (2018) found a certain relationship between the mechanical tension of plantar fascia and fiber morphology. Chen et al. (2019a,b) found that people who used forefoot strike were more likely to suffer from plantar fasciitis. Tas and Cetin (2019a) focused on the relationship between plantar pressure distribution and the morphology and mechanical properties of plantar fascia. Welte et al. (2021) revealed the effect of plantar fascia extensibility on the windlass mechanism of plantar fascia. Wang et al. (2019) illustrated the morphology and mechanical properties of plantar fascia in normal feet. These studies strengthen the understanding of the mechanical properties of plantar fascia in normal feet. However, to the author's knowledge, the morphology and mechanical properties of the whole plantar fascia of flexible flatfeet have not been reported to date.

Flatfoot is a common foot posture abnormality, with the highest incidence of 78% (Sung, 2016), and is characterized by a low medial longitudinal arch (Pehlivan et al., 2009). Flatfoot can be divided into rigid flatfoot and flexible flatfoot. Rigid flatfoot means that the medial longitudinal arch is always missing in both load-bearing and nonload-bearing positions. Flexible flatfoot means that the medial longitudinal arch is missing only in the load-bearing position, while in the nonload-bearing position, it is the same as that of a normal foot (Carr et al., 2016). The abnormal structural changes of the flexible flatfoot under load will gradually lead to changes in the morphology and mechanical properties of the plantar fascia, which may lead to plantar fasciitis and other diseases. The changes in the morphology and mechanical properties of plantar fascia will in turn affect the foot kinematics of patients with flatfoot, resulting in clinical symptoms such as patellar tendinopathy and medial tibial stress syndrome (Kohls-Gatzoulis et al., 2004; Van der Worp et al., 2011; Hamstra-Wright et al., 2015). Studies have shown that the potential cause of plantar fasciitis is the abnormal morphology and mechanical properties of plantar fascia (Wearing et al., 2006; Wu et al., 2011).

Therefore, the objective of this study was to investigate the morphology and mechanical properties of plantar fascia of patients with flexible flatfoot by B-mode ultrasound and shear wave elastography (SWE) *in vivo*. A comprehensive analysis was conducted combined with plantar pressure measurement. The results of the study may provide a meaningful reference and basis for analysis of the pathological mechanism and rehabilitation in patients with flexible flatfoot as well as more accurate definitions for foot finite element models.

METHODS

Ethics Statement

This study was based on the principles outlined in the Helsinki Declaration, which was approved by the Ethics Committee of the Second Hospital of Jilin University (No. 2020085). All volunteers who participated in the study signed written informed consent agreements.

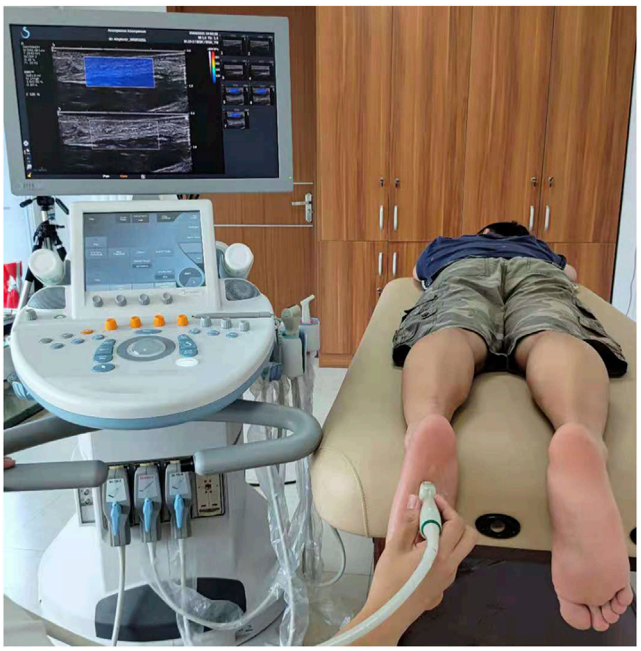

FIGURE 1 | The experimental device and the position of the subjects.

Selection of Research Subjects

The subjects of this experiment were patients with flexible flatfeet. They had the typical characteristics in that the medial longitudinal arch was missing only in the load-bearing position, while in the nonload-bearing position, it was the same as that of a normal foot (Carr et al., 2016). An intelligent scanner was employed to confirm the diagnosis and severity of flatfeet, of which the diagnostic principle was the arch index proposed by Cavanagh et al. (1987). The arch index was widely accepted and adopted (Wearing et al., 2004; Wong et al., 2012; Nirenberg et al., 2020; Wang et al., 2020). The inclusion criteria were as follows: 1) healthy male, 20–30 years old; 2) the diagnosis being flexible flatfeet; and 3) no history of other foot diseases. The exclusion criteria were as follows: 1) rigid flatfeet; 2) a history of foot trauma or surgery; 3) presence of systemic diseases that may affect plantar fascia, such as rheumatoid arthritis, diabetes, and gout; and 4) the presence of diseases that affect local plantar fascia, such as calcaneal spur or nodular fasciitis and plantar fibromatosis. Finally, 10 volunteers with 15 flexible flatfeet were included, and the basic characteristics of the volunteers were age, 26.2 ± 1.6 years; weight, 65.2 ± 2.2 kg; height, 175.2 ± 2.7 cm.

Test Device and Procedure

The subjects were asked to avoid intense sports 1 week before the test. B-mode and SWE mode of an Aixplorer ultrasonic scanner (Aixplorer ultrasonic imager, Aix-en-Provence, France) were used to measure the thickness and Young's modulus of plantar fascia, respectively. The linear transducer frequency was 10–2 MHz

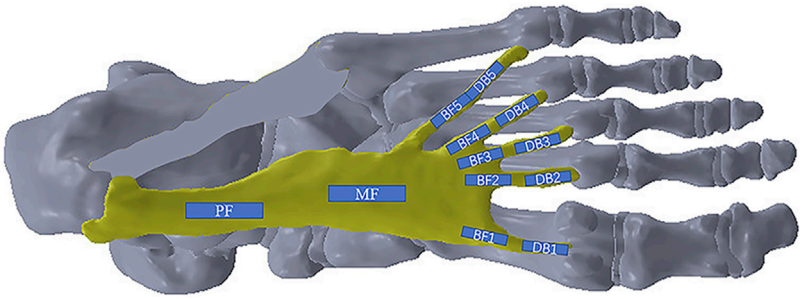

FIGURE 2 | The measuring positions of the plantar fascia.

for this study. The sampling depth was adjusted according to the positions of plantar fascia. It was set at 1.5–2.5 cm to include the whole plantar fascia, and the mechanical index was 1.0 in this study. During measurement, each subject lay prone on the examination bed, with the lower limbs straight and the feet hanging naturally (Haen et al., 2017) on the edge of the examination bed (**Figure 1**). The upper body and legs were relaxed.

In order to observe the entire changes in the plantar fascia, it was divided into four main regions: proximal fascia (PF), middle fascia (MF), five branches of fascia (BF1-BF5), and five distal branches (DB1-DB5), 12 positions in total (**Figure 2**). The PF was measured at a point 1 cm away from the insertion to the calcaneus. The location of the five DBs was defined as the farthest end where the plantar fascia has not been fused with joint capsule. The ultrasonic transducer was parallel to the plantar fascia, and the thickness of plantar fascia was measured in the middle of every position. Subsequently, the elastic measurement via SWE was performed. The width of the square-shaped elastography window (region of interest, ROI) was as large as possible, and the height was set to include the complete plantar fascia. Q-Box^{TM}Trace was used to measure Young's modulus (maximum, minimum, and average, in kPa) of plantar fascia with a length of 1 cm at each position, and Young's modulus scale was adjusted to 0–600 kPa (Wang et al., 2019). Additionally, the mean Young's modulus value was used for the data analysis in the study. At each position, Young's modulus and thickness of plantar fascia were measured three times.

Plantar Pressure Measurement

FreeStep (Sensor Medica, Italy) was employed to detect the plantar pressure of the subjects during level walking. Subjects were requested to walk normally, without rushing, acceleration, or deceleration. Data were collected barefoot at a self-selected speed (Rao et al., 2011; Hillstrom et al., 2013) along a 2 m walkway, and the walking velocity was 1.33 ± 0.97 m/s. The peak pressures under the first to fifth MH were measured during the push-off stage.

Statistical Analysis

IBM Statistical Package for the Social Sciences (SPSS) statistical software version 26.0 (SPSS Inc., Chicago, IL, United States) was used to analyze all the data. The 95% confidence interval (95% CI) and intragroup correlation coefficient ($ICC_{1,1}$) were used to measure and evaluate the reliability of plantar fascia thickness and Young's modulus. Generally, the values of $ICC_{1,1}$ in the ranges of 0–0.40, 0.41–0.6, 0.61–0.79, and 0.8–1.0, respectively, indicate poor, medium, good, and excellent reliability. At the same time, the one-way analysis of variance (one-way ANOVA) was used to compare the differences between different positions of plantar fascia. If the result of one-way ANOVA was $p < 0.05$, least significant difference was used to compare the differences between every two positions of plantar fascia. For least significant difference, P values we used had been corrected by the number of pairwise comparisons. Statistical difference was defined as $p < 0.05$. In order to better understand the spatial distribution in thickness and Young's modulus of plantar fascia, an exponential function (first-order exponential decay) was used to fit and analyze the variation trend of plantar fascia from the calcaneal to the five DB.

TABLE 1 | Intragroup correlation results of thickness and Young's modulus in 15 flexible flatfeet.

Foot identity	Thickness		Young's modulus	
	$ICC_{1,1}$ 95%CI	95%CI	$ICC_{1,1}$	95%CI
#1	0.994	(0.984, 0.998)	0.999	(0.998,1.000)
#2	0.991	(0.977, 0.997)	0.995	(0.987,0.999)
#3	0.994	(0.985, 0.998)	0.996	(0.989,0.999)
#4	0.987	(0.964, 0.996)	0.999	(0.996,1.000)
#5	0.981	(0.950, 0.994)	0.998	(0.994,0.999)
#6	0.986	(0.963, 0.996)	0.997	(0.991, 0.999)
#7	0.977	(0.938, 0.993)	0.996	(0.989,0.999)
#8	0.995	(0.986, 0.998)	0.988	(0.968,0.996)
#9	0.988	(0.969, 0.996)	0.992	(0.979,0.998)
#10	0.979	(0.944, 0.993)	0.996	(0.990, 0.999)
#11	0.979	(0.945, 0.993)	0.995	(0.987, 0.999)
#12	0.976	(0.938, 0.993)	0.996	(0.989, 0.999)
#13	0.981	(0.950, 0.994)	0.985	(0.961, 0.995)
#14	0.981	(0.951, 0.994)	0.993	(0.980, 0.998)
#15	0.988	(0.969, 0.996)	0.999	(0.996,1.000)

RESULTS

Intragroup Correlation Results of Thickness and Young's Modulus

The intragroup correlation results of the thickness and Young's modulus of the 15 flatfeet are listed in **Table 1**. The $ICC_{1,1}$ ranged

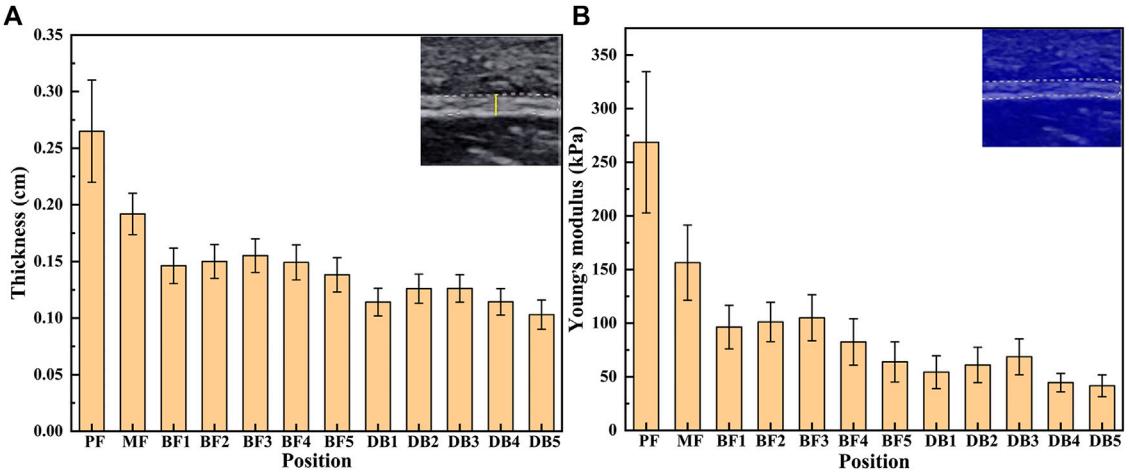

FIGURE 3 | The thickness **(A)** and Young's modulus **(B)** of plantar fascia of 15 flexible flatfeet.

from 0.976 to 0.995 and the corresponding 95% CI was 0.938, 0.998 for thickness of plantar fascia. The $ICC_{1,1}$ ranged from 0.985 to 0.999 and the 95% CI was 0.961, 1.000 for Young's modulus of plantar fascia.

Distribution Pattern of Thickness and Young's Modulus of Plantar Fascia

The results of thickness and Young's modulus of plantar fascia of 15 flexible flatfeet are shown in **Figure 3**. The results showed that both the thickness and Young's modulus of plantar fascia decreased gradually from the proximal end to the distal end. Among the five DB, the thickness and Young's modulus of the second and third branches were larger than the other three.

The one-way ANOVA was used to compare the differences between different positions of plantar fascia. If the result of one-way ANOVA was $p < 0.05$, least significant difference was used to compare the differences between every two positions of plantar fascia. The one-way ANOVA results showed that the differences in thickness and Young's modulus between different positions were statistically significant ($p < 0.05$). Least significant difference results showed that, in terms of plantar fascia thickness, PF > MF > all the five BFs > all the five DBs. Among the five DBs, DB2 and DB3 > DB1 and DB4 > DB5. The differences were statistically significant ($p < 0.05$). There was no statistical difference between DB2 and DB3, and there was also no statistical difference between DB1 and DB4 (**Table 2**). For Young's modulus, PF > MF > all the five BF > the corresponding position of DB. Among the five DBs, DB2 > DB4 and DB5; DB3 > DB1 and DB4 and DB5; DB1 > DB5. All the differences were statistically significant ($p < 0.05$). There was no statistical difference between DB2 and DB3, and no statistical difference was found between DB2 and DB1. There was also no statistical difference between DB4 and DB5 (**Table 3**).

Peak Pressure Distribution Under Five MHs

The peak pressure under five MHs of 15 flexible flatfeet is shown in **Figure 4**. The pressures under the second and third MH were higher than those under the other three MH, and the differences were statistically significant ($p < 0.05$) (**Table 4**). This distribution pattern is similar to the thickness and Young's modulus in the five DBs.

Spatial Distribution of Plantar Fascia Thickness and Young's Modulus

In order to better understand the spatial distribution in thickness and Young's modulus of plantar fascia, an exponential function (first-order exponential decay) was used to fit and analyze the variation trend of plantar fascia from the calcaneal to the five DB.

The spatial distribution of plantar fascia thickness and Young's modulus of foot #1 is shown in **Figure 5**. The results showed that the thickness and Young's modulus of plantar fascia were the largest at the calcaneus tubercle, and the thickness and Young's modulus of five fascial bundles gradually decreased as plantar fascia extended from the calcaneus to the five toes. The spatial distribution of thickness and Young's modulus in the other 14 flexible flatfeet also showed a similar tendency. The thickness and Young's modulus of plantar fascia of 15 flatfeet at PF and five DBs are shown in **Figure 6**.

DISCUSSION

This study investigated the morphology and mechanical properties of plantar fascia of patients with flexible flatfoot by B-mode ultrasound and ultrasonic elastography *in vivo*. A comprehensive analysis was conducted combined with plantar pressure measurements.

In order to evaluate the accuracy of the data, the repeatability of the thickness and Young's modulus data was analyzed in all 15 flexible flatfeet. The results showed that all the values of $ICC_{1,1}$ were more than 0.9, which indicated that the data of the study had good reliability. At the same time, a previous study reported that B-mode ultrasound was a reliable and reproducible method for detecting the thickness of plantar fascia and SWE mode was a reliable and reproducible method for detecting the elasticity of plantar fascia (Wang et al., 2019).

TABLE 2 | *P* value of least significant difference results between different positions in thickness of plantar fascia.

Position/ Thickness (mm)	MF	BF1	BF2	BF3	BF4	BF5	DB1	DB2	DB3	DB4	DB5
PF (0.265 ± 0.045)	0.000[a]	0.000[a]	0.000[a]	0.000[a]	0.000[a]	0.000[a]	0.000[a]	0.000[a]	0.000[a]	0.000[a]	0.000[a]
MF (0.192 ± 0.018)	—	0.000[a]	0.000[a]	0.000[a]	0.000[a]	0.000[a]	0.000[a]	0.000[a]	0.000[a]	0.000[a]	0.000[a]
BF1 (0.146 ± 0.016)	0.000[a]	—	0.33	0.024[a]	0.452	0.048[a]	0.000[a]	0.000[a]	0.000[a]	0.000[a]	0.000[a]
BF2 (0.150 ± 0.015)	0.000[a]	0.33	—	0.2	0.824	0.003[a]	0.000[a]	0.000[a]	0.000[a]	0.000[a]	0.000[a]
BF3 (0.155 ± 0.015)	0.000[a]	0.024[a]	0.2	—	0.133	0.000[a]	0.000[a]	0.000[a]	0.000[a]	0.000[a]	0.000[a]
BF4 (0.149 ± 0.015)	0.000[a]	0.452	0.824	0.133	—	0.006[a]	0.000[a]	0.000[a]	0.000[a]	0.000[a]	0.000[a]
BF5 (0.138 ± 0.015)	0.000[a]	0.048[a]	0.003[a]	0.000[a]	0.006[a]	—	0.000[a]	0.002[a]	0.003[a]	0.000[a]	0.000[a]
DB1 (0.114 ± 0.012)	0.000[a]	0.000[a]	0.000[a]	0.000[a]	0.000[a]	0.000[a]	—	0.003[a]	0.003[a]	0.942	0.000[a]
DB2 (0.126 ± 0.013)	0.000[a]	0.000[a]	0.000[a]	0.000[a]	0.000[a]	0.002[a]	0.003[a]	—	0.96	0.004[a]	0.000[a]
DB3 (0.126 ± 0.012)	0.000[a]	0.000[a]	0.000[a]	0.000[a]	0.000[a]	0.003[a]	0.003[a]	0.96	—	0.003[a]	0.000[a]
DB4 (0.114 ± 0.012)	0.000[a]	0.000[a]	0.000[a]	0.000[a]	0.000[a]	0.000[a]	0.942	0.004[a]	0.003[a]	—	0.004[a]
DB5 (0.103 ± 0.013)	0.000[a]	0.000[a]	0.000[a]	0.000[a]	0.000[a]	0.000[a]	0.006[a]	0.000[a]	0.000[a]	0.004[a]	—

[a]*Difference was statistically significant.*

P *values have been corrected (multiplied by k); k represents the number of pairwise comparisons. There were 12 positions; thus, k = 66.*

"/" = the same position.

TABLE 3 | *P* value of least significant difference results between different positions in Young's modulus of plantar fascia.

Position/ Young's modulus (KPa)	MF	BF1	BF2	BF3	BF4	BF5	DB1	DB2	DB3	DB4	DB5
PF (268.662 ± 65.970)	0.000[a]	0.000[a]	0.000[a]	0.000[a]	0.000[a]	0.000[a]	0.000[a]	0.000[a]	0.000[a]	0.000[a]	0.000[a]
MF (156.407 ± 35.046)	—	0.000[a]	0.000[a]	0.000[a]	0.000[a]	0.000[a]	0.000[a]	0.000[a]	0.000[a]	0.000[a]	0.000[a]
BF1 (96.302 ± 20.356)	0.000[a]	—	0.399	0.126	0.015[a]	0.000[a]	0.000[a]	0.000[a]	0.000[a]	0.000[a]	0.000[a]
BF2 (101.060 ± 18.322)	0.000[a]	0.399	—	0.492	0.001[a]	0.000[a]	0.000[a]	0.000[a]	0.000[a]	0.000[a]	0.000[a]
BF3 (104.938 ± 21.512)	0.000[a]	0.126	0.492	—	0.000[a]	0.000[a]	0.000[a]	0.000[a]	0.000[a]	0.000[a]	0.000[a]
BF4 (82.553 ± 21.637)	0.000[a]	0.015[a]	0.001[a]	0.000[a]	—	0.001[a]	0.000[a]	0.000[a]	0.013[a]	0.000[a]	0.000[a]
BF5 (63.860 ± 18.791)	0.000[a]	0.000[a]	0.000[a]	0.000[a]	0.001[a]	—	0.09	0.613	0.404	0.001[a]	0.000[a]
DB1 (54.271 ± 15.303)	0.000[a]	0.000[a]	0.000[a]	0.000[a]	0.000[a]	0.09	—	0.233	0.011[a]	0.084	0.024[a]
DB2 (61.004 ± 16.479)	0.000[a]	0.000[a]	0.000[a]	0.000[a]	0.000[a]	0.613	0.233	—	0.18	0.004[a]	0.001[a]
DB3 (68.567 ± 16.750)	0.000[a]	0.000[a]	0.000[a]	0.000[a]	0.13	0.404	0.011[a]	0.18	—	0.000[a]	0.000[a]
DB4 (44.500 ± 8.578)	0.000[a]	0.000[a]	0.000[a]	0.000[a]	0.000[a]	0.001[a]	0.084	0.004[a]	0.000[a]	—	0.598
DB5 (41.524 ± 10.270)	0.000[a]	0.000[a]	0.000[a]	0.000[a]	0.000[a]	0.000[a]	0.024[a]	0.001[a]	0.000[a]	0.598	—

[a]*Difference was statistically significant.*

P *values have been corrected (multiplied by k); k represents the number of pairwise comparisons. There were 12 positions; thus, k = 66.*

"/" = the same position.

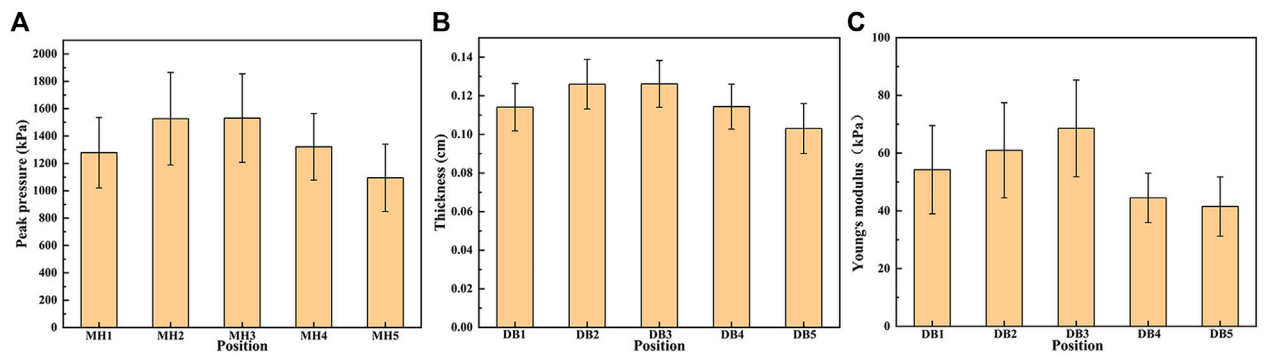

FIGURE 4 | The peak pressure under the five metatarsal heads (MH1–MH5) **(A)**, the thickness **(B),** and Young's modulus **(C)** in the five distal branches of the plantar fascia in 15 flatfeet.

Plantar fasciitis is one of the most common foot musculoskeletal diseases in primary diagnosis and treatment institutions (Thing et al., 2012; Young, 2012), and it is more likely to occur in patients with flatfoot than with normal foot (Riddle et al., 2003). It is characterized by heel pain after rest because it mainly affects the plantar fascia inserted into the

TABLE 4 | *P* value of least significant difference results between different positions in peak pressure.

Position	MH1	MH2	MH3	MH4	MH5
MH1 (1278.400 ± 258.050)	—	0.000[a]	0.000[a]	0.411	0.000[a]
MH2 (1526.400 ± 338.292)	0.000[a]	—	0.927	0.411	0.000[a]
MH3 (1531.200 ± 323.522)	0.000[a]	0.927	—	0.000[a]	0.000[a]
MH4 (1321.200 ± 243.951)	0.411	0.000[a]	0.000[a]	—	0.000[a]
MH5 (1094.800 ± 246.413)	0.000[a]	0.000[a]	0.000[a]	0.000[a]	—

[a]*Difference was statistically significant.*

P values have been corrected (multiplied by k); k represents the number of pairwise comparisons. There were five positions; thus, k = 10.

"/" = the same position.

calcaneus (Huang et al., 2000). The pain can also extend along the length of the plantar fascia (Thomas et al., 2016; Babatunde et al., 2019). In this study, the maximum Young's modulus of proximal plantar fascia was 387.1kPa, while that of a normal foot was about 300kPa (Wang et al., 2019). Studies showed that there was a positive correlation between Young's modulus and tendon force (Yeh et al., 2013; Yeh et al., 2016). Thus, the increased Young's modulus of the proximal plantar fascia indicates that the plantar fascia bears greater stress, leading more easily to the degeneration of plantar fascia (Huffer et al., 2017). The increase of Young's modulus in plantar fascia near calcaneus attachment in patients with flatfoot may provide a theoretical explanation for the high incidence of plantar fasciitis in patients with flatfoot.

The results of the study showed that the plantar fascia of the flexible flatfoot was spatially dependent from proximal to distal, and the thickness and Young's modulus of the five branches decreased gradually from proximal to distal. The differences between different parts were statistically significant. This feature of gradient changes is consistent with the results in normal plantar fascia (Wang et al., 2019). In the finite element model, the plantar fascia is often regarded as a linear elastic material, and the whole plantar fascia has the same Young's modulus (Phan et al., 2021). Thus, the spatial distribution feature (different Young's modulus in different regions) obtained in this study is helpful to define more accurate material properties for flatfeet finite element models to achieve more meaningful simulation results.

However, among the DB, Wang et al. (2019) showed that the thickness and Young's modulus between the five branches of the normal plantar fascia were the greatest under the first MH, while this study showed that the thickness and Young's modulus under the second and third MH were greater in patients with flexible flatfoot. At the same time, this study showed that the peak pressures under the second and third MH were greater than that under the fourth and fifth MH, which was consistent with the results of Buldt et al. (2018) and Hillstrom et al. (2013). It is speculated that this result may be due to the difference in the degree of collapse of the medial and lateral longitudinal arches in patients with flexible flatfoot. These results indicate that, in patients with flexible flatfoot, the degree of collapse of the medial longitudinal arch is more than that of the lateral arch, resulting in higher force and higher pressure on the medial side in the push-off phase. The stronger pressure stimulates plantar fascia, leading to its degeneration (Wearing et al., 2006). Shiotani et al. (2019) also noted that plantar fascia is mechanically stretched, so the morphology and mechanical properties of plantar fascia may be adapted to stress accumulation.

The center of pressure (COP) is defined as the centroid of the pressure distribution at a series of moments in time as the ground reaction is applied over the plantar surface of the foot (Cho and Choi, 2005). It was found that the peak pressures under the

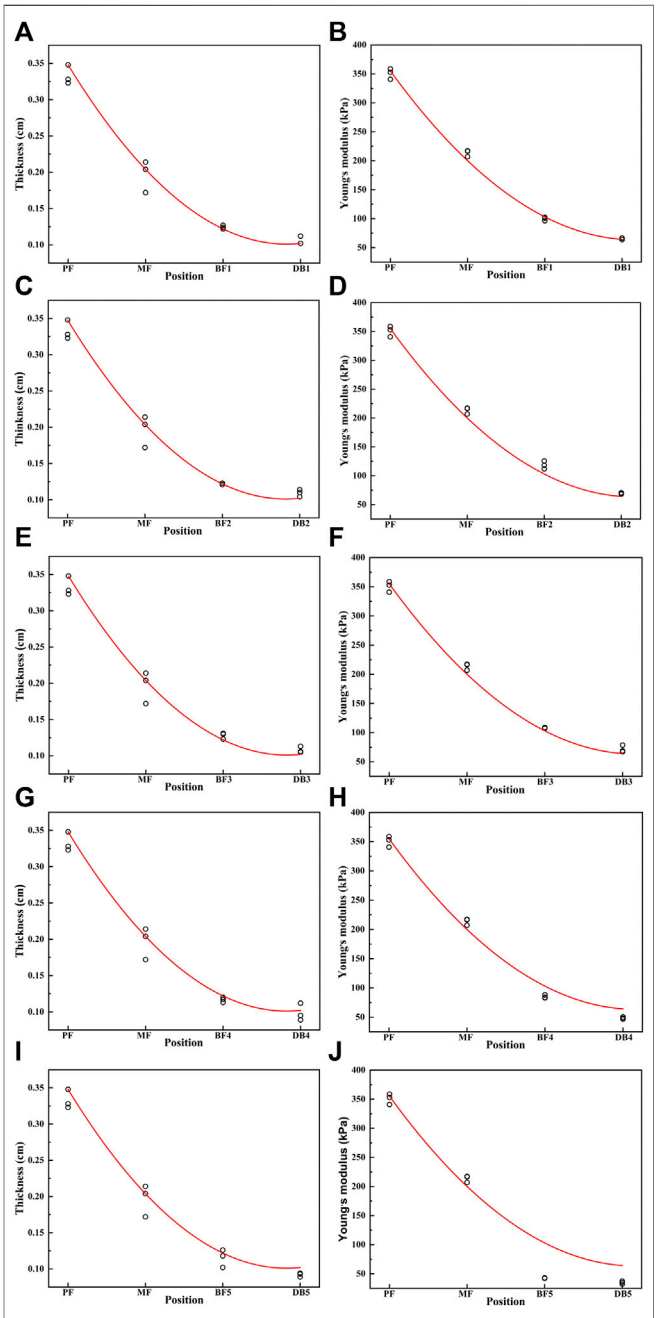

FIGURE 5 | The curve of the thickness and Young's modulus of the plantar fascia from the calcaneus to the five distal branches in foot #1: **(A)** thickness of the first branch, **(B)** Young's modulus of the first branch, **(C)** thickness of the second branch, **(D)** Young's modulus of the second branch, **(E)** thickness of the third branch, **(F)** Young's modulus of the third branch, **(G)** thickness of the forth branch, **(H)** Young's modulus of the forth branch, **(I)** thickness of the fifth branch, and **(J)** Young's modulus of the fifth branch.

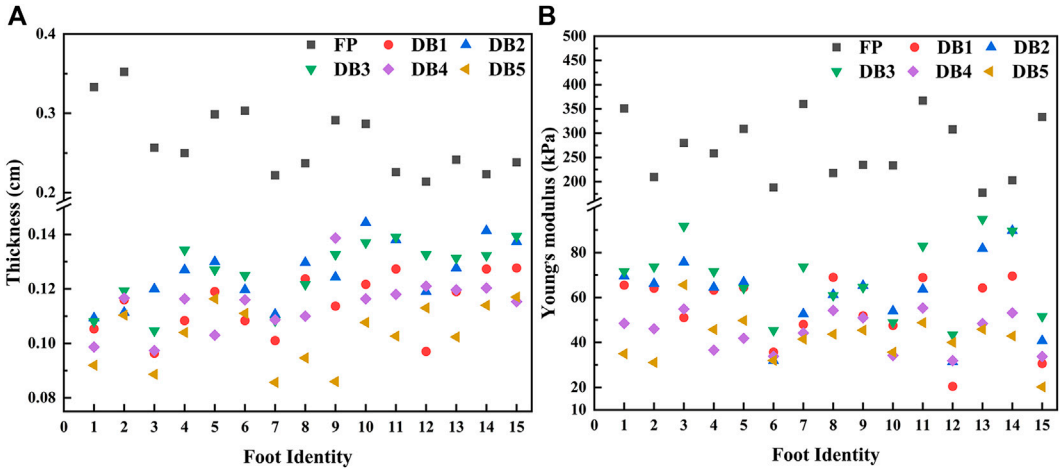

FIGURE 6 | Distribution of plantar fascia thickness **(A)** and Young's modulus **(B)** at proximal fascia (PF) and the five distal branches in 15 flatfeet.

second and third metatarsals were higher than those under the other metatarsals. Thus, the COP would move laterally from the first MH. These results were the same as those of Han et al. (2011). They found that, in the normal foot, the trajectory of the COP moved from the lateral heel, moved medially in forefoot, and then ended at the big toe. In flatfeet, the COP moved straight from the heel to the toe without medial shifting in the forefoot. There was a tendency for the COP in flatfoot to shift laterally in the forefoot than the COP in normal foot. These results also confirm our inference; that is, the medial longitudinal arch collapses more than the lateral arch in flatfoot, which leads to the higher force and higher pressure under the second and third metatarsals and the COP moving outward.

Morphologic and mechanical properties of the plantar fascia may be important factors affecting the plantar pressure distribution because the primary task of the plantar fascia is to stabilize the foot arches (McKeon et al., 2015). Studies (Tas and Cetin, 2019a) also show that there is a significant positive correlation between plantar pressure distribution and the thickness of plantar fascia. Higher plantar pressure may lead to plantar fascia hypertrophy. Foot orthoses could modify tissue loading by altering kinematics, kinetics, muscle activity, and sensory feedback (Mills et al., 2010), and they have been demonstrated to have a good therapeutic effect in plantar fasciitis (Buchbinder, 2004). The changes in morphology and mechanical properties of plantar fascia and peak pressure of the forefoot in patients with flexible flatfoot found in our study may provide the basis for the development of new foot orthoses for flexible flatfoot.

There were limitations in this study. Firstly, the sample size was limited to 15 cases, and there was no grading according to mild, moderate, and severe flexible flatfeet. However, the results showed that although the sample size is small and there may be some differences in disease degree among participants, the spatial distribution characteristics of thickness and Young's modulus of plantar fascia in all 15 flexible flat feet were similar, which indicated that the spatial distribution characteristics are less affected by the disease severity, and the research results may have broad representative significance. Secondly, this study did not include the control group, but our group has previously conducted and published one study on the morphology and mechanical properties of plantar fascia in normal feet (Wang et al., 2019). In addition, the age, height, and body weight of the volunteers who participated in this study are similar to those in our previous published work. Therefore, we cited and employed the published data (normal foot data) as the healthy control group in this study (Wang et al., 2019). Thirdly, though SWE has been used to evaluate the material properties of plantar fascia (Shiotani et al., 2019; Tas and Cetin, 2019b), studies have shown that the shear wave velocity of layered tissue is affected by its thickness and surrounding tissue properties (Helfenstein-Didier et al., 2016; Martin et al., 2018, 2019; Sadeghi and Cortes, 2020); especially when the thickness of the relevant tissue is equal to or less than the wavelength, SWE is no longer applicable (Li et al., 2018). The thickness of plantar fascia measured in this study is millimeter, which is far greater than the wavelength. In addition, the results of Helfenstein-Didier et al. (2016) in measuring the human Achilles tendon show that there is a high correlation between the shear modulus measured by SWE and the new guided wave technology-phase velocity mode, even considering the influence of thickness. Therefore, although the results of the differences between different positions in plantar fascia as well as between patients with flexible flat feet and healthy volunteers in this study may not be affected, it is necessary to explore the influence of thickness on the properties of plantar fascia materials by using guided wave technology in the future.

CONCLUSION

This study found a gradient distribution in that the thickness and Young's modulus gradient decreased from the proximal end to the distal end of plantar fascia in the longitudinal arch of flexible flatfeet. In the transverse arch, the thickness and Young's

modulus under the second and third DB were larger than those under the other three DB in flexible flatfoot, and the peak pressures under the second and third MH were also larger than those under the other three MH in patients with flexible flatfoot. These findings deepen our understanding of the changes of biomechanical properties and may be meaningful for the study of pathological mechanisms and therapy for flexible flatfoot.

DATA AVAILABILITY STATEMENT

The original contributions presented in the study are included in the article/Supplementary Material; further inquiries can be directed to the corresponding authors.

ETHICS STATEMENT

The studies involving human participants were reviewed and approved by the Ethics Committee of the Second Hospital of Jilin University (No. 2020085). The patients/participants provided their written informed consent to participate in this study.

AUTHOR CONTRIBUTIONS

ZQ and ZJ were responsible for the experiments and manuscript preparation. JW, FC, and LR participated in discussions and revisions. JL and LR worked as supervisors for all procedures.

FUNDING

This research was supported by the project of National Natural Science Foundation of China (No. 52175270), the Key Project of the National Natural Science Foundation of China (No. 91848204), National Natural Science Foundation of China (No. 52005209), the Interdisciplinary Research Funding Program for Doctoral Students of Jilin University (No. 101832020DJX049), and China Postdoctoral Science Foundation (No. 2021T140260 and No. 2021M691206).

ACKNOWLEDGMENTS

The authors would like to thank all the volunteers who contributed to this study.

REFERENCES

Babatunde, O. O., Legha, A., Littlewood, C., Chesterton, L. S., Thomas, M. J., Menz, H. B., et al. (2019). Comparative Effectiveness of Treatment Options for Plantar Heel Pain: a Systematic Review with Network Meta-Analysis. *Br. J. Sports Med.* 53, 182–194. doi:10.1136/bjsports-2017-098998

Buchbinder, R. (2004). Plantar Fasciitis. *N. Engl. J. Med.* 350, 2159–2166. doi:10.1056/NEJMcp032745

Buldt, A. K., Forghany, S., Landorf, K. B., Levinger, P., Murley, G. S., and Menz, H. B. (2018). Foot Posture Is Associated with Plantar Pressure during Gait: A Comparison of normal, Planus and Cavus Feet. *Gait & Posture* 62, 235–240. doi:10.1016/j.gaitpost.2018.03.005

Carr, J. B., 2nd, Yang, S., and Lather, L. A. (2016). Pediatric Pes Planus: A State-Of-The-Art Review. *Pediatrics* 137, e20151230. doi:10.1542/peds.2015-1230

Cavanagh, P. R., Rodgers, M. M., and liboshi, A. (1987). Pressure Distribution under Symptom-free Feet during Barefoot Standing. *Foot & Ankle* 7, 262–278. doi:10.1177/107110078700700502

Chen, T. L.-W., Agresta, C. E., Lipps, D. B., Provenzano, S. G., Hafer, J. F., Wong, D. W.-C., et al. (2019a). Ultrasound Elastographic Assessment of Plantar Fascia in Runners Using Rearfoot Strike and Forefoot Strike. *J. Biomech.* 89, 65–71. doi:10.1016/j.jbiomech.2019.04.013

Chen, T. L.-W., Wong, D. W.-C., Wang, Y., Lin, J., and Zhang, M. (2019b). Foot Arch Deformation and Plantar Fascia Loading during Running with Rearfoot Strike and Forefoot Strike: A Dynamic Finite Element Analysis. *J. Biomech.* 83, 260–272. doi:10.1016/j.jbiomech.2018.12.007

Cho, W. H., and Choi, H. (2005). Center of Pressure (COP) during the Postural Balance Control of High-Heeled Woman. *Conf. Proc. IEEE Eng. Med. Biol. Soc.* 2005, 2761–2764. doi:10.1109/IEMBS.2005.1617044

Guo, J., Liu, X., Ding, X., Wang, L., and Fan, Y. (2018). Biomechanical and Mechanical Behavior of the Plantar Fascia in Macro and Micro Structures. *J. Biomech.* 76, 160–166. doi:10.1016/j.jbiomech.2018.05.032

Haen, T. X., Roux, A., Soubeyrand, M., and Laporte, S. (2017). Shear Waves Elastography for Assessment of Human Achilles Tendon's Biomechanical Properties: an Experimental Study. *J. Mech. Behav. Biomed. Mater.* 69, 178–184. doi:10.1016/j.jmbbm.2017.01.007

Hamstra-Wright, K. L., Bliven, K. C. H., and Bay, C. (2015). Risk Factors for Medial Tibial Stress Syndrome in Physically Active Individuals Such as Runners and Military Personnel: a Systematic Review and Meta-Analysis. *Br. J. Sports Med.* 49, 362–369. doi:10.1136/bjsports-2014-093462

Han, J. T., Koo, H. M., Jung, J. M., Kim, Y. J., and Lee, J. H. (2011). Differences in Plantar Foot Pressure and COP between Flat and Normal Feet during Walking. *J. Phys. Ther. Sci.* 23, 683–685. doi:10.1589/jpts.23.683

Helfenstein-Didier, C., Andrade, R. J., Brum, J., Hug, F., Tanter, M., Nordez, A., et al. (2016). In Vivoquantification of the Shear Modulus of the Human Achilles Tendon during Passive Loading Using Shear Wave Dispersion Analysis. *Phys. Med. Biol.* 61, 2485–2496. doi:10.1088/0031-9155/61/6/2485

Hicks, J. H. (1954). The Mechanics of the Foot. II. The Plantar Aponeurosis and the Arch. *J. Anat.* 88, 25–30.

Hillstrom, H. J., Song, J., Kraszewski, A. P., Hafer, J. F., Mootanah, R., Dufour, A. B., et al. (2013). Foot Type Biomechanics Part 1: Structure and Function of the Asymptomatic Foot. *Gait & Posture* 37, 445–451. doi:10.1016/j.gaitpost.2012.09.007

Huang, H. H., Qureshi, A. A., and Biundo, J. J., Jr. (2000). Sports and Other Soft Tissue Injuries, Tendinitis, Bursitis, and Occupation-Related Syndromes. *Curr. Opin. Rheumatol.* 12, 150–154. doi:10.1097/00002281-200003000-00009

Huffer, D., Hing, W., Newton, R., and Clair, M. (2017). Strength Training for Plantar Fasciitis and the Intrinsic Foot Musculature: A Systematic Review. *Phys. Ther. Sport* 24, 44–52. doi:10.1016/j.ptsp.2016.08.008

Ker, R. F., Bennett, M. B., Bibby, S. R., Kester, R. C., and Alexander, R. M. (1987). The spring in the Arch of the Human Foot. *Nature* 325, 147–149. doi:10.1038/325147a0

Kohls-Gatzoulis, J., Angel, J. C., Singh, D., Haddad, F., Livingstone, J., and Berry, G. (2004). Tibialis Posterior Dysfunction: a Common and Treatable Cause of Adult Acquired Flatfoot. *BMJ* 329, 1328–1333. doi:10.1136/bmj.329.7478.1328

Martin, J. A., Brandon, S. C. E., Keuler, E. M., Hermus, J. R., Ehlers, A. C., Segalman, D. J., et al. (2018). Gauging Force by Tapping Tendons. *Nat. Commun.* 9, 1592. doi:10.1038/s41467-018-03797-6

Martin, J. A., Schmitz, D. G., Ehlers, A. C., Allen, M. S., and Thelen, D. G. (2019). Calibration of the Shear Wave Speed-Stress Relationship in *Ex Vivo* Tendons. *J. Biomech.* 90, 9–15. doi:10.1016/j.jbiomech.2019.04.015

Mckeon, P. O., Hertel, J., Bramble, D., and Davis, I. (2015). The Foot Core System: a New Paradigm for Understanding Intrinsic Foot Muscle Function. *Br. J. Sports Med.* 49, 290. doi:10.1136/bjsports-2013-092690

Mills, K., Blanch, P., Chapman, A. R., Mcpoil, T. G., and Vicenzino, B. (2010). Foot Orthoses and Gait: a Systematic Review and Meta-Analysis of Literature

Pertaining to Potential Mechanisms. *Br. J. Sports Med.* 44, 1035–1046. doi:10.1136/bjsm.2009.066977

Nirenberg, M., Ansert, E., Campbell, J., and Curran, M. (2020). Forensic Implications of Foot Arch index Comparison between Dynamic Bare Footprints and Shoe Insole Foot Impressions. *Sci. Justice* 60, 375–380. doi:10.1016/j.scijus.2020.03.001

Orchard, J. (2012). Plantar Fasciitis. *BMJ* 345: e6603. doi:10.1136/bmj.e6603

Pehlivan, O., Cilli, F., Mahirogullari, M., Karabudak, O., and Koksal, O. (2009). Radiographic Correlation of Symptomatic and Asymptomatic Flexible Flatfoot in Young Male Adults. *Int. Orthopaedics (Sicot)* 33, 447–450. doi:10.1007/s00264-007-0508-5

Phan, P. K., Vo, A. T. N., Bakhtiarydavijani, A., Burch, R., Smith, B., Ball, J. E., et al. (2021). In Silico Finite Element Analysis of the Foot Ankle Complex Biomechanics: A Literature Review. *J. Biomech. Eng.* 143. doi:10.1115/1.4050667

Rao, S., Song, J., Kraszewski, A., Backus, S., Ellis, S. J., Md, J. T. D., et al. (2011). The Effect of Foot Structure on 1st Metatarsophalangeal Joint Flexibility and Hallucal Loading. *Gait & Posture* 34, 131–137. doi:10.1016/j.gaitpost.2011.02.028

Riddle, D. L., Pulisic, M., Pidcoe, P., and Johnson, R. E. (2003). Risk Factors for Plantar Fasciitis. *The J. Bone Jt. Surgery-American Volume* 85, 872–877. doi:10.2106/00004623-200305000-00015

Sadeghi, S., and Cortes, D. H. (2020). Measurement of the Shear Modulus in Thin-Layered Tissues Using Numerical Simulations and Shear Wave Elastography. *J. Mech. Behav. Biomed. Mater.* 102, 103502. doi:10.1016/j.jmbbm.2019.103502

Shiotani, H., Yamashita, R., Mizokuchi, T., Naito, M., and Kawakami, Y. (2019). Site- and Sex-Differences in Morphological and Mechanical Properties of the Plantar Fascia: A Supersonic Shear Imaging Study. *J. Biomech.* 85, 198–203. doi:10.1016/j.jbiomech.2019.01.014

Stecco, C., Corradin, M., Macchi, V., Morra, A., Porzionato, A., Biz, C., et al. (2013). Plantar Fascia Anatomy and its Relationship with Achilles Tendon and Paratenon. *J. Anat.* 223, 665–676. doi:10.1111/joa.12111

Sung, P. S. (2016). The Ground Reaction Force Thresholds for Detecting Postural Stability in Participants with and without Flat Foot. *J. Biomech.* 49, 60–65. doi:10.1016/j.jbiomech.2015.11.004

Tas, S., and Cetin, A. (2019a). An Investigation of the Relationship between Plantar Pressure Distribution and the Morphologic and Mechanic Properties of the Intrinsic Foot Muscles and Plantar Fascia. *Gait Posture* 72, 217–221. doi:10.1016/j.jbiomech.2015.11.004

Taş, S., and Çetin, A. (2019b). Mechanical Properties and Morphologic Features of Intrinsic Foot Muscles and Plantar Fascia in Individuals with Hallux Valgus. *Acta Orthopaedica et Traumatologica Turcica* 53, 282–286. doi:10.1016/j.aott.2019.03.009

Thing, J., Maruthappu, M., and Rogers, J. (2012). Diagnosis and Management of Plantar Fasciitis in Primary Care. *Br. J. Gen. Pract.* 62, 443–444. doi:10.3399/bjgp12X653769

Thomas, M. J., Menz, H. B., and Mallen, C. D. (2016). Plantar Heel Pain. *BMJ* 353, i2175. doi:10.1136/bmj.i2175

Van Der Worp, H., Van Ark, M., Roerink, S., Pepping, G.-J., Van Den Akker-Scheek, I., and Zwerver, J. (2011). Risk Factors for Patellar Tendinopathy: a Systematic Review of the Literature. *Br. J. Sports Med.* 45, 446–452. doi:10.1136/bjsm.2011.084079

Wang, K., Liu, J., Wu, J., Qian, Z., Ren, L., and Ren, L. (2019). Noninvasive *In Vivo* Study of the Morphology and Mechanical Properties of Plantar Fascia Based on Ultrasound. *Ieee Access* 7, 53641–53649. doi:10.1109/Access.2019.2909409

Wang, Y.-T., Chen, J.-C., and Lin, Y.-S. (2020). Effects of Artificial Texture Insoles and Foot Arches on Improving Arch Collapse in Flat Feet. *Sensors* 20, 3667. doi:10.3390/s20133667

Wearing, S. C., Hills, A. P., Byrne, N. M., Hennig, E. M., and Mcdonald, M. (2004). The Arch index: a Measure of Flat or Fat Feet? *Foot Ankle Int.* 25, 575–581. doi:10.1177/107110070402500811

Wearing, S. C., Smeathers, J. E., Urry, S. R., Hennig, E. M., and Hills, A. P. (2006). The Pathomechanics of Plantar Fasciitis. *Sports Med.* 36, 585–611. doi:10.2165/00007256-200636070-00004

Welte, L., Kelly, L. A., Kessler, S. E., Lieberman, D. E., D'andrea, S. E., Lichtwark, G. A., et al. (2021). The Extensibility of the Plantar Fascia Influences the Windlass Mechanism during Human Running. *Proc. R. Soc. B.* 288, 20202095. doi:10.1098/rspb.2020.2095

Wong, C. K., Weil, R., and De Boer, E. (2012). Standardizing Foot-type Classification Using Arch index Values. *Physiother. Can.* 64, 280–283. doi:10.3138/ptc.2011-40

Wu, C.-H., Chang, K.-V., Mio, S., Chen, W.-S., and Wang, T.-G. (2011). Sonoelastography of the Plantar Fascia. *Radiology* 259, 502–507. doi:10.1148/radiol.11101665

Yeh, C.-L., Kuo, P.-L., Gennisson, J.-L., Brum, J., Tanter, M., and Li, P.-C. (2016). Shear Wave Measurements for Evaluation of Tendon Diseases. *IEEE Trans. Ultrason. Ferroelect., Freq. Contr.* 63, 1906–1921. doi:10.1109/TUFFC.2016.2591963

Yeh, C.-L., Kuo, P.-L., and Li, P.-C. (2013). Correlation between the Shear Wave Speed in Tendon and its Elasticity Properties. *2013 Ieee Int. Ultrason. Symp. (Ius)*, 9–12. doi:10.1109/Ultsym.2013.0003

Young, C. (2012). Plantar Fasciitis. *Ann. Intern. Med.* 156, ITC1–1. ITC1-2, ITC1-3, ITC1-4, ITC1-5, ITC1-6, ITC1-7, ITC1-8, ITC1-9, ITC1-10, ITC11-11, ITC11-12, ITC11-13, ITC11-14, ITC11-15; quiz ITC11-16. doi:10.7326/0003-4819-156-1-201201030-01001

Conflict of Interest: The authors declare that the research was conducted in the absence of any commercial or financial relationships that could be construed as a potential conflict of interest.

Publisher's Note: All claims expressed in this article are solely those of the authors and do not necessarily represent those of their affiliated organizations, or those of the publisher, the editors and the reviewers. Any product that may be evaluated in this article, or claim that may be made by its manufacturer, is not guaranteed or endorsed by the publisher.

frontiers in Bioengineering and Biotechnology

ORIGINAL RESEARCH
published: 25 November 2021
doi: 10.3389/fbioe.2021.732628

Effect of Exercise Volume on Plantar Microcirculation and Tissue Hardness in People With Type 2 Diabetes

Weiyan Ren[1†], Yijie Duan[2†], Yih-Kuen Jan[2,3], Wenqiang Ye[2], Jianchao Li[2], Wei Liu[2], Hongmei Liu[1,2], Junchao Guo[1], Fang Pu[2] and Yubo Fan[2,4*]*

[1]Key Laboratory of Rehabilitation Technical Aids for Old-Age Disability, Key Laboratory of Human Motion Analysis and Rehabilitation Technology of the Ministry of Civil Affairs, National Research Center for Rehabilitation Technical Aids, Beijing, China, [2]Key Laboratory for Biomechanics and Mechanobiology of Chinese Education Ministry, Beijing Advanced Innovation Center for Biomedical Engineering, School of Biological Science and Medical Engineering, Beihang University, Beijing, China, [3]Rehabilitation Engineering Laboratory, Department of Kinesiology and Community Health, University of Illinois at Urbana-Champaign, Champaign, IL, United States, [4]School of Engineering Medicine, Beihang University, Beijing, China

OPEN ACCESS

Edited by:
Zhi-Yong Li,
Southeast University, China

Reviewed by:
Panagiotis Chatzistergos,
Staffordshire University,
United Kingdom
Saldy Yusuf,
Hasanuddin University, Indonesia

***Correspondence:**
Fang Pu
pufangbme@buaa.edu.cn
Yubo Fan
yubofan@buaa.edu.cn

[†]These authors have contributed equally to this work and share first authorship

Specialty section:
This article was submitted to Biomechanics, a section of the journal Frontiers in Bioengineering and Biotechnology

Received: 29 June 2021
Accepted: 11 November 2021
Published: 25 November 2021

Citation:
Ren W, Duan Y, Jan Y-K, Ye W, Li J, Liu W, Liu H, Guo J, Pu F and Fan Y (2021) Effect of Exercise Volume on Plantar Microcirculation and Tissue Hardness in People With Type 2 Diabetes. Front. Bioeng. Biotechnol. 9:732628. doi: 10.3389/fbioe.2021.732628

Objective: Exercise has been reported to be beneficial for people with type 2 diabetes (T2DM), but exercise, especially weight-bearing exercise, may increase the risk of diabetic foot ulcers (DFUs). This study aimed to explore the associations between different volumes of weight-bearing physical activities and plantar microcirculation and tissue hardness in people with T2DM.

Methods: 130 elderly people with T2DM were enrolled for this cross-sectional study. They were classified into the high exercise volume group and the low exercise volume group based on their weekly energy expenditure (metabolic equivalents per week) in the past year. Weekly energy expenditure was calculated using the International Physical Activity Questionnaire and the Compendium of Physical Activities. The plantar oxygen saturation (SO_2) and soft tissue hardness of each participant's right foot were measured.

Results: A total of 80 participants completed the trial. The average exercise energy expenditure of the high exercise volume group and the low exercise volume group were significantly different ($p < 0.05$). The results showed that the SO_2 of the high exercise volume group (67.25 ± 6.12%) was significantly higher than the low exercise volume group (63.75 ± 8.02%, $p < 0.05$). The plantar tissue hardness of the high exercise volume group was lower than the low exercise volume group in the big toe, midfoot and hindfoot regions ($p < 0.05$).

Conclusion: This study demonstrates that higher volumes of exercise are associated with better plantar microcirculation and lower plantar tissue hardness in people with T2DM. The findings of this study indicate that weight-bearing exercise may not increase risk of developing diabetic foot ulcers.

Keywords: diabetic foot, weight-bearing exercise, plantar microcirculation, tissue hardness, exercise volume

INTRODUCTION

Diabetic foot ulcers (DFUs) are one of the most common and serious complications of diabetes mellitus (DM). A global survey on diabetes-related complications showed that one-third of people with diabetes suffered complications in the lower extremity (Zhang et al., 2020); and diabetes-related lower extremity amputations accounted for 30–65% of all amputations (Narres et al., 2017). DFUs can have a huge negative impact on the physical health and quality of life of people with diabetes.

Microvascular dysfunction (Greenman et al., 2005; Chao and Cheing, 2009), abnormal plantar stress (Jan et al., 2013b; Pu et al., 2018), increased plantar tissue hardness (Mithraratne et al., 2012; Jan et al., 2013a) and peripheral neuropathy (Bowering, 2001; Caselli et al., 2002) are major factors causing the development of DFUs. Research studies have shown that people with diabetes exhibit microvascular dysfunction, including a lower level of oxygen saturation of plantar tissue (Greenman et al., 2005; Chao and Cheing, 2009). Besides, the increased hardness of plantar tissue causes an increase in peak plantar pressure (Jan et al., 2013a; Teoh and Lee, 2020), which may gradually reduce the capacity to attenuate the ground impact in diabetic plantar tissue. Peripheral neuropathy can lead to a loss of protective sensation in people with diabetes, and also further aggravates microvascular dysfunction, as well as cause dry skin and musculoskeletal deformities (Armstrong et al., 2017). Although the relationships among oxygen saturation, plantar tissue hardness, neuropathy, and the occurrence of ulcerations are still unclear, these factors may play an important role in predicting and assessing the risk of DFUs.

Exercise is one of the most effective methods for managing the complications of diabetes, and has been shown to improve blood glucose levels, ankle brachial index, cardiopulmonary endurance, and muscle strength (Liao et al., 2019; Verboven et al., 2019). Moreover, weight-bearing exercise has been reported to improve tissue tolerance and significantly increase the achievable walking distance and step count of people with diabetic peripheral neuropathy (DPN) (Mueller and Maluf, 2002; Mueller et al., 2013; Kluding et al., 2017). Diloreto et al. also found that daily physical activity with an energy expenditure at 27 Mets·h/week (more than 10 Mets·h/week recommended by the American Diabetes Association) had a significant positive effect on the physical fitness of people with type 2 diabetes (Di Loreto et al., 2005; Association, 2020). However, the effects of exercise volumes of weight-bearing exercise on the risk of developing DFUs remain unclear (Liao et al., 2019). Exercise can improve endothelial function and blood circulation in the lower extremity (Mueller et al., 2013; Liao et al., 2019), which may be beneficial to improve microvascular function in people with type 2 diabetes (Mueller and Maluf, 2002; Kluding et al., 2017). On the other hand, the greater accumulated stress on plantar soft tissues caused by high volume of exercise, especially weight-bearing exercise, may increase the degree of compression of plantar tissue, and the occlusion duration of microvessels. The impaired plantar microcirculation under the accumulated stimulation of repeated mechanical loading may be more prone to cause tissue damage to the fragile foot tissue in people with type 2 diabetes (Chao et al., 2011). Particularly in people with diabetes and peripheral neuropathy, the dysfunction in the regulation of microvascular system, dry skin and musculoskeletal deformity caused by peripheral neuropathy can increase the vulnerability of plantar tissue to compressed damage during these physical activities (Mueller and Maluf, 2002; Jan et al., 2013b; Pu et al., 2018). Therefore, exploring the long-term effects of weight-bearing exercise with high exercise volume on the plantar microcirculation and soft tissue hardness in the diabetic foot may help to understand the risk of developing DFUs. This information may be used to develop appropriate exercise plans for people with type 2 diabetes.

The aim of this study was to compare the difference of plantar microcirculation and tissue hardness in people with type 2 diabetes who performed long-term weight-bearing exercise at high and low exercise volume. We hypothesized that participants with type 2 diabetes in the high exercise volume group would have better oxygen supply to the plantar foot and lower plantar hardness compared to the low exercise volume group.

MATERIALS AND METHODS

This is a cross-sectional observation study designed to explore the difference of plantar microcirculation and tissue hardness (the important factors in the development of DFUs) of the foot of people with diabetes who had habitual physical activity at high and low levels of exercise volume.

This study was conducted in accordance with clinical protocols approved by the institutional review board of Affiliated Hospital of National Research Center for Rehabilitation Technical Aids (20190101) and the Declaration of Helsinki (2013 revision). All participants were briefed on the study purposes and procedures and gave written informed consent prior to participation.

Participants

A total of 130 people with diabetes confirmed their willingness to participate in this study through a public recruitment drive in the local communities and hospitals. The inclusion criteria were: 1) diagnosed type 2 diabetes, 2) ≥40 ages, 3) no symptoms such as redness, callus, inflammation, or wounds on the skin of the feet or legs, and no history of amputation, 4) no diseases such as systematic inflammation, lower extremity edema, malignant tumor, and 5) performed regular physical activities over the course of 1 year with at least 150 min/week, with no more than two consecutive days without activity (Association, 2020) before being enrolled in this study. A total of 104 participants met the inclusion criteria and were enrolled in this study.

Physiological Information Recording and Assessment

Demographics and medical history were discussed and recorded at the initial assessment. In this study, 10 g Semmes-Weinstein monofilament and vibration perception threshold testing were

used to evaluate whether participants had sensory neuropathy. For this test, 10 g monofilament was compressed perpendicular to the four areas of foot (1st, 3rd, and 5th metatarsal heads and distal hallux) for 1 s and then removed. It was considered normal large-fiber nerve function if the patient could feel the touch of the monofilament at all four areas. Moreover, a biothesiometer was placed over the dorsal hallux and the amplitude of vibration was increased until participants could detect it. The protective sensation was considered normal if a participant's vibration perception threshold was smaller than 25 V (Boulton et al., 2008). No abnormal test would rule out diabetic peripheral neuropathy. Otherwise, a participant was confirmed as a diabetic with peripheral neuropathy (Boulton et al., 2008; Schaper et al., 2020). Care was taken to avoid performing the test on callous tissue.

Assessment of Physical Activity

The type, frequency and duration of weekly physical activity performed over the course of 1 year was recorded for each participant. This was assessed using the International Physical Activity Questionnaire (IPAQ) that has been proven to be a validated tool for physical activity assessment (Mynarski et al., 2012). The level of metabolic equivalent (MET) rating was determined based on the compendium of physical activities (Ainsworth et al., 2011), including step counts, duration and distance travelled, and the type of exercise described by the participants (Mynarski et al., 2012; Lalli et al., 2013; Ainsworth, 2014). All recorded activities and corresponding MET values in this study were as follows: walking (2.5 mph-2.8 mph, and 3 Mets), brisk walking (3.5–4.0 mph, 4.3 Mets), square dancing (5 Mets), table tennis (4 Mets), tennis (4.5 Mets), golf (4.8 Mets), billiards (2.5 Mets), cycling (4 Mets), and Tai Chi (3 Mets) (Ainsworth et al., 2011).

The weekly sum of each participant's energy expenditure through physical activity was calculated using the **Eq. 1** (Knowler et al., 2002). Diloreto et al. recommended that 27 Mets·h/week can be a reasonable target of energy expenditure for sedentary people with diabetes due to its great benefits associated with HbA1c, BMI, heart rate, and 10-years coronary heart disease risk (Di Loreto et al., 2005). Therefore, people with diabetes in this study were classified into the high exercise volume (HEV) group and the low exercise volume (LEV) group according to whether their energy expenditure exceeded 27 Mets·h/week.

$$\text{Energy Expenditure} = \sum \text{Met}_i \times \text{T}_i \quad (1)$$

In which, i represents different activity models, Met_i represents the metabolic equivalent rating corresponding to different activities, and T_i represents the time spent in different activities.

Assessment of Plantar Microcirculation and Tissue Hardness

All tests were performed in a climate-controlled room at 24°C with participants in a supine position. Every participants started with a 30 min resting period before measurements. A Shore durometer (Model 1,600, Type OO, Rex Co., Buffalo Grove, United States) was used to measure the tissue hardness in the plantar regions (big toe, little toes, medial metatarsal, middle metatarsal, lateral metatarsal, medial arch, lateral arch, medial heel, and lateral heel) of each participant's right foot. It was designed to test the hardness of soft materials such as animal tissue, foams, sponge rubber, and gels. The similar durometer has been used in several studies to assess plantar hardness in people with diabetes (Thomas et al., 2003; Periyasamy et al., 2012).

During measurement, the durometer was pressed perpendicular to the plantar skin surface and expresses the hardness in degrees of Shore (unit: °shore). A lower Shore value indicates a softer material. Each region was measured 5 times sequentially and the mean was calculated for comparisons. Care was taken to avoid testing areas with prominent bones or callus tissue. The tissue hardness of the little toes was the average of the four little toes. The tissue hardness of the forefoot region was the average of the medial metatarsal, middle metatarsal and lateral metatarsal. The tissue hardness of the midfoot region was the average of the medial arch and lateral arch. The tissue hardness of the hindfoot region was the average of the medial heel and lateral heel (**Figure 1**).

After measuring the plantar tissue hardness, a moorVMS-OXY monitor (Probe OP17-1,000, Moor Instruments, Axminster, United Kingdom) was used to monitor the plantar microcirculation. This device uses a white light spectroscopy method and transmits the 6 mW white light (400–700 nm wave length) into tissue via fiber optics in order to assess tissue oxygen saturation and temperature. The probe was attached to the skin surface of the right plantar big toe area with adhesive tapes to limit movement artefacts during the measurement. The plantar tissue oxygen saturation (SO_2) and skin temperature (Temp) of each participant in the supine position were recorded for 2 min (Newton et al., 2005; Ladurner et al., 2009).

Sample Size

The required sample size was calculated using Power Analysis and Sample Size (PASS 15) software set for *t* test. This study assumed that the mean and standard deviation (SD) of cutaneous oxygen saturation in people with diabetes was equivalent to that of a prior study (64.1 ± 4.0%) (Kabbani et al., 2013), and the mean difference between two groups was equivalent to that of Charles et al.'s study (3.9%) (Ezema et al., 2019). A minimum of 24 participants per group was needed at a power of 90% and an alpha level of 0.05. This study assumed a drop-out rate of 20%, and considered that more than half of the participants may not regularly perform physical activities over the course of 1 year with at least 150 min/week (one of the inclusion criteria) (Wen et al., 2011). Therefore, at least 120 participants were recruited for this study.

Data and Statistical Analyses

The mean values of SO_2 and Temp from each participant's right plantar big toe region, and the mean values of tissue hardness in five plantar regions (big toe, little toes, forefoot, midfoot, and hindfoot) of each participant's right foot, were calculated.

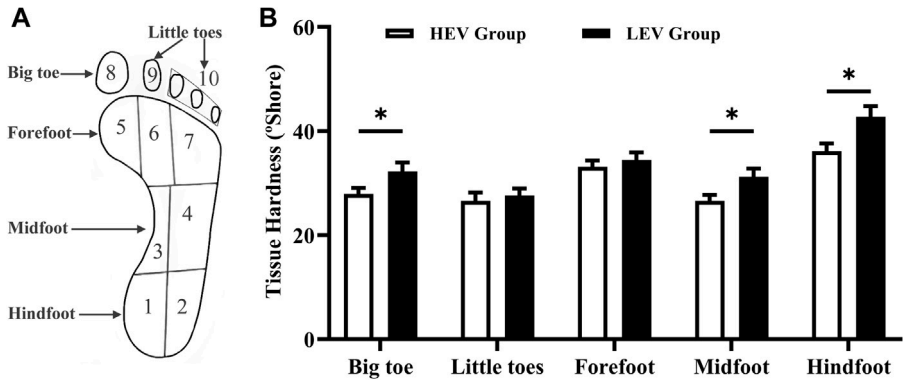

FIGURE 1 | (A) Division of the foot. **(B)** Results of tissue hardness of plantar tissue in participants (Mean with SEM). The tissue hardness of the little toes was the average of area 8 and area 9; the tissue hardness of the forefoot was the average of area 5, area 6 and area 7; the tissue hardness of the midfoot was the average of area 3 and area 4; the tissue hardness of the hindfoot was the average of area 1 and area 2. HEV: High Exercise Volume (≥27 Mets·h/week); LEV: Low Exercise Volume (<27 Mets·h/week); SEM: standard error of mean. * indicates a significant difference between the HEV group (n = 45) and LEV group (n = 35) (p < 0.05).

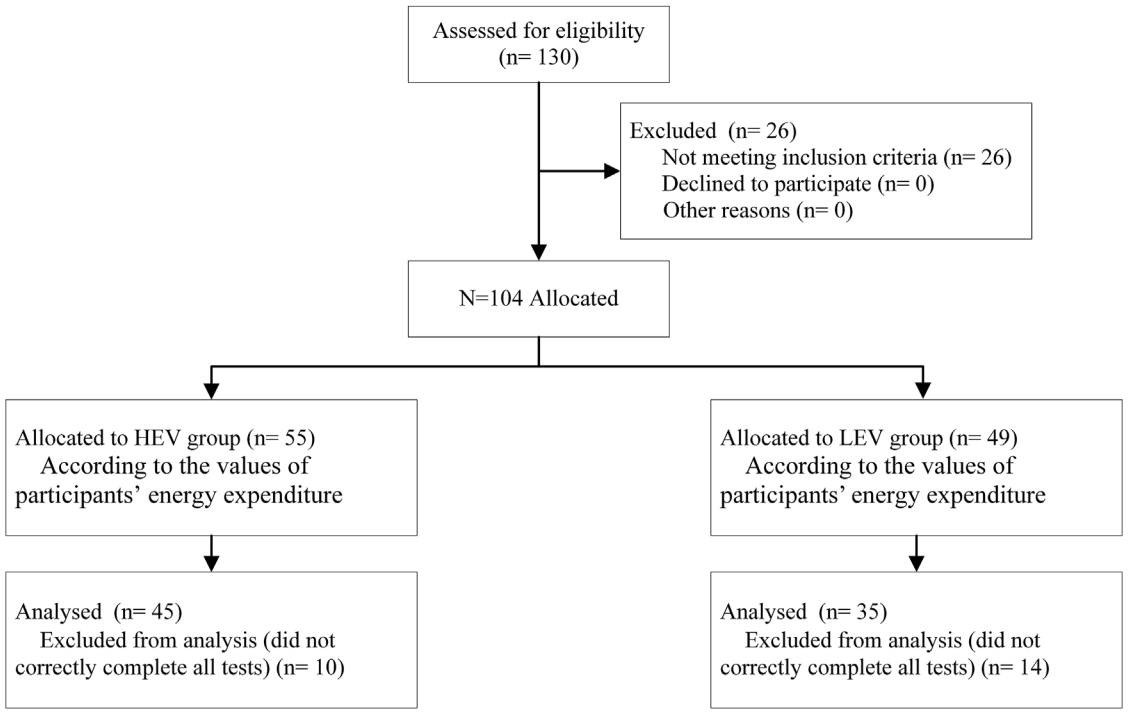

FIGURE 2 | Enrollment diagram of all participants.

Considering that peripheral neuropathy is an important factor in contributing to the development of diabetic foot ulcers (Armstrong et al., 2017), this study also preliminarily observed differences in the mean values of SO2, Temp and plantar soft tissue hardness between people with diabetic peripheral neuropathy and people without diabetic peripheral neuropathy. In addition, plantar soft tissue may be subjected to different levels of accumulated pressure stimuli under various exercise types, which may be related to the occurrence and development of diabetic foot ulcers (Burnfield et al., 2004; Lam et al., 2019). This study conducted a preliminary comparison of the mean values of SO2, Temp and plantar soft tissue hardness among people with different exercise types.

An independent t test or Mann-Whitney U test (based on the normality of the variables, as tested by a Shapiro-Wilk test) was used to evaluate differences in microcirculation and plantar hardness between the HEV group and LEV group. A Spearman or Pearson correlation analysis (based on the normality of the variables, as tested by a Shapiro-Wilk test) was used to test the relationship between tissue hardness and

TABLE 1 | Demographic and physiological information of participants in HEV and LEV groups (Mean ± SD).

Variables	HEV group	LEV group
Gender (Male/Female)	21/24	14/21
Age (years)	66.67 ± 4.55	65.85 ± 8.09
BMI (kg/m^2)	25.57 ± 3.22	26.49 ± 3.80
SBP (mmHg)	136.17 ± 14.05	132.04 ± 14.73
DBP (mmHg)	72.51 ± 8.78	72.11 ± 9.32
Heart rate (bpm)	72.94 ± 10.91	72.54 ± 9.53
Duration of diabetes (years)	13.19 ± 9.05	11.68 ± 7.61
Fasting blood glucose (mmol/L)	7.31 ± 1.51	7.63 ± 1.60
ABI	1.08 ± 0.16	1.07 ± 0.11
Diabetic peripheral neuropathy	8 (17.8%)	5 (14.3%)

HEV: high exercise volume; LEV: low exercise volume; BMI: body mass index; SBP: systolic blood pressure; DBP: diastolic blood pressure; ABI: Ankle brachial index. There was no significant difference in all parameters between the HEV, group and LEV, group.

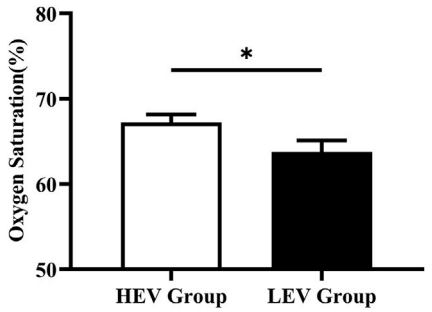

FIGURE 3 | Results of oxygen saturation of plantar tissue in participants (Mean with SEM). HEV: High Exercise Volume (≥27 Mets·h/week); LEV: Low Exercise Volume (<27 Mets·h/week); SEM: standard error of mean. * indicates a significant difference between the HEV group (n < 45) and LEV group (n < 35) (p < 0.05).

microcirculation. The results were expressed as mean ± SD. A statistical significance level of 0.05 was used. All statistical analyses were performed in SPSS (Version 26.0, IBM, Armonk, NY, United States).

RESULTS

A total of 80 participants completed all tests (**Figure 2**). Among them, 45 people with diabetes were classified as the HEV group, including eight people with DPN. The remaining 35 participants were classified as the LEV group, including five people with DPN. Participant characteristics are shown in **Table 1**. There was no significant difference in these parameters (age, body mass index, systolic blood pressure, diastolic blood pressure, heart rate, duration of diabetes, fasting blood glucose, and ankle brachial index) between the HEV group and LEV group. The average exercise energy expenditure of the HEV group and the LEV group were 51.69 ± 21.51 Mets·h/week and 18.34 ± 4.55 Mets·h/week (p < 0.05), respectively (**Table 1**).

In the HEV group, in addition to walking, 14 of the participants without DPN routinely engaged in one or more of the following weight-bearing activities; brisk walking, square dancing, ball games (table tennis, tennis, golf, and billiards), cycling, and Tai Chi. Among them, one participant did brisk walking at about 3.7 mph every day; five participants engaged in square dancing every week; four participants engaged in ball games every week; two participants went cycling daily; and two participants did Tai Chi every day. For the other 31 participants in this group, the only routine daily physical activity was walking. Similarly, in the LEV group, the only routine physical activity was walking, but with a lower energy expenditure.

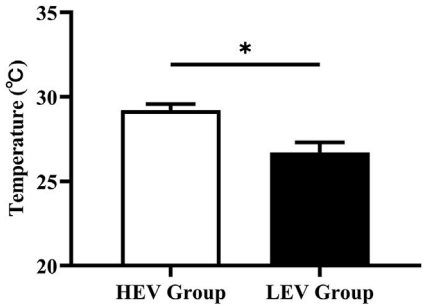

FIGURE 4 | Results of skin temperature of plantar tissue in participants (Mean with SEM). HEV: High Exercise Volume (≥27 Mets·h/week); LEV: Low Exercise Volume (<27 Mets·h/week); SEM: standard error of mean. * indicates a significant difference between the HEV group (n < 45) and LEV group (n < 35) (p < 0.05).

Effects of Weight-Bearing Exercise on Plantar Microcirculation

The plantar oxygen saturation (SO_2) and skin temperature (Temp) of both groups were recorded and analyzed (**Figures 3, 4**). The results showed that the plantar SO_2 (67.25 ± 6.12%) and plantar Temp (29.22 ± 2.44°C) in the HEV group were both significantly higher than the LEV group (SO_2: 63.75 ± 8.02%, p = 0.030; Temp: 26.72 ± 3.47°C, p = 0.001), respectively.

Table 2 shows the SO_2 and Temp for participants without diabetic peripheral neuropathy (Non-DPN) and DPN. The mean SO_2 and Temp of participants in the HEV group was higher than the LEV group. In the HEV group, the mean SO_2 of the DPN participants was lower than the Non-DPN participants. From **Table 2**, it can be seen that the mean SO_2 and mean Temp (except for Tai Chi) for participants in the sub-group "Walking + other weight-bearing activities" was higher than participants with "Only walking".

Effect of Weight-Bearing Exercise on Plantar Tissue Hardness

Figure 1 compares the plantar tissue hardness between the HEV and LEV group. The results showed that the mean tissue hardness in the HEV group was lower than that of the LEV group, with a significant difference at the big toe region (HEV: 27.89 ± 7.72°Shore, LEV: 32.25 ± 9.94°Shore; p = 0.030), midfoot (HEV: 26.59 ± 7.59°Shore, LEV: 31.20 ± 9.30°Shore; p = 0.034),

TABLE 2 | Plantar SO_2 and Temp for Non-DPN and DPN participants in the HEV and LEV groups, and for Non-DPN participants performing different physical activities in the HEV group (Participants in LEV group did not engage in any form of exercise other than walking; Mean ± SD).

	HEV group		LEV group	
	Non-DPN (*n* = 37)	**DPN (*n* = 8)**	**Non-DPN (*n* = 30)**	**DPN (*n* = 5)**
SO2 (%)	67.69 ± 6.37	65.23 ± 4.52	63.78 ± 8.30	63.56 ± 6.83
Temp (°C)	29.13 ± 2.57	29.62 ± 1.76	26.77 ± 3.54	26.40 ± 3.33

	Only walking in HEV group (n = 23)	**Walking + other weight-bearing activities in HEV group**				
		Brisk walking (*n* = 1)	**Square dancing (*n* = 5)**	**Ball games (n = 4)**	**Cycling (*n* = 2)**	**Tai Chi (*n* = 2)**
SO2 (%)	66.07 ± 6.33	70.90	68.28 ± 8.14	70.90 ± 5.93	73.07 ± 2.77	71.38 ± 1.81
Temp (°C)	28.87 ± 2.83	31.07	29.38 ± 2.59	29.32 ± 2.11	31.57 ± 0.03	28.02 ± 1.39

DPN: diabetic peripheral neuropathy; HEV: high exercise volume; LEV: low exercise volume; SO2: plantar oxygen saturation; Temp: skin temperature.

TABLE 3 | Plantar soft tissue hardness for Non-DPN and DPN participants in the HEV and LEV groups, and for Non-DPN participants performing different physical activities in the HEV group (Participants in LEV group did not engage in any form of exercise other than walking; Mean ± SD).

		HEV group		LEV group	
		Non-DPN (*n* = 37)	**DPN (*n* = 8)**	**Non-DPN (*n* = 30)**	**DPN (*n* = 5)**
Soft tissue (°shore)	Big toe	26.01 ± 6.47	36.60 ± 7.34	32.19 ± 10.43	32.60 ± 7.15
	Little toes	24.62 ± 8.78	35.68 ± 13.90	27.55 ± 8.36	27.76 ± 7.56
	Forefoot	31.41 ± 7.65	40.83 ± 6.48	34.45 ± 8.85	34.37 ± 7.93
	Midfoot	24.84 ± 6.39	34.69 ± 7.80	31.53 ± 9.71	29.20 ± 6.73
	Hindfoot	33.90 ± 9.19	46.15 ± 8.66	42.81 ± 12.84	42.04 ± 8.77

		Only walking in HEV group (*n* = 23)	**Walking + other weight-bearing activities in HEV group**				
			Brisk walking (*n* = 1)	**Square dancing (*n* = 5)**	**Ball games (*n* = 4)**	**Cycling (*n* = 2)**	**Tai Chi (*n* = 2)**
Soft tissue (°shore)	Big toe	25.29 ± 6.94	29.40	28.64 ± 6.54	28.40 ± 5.93	20.10 ± 4.38	27.10 ± 1.27
	Little toes	23.94 ± 8.83	35.60	29.16 ± 8.54	27.15 ± 9.64	15.50 ± 0.99	19.60 ± 3.11
	Forefoot	30.81 ± 8.09	34.47	31.84 ± 6.19	36.03 ± 8.01	25.33 ± 4.81	32.57 ± 10.98
	Midfoot	24.76 ± 6.92	27.30	21.80 ± 4.08	28.48 ± 6.54	21.80 ± 5.23	27.85 ± 7.14
	Hindfoot	34.39 ± 10.24	28.60	30.64 ± 6.30	38.75 ± 7.24	28.90 ± 10.32	34.30 ± 8.91

DPN: diabetic peripheral neuropathy; HEV: high exercise volume; LEV: low exercise volume.

and hindfoot (HEV: 36.08 ± 10.17°Shore, LEV: 42.70 ± 12.23°Shore; $p = 0.010$).

It was also found that SO_2 and Temp were negatively correlated with the tissue hardness of the big toe region (SO_2: R = −0.299, $p = 0.007$; Temp: R = −0.311, $p = 0.005$).

Within the HEV group, the mean plantar tissue hardness of all regions of the foot for the DPN participants was higher than that of the Non-DPN participants. For DPN participants, the mean plantar tissue hardness in the HEV group was higher than the LEV group. Also, the plantar tissue hardness in the Non-DPN participants in the HEV group varied depending on the type of routine physical activities typically performed. Four participants who played ball games and one participant who did brisk walking had a higher tissue hardness in the forefoot region than other participants, while two participants who routinely cycled had the lowest tissue hardness (**Table 3**).

DISCUSSION

This study analyzed the association between exercise volume and plantar microcirculation and soft tissue hardness in people with type 2 diabetes. The results showed that participants with higher volume of habitual exercise had better oxygen supply and basal skin temperature and lower soft tissue hardness of the foot, compared to participants with lower volume of habitual exercise. These findings suggest that weight-bearing exercise with high exercise volume might be associated with better microcirculation function and softer plantar tissue, which may not increase the risk of developing foot ulcers.

Previous studies reported that exercise can increase insulin sensitivity in people with diabetes and promote the production of endothelium-dependent vasodilator nitric oxide, thus improving endothelial and microvascular function and promoting metabolism in the lower extremities (Kluding et al., 2017). Studies have also shown that a high stress stimulus can increase vessel diameter and arterial compliance, and was beneficial for the cardiopulmonary and vascular function (Huonker et al., 1996; Mueller and Maluf, 2002). Charles et al. also found that people with diabetes who engaged in an eight-week aerobics programme (bicycle) had a 3.9% increase in peripheral oxygen saturation compared to the control group (Ezema et al., 2019). Demachi et al. reported that skin temperature gradually increases with the duration of exercise (Demachi et al., 2013). Similarly, this current study found that the high exercise volume group (≥27 Mets·h/week) had higher

plantar SO2 and basal Temp in comparison with the low exercise volume group (<27 Mets·h/week) (**Figures 3**, **4**). Moreover, participants in the sub-group "Walking + other weight-bearing activities" had a higher mean SO_2 and Temp than participants with "Only walking". This may be due to the higher energy requirements when performing more than one routine exercise (Walking + other weight-bearing activities: 67.66 ± 29.55 Mets·h/week; Only walking: 41.54 ± 8.06 Mets·h/week). Sivanandam et al. demonstrated that the foot temperature of people with diabetes was significantly lower than that of healthy people (Sivanandam et al., 2012). Decreased skin temperature may be related to poor microvascular perfusion of the lower extremity in people with diabetes, which further aggravates microvascular dysfunction and leads to the occurrence of DFUs. The results of this study suggest that weight-bearing exercise with high exercise volume has a more positive effect on circulation and the nutrient supply to the plantar microvasculature, implying that the active weight-bearing exercise may be associated with lower risk of DFUs.

Some studies reported that the abnormal increase of plantar skin temperature may indicate the occurrence of some pathologic factors (e.g., peripheral neuropathy (Yavuz et al., 2019) and inflammation responses (van Netten et al., 2014)). However, the study of Kokate et al. demonstrated that the damage of deep tissue would occur under the pressure stimulus at temperature above 35°C in a reliable porcine model, and no damage was observed in the superficial or deep tissues with a temperature of 25°C under the pressure stimulus (Kokate et al., 1995). In this study, we compared the basal foot temperature of people with diabetes with different exercise volumes, none of the participants had a diabetic foot ulcer history and their plantar temperature did not exceed 35°C. Therefore, the mean temperature of the high exercise volume group was higher than that of the low exercise volume group, which may be due to the improvement of lower extremity microvascular perfusion in people with diabetes caused by higher volume of habitual exercise.

In this study, a OO Shore durometer was used to assess the plantar soft tissue hardness in people with diabetes. The results showed that compared to the low exercise volume group, people with diabetes in the high exercise volume group who actively engaged in weight-bearing exercise had a significantly lower plantar tissue hardness (**Figure 1**). According to the Physical Stress Theory proposed by Muller et al. (Mueller and Maluf, 2002; Kluding et al., 2017), tissues have different adaptive responses to external physical stress stimulation, including decreased tolerance (e.g., atrophy), maintenance, increased tolerance (e.g., hypertrophy), injury, and death. Maintenance seems to be a tissue homeostasis, physical stress stimulus below the maintenance range may result in tissue atrophy, and physical stress stimulus above the maintenance range may result in increased tolerance (Mueller and Maluf, 2002; Kluding et al., 2017). Therefore, people with diabetes in the high exercise volume group who showed a lower plantar tissue hardness may be due to the enhanced tissue adaptability under suitable repeated stress stimulus among the maintenance range. Decreased tolerance (e.g., atrophy) in the low exercise volume group may be more prone to tissue damage and cuticle thickening under mild external stress stimulus, which further leads to callus formation and an increased risk of DFUs. Some studies also reported that higher and long-term repetitive physical stress can increase collagen content and the diameter of collagen fibers, thicken skin and increase skin strength, which is beneficial to distribute plantar pressure and decrease the risk of skin breakdown (Sanders et al., 1995; Mueller and Maluf, 2002). Therefore, the mechanical stress stimulation during weight-bearing exercise in the high exercise volume group examined in this study could be expected to increase the stress tolerance threshold of plantar tissue and improve skin health.

The lower plantar tissue hardness of people with diabetes in the high exercise volume group could also be due to the improved blood circulation in the foot and enhanced protective response of tissue microvessels under stress. Mithraratne et al. demonstrated a negative correlation between the hardness of plantar tissue and the level of blood supply in the arteries of the foot (Mithraratne et al., 2012). Exercise can improve blood flow and oxygen saturation levels, which has been shown to reduce local hypoxia and waste accumulation in the foot tissue of people with diabetes (Kluding et al., 2017; Reis et al., 2019), and improve the plantar tissue viability and tolerance under an external stimulus (Jan et al., 2013b). From this study, it is evident that tissue hardness of the foot is negatively correlated with SO2 and Temp, which further confirms the above interpretation. It indicates that weight-bearing exercise with habitual high exercise volume can improve the biomechanical properties and microcirculation in the feet of people with diabetes, which can interact to play a positive role in protecting overall foot health.

In this study, eight participants were confirmed as diabetic peripheral neuropathy in the high exercise volume group (17.8%), and five participants were confirmed as diabetic peripheral neuropathy in the low exercise volume group (14.3%). This study found that the plantar SO_2 of DPN participants was slightly lower than the Non-DPN participants in the high exercise volume group (65.23 ± 4.52 vs 67.69 ± 6.37; unit: %), and the DPN participants had the highest plantar tissue hardness value (Big toe: 36.60 ± 7.34; Little toes: 35.68 ± 13.90; Forefoot: 40.83 ± 6.48; Midfoot: 34.69 ± 7.80; Hindfoot: 46.15 ± 8.66; unit: °shore). This may be due to the reduced tissue deformability and perception to external mechanical stress caused by diabetic neuropathy. For people with diabetes and neuropathy, the loss of protective sensations in the foot, dysfunction in sweat glands, bone deformities and abnormal stress distribution would further accelerate plantar tissue stiffening (Bowering, 2001; Sun et al., 2011). The impaired microvascular regulation caused by neuropathy can hinder the oxygenation capacity and waste removal capability of foot tissue under mechanical stress. This may be the reason for the decreased SO_2 and increased tissue hardness in DPN participants in the high exercise volume group (Edmonds et al., 1982; Stevens et al., 1991). Although it has been reported that moderate walking speed does not increase the incidence and recurrence of foot ulcers in people with DPN (LeMaster et al., 2008), a higher tissue hardness and lower SO_2 are thought to increase the risk of developing foot ulcers (Murray et al., 1996; Jan et al., 2013a). Therefore, neuropathy may be an important consideration when people with diabetes engage in exercise, and it is necessary for people with DPN to carefully

choose the type and intensity of weight-bearing exercise. In the future, it is still necessary to expand the sample size and conduct a similar study on people with diabetic peripheral neuropathy to clarify the impact of weight-bearing exercise on the risk of diabetic foot ulcers in people with diabetic peripheral neuropathy.

In addition, the results of this study showed that participants who regularly went for brisk walk and participated in ball games had higher plantar tissue hardness in the forefoot region. Participants with brisk walking had the highest plantar tissue hardness in the hindfoot region (**Table 3**). Burnfield et al. found that faster walking increased the plantar pressure around the toes, medial metatarsal heads and heel when healthy elderly people walked at different speeds (57, 80, 97 m/min) (Burnfield et al., 2004). Similarly, Lam et al. reported that playing table tennis produced higher peak pressure in the total foot during side-step and cross-step footwork in comparison with one-step footwork (Lam et al., 2019). This suggests that the high hardness in participants of this study who routinely participated in brisk walking and ball games (table tennis, tennis, golf, and billiards) may be related to the repetitive high plantar pressure acting on the plantar soft tissues during exercise. Such a high-magnitude pressure stimulus for a brief duration may cause excessive physical stress to plantar tissue, and further cause callus formation and tissue damage (Murray et al., 1996; Mueller and Maluf, 2002). However, the effect of different types of exercise on the risk of developing DFUs needs further exploration.

There are some limitations to this study that should be noted. Firstly, the durometer works on the principle of indentation to characterize the plantar tissue hardness, ignoring the non-linear viscoelastic behaviour and tissue thickness. Subsequent studies can use ultrasound imaging to explore the biomechanical properties of plantar tissue in more detail. Secondly, this study only considered a limited number of physical activities with moderate intensity, and the predominant exercise performed across all participants was walking. The influence of accumulated stress and different activity patterns on the risk of developing DFUs needs further study. Thirdly, the impact of exercise on other DFUs risk factors such as transcutaneous oxygen tension ($TcPO_2$), the microvascular response to mechanical stress, musculoskeletal deformities and callus formation of the foot may be considered in future studies. Fourthly, participants in this study had not yet developed foot ulcers. Because the relationships between foot ulcers and tissue hardness, and oxygen saturation are still unclear, follow-up studies should determine whether lower oxygen saturation and higher plantar tissue hardness in the low exercise volume group with diabetic peripheral neuropathy is associated with higher incidence of diabetic foot ulcers.

CONCLUSION

In conclusion, this study found that higher volumes of habitual weight-bearing exercise in people with type 2 diabetes are associated with better plantar tissue oxygenation and lower plantar tissue hardness. These changes may decrease the risk of developing diabetic foot ulcers.

DATA AVAILABILITY STATEMENT

The original contributions presented in the study are included in the article/Supplementary Material, further inquiries can be directed to the corresponding authors.

ETHICS STATEMENT

The studies involving human participants were reviewed and approved by the institutional review board of Affiliated Hospital of National Research Center for Rehabilitation Technical Aids (20190101) and the Declaration of Helsinki (2013 revision). The patients/participants provided their written informed consent to participate in this study.

AUTHOR CONTRIBUTIONS

Methodology, YF, FP, and Y-KJ; formal analysis, WR and YD; investigation, WY, WL, HL, and JG; data curation, WR, YD, and WY; writing—original draft preparation, WR and YD; writing—review and editing, FP and Y-KJ; funding acquisition, WR, YF and FP. All authors have read and agreed to the published version of the manuscript.

FUNDING

This research was funded by the National Natural Science Foundation of China (Grant Nos 11902089, 11672027, U20A20390, and 11827803), and Beijing Municipal Science and Technology Commission (Grant Number Z171100000517010).

ACKNOWLEDGMENTS

The authors thank all subjects who participated in this study.

REFERENCES

Ainsworth, B. E., Haskell, W. L., Herrmann, S. D., Meckes, N., Bassett, D. R., Jr., Tudor-Locke, C., et al. (2011). 2011 Compendium of Physical Activities. *Med. Sci. Sports Exer* 43 (8), 1575–1581. doi:10.1249/MSS.0b013e31821ece12

Ainsworth, B. E. (2014). "How to Assess the Energy Costs of Exercise and Sport," in *Sports Nutrition*. Editor R. J. Maughan. 1st ed (UK: John Wiley & Sons), 67.

Armstrong, D. G., Boulton, A. J. M., and Bus, S. A. (2017). Diabetic Foot Ulcers and Their Recurrence. *N. Engl. J. Med.* 376 (24), 2367–2375. doi:10.1056/NEJMra1615439

Association, A. D. (2020). 5. Facilitating Behavior Change and Well-Being to Improve Health Outcomes: Standards of Medical Care in Diabetes-2020. *Dia Care* 43 (1), S48–S65. doi:10.2337/dc20-S005

Boulton, A. J. M., Armstrong, D. G., Albert, S. F., Frykberg, R. G., Hellman, R., Kirkman, M. S., et al. (2008). Comprehensive Foot Examination and Risk Assessment: A Report of the Task Force of the Foot Care Interest Group of the

American Diabetes Association, with Endorsement by the American Association of Clinical Endocrinologists. *Diabetes Care* 31 (8), 1679–1685. doi:10.2337/dc08-9021

Bowering, C. K. (2001). Diabetic Foot Ulcers. Pathophysiology, Assessment, and Therapy. *Can. Fam. Physician* 47 (5), 1007–1016.

Burnfield, J. M., Few, C. D., Mohamed, O. S., and Perry, J. (2004). The Influence of Walking Speed and Footwear on Plantar Pressures in Older Adults. *Clin. Biomech.* 19 (1), 78–84. doi:10.1016/j.clinbiomech.2003.09.007

Caselli, A., Pham, H., Giurini, J. M., Armstrong, D. G., and Veves, A. (2002). The Forefoot-To-Rearfoot Plantar Pressure Ratio Is Increased in Severe Diabetic Neuropathy and Can Predict Foot Ulceration. *Diabetes Care* 25 (6), 1066–1071. doi:10.2337/diacare.25.6.1066

Chao, C. Y. L., and Cheing, G. L. Y. (2009). Microvascular Dysfunction in Diabetic Foot Disease and Ulceration. *Diabetes Metab. Res. Rev.* 25 (7), 604–614. doi:10.1002/dmrr.1004

Chao, C. Y. L., Zheng, Y.-P., and Cheing, G. L. Y. (2011). *Epidermal Thickness and Biomechanical Properties of Plantar Tissues in Diabetic Foot. Ultrasound Med. Biol.* 37 (7), 1029–1038. doi:10.1016/j.ultrasmedbio.2011.04.004

Demachi, K., Yoshida, T., Kume, M., Tsuji, M., and Tsuneoka, H. (2013). The Influence of Internal and Skin Temperatures on Active Cutaneous Vasodilation under Different Levels of Exercise and Ambient Temperatures in Humans. *Int. J. Biometeorol.* 57 (4), 589–596. doi:10.1007/s00484-012-0586-y

Di Loreto, C., Fanelli, C., Lucidi, P., Murdolo, G., De Cicco, A., Parlanti, N., et al. (2005). Make Your Diabetic Patients Walk: Long-Term Impact of Different Amounts of Physical Activity on Type 2 Diabetes. *Diabetes Care* 28 (6), 1295–1302. doi:10.2337/diacare.28.6.1295

Edmonds, M. E., Roberts, V. C., and Watkins, P. J. (1982). Blood Flow in the Diabetic Neuropathic Foot. *Diabetologia* 22 (1), 9–15. doi:10.1007/bf00253862

Ezema, C. I., Omeh, E., Omeh, E., Onyeso, O. K. K., Anyachukwu, C. C., Nwankwo, M. J., et al. (2019). The Effect of an Aerobic Exercise Programme on Blood Glucose Level, Cardiovascular Parameters, Peripheral Oxygen Saturation, and Body Mass Index Among Southern Nigerians with Type 2 Diabetes Mellitus, Undergoing Concurrent Sulfonylurea and Metformin Treatment. *Malaysian J. Med. Sci.* 26 (5), 88–97. doi:10.21315/mjms2019.26.5.8

Greenman, R. L., Panasyuk, S., Wang, X., Lyons, T. E., Dinh, T., Longoria, L., et al. (2005). Early Changes in the Skin Microcirculation and Muscle Metabolism of the Diabetic Foot. *The Lancet* 366 (9498), 1711–1717. doi:10.1016/s0140-6736(05)67696-9

Huonker, M., Halle, M., and Keul, J. (1996). Structural and Functional Adaptations of the Cardiovascular System by Training. *Int. J. Sports Med.* 17 (3), S164–S172. doi:10.1055/s-2007-972919

Jan, Y.-K., Lung, C.-W., Cuaderes, E., Rong, D., and Boyce, K. (2013a). Effect of Viscoelastic Properties of Plantar Soft Tissues on Plantar Pressures at the First Metatarsal Head in Diabetics with Peripheral Neuropathy. *Physiol. Meas.* 34 (1), 53–66. doi:10.1088/0967-3334/34/1/53

Jan, Y.-K., Shen, S., Foreman, R. D., and Ennis, W. J. (2013b). Skin Blood Flow Response to Locally Applied Mechanical and thermal Stresses in the Diabetic Foot. *Microvasc. Res.* 89, 40–46. doi:10.1016/j.mvr.2013.05.004

Kabbani, M., Rotter, R., Busche, M., Wuerfel, W., Jokuszies, A., Knobloch, K., et al. (2013). Impact of Diabetes and Peripheral Arterial Occlusive Disease on the Functional Microcirculation at the Plantar Foot. *Plast. Reconstr. Surg. Glob. open* 1 (7), e48. doi:10.1097/GOX.0b013e3182a4b9cb

Kluding, P. M., Bareiss, S. K., Hastings, M., Marcus, R. L., Sinacore, D. R., and Mueller, M. J. (2017). Physical Training and Activity in People with Diabetic Peripheral Neuropathy: Paradigm Shift. *Phys. Ther.* 97 (1), 31–43. doi:10.2522/ptj.20160124

Knowler, W. C., Barrett-Connor, E., Fowler, S. E., Hamman, R. F., Lachin, J. M., Walker, E. A., et al. (2002). Reduction in the Incidence of Type 2 Diabetes with Lifestyle Intervention or Metformin. *N. Engl. J. Med.* 346 (6), 393–403. doi:10.1056/nejmoa012512

Kokate, J. Y., Leland, K. J., Held, A. M., Hansen, G. L., Kveen, G. L., Johnson, B. A., et al. (1995). Temperature-modulated Pressure Ulcers: a Porcine Model. *Arch. Phys. Med. Rehabil.* 76 (7), 666–673. doi:10.1016/s0003-9993(95)80637-7

Ladurner, R., Feilitzsch, M., Steurer, W., Coerper, S., Königsrainer, A., and Beckert, S. (2009). The Impact of a Micro-lightguide Spectrophotometer on the Intraoperative Assessment of Hepatic Microcirculation: A Pilot Study. *Microvasc. Res.* 77 (3), 387–388. doi:10.1016/j.mvr.2009.01.008

Lalli, P., Chan, A., Garven, A., Midha, N., Chan, C., Brady, S., et al. (2013). Increased Gait Variability in Diabetes Mellitus Patients with Neuropathic Pain. *J. Diabetes its Complications* 27 (3), 248–254. doi:10.1016/j.jdiacomp.2012.10.013

Lam, W.-K., Fan, J.-X., Zheng, Y., and Lee, W. C.-C. (2019). Joint and Plantar Loading in Table Tennis Topspin Forehand with Different Footwork. *Eur. J. Sport Sci.* 19 (4), 471–479. doi:10.1080/17461391.2018.1534993

LeMaster, J. W., Mueller, M. J., Reiber, G. E., Mehr, D. R., Madsen, R. W., and Conn, V. S. (2008). Effect of Weight-Bearing Activity on Foot Ulcer Incidence in People with Diabetic Peripheral Neuropathy: Feet First Randomized Controlled Trial. *Phys. Ther.* 88 (11), 1385–1398. doi:10.2522/ptj.20080019

Liao, F., An, R., Pu, F., Burns, S., Shen, S., and Jan, Y.-K. (2019). Effect of Exercise on Risk Factors of Diabetic Foot Ulcers. *Am. J. Phys. Med. Rehabil.* 98 (2), 103–116. doi:10.1097/phm.0000000000001002

Mithraratne, K., Ho, H., Hunter, P. J., and Fernandez, J. W. (2012). Mechanics of the Foot Part 2: A Coupled Solid-Fluid Model to Investigate Blood Transport in the Pathologic Foot. *Int. J. Numer. Meth. Biomed. Engng.* 28 (10), 1071–1081. doi:10.1002/cnm.2493

Mueller, M. J., and Maluf, K. S. (2002). Tissue Adaptation to Physical Stress: A Proposed "physical Stress Theory" to Guide Physical Therapist Practice, Education, and Research. *Phys. Ther.* 82 (4), 383–403. doi:10.1093/ptj/82.4.383

Mueller, M. J., Tuttle, L. J., LeMaster, J. W., Strube, M. J., McGill, J. B., Hastings, M. K., et al. (2013). Weight-Bearing versus Nonweight-Bearing Exercise for Persons with Diabetes and Peripheral Neuropathy: A Randomized Controlled Trial. *Arch. Phys. Med. Rehabil.* 94 (5), 829–838. doi:10.1016/j.apmr.2012.12.015

Murray, H. J., Young, M. J., Hollis, S., and Boulton, A. J. M. (1996). The Association between Callus Formation, High Pressures and Neuropathy in Diabetic Foot Ulceration. *Diabet. Med.* 13 (11), 979–982. doi:10.1002/(sici)1096-9136(199611)13:11<979:aid-dia267>3.0.co;2-a

Mynarski, W., Psurek, A., Borek, Z., Rozpara, M., Grabara, M., and Strojek, K. (2012). Declared and Real Physical Activity in Patients with Type 2 Diabetes Mellitus as Assessed by the International Physical Activity Questionnaire and Caltrac Accelerometer Monitor: A Potential Tool for Physical Activity Assessment in Patients with Type 2 Diabetes Mellitus. *Diabetes Res. Clin. Pract.* 98 (1), 46–50. doi:10.1016/j.diabres.2012.05.024

Narres, M., Kvitkina, T., Claessen, H., Droste, S., Schuster, B., Morbach, S., et al. (2017). Incidence of Lower Extremity Amputations in the Diabetic Compared with the Non-diabetic Population: A Systematic Review. *Plos One* 12 (8), e0182081. doi:10.1371/journal.pone.0182081

Newton, D. J., Bennett, S. P., Fraser, J., Khan, F., Belch, J. J. F., Griffiths, G., et al. (2005). Pilot Study of the Effects of Local Pressure on Microvascular Function in the Diabetic Foot. *Diabet Med.* 22 (11), 1487–1491. doi:10.1111/j.1464-5491.2005.01659.x

Periyasamy, R., Gandhi, T. K., Das, S. R., Ammini, A. C., and Anand, S. (2012). A Screening Computational Tool for Detection of Diabetic Neuropathy and Non-neuropathy in Type-2 Diabetes Subjects. *J. Med. Imaging Hlth Inform.* 2 (3), 222–229. doi:10.1166/jmihi.2012.1093

Pu, F., Ren, W., Fu, H., Zheng, X., Yang, M., Jan, Y.-K., et al. (2018). Plantar Blood Flow Response to Accumulated Pressure Stimulus in Diabetic People with Different Peak Plantar Pressure: a Non-randomized Clinical Trial. *Med. Biol. Eng. Comput.* 56 (7), 1127–1134. doi:10.1007/s11517-018-1836-x

Reis, J. F., Fatela, P., Mendonca, G. V., Vaz, J. R., Valamatos, M. J., Infante, J., et al. (2019). Tissue Oxygenation in Response to Different Relative Levels of Blood-Flow Restricted Exercise. *Front. Physiol.* 10, 407. doi:10.3389/fphys.2019.00407

Sanders, J. E., Goldstein, B. S., and Leotta, D. F. (1995). Skin Response to Mechanical Stress: Adaptation rather Than Breakdown-A Review of the Literature. *J. Rehabil. Res. Dev.* 32 (3), 214–226.

Schaper, N. C., Netten, J. J., Apelqvist, J., Bus, S. A., Hinchliffe, R. J., Lipsky, B. A., et al. (2020). Practical Guidelines on the Prevention and Management of Diabetic Foot Disease (IWGDF 2019 Update). *Diabetes Metab. Res. Rev.* 36, e3266. doi:10.1002/dmrr.3266

Sivanandam, S., Anburajan, M., Venkatraman, B., Menaka, M., and Sharath, D. (2012). Medical Thermography: a Diagnostic Approach for Type 2 Diabetes Based on Non-contact Infrared thermal Imaging. *Endocrine* 42 (2), 343–351. doi:10.1007/s12020-012-9645-8

Stevens, M. J., Edmonds, M. E., Douglas, S. L. E., and Watkins, P. J. (1991). Influence of Neuropathy on the Microvascular Response to Local Heating in the Human Diabetic Foot. *Clin. Sci.* 80 (3), 249–256. doi:10.1042/cs0800249

Sun, J.-H., Cheng, B. K., Zheng, Y.-P., Huang, Y.-P., Leung, J. Y., and Cheing, G. L. (2011). Changes in the Thickness and Stiffness of Plantar Soft Tissues in People with Diabetic Peripheral Neuropathy. *Arch. Phys. Med. Rehabil.* 92 (9), 1484–1489. doi:10.1016/j.apmr.2011.03.015

Teoh, J. C., and Lee, T. (2020). Identification of Potential Plantar Ulceration Among Diabetes Patients Using Plantar Soft Tissue Stiffness. *J. Mech. Behav. Biomed. Mater.* 103, 103567. doi:10.1016/j.jmbbm.2019.103567

Thomas, V. J., Patil, K. M., Radhakrishnan, S., Narayanamurthy, V. B., and Parivalavan, R. (2003). The Role of Skin Hardness, Thickness, and Sensory Loss on Standing Foot Power in the Development of Plantar Ulcers in Patients with Diabetes Mellitus-A Preliminary Study. *The Int. J. Lower Extremity Wounds* 2 (3), 132–139. doi:10.1177/1534734603258601

van Netten, J. J., Prijs, M., van Baal, J. G., Liu, C., van der Heijden, F., and Bus, S. A. (2014). Diagnostic Values for Skin Temperature Assessment to Detect Diabetes-Related Foot Complications. *Diabetes Technol. Ther.* 16 (11), 714–721. doi:10.1089/dia.2014.0052

Verboven, M., Van Ryckeghem, L., Belkhouribchia, J., Dendale, P., Eijnde, B. O., Hansen, D., et al. (2019). Effect of Exercise Intervention on Cardiac Function in Type 2 Diabetes Mellitus: A Systematic Review. *Sports Med.* 49 (2), 255–268. doi:10.1007/s40279-018-1003-4

Wen, C. P., Wai, J. P. M., Tsai, M. K., Yang, Y. C., Cheng, T. Y. D., Lee, M.-C., et al. (2011). Minimum Amount of Physical Activity for Reduced Mortality and Extended Life Expectancy: a Prospective Cohort Study. *The Lancet* 378 (9798), 1244–1253. doi:10.1016/s0140-6736(11)60749-6

Yavuz, M., Ersen, A., Hartos, J., Lavery, L. A., Wukich, D. K., Hirschman, G. B., et al. (2019). Temperature as a Causative Factor in Diabetic Foot Ulcers: A Call to Revisit Ulceration Pathomechanics. *J. Am. Podiatric Med. Assoc.* 109 (5), 345–350. doi:10.7547/17-131

Zhang, Y., Lazzarini, P. A., McPhail, S. M., van Netten, J. J., Armstrong, D. G., and Pacella, R. E. (2020). Global Disability Burdens of Diabetes-Related Lower-Extremity Complications in 1990 and 2016. *Dia Care* 43 (5), 964–974. doi:10.2337/dc19-1614

Conflict of Interest: The authors declare that the research was conducted in the absence of any commercial or financial relationships that could be construed as a potential conflict of interest.

Publisher's Note: All claims expressed in this article are solely those of the authors and do not necessarily represent those of their affiliated organizations, or those of the publisher, the editors and the reviewers. Any product that may be evaluated in this article, or claim that may be made by its manufacturer, is not guaranteed or endorsed by the publisher.

frontiers in Bioengineering and Biotechnology

ORIGINAL RESEARCH
published: 29 November 2021
doi: 10.3389/fbioe.2021.753897

An Exploratory Analysis of the Role of Adipose Characteristics in Fulltime Wheelchair Users' Pressure Injury History

Sharon Eve Sonenblum[1], Megan Measel[2], Stephen H. Sprigle[1,3], John Greenhalgh[4] and John McKay Cathcart[5]*

[1]Rehabilitation Engineering and Applied Research Laboratory, The George W. Woodruff School of Mechanical Engineering, Georgia Institute of Technology, Atlanta, GA, United States, [2]Wallace H. Coulter Department of Biomedical Engineering, Georgia Institute of Technology, Atlanta, GA, United States, [3]College of Design, Georgia Institute of Technology, Atlanta, GA, United States, [4]FONAR Corporation, Melville, NY, United States, [5]School of Health Sciences, Ulster University, Northern Ireland, Coleraine, United Kingdom

OPEN ACCESS

Edited by:
Peter Pivonka, Queensland University of Technology, Australia

Reviewed by:
Jicheng Fu, University of Central Oklahoma, United States
Anke Scheel-Sailer, Swiss Paraplegic Center, Switzerland
Yi-Ting Tzen, University of Texas Southwestern Medical Center, United States

***Correspondence:**
Sharon Eve Sonenblum
ss427@gatech.edu

Specialty section:
This article was submitted to Biomechanics, a section of the journal Frontiers in Bioengineering and Biotechnology

Received: *05 August 2021*
Accepted: *26 October 2021*
Published: *29 November 2021*

Citation:
Sonenblum SE, Measel M, Sprigle SH, Greenhalgh J and Cathcart JM (2021) An Exploratory Analysis of the Role of Adipose Characteristics in Fulltime Wheelchair Users' Pressure Injury History. Front. Bioeng. Biotechnol. 9:753897. doi: 10.3389/fbioe.2021.753897

Aim: The goals of this study were 1) to identify the relationship between adipose (subcutaneous and intramuscular) characteristics and pressure injury (PrI) history in wheelchair users and 2) to identify subject characteristics, including biomechanical risk, that are related to adipose characteristics.

Materials and Methods: The buttocks of 43 full-time wheelchair users with and without a history of pelvic PrIs were scanned in a seated posture in a FONAR UPRIGHT® MRI. Intramuscular adipose (the relative difference in intensity between adipose and gluteus maximus) and the subcutaneous adipose characteristics (the relative difference in intensity between subcutaneous adipose under and surrounding the ischium) were compared to PrI history and subject characteristics.

Results: Participants with a history of PrIs had different subcutaneous fat (subQF) characteristics than participants without a history of PrIs. Specifically, they had significantly darker adipose under the ischium than surrounding the ischium (subQF effect size = 0.21) than participants without a history of PrIs (subQF effect size = 0.58). On the other hand, only when individuals with complete fat infiltration (n = 7) were excluded did individuals with PrI history have more fat infiltration than those without a PrI history. The presence of spasms (μ intramuscular adipose, 95% CI with spasms 0.642 [0.430, 0.855], without spasms 0.168 [–0.116, 0.452], $p = 0.01$) and fewer years using a wheelchair were associated with leaner muscle (Pearson Corr = –0.442, $p = 0.003$).

Conclusion: The results of the study suggest the hypothesis that changes in adipose tissue under the ischial tuberosity (presenting as darker SubQF) are associated with increased biomechanical risk for pressure injury. Further investigation of this hypothesis, and the role of intramuscular fat infiltration in PrI development, may help our understanding of PrI etiology. It may also lead to clinically useful diagnostic techniques that can identify changes in adipose and biomechanical risk to inform early preventative interventions.

Keywords: adipose, pressure injury, pressure ulcer, MRI, biomechanical risk, wheelchair, spinal cord injury

INTRODUCTION

Full-time wheelchair users are at a higher risk for pressure injuries (PrIs) due to continuous, high magnitude loading and lack of sensation (Bergstrom et al., 1995; Salzberg, et al., 1996). Disability categories with the highest PrI prevalence include paraplegia/quadriplegia, spina bifida, Alzheimer disease, hemiplegia, cerebral palsy, Parkinson disease, and multiple sclerosis (Sprigle et al., 2020). Previous research has identified many risk factors such as age, poor nutrition, and shearing, which significantly add to an individual's PrI risk (Braden and Bergstrom, 1987; European Pressure Ulcer Advisory Panel, National Pressure Injury Advisory Panel and Pan Pacific Pressure Injury Alliance, 2019). Investigation into the role of adipose and its relationship to tissue tolerance and PrI risk has been limited, despite considerable evidence on the effect of adipose on an individual's health (Garcia and Thomas 2006; Lemmer, Alvarado et al., 2019; Bogie, Schwartz et al., 2020).

There are multiple kinds of adipose depots, such as visceral, intramuscular, and subcutaneous, that differ in adipose characteristics. Intramuscular adipose tissue (IMAT) is the sum of the fat that lies underneath the fascia and between muscle groups and the fat that is infiltrated between and/or within the muscle fibers. Subcutaneous fat (SubQF), by definition, exists deep to the epidermis and dermis and represents the majority of body fat.

The majority of research about adipose is not focused on pressure injuries but on obesity, diabetes, and related disciplines. IMAT in obese and glucose-tolerant individuals has been found to be associated with decreased muscle quality and increased insulin resistance, which increases the risk for type 2 diabetes (Goodpaster, Thaete et al., 2000; Addison, Marcus et al., 2014). Like IMAT, previous research has shown that SubQF located in the abdominal region has been correlated with insulin resistance. However, in the gluteal–femoral region, the SubQF tissue has been shown to protect against metabolic dysregulation and insulin resistance (Patel and Abate 2013; Addison, Marcus et al., 2014). Additionally, lower body SubQF has been found to protect systemic glucose homeostasis and inhibit obesity-induced muscle pathophysiology (Booth, Magnuson et al., 2018). Previous research suggested that the protection might be due to fat storage capacity (Grundy 2015; Booth, Magnuson et al., 2018). As a result, this would increase blood flow, since an increased insulin resistance is correlated to decreased skin blood flow regulation (Snijder et al., 2005; Yim, Heshka et al., 2008; Liao, Burns et al., 2013; Bhattacharya and Mishra 2015; Lambadiari, Triantafyllou et al., 2015).

In early studies, IMAT has been found to be directly correlated with PrI history in individuals with a spinal cord injury (Ogawa, Lester et al., 2017; Lemmer, Alvarado et al., 2019). A follow-up study on individuals with spinal cord injuries found that IMAT was correlated with circulatory adipogenic and myogenic biomarkers (Bogie, Schwartz et al., 2020). Although IMAT is common, the mechanisms for its development and effects remain unknown. Therefore, understanding the individual characteristics that predict IMAT for a wheelchair user (e.g., age, years of immobility, spasticity, etc.) may inform the physiology behind the infiltration process. With this knowledge, future interventions may target improvement of muscle quality. Furthermore, it would be beneficial to confirm previous results regarding the relationship between IMAT and PrI development in a larger population of wheelchair users.

Contrary to the role of IMAT, a loss of subcutaneous fat (SubQF) has been shown to increase PrI risk (Garcia and Thomas 2006; Sonenblum, Seol et al., 2020). Obesity, exercise, and hypoxia can all change the characteristics of adipose (Alkhouli, Mansfield et al., 2013; Frayn and Karpe 2014; Lempesis et al., 2020). Furthermore, adipogenesis is a mechanosensitive process (Hara, Wakino et al., 2011; Levy, Enzer et al., 2012). Therefore, the constant loading experienced by wheelchair users who sit nearly 12 h/day (Sonenblum and Sprigle 2011; Sonenblum, Sprigle et al., 2012) has significant potential to change the characteristics of the SubQF of wheelchair users. To date, these changes have not been studied.

Biomechanical risk is an intrinsic characteristic of an individual's soft tissue to deform in response to extrinsic applied forces, and it is associated with PrI risk (Sonenblum, Seol et al., 2020). Understanding biomechanical risk is critical for assessing PrI risk and optimizing PrI prevention, but changes that occur in SubQF and how they influence biomechanical risk have not yet been studied. Furthermore, understanding what subject characteristics are associated with change in SubQF characteristics may help identify factors that assist in PrI prevention.

This study sought to accomplish two goals: (1) to identify the relationship between adipose (SubQF and IMAT) characteristics and PrI history in wheelchair users and 2) to identify subject characteristics, including biomechanical risk, that are related to adipose (SubQF and IMAT) characteristics. Because the changes in adipose are poorly understood, we also investigated whether IMAT was associated with SubQF characteristics.

METHODS

Subjects

Forty-three individuals who use wheelchairs as their primary mobility device were included in this exploratory secondary analysis. Participants were recruited from either the New York, Colorado, Georgia, or New Jersey area. This study was approved by institutional review boards at a primary research site and multiple clinical sites. All participants reviewed and signed the informed consent form as approved by their local institutional review board prior to participation in the study. Inclusion criteria required that the participants must have been using a wheelchair for at least 2 years and were able to remain stable while seated on flat foam in the MRI environment. If the participants had a current PrI, they could not be on restricted sitting time or be considered at risk from sitting on the test cushions or performing additional transfers. A subset of this population has been published previously in Sonenblum, Seol et al. (2020).

Study Protocol

Each subject had their characteristics, such as age, body mass index (BMI), PrI history, and presence of spasticity, collected *via*

a self-reported health form. Participants reported a PrI history if they had experienced at least one prior PrI at an ischium or in the sacral/coccygeal region, and at which location(s) they had experienced the PrIs. Participants' buttocks were scanned while they sat in a FONAR UPRIGHT® MRI. Since these scans were originally taken for the purpose of measuring seated tissue deformation, a FONAR UPRIGHT® MRI was used, and T1-weighted (RF spoiled) 3D in-phase gradient echo scans were taken with participants seated. Scans had a 280-mm field of view with 3.0 mm contiguous slices in the sagittal plane. The field of view was centered on the right ischial tuberosity for most participants, unless participants had an active pressure ulcer on that side or any hardware that would cause an artifact in the MRI (such as a hip implant), in which case the left ischial tuberosity was the center of the field of view. Most participants were scanned while seated on an $18'' \times 18''$ cushion made with flat $3''$ HR45 foam. However, five participants were not studied in this condition. Therefore, for this analysis, scans collected on a Matrx Vi (Invacare, n = 4), or Embrace (Permobil, n = 1) were used. Both the Embrace and Matrx Vi are contoured foam cushions, as opposed to flat foam, but they created a similar loaded condition to study the adipose characteristics of the buttocks.

Expert clinicians assisted with seating the subjects to have their pelvis in a neutral posture. The footrest was also adjusted to properly load the thighs and to keep the knees and hips close to 90° of flexion (Sonenblum, Seol et al., 2020).

An additional subject characteristic was measured with subjects seated on the same reference foam on which they were imaged. Compressible hip breadth was measured by measuring the bi-trochanteric distance twice: once with no tissue compression and once with maximum compression (i.e., until the tissue could not be compressed any farther), and the difference between the two was computed.

Data Processing

MRI Image Processing

The raw DICOM scans were imported into MRI analysis software, AnalyzePro (AnalyzeDirect, Overland Park, KS), for review and segmentation of the pelvis, gluteus maximus, and the subcutaneous fat of the side of the buttocks included in the MRI. Trained researchers under the supervision of an experienced radiographer (Cathcart) performed the segmentations for a single slice of the MRI scans located at the peak of the ischial tuberosity in the sagittal plane. Skin was included within the subcutaneous fat segmentation when visible since the scan resolution did not allow for separate segmentation of the two. The region pixel intensities and the coordinate location points from the adipose and gluteus maximus segmentations from the sagittal slice were extracted and interpreted using MATLAB R2020a (MathWorks, Natick, MA).

Measures associated with biomechanical risk included bulk tissue thickness and sagittal radius of curvature, and their calculations have been described previously (Sonenblum et al., 2020). Briefly, bulk tissue thickness is defined as the average tissue thickness under the ischial tuberosity measured in an oblique plane in a region 50 mm long. The radius of curvature is computed in a 50-mm region centered at the peak of the ischial tuberosity in the sagittal plane.

Because the scans were taken with a planar surface coil (Quad-Z Planar) located in the axial plane under the wheelchair cushion, there was an image intensity gradient along an axis orthogonal to the coil, i.e., in the superior–inferior direction. Therefore, it was necessary to correct for this gradient to allow for accurate comparison between the gluteus maximus and adipose intensities when calculating intramuscular fat infiltration.

To correct for the image intensity gradient, we used a control MRI scan of a basketball filled with dilute nickel chloride (to mimic human tissue) that was placed on top of the Quad-Z Planar coil at its center (**Figure 1**) with the same sequence parameters used to scan participants. Because the basketball was filled with a homogenous fluid, the smooth variation in pixel brightness from point to point (voxel to voxel) can be attributed to voxel distance from the conductive elements of the receiver coil. Therefore, a normalization curve was defined to represent the variation in intensity of the image using the power function through MATLAB's Curve Fitting Tool as a function of distance across the vertical axis of the scan (the superior–inferior direction). Sagittal voxel intensities in the buttocks scans were corrected by subtracting the normalization curve from the original scan intensities.

Intramuscular Adipose Tissue

To study the IMAT within the gluteus maximus, which resides predominantly posterior to the gluteus maximus (Sonenblum, Seol et al., 2020), adipose included in IMAT analysis was constrained to the region posterior to the ischial tuberosity and inferior to the gluteus maximus (**Figure 2**).

Several approaches were considered to quantify IMAT in the gluteus maximus. Methods like the midpoint method and the Otsu Method (Gorgey, Ogawa et al., 2017; Ogawa, Lester et al., 2017) rely on identifying adipose and gluteus intensities within the gluteus maximus and computing a cutoff threshold. While this is effective in many cases, for subjects with very lean gluteus

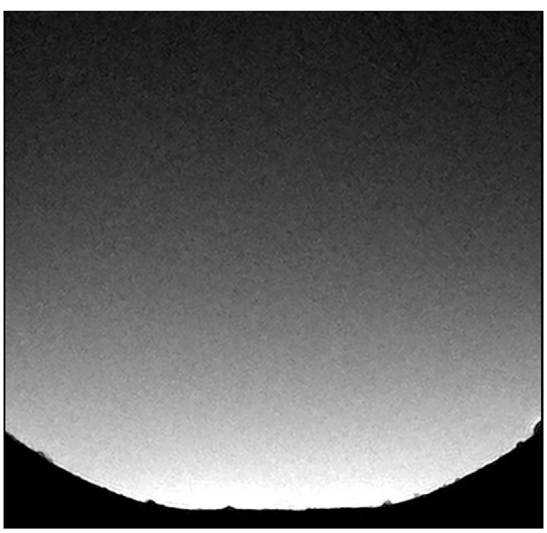

FIGURE 1 | The control scan of a basketball filled with dilute nickel chloride that was used to find the power function (i.e., normalization curve) for normalizing the intensity gradient in scans of the buttocks.

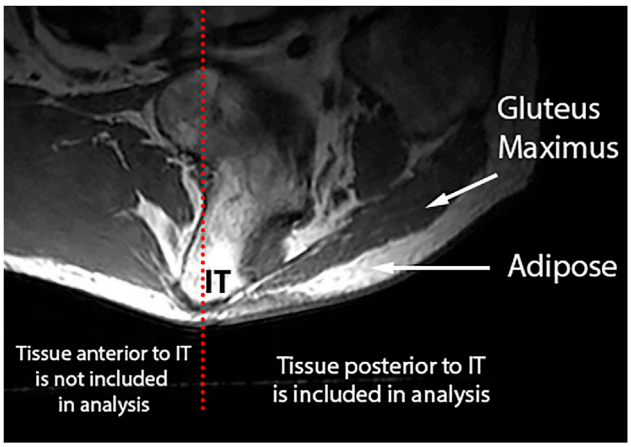

FIGURE 2 | IMAT is calculated using the gluteus maximus and SubQF intensities posterior to the ischial tuberosity.

maximi (i.e., no IMAT) or fully adipose infiltrated muscle (i.e., no discernable muscle tissue), identifying separate tissue types and therefore an intensity cutoff threshold is not effective.

Instead, we reported an effect size for each participant. The IMAT effect size is a standardized magnitude of difference between the corrected intensities of the gluteus maximus and the SubQF inferior to the gluteus (**Eq. 1**). Higher IMAT effect sizes indicated less IMAT within the gluteus maximus, while values closer to zero or even negative IMAT effect sizes indicate significant amounts of IMAT in the gluteus maximus.

Equation 1. IMAT effect size is the relative difference in intensity between adipose and gluteus maximus.

$$IMAT\ effect\ size = \frac{mean\ intensity\ of\ the\ adipose - mean\ intensity\ of\ the\ gluteus\ maximus}{pooled\ standard\ deviation\ of\ intensities\ in\ both\ tissues} \quad (1)$$

This approach was correlated (Pearson Corr = −0.601, p = 0.003) with the midpoint method for participants not at the extremes of low or high IMAT (e.g., the interquartile range). Furthermore, MRI scans were subjectively categorized based on who had low, medium, and high fat infiltration, and the effect size accurately predicted these categorizations.

Subcutaneous Adipose (SubQF) Tissue

Since the adipose under the pelvis is the most susceptible area to PrIs, we evaluated the SubQF under the ischium and compared it with the segmented SubQF surrounding the ischium in the sagittal plane (**Figure 3**). First, we located all SubQF inferior to a location 10 mm superior to the peak of the ischium. Then, we further divided this segment of SubQF into two regions: 1) under the ischium included 5 mm anterior and posterior of the ischium from 10 mm superior to the most inferior aspect of the ischial tuberosity, and 2) surrounding the ischium included regions anterior and posterior to the region under the ischium. This constrained the adipose included in analysis and avoided unintentional inclusion of visceral adipose. To describe the characteristics of the SubQF for each individual, we quantified the standardized magnitude of the difference in intensity under the ischium versus surrounding the ischium using the effect size (**Eq. 2**).

Equation 2. SubQF effect size is the relative difference in intensity between SubQF under and surrounding the ischium.

$$SubQF\ effect\ size = \frac{mean\ intensity\ of\ adipose\ surrounding\ the\ ischium - mean\ intensity\ of\ adipose\ under\ the\ ischium}{pooled\ standard\ deviation\ of\ intensities\ in\ both\ regions} \quad (2)$$

Data Analysis

The goals of this study were to identify the relationship between adipose characteristics and PrI history in wheelchair users and to identify subject characteristics that are related to adipose characteristics. To accomplish these goals, one-way ANOVA tests were run comparing adipose characteristics across individuals with and without a history of PrIs. Statistics were computed using Minitab 18.1. Four subject characteristics were considered: BMI, years using a wheelchair, presence of spasticity, and compressible hip breadth. All but hip breadth were assessed *via* self-report. The relationship between adipose characteristics

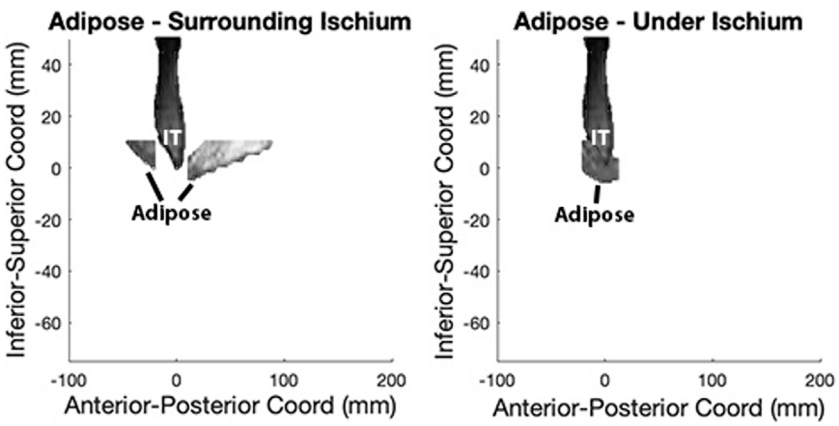

FIGURE 3 | SubQF effect size is calculated using adipose under and surrounding the ischium in the sagittal plane.

TABLE 1 | Participant characteristics.

	All		WC user No Hx (n = 21)		WC user PrI Hx (n = 22)	
	Mean (SD)	**Median (min–max)**	**Mean (SD)**	**Median (min–max)**	**Mean (SD)**	**Median (min–max)**
Age (years, n = 43)	46.8 (11.3)	47.0 (18.0–73.0)	44.8 (13.5)	46.0 (18.0–73.0)	48.8 (8.7)	48.5 (34.0–66.0)
BMI (n = 43)	23.9 (4.8)	23.1 (14.6–34.5)	24.5 (5.0)	23.9 (14.6–34.5)	23.3 (4.6)	21.5 (14.9–33.5)
Years using wheelchair (n = 43)	15.3 (12.2)	10.0 (2.0–46.0)	10.7 (9.3)	6.5 (2.0–37.0)	19.6 (13.3)	16.3 (3.0–46.0)
Compressible hip breadth (inches) (n = 39)	1.4 (0.8)	1.3 (0.3–3.0)	1.7 (0.8)	1.8 (0.5–3.0)	1.1 (0.8)	0.8 (0.3–3.0)
Sex	N	%	N	%	N	%
Female	8	19%	6	29%	2	9%
Male	35	81%	15	71%	20	91%
Diagnosis						
SCI	36	84%	17	81%	19	86%
Other	7	6%	4	19%	3	14%
Injury completeness (n = 41)						
Complete	22	54%	10	48%	12	60%
Incomplete	19	46%	11	52%	8	40%
Spasms (n = 38)						
Yes	24	63%	10	56%	14	70%
No	14	37%	8	44%	6	30%
Race						
Asian American	1	2%	1	5%		
Black/African American	2	5%	1	5%	1	5%
White	33	77%	16	76%	17	77%
Hispanic or Latino	5	12%	2	9%	3	14%
Two or More Races	1	2%			1	5%
Other	1	2%	1	5%	74">	86">

(SubQF effect size and IMAT effect size) and continuous characteristics—BMI, years using a wheelchair, and compressible hip breadth—were investigated with a correlation, while the presence of spasticity was studied with a one-way ANOVA.

To understand if adipose characteristics played a role in deformation of the seated buttocks, correlations were calculated between adipose characteristics (i.e., SubQF effect size and IMAT effect size) and bulk tissue thickness and sagittal radius of curvature. Finally, a correlation was calculated to investigate a relationship between subcutaneous adipose and intramuscular adipose characteristics.

RESULTS

Participants

Participants were predominantly men (81%) with spinal cord injuries (84%) (**Table 1**). The remaining participants had spinal cord disorders such as spinal bifida (n = 4) and spinal cord stroke (n = 1), while one participant had multiple sclerosis and one had fronto-temporal degeneration. They ranged in age from 18 to 73 years old and had between 2 and 46 years of experience using a wheelchair as their primary mobility device. Additional characteristics are presented in **Table 1** for all participants where responses and/or measurements were available.

Adipose Characteristics and Pressure Injuries

Subcutaneous Adipose

Characteristics of the adipose tissue underneath the ischium were different than the surrounding adipose in some people, leading to larger SubQF effect sizes. Larger, positive SubQF effect sizes indicate that the adipose under the ischium is darker than surrounding adipose (**Table 2**; **Figure 4**). Greater negative SubQF effect sizes indicate that the tissue under the ischium is brighter than the tissue surrounding the ischium.

Participants with a history of PrIs had a significantly greater SubQF effect size than participants without a history of PrIs (difference in effect size μ [95% CI] = −0.370 [−0.684, −0.555], p = 0.022).

A closer look at participants with a history of ischial PrIs (i.e., 12 of the overall 22 participants with pelvic PrIs, excluding the 10 that had sacral/coccygeal PrI) revealed darker tissue surrounding the ischium (**Figure 5**). Among participants with bright adipose surrounding the ischium (e.g., >2,200), only three had a history of ischial PrIs. Specifically, participants with a history of PrIs had darker adipose under the ischium relative to the surrounding ischium.

Intramuscular Adipose Tissue

Intramuscular adipose tissue varied, including very lean subjects with high effect sizes, such as the example on the left in **Figure 6** (IMAT effect size = 0.689, gluteus maximus intensity darker than SubQF intensity), subjects with some IMAT present in the gluteus maximus (IMAT effect sizes >0), and subjects with complete fat infiltration. For these subjects with no muscle visible given all the adipose infiltration, IMAT effect size varied from −0.275 to −1.059 because the gluteus maximus intensity was brighter than the SubQF intensity (e.g., **Figure 6**, right).

One-way ANOVA showed that there was no relationship between fat infiltration and PrI history (**Table 2**). However, when individuals with complete fat infiltration (n = 7)

TABLE 2 | Adipose characteristics.

Variable	All (n = 43)	No PrI (n = 21)	Yes PrI (n = 22)	p-value
	Mean (SD)	Mean (SD)	Mean (SD)	
Adipose intensity surrounding the ischium	2,022 (671)	2,019 (657)	2,026 (700)	0.974
Adipose intensity under the ischium	1,707 (783)	1,873 (842)	1,548 (704)	0.176
SubQF effect size	0.40 (0.53)	0.21 (0.56)	0.58 (0.45)	0.022
Adipose intensity posterior to the ischium	1,517 (387)	1,586 (388)	1,451 (383)	0.258
Gluteus Maximus Intensity	1,324 (306)	1,313 (239)	1,334 (364)	0.831
IMAT effect size	0.50 (0.55)	0.59 (0.60)	0.41 (0.51)	0.280
Average bulk thickness (mm)	14.8 (6.1)	17.1 (7.1)	12.5 (3.9)	0.012
Sagittal radius of curvature (mm)	83.7 (38.1)	93.9 (44.7)	73.6 (27.5)	0.085

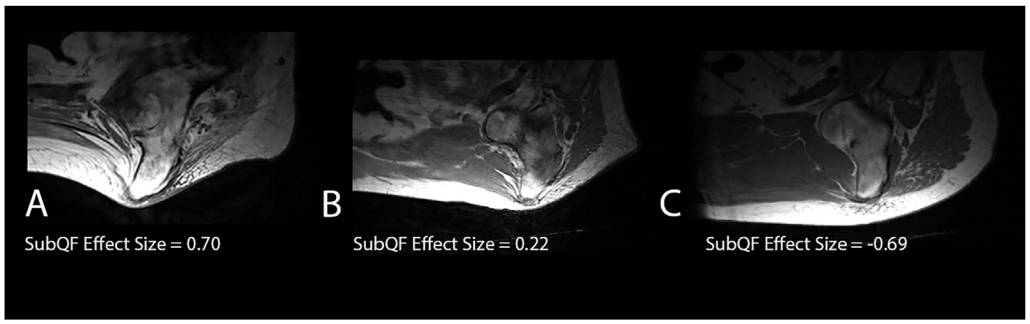

FIGURE 4 | Examples of subjects with different SubQF effect sizes. Subject A had a SubQF effect size of 0.7, indicating darker adipose under the ischium than surrounding the ischium, while subject B had a SubQF effect size of 0.22, indicating adipose under the ischium was only slightly darker than surrounding ischium. Subject C (SubQF effect size of −0.69) actually had brighter adipose under the ischium.

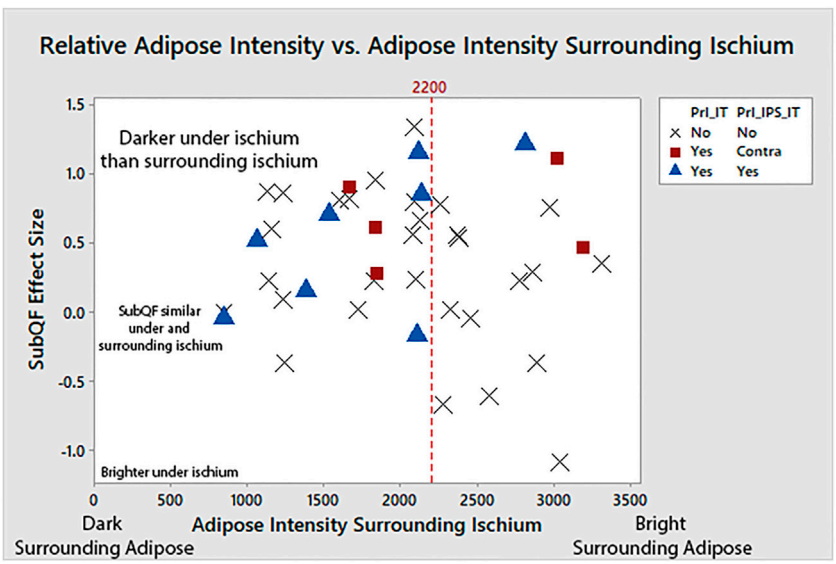

FIGURE 5 | Adipose under the ischium was darker than surrounding adipose (larger SubQF effect size) for people with a history of PrIs, indicating changes to adipose characteristics under the ischium. People with ischial PrIs were also less likely to have bright surrounding adipose.

(i.e., their muscle is indistinguishable from the adipose) were excluded, individuals with PrI history had more fat infiltration than those without a PrI history (IMAT effect size with PrIs n = 19 and μ, 95% CI = 0.56 [0.428, 0.693] vs. without n = 17 and μ = 0.86 [0.716, 0.997], difference in IMAT effect size μ, 95% CI = 0.29 [0.102, 0.471], p = 0.004).

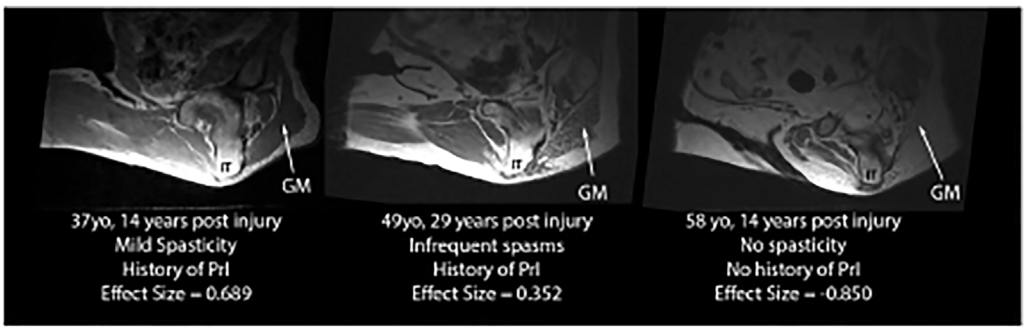

FIGURE 6 | Examples of IMAT effect sizes varying from lean (IMAT effect size = 0.689) to full fat infiltration (IMAT effect size = −0.850).

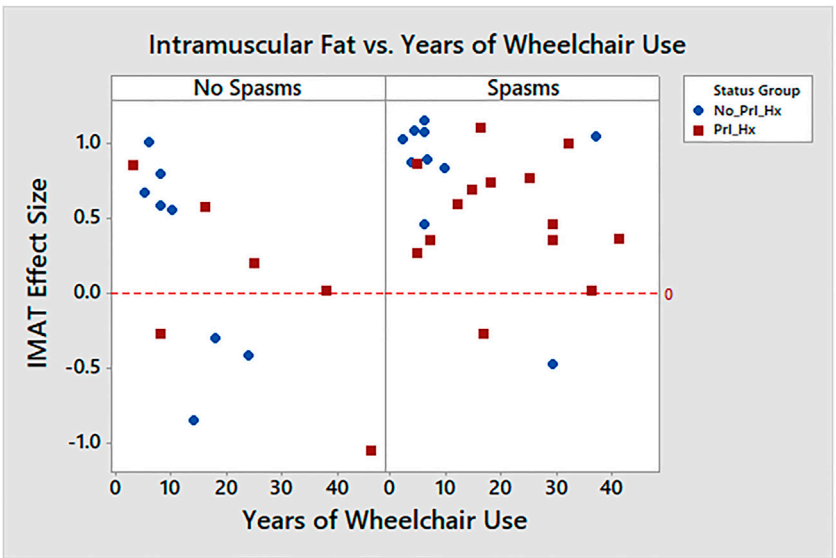

FIGURE 7 | Intramuscular fat vs. years of wheelchair use per spasticity.

Adipose Characteristics and Individual Characteristics

Subcutaneous Adipose

Patient characteristics were not predictive of subcutaneous adipose characteristics. Specifically, there was no significant correlation between the differences in adipose inferior to the ischium versus surrounding the ischium (SubQF effect size) and BMI, years using wheelchair, or compressible hip breadth. Furthermore, one-way ANOVA tests revealed no differences in subcutaneous effect sizes according to the presence of spasms.

Intramuscular Adipose Tissue

Some patient characteristics were associated with intramuscular adipose (**Figure 7**). Specifically, the presence of spasms was associated with a greater IMAT effect size, or leaner muscle (μ, 95% CI with spasms 0.642 [0.430, 0.855], without spasms 0.168 [−0.116, 0.452], $p = 0.01$). BMI was not associated with intramuscular adipose (Pearson Corr = −0.148, $p = 0.339$) nor was compressible hip breadth (Pearson Corr = −0.193, $p = 0.239$), but years using a wheelchair was negatively correlated with IMAT effect size (Pearson Corr = −0.442, $p = 0.003$), suggesting more fat infiltration with more years in the wheelchair.

Adipose Characteristics and Biomechanical Risk

Subcutaneous Adipose

Subcutaneous effect size was negatively correlated with tissue thickness (Pearson Corr = −0.489, $p < 0.01$) and sagittal radius of curvature = −0.564, $p < 0.01$). That is, as SubQF effect size goes up (darker adipose under IT), tissue thickness goes down, and the radius of curvature goes down or the shape becomes more peaked. In other words, darker adipose under the IT is associated with a higher biomechanical risk.

Intramuscular Adipose

Intramuscular adipose (IMAT effect size) was not related to either tissue thickness or radius of curvature of the seated buttocks (Pearson Corr = 0.092 and = −0.073 respectively).

Intramuscular Adipose vs. Subcutaneous Adipose

SubQF effect size was not related to IMAT effect size (Pearson Corr = −0.100).

DISCUSSION

This study is the first to integrate an assessment of both subcutaneous and intramuscular adipose in wheelchair users and to assess how adipose relates both to PrI risk and biomechanical risk (i.e., the tissue response to loading).

Tissue with darker subcutaneous adipose under the IT compared with surrounding adipose measured with an MRI was associated with a higher biomechanical risk when seated. These individuals were also more likely to have a history of PrIs, but not necessarily at the ipsilateral ischial tuberosity that was studied. The relationship between adipose and tissue tolerance likely evolves over time in response to load. Buttocks with good structural integrity and low biomechanical risk, such as the buttocks of an able-bodied adult, provide ample protection from development of PrIs.

There are a number of physiological reasons why changes to adipose characteristics might occur over time for wheelchair users and consequently influence tissue tolerance and biomechanical risk. Studies have shown that exposure to mild, prolonged hypoxia increases fat storage and decreases proinflammatory gene expression. In contrast, acute exposure to severe hypoxia decreases fat storage and increases proinflammatory expression (Lempesis et al., 2020). Loading over time will also bring about changes to the mechanical structure of the subcutaneous adipose (Edsberg, Cutway et al., 2000; Edsberg, Natiella et al., 2001). For example, omental adipose has a higher proportion of fibrous proteins than subcutaneous adipose (Alkhouli et al., 2013). Thus, if the tissue were to differentiate in response to load, the distribution of fibrous proteins might change. Additionally, the extracellular matrix of adipose is composed primarily of collagen, yet elastin provides greater distensibility (Alkhouli et al., 2013). Therefore, a change in the distribution of collagen and elastin would result in a change in mechanical properties and biomechanical risk. Finally, lipid formation is known to change in response to load (Hara et al., 2011), and this may also affect the mechanical properties and, thus, the biomechanical risk (Ben-Or Frank et al., 2015).

Clinically, the association between adipose characteristics and biomechanical risk presents an opportunity both for assessment and intervention. For years, clinicians have been assessing tissue quality *via* palpation. The results of this study suggest that palpation may be augmented with an objective assessment of SubQF adipose quality to understand biomechanical risk and tissue tolerance. As MRI is not practical for regular clinical use, this would require clinically viable tools to assess SubQF quality, whether *via* imaging, assessment of mechanical properties, or an alternative approach. Furthermore, if changes in mechanical structure of the adipose increases risk, improving the SubQF quality could be an interventional goal. Lastly, combined with the finding that there is little gluteus maximus coverage of the ischium while seated (Sonenblum et al., 2020), these results provide further evidence that adipose plays an important role in PrI development.

In terms of intramuscular adipose tissue, our results contrasted with the studies of Lemmer, Alvarado et al. (2019) and Wu and Bogie (2013). Our study found that there was no relationship between the amount of fat infiltration and PrI history, which was unanticipated. It is possible that when studying such small sample sizes as done in Lemmer, Alvarado et al. (2019) (n = 38, but only n = 11 did not have a PrI history) and Wu and Bogie (2013) (n = 10 wheelchair users), IMAT was serving as a proxy for other effects such as time since injury, or in the present study, time since injury could be confounding the effect of IMAT. It is also worth noting that the methodology used to measure IMAT was different between these studies. Lemmer, Alvarado et al., (2019) and Wu and Bogie (2013) used CT scans to measure IMAT, which allowed for a more precise calculation of the ratio of adipose and muscle than is possible using MRI. On the other hand, CT scans come with increased radiation exposure and a supine posture that was undesirable for the present data collection approach.

However, when the completely fat-infiltrated subjects (IMAT effect size <0, or gluteus maximus intensity > adipose intensity) were excluded in our study, subjects with a higher amount of fat infiltration were more likely to have a history of PrI. Fat infiltration increases insulin resistance (Kalyani et al., 2014), which may be associated with decreased microvascular flow to the skeletal muscle and could explain the increased risk in this subset of the population. The difference in findings between people with partial fat infiltration and full fat infiltration may indicate that people who are fully fat infiltrated may have a different pathology of fat infiltration, making fat infiltration contribute less to their risk for PrI. For example, one participant experienced fat infiltration secondary to chemotherapy. Another possibility is that the properties and oxygen demand of the fully infiltrated muscle are different than that of the partially infiltrated muscle. Previous research has shown that in the abdominal region, subcutaneous fat has been correlated with insulin resistance (Patel and Abate, 2013). However, in the gluteal–femoral region, subcutaneous adipose tissue has been shown to increase insulin, which would increase blood flow (Snijder et al., 2005; Yim et al., 2008; Lambadiari et al., 2015). If the IMAT properties conformed to properties similar to SubQF upon full fat infiltration, then this could explain a change in perfusion and risk. At the same time, oxygen requirements are lower with enlarged fat cells, which may be the phenotype present in a fully infiltrated muscle (Frayn and Karpe, 2014). However, additional research would need to be conducted to confirm these new hypotheses.

Since BMI is a common method used to measure an individual's body fat, one would expect that the amount of fat infiltration and BMI would be directly correlated. However, there was no relationship between fat infiltration and BMI. This is consistent with Bogie et al. (2020). Time since injury is a much stronger predictor of IMAT, suggesting that the process occurs at some point after injury, likely as a result of disuse and atrophy, in response to myogenic and adipogenic markers identified in (Bogie et al., 2020). BMI (i.e., body weight and height) was self-reported in this study, so the accuracy of BMI values is unknown. However, our findings were similar when analyzed as SCI-adjusted BMI category, which would be less sensitive to precise weight measurements.

Limitations

The MRI scans used in this study were not optimized for studying intramuscular or SubQF adipose. There are imaging protocols that would provide more detailed information about the adipose, such as a Dixon protocol. Furthermore, the characteristics and etiology of the darker presentation of SubQF observed would be more thoroughly investigated using histology and mechanical testing as opposed to MRI. However, we believe that the results of this investigation provide important preliminary results to drive future work, in which histology and mechanical testing will relate the imaging results to specific changes in adipose characteristics.

While this study explored a large group of individuals with and without PrI history, there was a difference in the years of wheelchair use between the two groups that may have impacted IMAT analysis. Additional factors and comorbidities, such as chemotherapy or diabetes, were also not analyzed but may have influenced IMAT. Further studies that will include longitudinal analysis and consideration of additional factors and comorbidities would be beneficial to better understand the natural history of fat infiltration.

The few participants who used a wheelchair for reasons other than a spinal cord injury may expect a different adipose and muscle presentation given the differences in autonomic nervous system function. However, variability in nervous system function among individuals with SCI also exists, and this is best addressed by studying a larger population.

CONCLUSION

The results of the study suggest a hypothesis that changes in adipose tissue under the ischial tuberosity are associated with increased biomechanical risk for pressure injury. Further investigation of this hypothesis is warranted, including histology to understand the specific changes in tissue characteristic associated with darker fat, mechanical testing to identify changes in mechanical properties, and measurement of blood flow responses in regions with dark adipose. Further investigation of this hypothesis may lead to clinically useful diagnostic techniques that can identify changes in adipose and biomechanical risk to inform early preventative interventions.

DATA AVAILABILITY STATEMENT

The raw data supporting the conclusions of this article will be made available by the authors, without undue reservation.

ETHICS STATEMENT

The studies involving human participants were reviewed and approved by institutional review boards at the Georgia Institute of Technology and multiple clinical sites. The patients/participants provided their written informed consent to participate in this study.

AUTHOR CONTRIBUTIONS

SES and SHS designed the original study methods including research questions and data collection approach, and secured funding. SES provided study oversight and the analysis plan for this manuscript. SES drafted, revised, and submitted the manuscript. MM conducted the data analysis for this manuscript and contributed significantly to the initial manuscript draft and revisions. SHS provided critical insights to data analysis and revised the draft manuscript. JG was instrumental in developing the MRI data collection protocols and the gradient correction approach, participated in data collection, and revised the manuscript. JC supervised MRI analysis, provided expertise as a radiographer, and revised the manuscript.

FUNDING

This study was completed as part of a Field Initiated Project (grant 90IF0120), which was funded by the National Institute on Disability, Independent Living, and Rehabilitation Research (NIDILRR). This work was also supported by donations from Ride Designs and the Robert H. Graebe Foundation.

ACKNOWLEDGMENTS

The authors acknowledge and thank the clinical team, Kelly Waugh, PT, MAPT, ATP, Mary Shea, MA, OTR, ATP, and Trevor Dyson-Hudson, PhD for their efforts collecting high quality data for this study. Finally, the authors also acknowledge our research participants, who contributed their time, along with patience and enthusiasm, and without whom this work could not have been completed.

REFERENCES

Addison, O., Marcus, R. L., LaStayo, P. C., and Ryan, A. S. (20142014). Intermuscular Fat: A Review of the Consequences and Causes. *Int. J. Endocrinol.* 2014, 309570. doi:10.1155/2014/309570

Alkhouli, N., Mansfield, J., Green, E., Bell, J., Knight, B., Liversedge, N., et al. (2013). The Mechanical Properties of Human Adipose Tissues and Their Relationships to the Structure and Composition of the Extracellular Matrix. *Am. J. Physiology-Endocrinology Metab.* 305 (12), E1427–E1435. doi:10.1152/ajpendo.00111.2013

Ben-Or Frank, M., Shoham, N., Benayahu, D., and Gefen, A. (2015). Effects of Accumulation of Lipid Droplets on Load Transfer between and within Adipocytes. *Biomech. Model. Mechanobiol* 14 (1), 15–28. doi:10.1007/s10237-014-0582-8

Bergstrom, N., Braden, B., Boynton, P., and Bruch, S. (1995). Using a Research-Based Assessment Scale in Clinical Practice. *Nurs. Clin. North. Am.* 30 (3), 539–551.

Bhattacharya, S., and Mishra, R. K. (2015). Pressure Ulcers: Current Understanding and Newer Modalities of Treatment. *Indian J. Plast. Surg.* 48 (1), 4–16. doi:10.4103/0970-0358.155260

Bogie, K. M., Schwartz, K., Li, Y., Wang, S., Dai, W., and Sun, J. (2020). Exploring Adipogenic and Myogenic Circulatory Biomarkers of Recurrent Pressure Injury Risk for Persons with Spinal Cord Injury. *J. Circ. Biomark* 9, 1–7. doi:10.33393/jcb.2020.2121

Booth, A. D., Magnuson, A. M., Fouts, J., Wei, Y., Wang, D., Pagliassotti, M. J., et al. (2018). Subcutaneous Adipose Tissue Accumulation Protects Systemic Glucose Tolerance and Muscle Metabolism. *Adipocyte* 7 (4), 261–272. doi:10.1080/21623945.2018.1525252

Braden, B., and Bergstrom, N. (1987). A Conceptual Schema for the Study of the Etiology of Pressure Sores. *Rehabil. Nurs. J.* 12 (1). doi:10.1002/j.2048-7940.1987.tb00541.x

Edsberg, L. E., Cutway, R., Anain, S., and Natiella, J. R. (2000). Microstructural and Mechanical Characterization of Human Tissue at and Adjacent to Pressure Ulcers. *J. Rehabil. Res. Dev.* 37 (4), 463–471.

Edsberg, L. E., Natiella, J. R., Baier, R. E., and Earle, J. (2001). Microstructural Characteristics of Human Skin Subjected to Static versus Cyclic Pressures. *J. Rehabil. Res. Dev.* 38 (5), 477–486.

European Pressure Ulcer Advisory Panel, National Pressure Injury Advisory Panel and Pan Pacific Pressure Injury Alliance (2019). *Prevention and Treatment of Pressure Ulcers/Injuries: Clinical Practice Guideline*. Editor E. Haesler (EPUAP/NPIAP/PPPIA).

Frayn, K. N., and Karpe, F. (2014). Regulation of Human Subcutaneous Adipose Tissue Blood Flow. *Int. J. Obes.* 38 (8), 1019–1026. doi:10.1038/ijo.2013.200

Garcia, A. D., and Thomas, D. R. (2006). Assessment and Management of Chronic Pressure Ulcers in the Elderly. *Med. Clin. North America* 90 (5), 925–944. doi:10.1016/j.mcna.2006.05.018

Goodpaster, B. H., Thaete, F. L., and Kelley, D. E. (2000). Thigh Adipose Tissue Distribution Is Associated with Insulin Resistance in Obesity and in Type 2 Diabetes Mellitus. *Am. J. Clin. Nutr.* 71 (4), 885–892. doi:10.1093/ajcn/71.4.885

Gorgey, A., Ogawa, M., Lester, R., and Akima, H. (2017). Quantification of Intermuscular and Intramuscular Adipose Tissue Using Magnetic Resonance Imaging after Neurodegenerative Disorders. *Neural Regen. Res.* 12 (12), 2100. doi:10.4103/1673-5374.221170

Grundy, S. M. (2015). Adipose Tissue and Metabolic Syndrome: Too Much, Too Little or Neither. *Eur. J. Clin. Invest.* 45 (11), 1209–1217. doi:10.1111/eci.12519

Hara, Y., Wakino, S., Tanabe, Y., Saito, M., Tokuyama, H., Washida, N., et al. (2011). Rho and Rho-Kinase Activity in Adipocytes Contributes to a Vicious Cycle in Obesity that May Involve Mechanical Stretch. *Sci. Signal.* 4 (157), ra3. doi:10.1126/scisignal.2001227

Lambadiari, V., Triantafyllou, K., and Dimitriadis, G. D. (2015). Insulin Action in Muscle and Adipose Tissue in Type 2 Diabetes: The Significance of Blood Flow. *Wjd* 6 (4), 626–633. doi:10.4239/wjd.v6.i4.626

Lemmer, D. P., Alvarado, N., Henzel, K., Richmond, M. A., McDaniel, J., Graebert, J., et al. (2019). What Lies beneath: Why Some Pressure Injuries May Be Unpreventable for Individuals with Spinal Cord Injury. *Arch. Phys. Med. Rehabil.* 100 (6), 1042–1049. doi:10.1016/j.apmr.2018.11.006

Lempesis, I. G., van Meijel, R. L. J., Manolopoulos, K. N., and Goossens, G. H. (2020). Oxygenation of Adipose Tissue: A Human Perspective. *Acta Physiol. (Oxf)* 228 (1), e13298. doi:10.1111/apha.13298

Levy, A., Enzer, S., Shoham, N., Zaretsky, U., and Gefen, A. (2012). Large, but Not Small Sustained Tensile Strains Stimulate Adipogenesis in Culture. *Ann. Biomed. Eng.* 40 (5), 1052–1060. doi:10.1007/s10439-011-0496-x

Liao, F., Burns, S., and Jan, Y.-K. (2013). Skin Blood Flow Dynamics and its Role in Pressure Ulcers. *J. Tissue Viability* 22 (2), 25–36. doi:10.1016/j.jtv.2013.03.001

Ogawa, M., Lester, R., Akima, H., and Gorgey, A. S. (2017). Quantification of Intermuscular and Intramuscular Adipose Tissue Using Magnetic Resonance Imaging after Neurodegenerative Disorders. *Neural Regen. Res.* 12 (12), 2100–2105. doi:10.4103/1673-5374.221170

Patel, P., and Abate, N. (2013). Body Fat Distribution and Insulin Resistance. *Nutrients* 5 (6), 2019–2027. doi:10.3390/nu5062019

Salzberg, C. A., Byrne, D. W., Cayten, C. G., van Niewerburgh, P., Murphy, J. G., and Viehbeck, M. (1996). A New Pressure Ulcer Risk Assessment Scale for Individuals with Spinal Cord Injury1. *Am. J. Phys. Med. Rehabil.* 75 (2), 96–104. doi:10.1097/00002060-199603000-00004

Snijder, M. B., Visser, M., Visser, M., Dekker, J. M., Goodpaster, B. H., Harris, T. B., et al. (2005). Low Subcutaneous Thigh Fat Is a Risk Factor for Unfavourable Glucose and Lipid Levels, Independently of High Abdominal Fat. The Health ABC Study. *Diabetologia* 48 (2), 301–308. doi:10.1007/s00125-004-1637-7

Sonenblum, S. E., Sprigle, S., and Lopez, R. A. (2012). Manual Wheelchair Use: Bouts of Mobility in Everyday Life. *Rehabil. Res. Pract.* 2012, 753165. doi:10.1155/2012/753165

Sonenblum, S. E., Seol, D., Sprigle, S. H., and Cathcart, J. M. (2020). Seated Buttocks Anatomy and its Impact on Biomechanical Risk. *J. Tissue Viability* 29 (2), 69–75. doi:10.1016/j.jtv.2020.01.004

Sonenblum, S. E., and Sprigle, S. (2011). Distinct Tilting Behaviours with Power Tilt-In-Space Systems. *Disabil. Rehabil. Assistive Techn.* 6 (6), 526–535. doi:10.3109/17483107.2011.580900

Sprigle, S., McNair, D., and Sonenblum, S. (2020). Pressure Ulcer Risk Factors in Persons with Mobility-Related Disabilities. *Adv. Skin Wound Care* 33 (3), 146–154. doi:10.1097/01.asw.0000653152.36482.7d

Wu, G. A., and Bogie, K. M. (2013). Not just Quantity: Gluteus Maximus Muscle Characteristics in Able-Bodied and SCI Individuals - Implications for Tissue Viability. *J. Tissue Viability* 22 (3), 74–82. doi:10.1016/j.jtv.2013.03.003

Yim, J.-E., Heshka, S., Albu, J. B., Heymsfield, S., and Gallagher, D. (2008). Femoral-gluteal Subcutaneous and Intermuscular Adipose Tissues Have Independent and Opposing Relationships with CVD Risk. *J. Appl. Physiol.* 104 (3), 700–707. doi:10.1152/japplphysiol.01035.2007

Conflict of Interest: Author JG is employed by FONAR Corporation.

The remaining authors declare that the research was conducted in the absence of any commercial or financial relationships that could be construed as a potential conflict of interest.

frontiers in Bioengineering and Biotechnology

ORIGINAL RESEARCH
published: 10 December 2021
doi: 10.3389/fbioe.2021.731882

Hypertension and Stroke Cardiovascular Control Evaluation by Analyzing Blood Pressure, Cerebral Blood Flow, Blood Vessel Resistance and Baroreflex

Shoou-Jeng Yeh[1], *Chi-Wen Lung*[2,3], *Yih-Kuen Jan*[3], *Fang-Chuan Kuo*[4] *and Ben-Yi Liau*[5]*

[1]Section of Neurology and Neurophysiology, Cheng-Ching General Hospital, Taichung, Taiwan, [2]Department of Creative Product Design, Asia University, Taichung, Taiwan, [3]Rehabilitation Engineering Lab, Kinesiology and Community Health, Computational Science and Engineering, University of Illinois at Urbana-Champaign, Champaign, IL, United States, [4]Department of Physical Therapy, Hungkuang University, Taichung, Taiwan, [5]Department of Biomedical Engineering, Hungkuang University, Taichung, Taiwan

OPEN ACCESS

Edited by:
Massimiliano Zingales,
University of Palermo, Italy

Reviewed by:
Federica Cosentino,
Ri.MED Foundation, Italy
Weiwei Yan,
China Jiliang University, China

***Correspondence:**
Ben-Yi Liau
byliau@hk.edu.tw

Specialty section:
This article was submitted to Biomechanics, a section of the journal Frontiers in Bioengineering and Biotechnology

Received: 28 June 2021
Accepted: 15 November 2021
Published: 10 December 2021

Citation:
Yeh S-J, Lung C-W, Jan Y-K, Kuo F-C and Liau B-Y (2021) Hypertension and Stroke Cardiovascular Control Evaluation by Analyzing Blood Pressure, Cerebral Blood Flow, Blood Vessel Resistance and Baroreflex. Front. Bioeng. Biotechnol. 9:731882. doi: 10.3389/fbioe.2021.731882

Cardiovascular diseases have been the leading causes of mortality in Taiwan and the world at large for decades. The composition of cardiovascular and cerebrovascular systems is quite complicated. Therefore, it is difficult to detect or trace the related signs of cardiovascular and cerebrovascular diseases. The characteristics and changes in cardiopulmonary system disease can be used to track cardiovascular and cerebrovascular disease prevention and diagnosis. This can effectively reduce the occurrence of cardiovascular and cerebrovascular diseases. This study analyzes the variability in blood pressure, cerebral blood flow velocity and the interaction characteristics using linear and nonlinear approaches in stroke, hypertension and healthy groups to identify the differences in cardiovascular control in these groups. The results showed that the blood pressure and cerebral blood flow of stroke patients and hypertensive patients were significantly higher than those of healthy people (statistical differences ($p < 0.05$). The cerebrovascular resistance (CVR) shows that the CVR of hypertensive patients is higher than that of healthy people and stroke patients ($p < 0.1$), indicating that the cerebral vascular resistance of hypertensive patients is slightly higher. From the patient's blood flow and vascular characteristics, it can be observed that the cardiovascular system is different from those in healthy people. Baroreflex sensitivity (BRS) decreased in stroke patients ($p < 0.05$). Chaotic analysis revealed that the blood pressure disturbance in hypertensive patients has a higher chaotic behavior change and the difference in initial state sensitivity. Cross-correlation (CCF) analysis shows that as the course of healthy→hypertension→stroke progresses, the maximum CCF value decreases significantly ($p < 0.05$). That means that blood pressure and cerebral blood flow are gradually not well controlled by the self-regulation mechanism. In conclusion, cardiovascular control performance in hypertensive and stroke patients displays greater variation. This can be observed by the bio-signal analysis. This analysis could identify a measure for detecting and preventing the risk for hypertension and

stroke in clinical practice. This is a pilot study to analyze cardiovascular control variation in healthy, hypertensive and stroke groups.

Keywords: cardiovascular control, hypertension, stroke, blood pressure, cerebral blood flow, blood vessel resistance, baroreflex

1 INTRODUCTION

Cardiovascular diseases (CVD) have become a leading health care burden in many areas of the world. It was reported that high blood pressure is the main risk factor to induce CVD. Most deaths are caused by ischemic heart disease and ischemic stroke (Roth et al., 2020). Therefore, systolic blood pressure variability could be assessed as a stroke and CVD risk predictor in the hypertensive population (Pringle et al., 2003). Because CVD is common in most areas of the world, WHO established a CVD risk prediction chart to reduce the medical burden (WHO CVD risk chart working group, 2019). Moreover, blood pressure is highly related to CVD (Fuchs and Ethlton, 2020). Hypertension is high blood pressure in the blood vessels. In the brain, high blood pressure induces hypertrophy and remodels smooth muscle cells in the cerebral arteries (Yu et al., 2011). The changes in blood vessel wall composition leads to greater cerebral artery stiffness. Aortic stiffness could be an independent predictor of hypertensive-stroke patient (Baumbach et al., 1988; Laurent et al., 2003, Laurent et al., 2005; Benjo et al., 2007). The change in blood pressure is the earliest sign of abnormal cardiopulmonary circulation. The change in blood pressure causes considerable variation in the physiological feedback mechanism. The relationship between blood pressure and cerebral blood flow in the brain is cerebral autoregulation (CA). Cerebral autoregulation maintains cerebral blood flow to protect the brain by reducing the effect of blood pressure variation. Previous studies reported that impaired CA may be associated with higher stroke risk (Shekhar et al., 2017; Castro et al., 2018). Therefore, CA assessment is also important to predict and reduce CVD risk. CA measurement and evaluation may obtain a predictive value for the development of delayed cerebral ischemia and radiographic vasospasm (Tiecks et al., 1995; Aoi wt al., 2012; Oeinck et al., 2013; Ma et al., 2016; Crippa et al., 2018). Although some non-invasive approaches (ex. Cross-correlation function, chaotic analysis etc.) and devices (ex. Near-infrared spectroscopy, transcranial Doppler etc.) have been developed to assess CA, measuring CA is difficult and standard measurement is not currently available (Tiecks et al., 1995; Liau et al., 2010; Rivera-Lara et al., 2017; Xiong et al., 2017). On the other hand, few studies revealed the differences in physiological signals and properties between hypertension and stroke. The changes in the cardiovascular disease physiological parameter development process (healthy→hypertension→stroke) are not clear. The objective of this study was to apply linear and nonlinear physiological signal analysis methods to assess multiple blood pressure signal correlation effects on cerebral blood flow signals, blood vessel properties, baroreflex and CA in healthy people, hypertension and stroke patients. To the best of our knowledge, this is the first study to investigate bio-signal performance and differences. The findings from multiple views could be used to better understand the effects of various cardiovascular diseases on bio-signal variation and tissue properties as assessed using multi-correlation approaches.

2 MATERIALS AND METHODS

2.1 Subjects and Measurement

In this study, 3 groups were enrolled: 1) 11 healthy subjects (57.4 ± 8.4 years) that have no history of related cardiovascular diseases. 2) 11 hypertensive patients (50.8 ± 10.3 years) from the Neurology Section of Cheng-Ching General Hospital, Taiwan. Hypertension was according to WHO, 2003 that clinic blood pressure ≥140/90 mmHg (WHO, 2003). 3) 10 hypertensive stroke outpatients (56 ± 10.16 years) from the Neurology Section of Cheng-Ching General Hospital were enrolled in this study. These stroke patients have to qualify blood pressure level defined as a clinic blood pressure ≥140/90 mmHg (WHO, 2003). National Institutes of Health Stroke Scale, NIHSS <15. Stroke more than 7 days. The subjects in 3 groups were age-matched and none of the subjects were receiving any medication during the study period. Informed consent was received from all subjects prior to entry into the study. This study was approved by the Research Ethics Committee of Cheng-Ching General Hospital, Taiwan. Continuous arterial blood pressure signals were acquired via using the Finapres (Model 2,300, Ohemda, Englewood, CO, United States). Cerebral blood flow velocity signals were obtained through TCD (transcranial Doppler ultrasound, EME TC 2020, Nicolet instrument, Warwick, United Kingdom) in conjunction with a 5-MHz transducer fixed over the temporal bones by an elastic headband. Subjects lied down on a tilt-table that enabled a motor-driven change from a supine to an upright position at 75° within 4 s. Data acquisition was started after a 10-min relaxation period in the supine position. After that, continuous arterial blood pressure and cerebral blood flow velocity signals were acquired during both supine and 75° head-up tilt positions and then returned to supine and rest for 5 minutes. The experimental devices included a general-purpose data acquisition board with a computer and LabVIEW program for acquiring signal processing. This equipment was developed in our previous study (Chiu et al., 2007; Liau et al., 2010).

2.2 BP and CBFV Signals

Mean value estimation is based on every waveform peak and valley location. The mean arterial blood pressure (MABP) value was calculated using each pulse as follows:

$$MABP_i = \frac{1}{P_{i+1} - P_i} \sum_{k=P}^{P_{i+1}} BP(k) \quad (1)$$

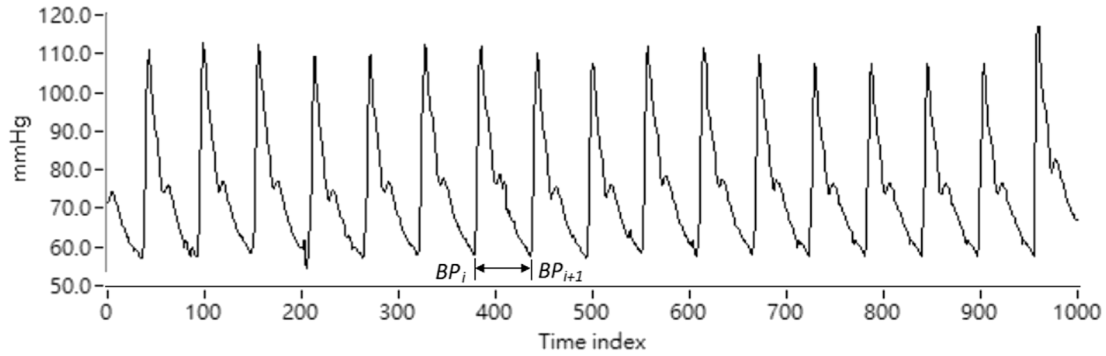

FIGURE 1 | Representation of the ABP signal.

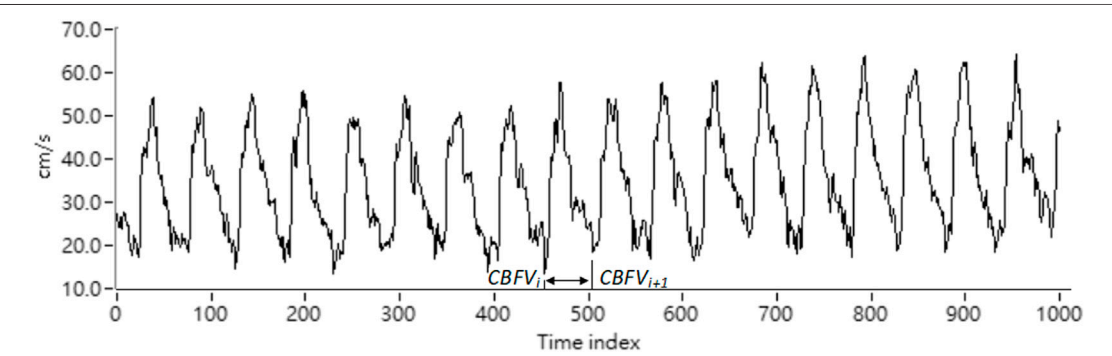

FIGURE 2 | Representation of the CBFV signal.

where *BP*(⊠)in **Eq. 1** is the arterial blood pressure pulse signal acquired by Finapres continuously. P_i is the wave-through time index in the *i*th BP pulse beat. Therefore, $MABP_i$ is the mean BP value calculated by the *i*th pulse beat. Representation of the BP signal is shown as **Figure 1**.On the other hand, mean cerebral blood flow velocity (MCBFV) could be obtained using **Eq. 2** as follows.

$$MCBFV_i = \frac{1}{V_{i+1} - V_i} \sum_{k=V}^{V_{i+1}} CBFV(k) \tag{2}$$

where *CBFV*(⊠) is the CBFV pulse signal continuously acquired by the TCD. *Vi* is the time index of the wave-through in the CBFV signal corresponding to the *i*th pulse beat. *MCBFVi* is the mean CBFV value for the *i*th pulse beat. The CBFV signal representation is shown as **Figure 2**.

2.3 Methodology

2.3.1 Resistance Index

Resistance index is a measure of peripheral blood flow resistance. Low vascular resistance has a higher diastolic blood flow velocity characteristic, and will have a lower RI. A high vascular resistance has a lower diastolic blood flow velocity characteristic, and will produce a higher RI. RI can be calculated using the following formula, SCBFV is the systolic blood flow velocity, and DCBFV is the diastolic blood flow velocity. RI can be obtained by **Eq. 3** as below (Hilz et al., 2004).

$$\text{RI} = \frac{SCBFV - DCBFV}{SCBFV} \tag{3}$$

2.3.2 Pulsatility Index

The pulsation index is a measurement that describes the type of signal waveform. Low intracranial vascular resistance will reduce PI, and rising intracranial pulsations have been found to be related to rising intracranial pressure. The normal PI range is between 0.5 and 1.4, less than 0.5 may be an ischemic flow pattern under vascular dilation, and greater than 1.5 may be a decrease in vascular compliance or an increase in intracranial pressure. PI can be calculated using the following formula, SCBFV is the systolic blood flow velocity, DCBFV is the diastolic blood flow velocity, and MCBFV is the average blood flow velocity. *PI* can be obtained by **Eq. 4** (Hilz et al., 2004)

$$\text{PI} = \frac{\text{SCBFV} - \text{DCBFV}}{\text{MCBFV}} \tag{4}$$

2.3.3 Cerebrovascular Resistance

The cerebrovascular resistance can be expressed as the ratio of the average pressure to the average cerebral blood flow rate. The unit is mmHg/(cm/s). CVR can be calculated using the following formula, where MABP is the average blood pressure and MCBFV is the average cerebral blood flow. *CVR* can be obtained using **Eq. 5** (Hilz et al., 2004)

$$CVR = \frac{MABP}{MCBFV} \tag{5}$$

2.3.4 Cross-Correlation Analysis

Cross-correlation analysis mainly observes the correlation between the two signals in the time domain. Taking the average cerebral blood flow signal and the average blood pressure signal as an example, the correlation and phase relationship between the average cerebral blood flow signal and the average blood pressure signal can be determined by the brain. The phase relationship between blood flow and blood pressure is used to explore the blood flow regulation mechanism using the cardiovascular system. Let the cross-correlation function be expressed as CCF(k), W is the length of the window, k is the number of peak-to-peak displacement points, N is the total length of the signal, and the MABP time series normalized with the average value is expressed as x(n), MCBFV time series is expressed as y(n), the time series of x(n) after band-pass filtering is expressed as, and the time series of y(n) after band-pass filtering is expressed as, then cross-correlation The analyzed formula is as follows (Chiu et al., 2001; Chiu et al., 2005; Liau et al., 2010; Fan et al., 2019):

$$CCF_i(k) = \frac{R^i_{\hat{x}\hat{y}}(k)}{\left[R^i_{\hat{x}\hat{x}}(0)R^i_{\hat{y}\hat{y}}(0)\right]^{\frac{1}{2}}}, \quad k = 0, \pm 1, \pm 2, \ldots, \quad i = 1 \text{ to } N - W + 1 \tag{6}$$

where

$$R^i_{\hat{x}\hat{y}}(k) = \begin{cases} \frac{1}{W}\sum_{j=i}^{i+W} \hat{x}(j)\hat{y}(j+k), & k = 0, 1, 2, \ldots \\ \frac{1}{W}\sum_{j=i}^{i+W} \hat{x}(j-k)\hat{y}(j), & k = 0, -1, -2, \ldots \end{cases}$$

$$R^i_{\hat{x}\hat{x}}(0) = \frac{1}{W}\sum_{j=i}^{i+W}\left[\hat{x}(j)\right]^2, \text{and } R^i_{\hat{y}\hat{y}}(0) = \frac{1}{W}\sum_{j=i}^{i+W}\left[\hat{y}(j)\right]^2$$

2.3.5 Baroreflex Sensitivity

The index is used to evaluate the pressure-sensitive reflex. In order to observe the changes in heart rate and blood pressure at the same time, the baroreflex sensitivity index observes the relationship between the heart rate signal and the blood pressure signal. Assuming that the systolic blood pressure sequence SBP is S(n), and the heartbeat interval RR interval is R(n), the baroreflex sensitivity (BRS) T(n) can be expressed as: (Karemaker and Wesseling, 2008):

$$T(n) = \sum_{k=1}^{n} \frac{R(k)}{S(k)} \tag{7}$$

2.3.6 Correlation Dimension

The correlation dimension (CD) can quantify the properties of the attractors from the time series and determine the singularity of the attractors, which is estimated by the correlation function by calculating the pairs of points where the attractors fall on the radius of the "sphere". The correlation function Cd(R) is defined as (Grassberger and Procaccia, 1983; Liau et al., 2008; Gao et al., 2011; Bolea et al., 2014):

$$C_d(R) = \lim_{N\to\infty}\left[\frac{1}{N^2}\sum_{i,j=1,i\neq j} H_E\left(R - \left|X_i - X_j\right|\right)\right] \tag{8}$$

N:number of points
H_E:Heaviside step function
$H_E = 1$, if R-$\left| X_i - X_j \right| \geqq 0$
$H_E = 0$, otherwise
(X_i, X_j)The Euclidean distance of an attractor in 1 dm dimension is:

$$\left|X_i - X_j\right| = \left[\left(x_{i,1} - x_{j,1}\right)^2 + \left(x_{i,2} - x_{j,2}\right)^2 + \cdots\left(x_{i,dm} - x_{j,dm}\right)^2\right]^{1/2}$$

The relationship between the correlation integral and R is: Cd(R)~R^{dc}, the logarithm of both sides can be obtained:

$$\log C_d(R) = d_c \log R + \text{constant}$$

2.3.7 Lyapunov Exponent

The Lyapunov exponent (LE) is used to quantitatively analyze the chaotic behavior by measuring the sensitivity of the attractor initial state. Its physical meaning is the exponential rate of the divergence of adjacent trajectories in the attractor. It is used to measure the degree of attraction or separation between two adjacent trajectories in phase space. For example: the initial distance between two points of adjacent trajectories is d_L (0), and then the distance becomes d_L(t) due to the trajectory divergence at time t, so$d_L(t) = d_L(0)e^{\lambda t}$. A positive LE value indicates that the system dynamic behavior is chaotic, and a negative value or zero indicates regular behavior. For an N-dimensional attractor, there will be N LE values. The algorithm for calculating LE is to obtain the maximum positive LE (that is, λ_1) in the time series. This method calculates the divergence rate of the reference trajectory and adjacent trajectories in the attractor. The maximum positive LE of the time series can be expressed as (Eckhardt and Yao, 1993; Rozenbaum et al., 2017):

$$\lambda_1 = \lim_{N\to\infty}\frac{1}{t_m - t_0}\sum_{i=1}^{m}\ln\frac{d_L'(t_i)}{d_L(t_{i-1})} \tag{9}$$

t_0:initial timet_m:the mth time.

2.3.8 Kolmogorov Entropy (K2)

Kolmogorov entropy is a quantitative method for measuring the degree of chaotic behavior. It can also be used to distinguish the

characteristics of dynamic systems: chaotic or non-chaotic. "Entropy" is adopted from the concept of thermodynamics as a method for expressing information characteristics, that is, the prediction of an uncertain system. The Kolmogorov entropy concept can be expressed as:

$$S(t_2) = S(t_1) + K(t_2 - t_1) \tag{10}$$

K stands for Kolmogorov entropy. The unit is bit/s. $S(t_1,t_2)$ is the amount of change in the time development information predicted by the initial information $S(t_1)$ after one (t_2—t_1) time. Assume that the initial entropy information is $S(t_1)$, after a time interval t_2—t_1, the information change to become $S(t_2)$. The change difference information is $K(t_2$—$t_1)$. Thus, it can be derived: $S(t_2) = S(t_1) + K(t_2$—$t_1)$. When $S(t_1) > S(t_2)$, so $K(t_2$—$t_1) = S(t_1)$—$S(t_2)$. Assume $S(t_1) = \ln C_d(R)$, $S(t_2) = \ln C_{d+1}(R)$. $C_d(R)$ is the signal correlation function. The equation for $K2$ is derived as below (Grassberger 1983; Zhang 2017):

$$K2 = \ln \frac{C_d(R)}{C_{d+1}(R)} \tag{11}$$

t-test was used to determine the significance of difference between healthy group and patient groups. The significance level was set to 0.05. All statistical tests were performed using SPSS 26 (IBM, Somers, NY, United States).

3 RESULTS

3.1 Blood Pressure and Cerebral Blood Flow

Figure 3 showed the comparison of differences in blood pressure and cerebral blood flow while in supine position among groups. From the systolic arterial blood pressure (SABP) and mean arterial blood pressure (MABP), it can be observed that stroke patients (SABP:177.0 ± 21.25 mmHg; MABP: 127.95 ± 18.66 mmHg)>hypertension patients (SABP:146.07 ± 26.04 mmHg; MABP: 106.55 ± 19.72 mmHg)>healthy people (SABP:120.94 ± 7.74 mmHg; MABP: 88.11 ± 7.76 mmHg). Both of these differences were significant ($p < 0.05$). Diastolic arterial blood pressure (DABP) is statistically different in stroke patients (DABP: 101.69 ± 18.02 mmHg) as opposed to hypertensive patients (DABP: 87.01 ± 18.16 mmHg) ($p < 0.05$). It can be seen that cardiovascular diseases (hypertension, stroke) do have obvious changing factors and trends to increase blood pressure. The systolic cerebral blood flow velocity (SCBFV) and mean cerebral blood flow velocity (MCBFV) showed that the value of stroke patients (SCBFV: 118.37 ± 60.42 cm/s; MCBFV: 73.99 ± 39.20 cm/s) was significantly higher than that of hypertension patients (SCBFV: 67.19 ± 21.84 cm/s; MCBFV: 36.84 ± 16.55 cm/s) and healthy people (SCBFV: 58.73 ± 9.62 cm/s; MCBFV: 38.82 ± 7.84 cm/s), and there was a statistical difference ($p < 0.05$). Diastolic cerebral blood flow velocity (DCBFV) is statistically different between stroke patients (DCBFV: 45.12 ± 24.78 cm/s) and healthy people (DCBFV: 23.69 ± 6.90 cm/s) ($p < 0.05$), and there is no significant difference in diastolic cerebral blood flow between hypertensive patients and stroke patients. **Figure 3** indicated the significant differences in blood pressure and cerebral blood flow while in supine position among healthy people, hypertensive patients, and stroke patients.

Figure 4 revealed the blood pressure and cerebral blood flow differences comparison in healthy people, hypertensive patients, and stroke patients in head-up tilt position. After interference induced by the tilting table, it can be seen that the SABP, MABP, and DABP values of stroke patients are significantly ($p < 0.05$) higher than those in healthy people ($SABP_{stroke}$:163.97 ± 19.55 mmHg; $MABP_{stroke}$:116.90 ± 12.78 mmHg; $DABP_{stroke}$: 94.71 ± 12.38 mmHg; $SABP_{healthy}$:128.83 ± 18.18 mmHg; $MABP_{healthy}$:95.0 ± 11.79 mmHg; $DABP_{healthy}$:76.30 ± 11.49 mmHg). On the other hand, the BP values of hypertensive patients between healthy and stroke patients were without significant difference and this might indicate an increasing BP trend toward abnormal. The cerebral blood flow velocity of stroke patients is higher than that of healthy people. The systolic cerebral blood flow velocity values revealed a significant statistical difference ($SCBFV_{stroke}$:114.18 ± 60.65 cm/s; $SCBFV_{healthy}$:60.87 ± 14.05 cm/s, $p < 0.05$).

3.2 Resistance Index, Pulsation Index) and Cerebrovascular Resistance

Figures 5, **6** show the resistance index (RI), pulsation index (PI), and cerebrovascular resistance (CVR) analysis results of the three groups in both supine and tilting positions, respectively. There is no obvious difference in movement and progress in RI and PI during position change. The CVR values indicated a slight statistical difference between healthy people and hypertensive patients ($CVR_{healthy}$: 2.32 ± 0.32; $CVR_{hypertension}$: 3.9 ± 2.78), hypertensive patients vs. stroke patients ($CVR_{hypertension}$: 3.9 ± 2.78; $CVR_{hypertension}$: 2.13 ± 1.03) while in supine position ($p < 0.1$). There was no significant difference in PI in the subjects tested this time. Only the PI values of hypertensive patients and stroke patients tended to be slightly higher than normal. The cerebrovascular resistance index CVR shows that the CVR of hypertensive patients is higher than that of normal people and stroke patients ($p < 0.1$), which shows that the cerebral vascular resistance of hypertensive patients is higher, but it is speculated that once a stroke develops, the cerebral vascular lesions Instead, it reduces the vascular resistance in the brain.

3.3 Analysis of Baroreflex

The pressure-sensitive reflex degree—baroreflex sensitivity (BRS) (also known as the pressure-sensitive reflex gain) is used as a measure of the autonomous control of the cardiovascular system. Usually BRS is a measure of the response of autonomic effectors to a given change in arterial pressure. When the position of a person changes from supine to a head-up position, blood pressure drops. This decreasing blood pressure can be compensated by the baroreflex through the conduction of the vagus nerve reflex. The sensory signal caused by the pressure receptor can inhibit the activity of the parasympathetic nerve and promote the activity of the sympathetic nerve, which increases the heart rate and

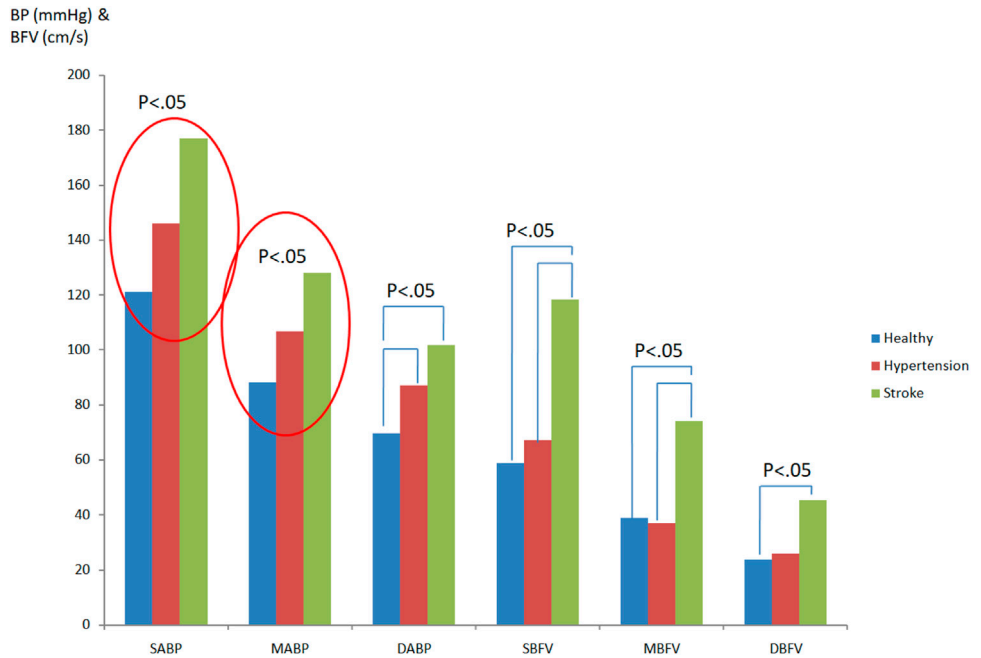

FIGURE 3 | Comparison of differences in blood pressure and cerebral blood flow while in supine position among groups.

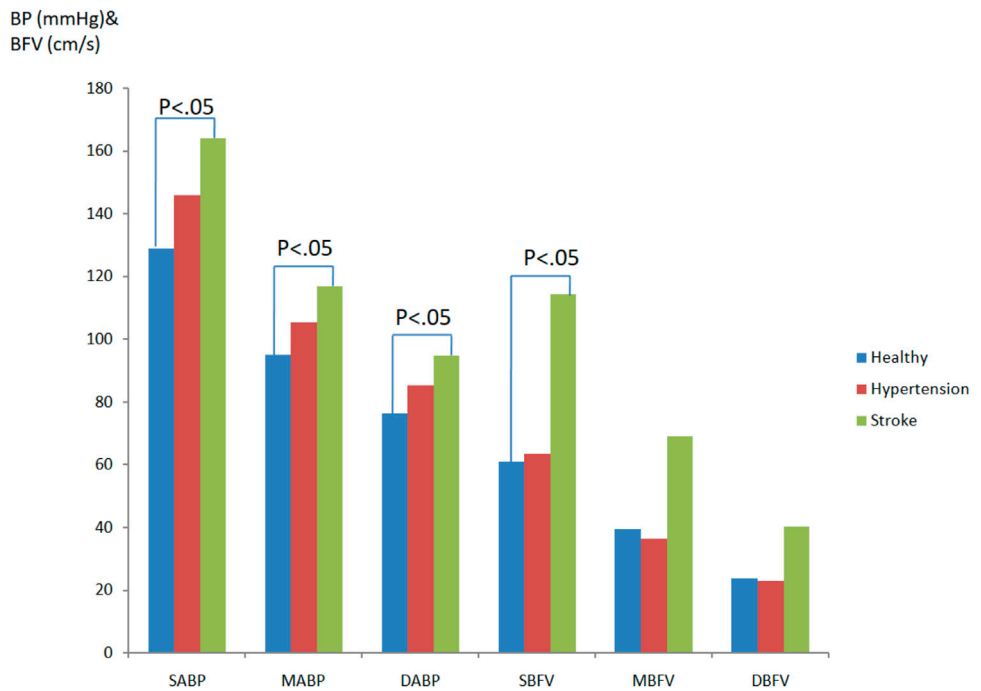

FIGURE 4 | Blood pressure and cerebral blood flow differences comparison in healthy people, hypertensivepatients, and stroke patients in head-up tilt position.

vasoconstriction, helping to maintain proper blood pressure when standing. **Figure 7** shows the baroreflex sensitivity analysis results of healthy people, hypertensive patients, and stroke patients. It shows that as the course of healthy→hypertension→stroke progresses, $BRS_{healthy}$ > $BRS_{hypertension}$ > BRS_{stroke}, and BRS decreases accordingly. Healthy people vs. hypertension (supine: $BRS_{healthy}$: 7.29 ± 0.88, $BRS_{hypertension}$: 6.1 ± 1.49; tilting: $BRS_{healthy}$: 6.43 ± 0.98,

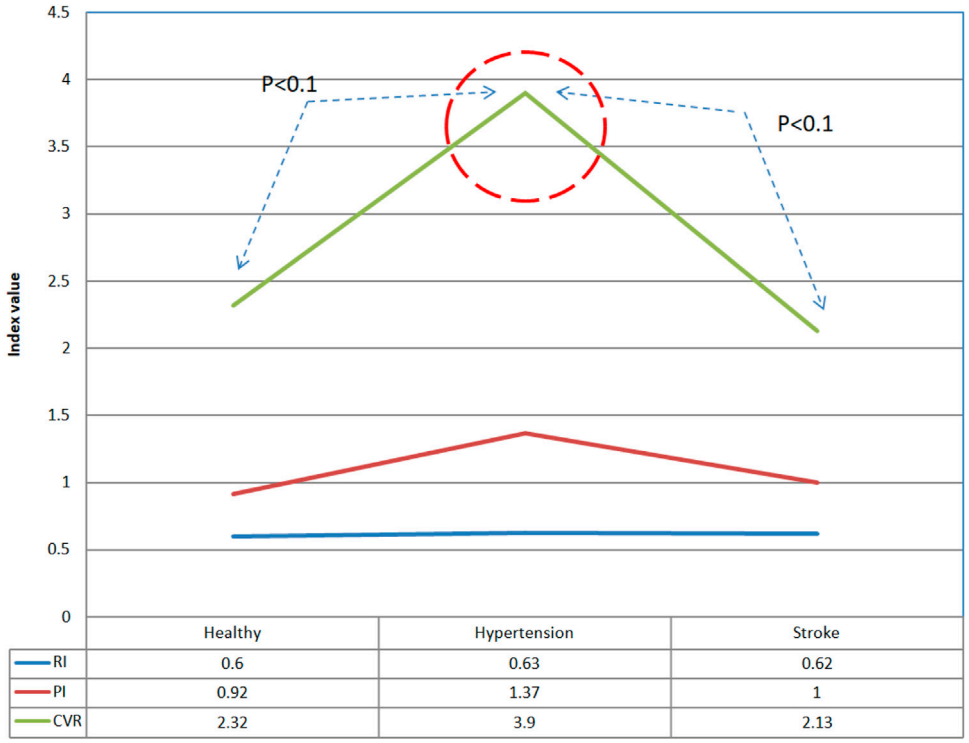

	Healthy	Hypertension	Stroke
RI	0.6	0.63	0.62
PI	0.92	1.37	1
CVR	2.32	3.9	2.13

FIGURE 5 | Comparison of differences in vascular resistance indexes between healthy people, hypertension patients, and stroke patients in supine position.

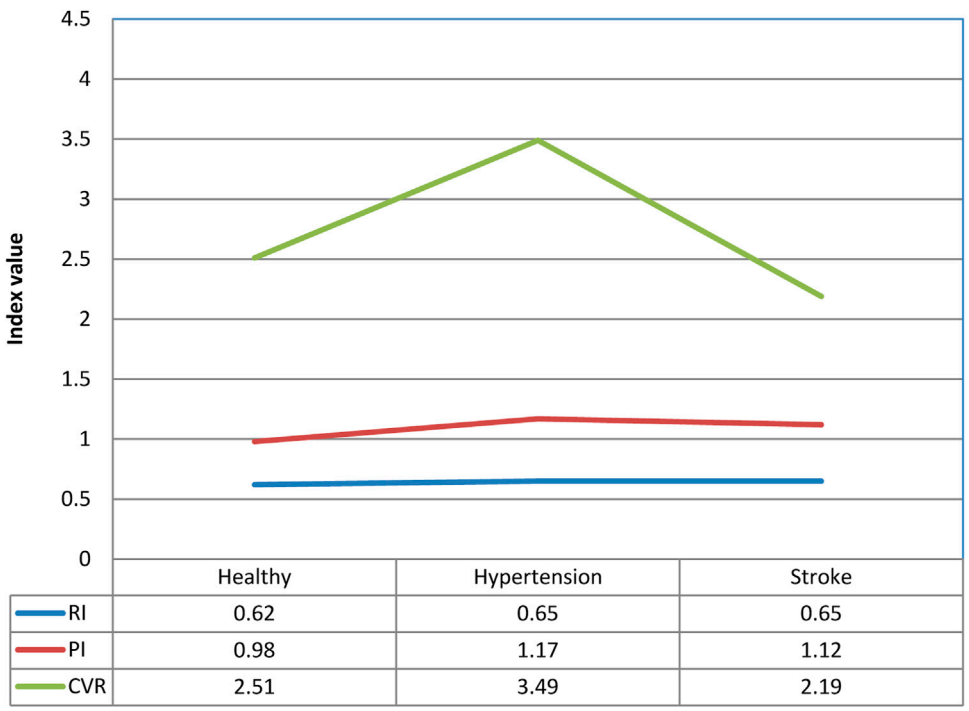

	Healthy	Hypertension	Stroke
RI	0.62	0.65	0.65
PI	0.98	1.17	1.12
CVR	2.51	3.49	2.19

FIGURE 6 | Comparison of differences in vascular resistance indexes of healthy people, hypertensive patients, and stroke patients in tilting position.

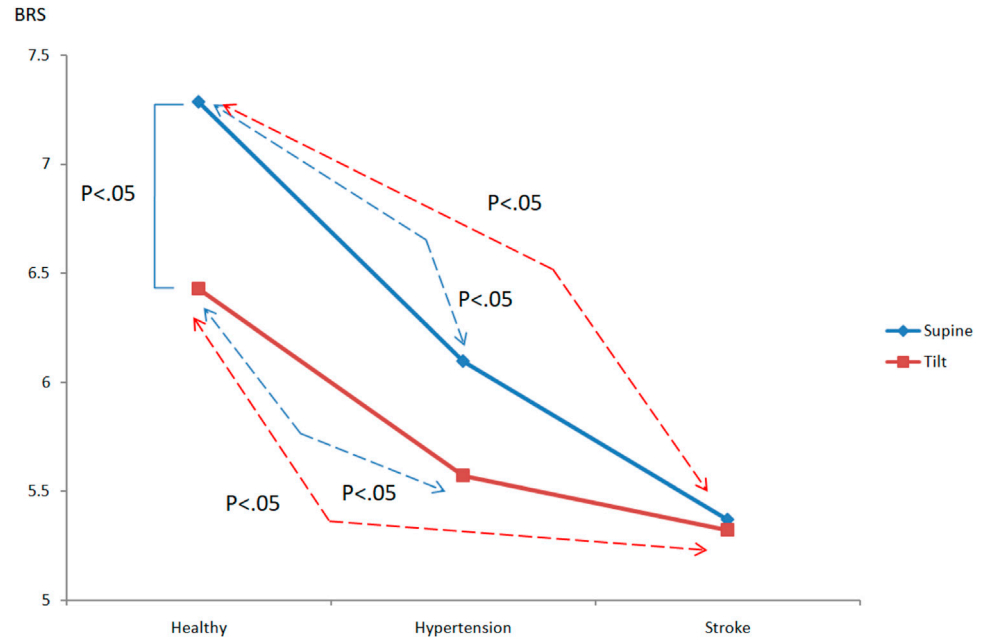

FIGURE 7 | Comparison of the differences in pressure reflex between healthy people, hypertensive patients, and stroke patients.

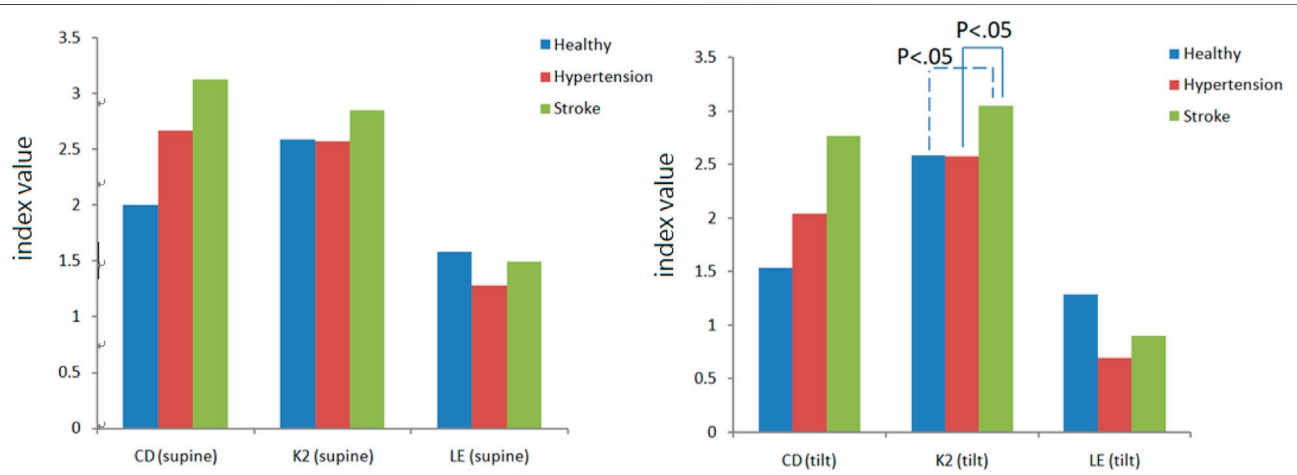

FIGURE 8 | Differences in blood pressure chaotic analysis of healthy people, hypertensive patients, and stroke patients.

$BRS_{hypertension}$: 5.57 ± 0.86), healthy people vs. stroke (supine: $BRS_{healthy}$: 7.29 ± 0.88, BRS_{stroke}: 5.37 ± 1.33; tilting: $BRS_{healthy}$: 6.43 ± 0.98, $BRS_{stroken}$: 5.32 ± 1.22), there are significant differences in both supine and tilting positions ($p < 0.05$).

3.4 Nonlinear Blood Pressure and Cerebral Blood Flow Analysis

There are three main parameters in chaotic analysis: 1. Correlation dimension (CD) represents the complexity of a system, and the higher the CD value, the higher the system complexity. 2. Lyapunov exponent (LE) represents the sensitivity of the initial system state. A positive LE value indicates that the system dynamic behavior is chaotic, and a negative value or zero indicates regular behavior. 3. Kolmogorov entropy (K2) is a quantitative method for the degree of chaotic behavior. It is used to predict the information loss rate of future behavior, that is, the degree of unpredictability. For a regular system, K2 is zero. For a completely random system, the K2 value is infinite. For a chaotic system, the K2 value is finite and positive. **Figure 8** is a comparison chart of the differences in blood pressure chaos analysis between healthy people, hypertensive patients, and stroke patients. It can be observed that the change trend between supine and head-up positions is close. After head-up

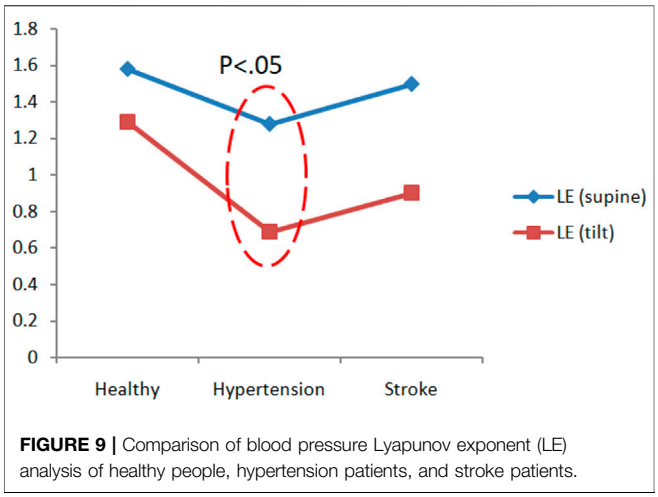

FIGURE 9 | Comparison of blood pressure Lyapunov exponent (LE) analysis of healthy people, hypertension patients, and stroke patients.

tilting, the K2 value of stroke patients is greater than that of hypertension patients and healthy people ($K2_{stroke}$:3.04 ± 0.28, $K2_{hypertension}$:2.58 ± 0.39, $K2_{healthy}$:2.59 ± 1.11), and there are statistical differences ($p < 0.05$) as shown in **Figure 8**. On the other hand, when the LE value changes posture in hypertensive patients, there is a statistically significant difference (Supine-$LE_{hypertension}$:1.28 ± 0.67,Tilt-$LE_{hypertension}$:0.69 ± 0.43$p < 0.05$), such as shown in **Figure 9**.

Figure 10 is a comparison chart of the chaotic analysis of cerebral blood flow in healthy people, hypertensive patients, and stroke patients. It can be observed that there is a significant difference ($p < 0.05$) in the K2 index between supine and tilting positions. While in supine position, the K2 value of stroke was higher than that of healthy people, with a statistical difference ($K2_{stroke}$: 3.74 ± 0.42, $K2_{healthy}$: 3.14 ± 0.59, $p < 0.05$). After head-up tilting, the K2 values of stroke patients were higher than those in hypertension patients and healthy people, and there was a statistical difference ($K2_{stroke}$:3.87 ± 1.03; $K2_{hypertension}$:3.24 ± 0.3; $K2_{healthy}$:2.80 ± 0.46, $p < 0.05$) as shown in **Figure 10**. When the LE value during changes posture in

TABLE 1 | Correlation analysis results for blood pressure and cerebral blood flow in each group.

	Supine			Tilting		
	Max CCF	Index	SD	Max CCF	Index	SD
Healthy	0.57	−1.9	015	0.53	−1.6	0.18
Hypertension	0.43*	−2.2	0.16	0.40	−2.5	0.19
Stroke	0.40**	−0.11	0.20	0.34	−3.52	0.22

*Max CCF, in supine (Healthy vs. Hypertension, *p < 0.05; Healthy vs. Stroke, **p < 0.05); max CCF, in tilting (Healthy vs. Hypertension, p < 0.05; Healthy vs. Stroke, p < 0.05).*

hypertensive patients, there is a statistically significant difference (supine $LE_{hypertension}$:1.11 ± 0.43; tilting $LE_{hypertension}$:0.64 ± 0.25, $p < 0.05$).

3.5 Cross-Correlation Function Analysis

3.5.1 Blood Pressure and Cerebral Blood Flow

Table 1 shows the correlation analysis results for blood pressure and cerebral blood flow in healthy people, hypertensive patients, and stroke patients. **Figure 11** shows the comparison of the maximum CCF differences between blood pressure and cerebral blood flow in healthy people, hypertensive patients, and stroke patients. The results show that as the course of healthy→ hypertension → stroke progresses with the maximum CCF value decreases indicated significantly differences (Healthy vs. Hypertension; Healthy vs. Stroke, $p < 0.05$). That means the relationship between blood pressure and cerebral blood flow decreased, reaching a statistical difference ($p < 0.05$). **Figures 12–14** show the correlation analysis between blood pressure and cerebral blood flow in typical healthy people, hypertensive patients, and stroke patients.

4 DISCUSSION

The time domain analysis results indicate that high blood pressure is one of the most important factors influencing the

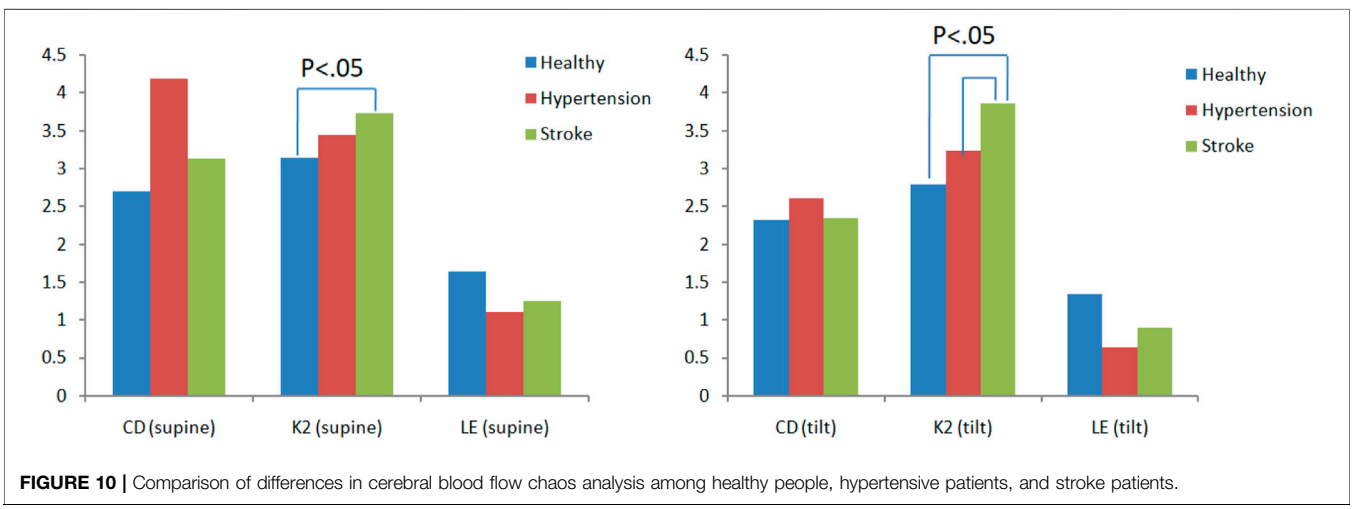

FIGURE 10 | Comparison of differences in cerebral blood flow chaos analysis among healthy people, hypertensive patients, and stroke patients.

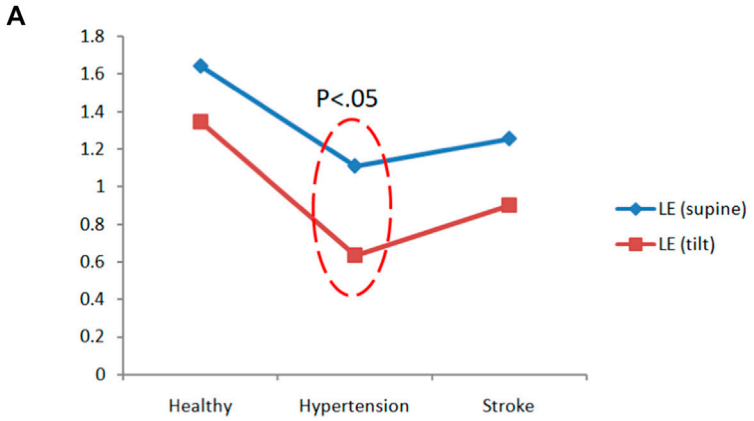

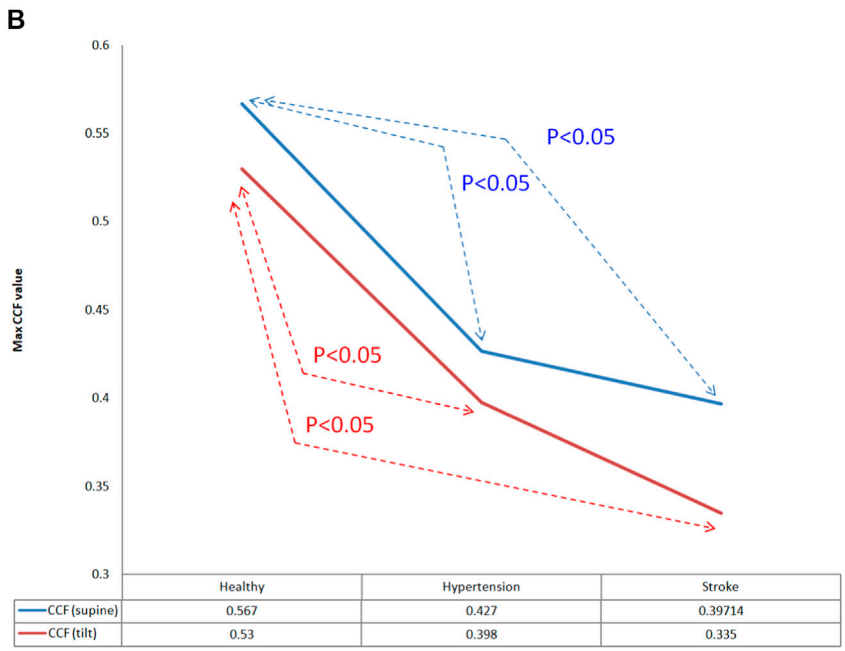

	Healthy	Hypertension	Stroke
CCF (supine)	0.567	0.427	0.39714
CCF (tilt)	0.53	0.398	0.335

FIGURE 11 | (A) Comparison of Lyapunov exponent (LE) analysis of cerebral blood flow in healthy people, hypertensive patients, and stroke patients. **(B)** Comparison of maximum CCF differences between blood pressure and cerebral blood flow in healthy people, hypertensive patients, and stroke patients.

stroke process. Higher blood pressure and blood flow increase the risk for stroke (Fuchs and Ethlton, 2020). Although there is no statistical difference between the average cerebral blood flow and the diastolic cerebral blood flow, it can be clearly observed that the CBFV value of stroke patients is higher than those in healthy and hypertensive patients. Therefore, it can also be inferred that the increase in blood pressure and blood flow is accompanied by a high risk for hypertension and stroke due to hypertrophy and smooth muscle cells remodeling (Yu et al., 2011). On the other hand, the blood vessel resistance index (RI) is a measure of peripheral blood flow resistance. Low vascular resistance has a higher diastolic blood flow velocity characteristic, and will have a lower RI value, and a high vascular resistance has a lower diastolic blood flow velocity characteristic and will induce a higher RI value (Hilz et al., 2004). The results showed that there was no significant difference in RI among the groups in this study. The pulsation index (PI) is a measurement that describes the type of signal waveform. Low intracranial vascular resistance will reduce PI, and rising intracranial pulsations have been found to be related to rising intracranial pressure. The general PI range is between 0.5 and 1.4, less than 0.5 may be an ischemic flow pattern under vascular dilation. PI range greater than 1.5 may indicate a decrease in vascular compliance or an increase in intracranial pressure (Hilz et al., 2004). Because the CVR value in the hypertension group is higher than those in other groups, it would indicate that blood vessel resistance increased and blood vessel characteristics were changed. Moreover, average PI value in hypertension group is 1.37 close to 1.4, it may reveal high blood pressure decrease

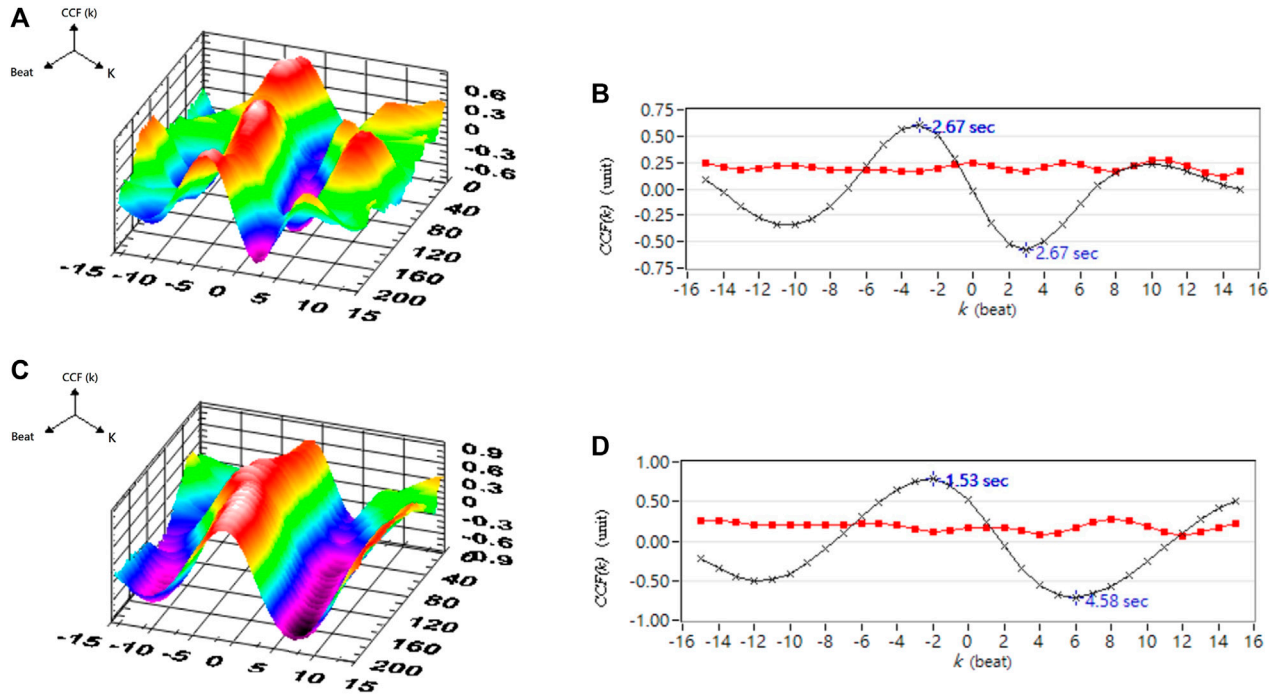

FIGURE 12 | A typical healthy person's blood pressure and cerebral blood flow correlation analysis. **(A)** 3D representative CCF figures in supine position. **(B)** 2D representative figures of CCF in supine position. **(C)** 3D representative figures of CCF in head-up tilt position. **(D)** 2D representative figures of CCF in head-up tilt position. CCF(k) is the CCF value in the time indices. The mean (–x–) and standard deviation (–■–) of CCF value in each time index k.

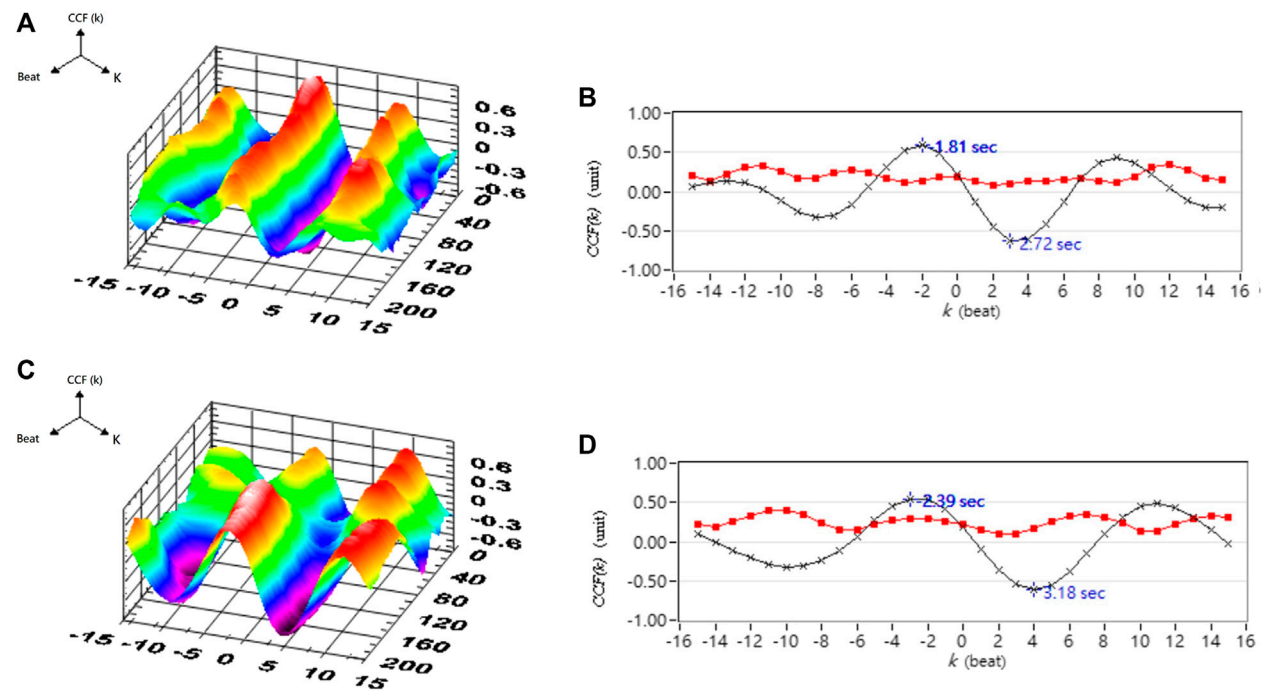

FIGURE 13 | Analysis results of correlation between blood pressure and cerebral blood flow in a typical hypertensive patient. **(A)** 3D representative figures of CCF in supine position. **(B)** 2D representative figures of CCF in supine position. **(C)** 3D representative CCF figures in head-up tilt position. **(D)** 2D representative CCF figures in head-up tilt position. CCF(k) is the CCF value in the time indices. The mean (–x–) and standard deviation (–■–) of CCF value in each time index k.

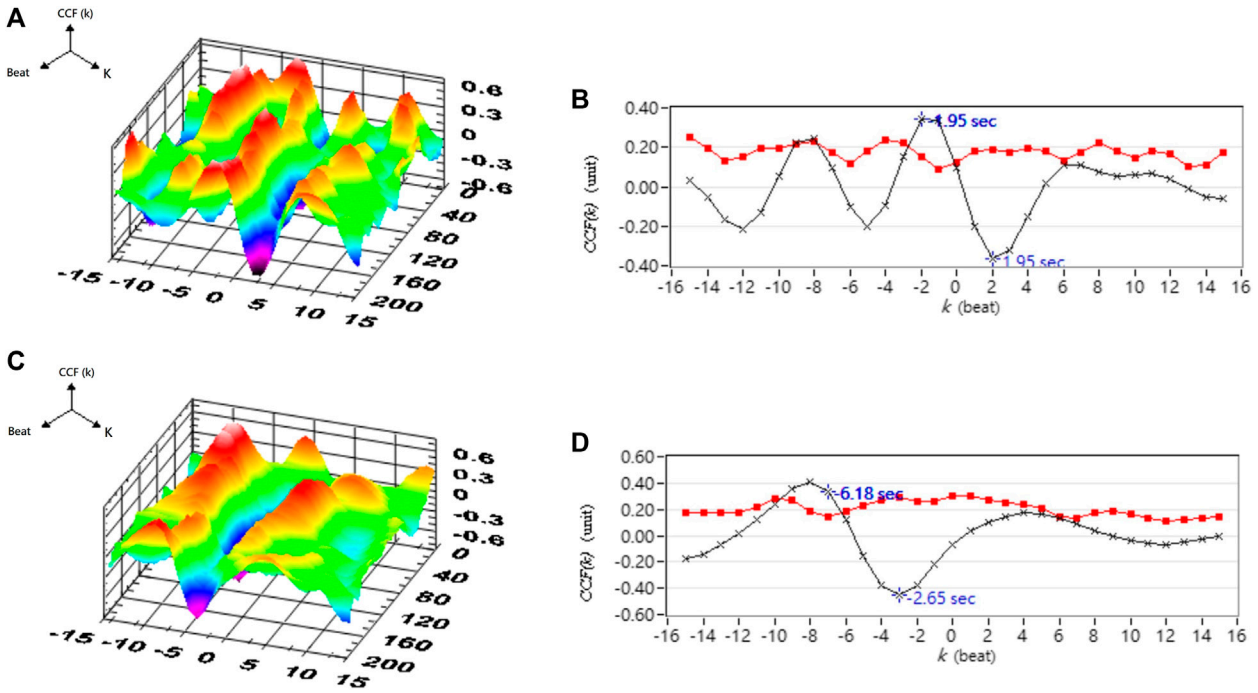

FIGURE 14 | Analysis results for the correlation between blood pressure and cerebral blood flow in a typical stroke patient. **(A)** 3D representative figures of CCF in supine position. **(B)** 2D representative figures of CCF in supine position. **(C)** 3D representative CCF figures in head-up tilt position. **(D)** 2D representative CCF figures in head-up tilt position. CCF(k) is the CCF value in the time indices. The mean (–x–) and standard deviation (–■–) of CCF value in each time index k.

vascular compliance or increase intracranial pressure (Hilz et al., 2004). From the baroreflex results, it can be inferred that the BRS receptor sensitivity in patients with hypertension and stroke is reduced, and it is unable to effectively sense the changes in blood pressure and regulate the cardiovascular system. If high blood pressure occurs, hypertension exceeds the normal pressure reflex receptor operating range (The average blood pressure is 60–120 mmHg), the individual cannot adjust their heartbeat, blood vessel radius and other factors through the autonomic nervous system to maintain normal cardiovascular system regulation. Therefore, dysfunctional baroreflex and hypertension would lead to stroke risk according to the results and previous studies (Kuusela et al., 2002; Yu et al., 2011; Fuchs et al., 2020).

Chaotic analysis can extract hidden behavior in a system. The K2 value is finite and positive for a chaotic system. Using the BP K2 results in chaotic analysis, it can be speculated that the changes in blood pressure in stroke patients are more unpredictable than in healthy people and hypertensive patients (Grassberger 1983; Zhang 2017). According to previous studies (Eckhardt and Yao, 1993; Rozenbaum et al., 2017), the difference in LE indicated that the blood pressure disturbance in hypertensive patients has a higher change in chaotic behavior and a difference in initial state sensitivity. On the other hand, nonlinear analysis of cerebral blood flow infers that the changes in cerebral blood flow in stroke patients is more unpredictable than in healthy people and hypertensive patients. This revealed that cerebral blood flow disturbance in hypertensive patients has a higher change in chaotic behavior and a difference in initial state sensitivity. Summarizing the chaotic analysis and baroreflex results, due to lower BRS value mean dysfunction baroreflex and it would induced circulation system to be more complicated (Kuusela et al., 2002), it can be inferred that changes in blood pressure and cerebral blood flow in patients with hypertension and stroke lead to higher chaotic behavior and changes in initial state sensitivity. CCF analysis indicated the interaction of circulation subsystems and it showed maximum CCF value decreasing significant in hypertension and stroke group respect to healthy group. This means that blood pressure and cerebral blood flow are gradually not affected by the autoregulation mechanism, and that the buffer between blood pressure and cerebral blood flow is dysfunctional. It can also be speculated that the incidence of stroke is increased.

5 CONCLUSION

This study demonstrated the results from assessing the link change in linear and nonlinear analysis in healthy, hypertensive and stroke groups. The significant differences might indicate high blood pressure would be a critical factor that affects cardiovascular control with regulation function and blood vessel properties in hypertension and stroke subjects. The results from this study revealed the time domain analysis included BP and BFV levels, BRS, CVR and CCF. The nonlinear measures included LE, and K2, which are suitable parameters to explore the hidden components of circulation

characteristics and performance in hypertensive and stroke patients. We speculate that an irregular cardiovascular system would tend toward dysfunction in various sub-systems and less predictable behavior. This could be as a measure for detecting and preventing the risk for hypertension and stroke in clinical practice (Faure and Korn, 1998; Rivera-Lara et al., 2017).

DATA AVAILABILITY STATEMENT

The raw data supporting the conclusion of this article will be made available by the author, without undue reservation.

ETHICS STATEMENT

The studies involving human participants were reviewed and approved by the Research Ethics Committee of Cheng-Ching General Hospital, Taiwan. The patients/participants provided their written informed consent to participate in this study.

AUTHOR CONTRIBUTIONS

Conceptualization and methodology, B-YL and S-JY; formal analysis, B-YL and Y-KJ; writing, B-YL, C-WL, F-CK, and Y-KJ; project administration, B-YL and S-JY All authors have read and agreed to the published version of the manuscript.

FUNDING

This work was supported by the Ministry of Science and Technology, Taiwan (MOST 108- 2221-E-241-008 and MOST 110-2637-E-241-002) to B-YL and S-JY.

ACKNOWLEDGMENTS

The authors would like to thank the National Science Council, Taiwan, ROC, for supporting this research under Contract Nos. MOST 108-2221-E-241-008 and MOST 110-2637-E-241-002.

REFERENCES

Aoi, M. C., Hu, K., Lo, M.-T., Selim, M., Olufsen, M. S., and Novak, V. (2012). Impaired Cerebral Autoregulation Is Associated with Brain Atrophy and Worse Functional Status in Chronic Ischemic Stroke. *PLoS ONE* 7 (10), e46794. doi:10.1371/journal.pone.0046794

Baumbach, G. L., and Heistad, D. D. (1988). Cerebral Circulation in Chronic Arterial Hypertension. *Hypertension* 12 (2), 89–95. doi:10.1161/01.hyp.12.2.89

Benjo, A., Thompson, R. E., Fine, D., Hogue, C. W., Alejo, D., Kaw, A., et al. (2007). Pulse Pressure Is an Age-independent Predictor of Stroke Development after Cardiac Surgery. *Hypertension* 50, 630–635. doi:10.1161/HYPERTENSIONAHA.107.095513

Bolea, J., Laguna, P., Remartínez, J. M., Rovira, E., Navarro, A., and Bailón, R. (2014). Methodological Framework for Estimating the Correlation Dimension in HRV Signals. *Comput. Math. Methods Med.* 2014, 129248. doi:10.1155/2014/129248

Castro, P., Azevedo, E., and Sorond, F. (2018). Cerebral Autoregulation in Stroke. *Curr. Atheroscler. Rep.* 20, 37. doi:10.1007/s11883-018-0739-5

Chiu, C.-C., and Yeh, S.-J. (2001). Assessment of Cerebral Autoregulation Using Time-Domain Cross-Correlation Analysis. *Comput. Biol. Med.* 31 (6), 471–480. doi:10.1016/s0010-4825(01)00015-4

Chiu, C. C., Yeh, S. J., and Chen, C. H. (2007). Self-organizing Arterial Pressure Pulse Classication Using Neural Networks: Theoretical Considerations and Clinical Applicability. *Comput. Biol. Med.* 30, 71–88.

Chiu, C. C., Yeh, S. J., and Liau, B. Y. (2005). Assessment of Cerebral Autoregulation Dynamics in Diabetics Using Time-Domain Cross-Correlation Analysis. *J. Med. Biol. Eng.* 25 (2), 53–59.

Crippa, I. A., Subirà, C., Vincent, J.-L., Fernandez, R. F., Hernandez, S. C., Cavicchi, F. Z., et al. (2018). Impaired Cerebral Autoregulation Is Associated with Brain Dysfunction in Patients with Sepsis. *Crit. Care* 22, 327. doi:10.1186/s13054-018-2258-8

Eckhardt, B., and Yao, D. (1993). Local Lyapunov Exponents in Chaotic Systems. *Physica D: Nonlinear Phenomena* 65, 100–108. doi:10.1016/0167-2789(93)90007-n

Fan, X., Li, X., and Yin, J. (2019). Dynamic Relationship between Carbon price and Coal price: Perspective Based on Detrended Cross-Correlation Analysis. *Energ. Proced.* 158, 3470–3475. doi:10.1016/j.egypro.2019.01.925

Faure, P., and Korn, H. (1998). A New Method to Estimate the Kolmogorov Entropy from Recurrence Plots: its Application to Neuronal Signals. *Physica D: Nonlinear Phenomena* 122, 265–279. doi:10.1016/s0167-2789(98)00177-8

Fuchs, F. D., and Whelton, P. K. (2020). High Blood Pressure and Cardiovascular Disease. *Hypertension* 75 (2), 285–292. doi:10.1161/hypertensionaha.119.14240

Gao, J., Hu, J., and Tung, W.-w. (2011). Facilitating Joint Chaos and Fractal Analysis of Biosignals through Nonlinear Adaptive Filtering. *PLoS ONE* 6 (9), e24331. doi:10.1371/journal.pone.0024331

Grassberger, P., and Procaccia, I. (1983). Estimation of the Kolmogorov Entropy from a Chaotic Signal. *Phys. Rev. A.* 28 (4), 2591–2593. doi:10.1103/physreva.28.2591

Grassberger, P., and Procaccia, I. (1983). Measuring the Strangeness of Strange Attractors. *Physica D: Nonlinear Phenomena* 9, 189–208. doi:10.1016/0167-2789(83)90298-1

Hilz, M. J., Kolodny, E. H., Brys, M., Stemper, B., Haendl, T., and Marthol, H. (2004). Reduced Cerebral Blood Flow Velocity and Impaired Cerebral Autoregulation in Patients with Fabry Disease. *J. Neurol.* 251 (5), 564–570. doi:10.1007/s00415-004-0364-9

Karemaker, J. M., and Wesseling, K. H. (2008). Variability in Cardiovascular Control: The Baroreflex Reconsidered. *Cardiovasc. Eng.* 8, 23–29. doi:10.1007/s10558-007-9046-4

Kuusela, T. A., Jartti, T. T., Tahvanainen, K. U. O., and Kaila, T. J. (2002). Terbutaline-Induced Heart Rate and Blood Pressure Changes. *Am. J. Physiol. Heart Circ. Physiol.* 282, H773–H781.

Laurent, S., Katsahian, S., Fassot, C., Tropeano, A.-I., Gautier, I., Laloux, B., et al. (2003). Aortic Stiffness Is an Independent Predictor of Fatal Stroke in Essential Hypertension. *Stroke* 34, 1203–1206. doi:10.1161/01.STR.0000065428.03209.64

Laurent, S. p., and Boutouyrie, P. (2005). Arterial Stiffness and Stroke in Hypertension. *CNS Drugs* 19 (1), 1–11. doi:10.2165/00023210-200519010-00001

Liau, B.-Y., Yeh, S.-J., Chiu, C.-C., and Tsai, Y.-C. (2008). Dynamic Cerebral Autoregulation Assessment Using Chaotic Analysis in Diabetic Autonomic Neuropathy. *Med. Bio Eng. Comput.* 46, 1–9. doi:10.1007/s11517-007-0243-5

Liau, B. Y., Chiu, C. C., and Yeh, S. J. (2010). Assessment of Dynamic Cerebral Autoregulation Using Spectral and Cross-Correlation Analyses of Different Antihypertensive Drug Treatments. *J. Med. Biol. Eng.* 30 (3), 169–176.

Ma, H., Guo, Z.-N., Liu, J., Xing, Y., Zhao, R., Yang, Y., et al. (2016). Temporal Course of Dynamic Cerebral Autoregulation in Patients with Intracerebral Hemorrhage. *Stroke* 47, 674–681. doi:10.1161/STROKEAHA.115.011453

Oeinck, M., Neunhoeffer, F., Buttler, K.-J., Meckel, S., Schmidt, B., Czosnyka, M., et al. (2013). Dynamic Cerebral Autoregulation in Acute Intracerebral Hemorrhage. *Stroke* 44, 2722–2728. doi:10.1161/STROKEAHA.113.001913

Pringle, E., Phillips, C., Thijs, L., Davidson, C., Staessen, J. A., de Leeuw, P. W., et al. (2003). Systolic Blood Pressure Variability as a Risk Factor for Stroke and

Cardiovascular Mortality in the Elderly Hypertensive Population. *J. Hypertens.* 21, 2251–2257. doi:10.1097/00004872-200312000-00012

Rivera-Lara, L., Zorrilla-Vaca, A., Geocadin, R. G., Healy, R. J., Ziai, W., and Mirski, M. A. (2017). Cerebral Autoregulation-Oriented Therapy at the Bedside. *Anesthesiology* 126 (6), 1187–1199. doi:10.1097/aln.0000000000001625

Rivera-Lara, L., Zorrilla-Vaca, A., Geocadin, R., Ziai, W., Healy, R., Thompson, R., et al. (2017). Predictors of Outcome with Cerebral Autoregulation Monitoring. *Crit. Care Med.* 45 (4), 695–704. doi:10.1097/CCM.0000000000002251

Roth, G. A., Mensah, G. A., Johnson, C. O., Addolorato, G., Ammirati, E., Baddour, L. M., et al. (2020). Global Burden of Cardiovascular Diseases and Risk Factors, 1990-2019: Update from the GBD 2019 Study. *J. Am. Coll. Cardiol.* 76 (5), 2982–3021. doi:10.1016/j.jacc.2020.11.010

Rozenbaum, E. B., Ganeshan, S., and Galitski, V. (2017). Lyapunov Exponent and Out-Of-Time-Ordered Correlator's Growth Rate in a Chaotic System. *Phys. Rev. Lett.* 118, 086801. doi:10.1103/PhysRevLett.118.086801

Shekhar, S., Liu, R., Travis, O. K., Roman, R. J., and Fan, F. (2017). Cerebral Autoregulation in Hypertension and Ischemic Stroke: a Mini Review. *J. Pharm. Sci. Exp. Pharmacol.* 2017 (1), 21–27.

Tiecks, F. P., Lam, A. M., Aaslid, R., and Newell, D. W. (1995). Comparison of Static and Dynamic Cerebral Autoregulation Measurements. *Stroke* 26 (6), 1014–1019. doi:10.1161/01.str.26.6.1014

WHO CVD risk chart working group (2019). World Health Organization Cardiovascular Disease Risk Charts: Revised Models to Estimate Risk in 21 Global Regions. *Lancet Glob. Health* 7 (10), e1332–e1345. doi:10.1016/S2214-109X(19)30318-3

WHO (2003), International Society of Hypertension Writing Group. *J. Hypertens.* 21 (11), 1983–1992.

Xiong, L., Liu, X., Shang, T., Smielewski, P., Donnelly, J., Guo, Z.-n., et al. (2017). Impaired Cerebral Autoregulation: Measurement and Application to Stroke. *J. Neurol. Neurosurg. Psychiatry* 88, 520–531. doi:10.1136/jnnp-2016-314385

Yu, J.-G., Zhou, R.-R., and Cai, G.-J. (2011). From Hypertension to Stroke: Mechanisms and Potential Prevention Strategies. *CNS Neurosci. Ther.* 17, 577–584. doi:10.1111/j.1755-5949.2011.00264.x

Zhang, X. D. (2017). "Entropy for the Complexity of Physiological Signal Dynamics,". Editor B. Shen (Springer Nature Singapore Pte Ltd.), Adv. Exp. Med. Biol., 1028, 39–53. doi:10.1007/978-981-10-6041-0_3

Conflict of Interest: The authors declare that the research was conducted in the absence of any commercial or financial relationships that could be construed as a potential conflict of interest.

Publisher's Note: All claims expressed in this article are solely those of the authors and do not necessarily represent those of their affiliated organizations, or those of the publisher, the editors and the reviewers. Any product that may be evaluated in this article, or claim that may be made by its manufacturer, is not guaranteed or endorsed by the publisher.

frontiers in Bioengineering and Biotechnology

ORIGINAL RESEARCH
published: 23 December 2021
doi: 10.3389/fbioe.2021.803725

Predicting Forefoot-Orthosis Interactions in Rheumatoid Arthritis Using Computational Modelling

*Emily S. Kelly[1], Peter R. Worsley[2], Catherine J. Bowen[2], Lindsey S. Cherry[2], Bethany E. Keenan[3], Christopher J. Edwards[4], Neil O'Brien[4], Leonard King[4] and Alex S. Dickinson[1]**

[1]School of Engineering, Faculty of Engineering and Physical Sciences, University of Southampton, Southampton, United Kingdom, [2]School of Health Sciences, Faculty of Environmental and Life Sciences, University of Southampton, Southampton, United Kingdom, [3]Cardiff School of Engineering and Cardiff University Brain Research Imaging Centre, Cardiff University, Cardiff, United Kingdom, [4]University Hospital Southampton NHS Foundation Trust, Southampton, United Kingdom

Foot orthoses are prescribed to reduce forefoot plantar pressures and pain in people with rheumatoid arthritis. Computational modelling can assess how the orthoses affect internal tissue stresses, but previous studies have focused on a single healthy individual. This study aimed to ascertain whether simplified forefoot models would produce differing biomechanical predictions at the orthotic interface between people with rheumatoid arthritis of varying severity, and in comparison to a healthy control. The forefoot models were developed from magnetic resonance data of 13 participants with rheumatoid arthritis and one healthy individual. Measurements of bony morphology and soft tissue thickness were taken to assess deformity. These were compared to model predictions (99th% shear strain and plantar pressure, max. pressure gradient, volume of soft tissue over 10% shear strain), alongside clinical data including body mass index and Leeds Foot Impact Scale–Impairment/Footwear score (LFIS-IF). The predicted pressure and shear strain for the healthy participant fell at the lower end of the rheumatoid models' range. Medial first metatarsal head curvature moderately correlated to all model predicted outcomes ($0.529 < r < 0.574$, $0.040 < p < 0.063$). BMI strongly correlated to all model predictions except pressure gradients ($0.600 < r < 0.652$, $p < 0.05$). There were no apparent relationships between model predictions and instances of bursae, erosion and synovial hypertrophy or LFIS-IF score. The forefoot models produced differing biomechanical predictions between a healthy individual and participants with rheumatoid arthritis, and between individuals with rheumatoid arthritis. Models capable of predicting subject specific biomechanical orthotic interactions could be used in the future to inform more personalised devices to protect skin and soft tissue health. While the model results did not clearly correlate with all clinical measures, there was a wide range in model predictions and morphological measures across the participants. Thus, the need for assessment of foot orthoses across a population, rather than for one individual, is clear.

Keywords: foot orthosis, computational modeling, FEA, tissue strain, deep tissue injury, foot

OPEN ACCESS

Edited by:
Fang Pu,
Beihang University, China

Reviewed by:
Chi-Wen Lung,
Asia University, Taiwan
Wenxin Niu,
Tongji University, China

****Correspondence:***
Alex S. Dickinson
alex.dickinson@soton.ac.uk

Specialty section:
This article was submitted to Biomechanics, a section of the journal Frontiers in Bioengineering and Biotechnology

Received: *28 October 2021*
Accepted: *07 December 2021*
Published: *23 December 2021*

Citation:
Kelly ES, Worsley PR, Bowen CJ, Cherry LS, Keenan BE, Edwards CJ, O'Brien N, King L and Dickinson AS (2021) Predicting Forefoot-Orthosis Interactions in Rheumatoid Arthritis Using Computational Modelling. Front. Bioeng. Biotechnol. 9:803725. doi: 10.3389/fbioe.2021.803725

INTRODUCTION

Rheumatoid arthritis (RA) is frequently characterized by deformities at the metatarsophalangeal (MTP) joints, frequently with erosion and subluxation of the first and fifth MTP joints (Bowen et al., 2011). Where RA has resulted in hallux valgus deformities, lateral displacement of the sesamoid bones is common (Nix et al., 2012). The surrounding soft tissues are also affected, with the plantar fat pad migrating distally from under the metatarsal heads increasing their vulnerability (Jaakkola and Mann, 2004). Bursae also pose problems, through inflammation or adventitial bursae formation as a response to friction and high pressures (Bowen et al., 2010; Van Hul et al., 2011). Associated with these morphological changes are pain, reduced foot function, and risk of soft tissue wounds (van der Leeden et al., 2006; Bowen et al., 2011). The most common sites of ulceration in the RA foot are the dorsal aspect of hammer toes (48%), the metatarsal heads (32%), and the medial aspect of the first MTP joint, with many ulcers reoccurring (Firth et al., 2008).

Generally, people with RA experience increased forefoot peak pressures compared to healthy individuals during weightbearing (Rosenbaum et al., 2006; Bowen et al., 2011; Carroll et al., 2015). Increased pressure has been shown to correlate to joint erosion and damage (Tuna et al., 2005; van der Leeden et al., 2006), but not pain, swelling or disability measures (van der Leeden et al., 2006; Konings-Pijnappels et al., 2019). Additionally, there may be limited associations between external pressures, which are easily measured, and internal tissue stresses, which are more indicative of injury (Linder-Ganz et al., 2007). Using Finite Element (FE) Analysis in other scenarios, elevated internal soft tissue stresses have been predicted around bony prominences with low soft tissue coverage, where compression also generates shear stresses (Takahashi et al., 2010). Many studies comparing plantar pressures to RA-related factors, such as pain or disability, are limited by measuring pressures barefoot rather than shod. Shoe choice is important in treating RA, as poorly-fitting footwear cause high pressures at the bony prominences of the metatarsal heads, particularly where joints are deformed (Woodburn and Helliwell, 1996).

Foot orthoses (FOs) are also prescribed to improve quality of life (QoL) by offloading painful regions. However, literature on the effectiveness of FOs in RA treatment is unclear. The effects of several footwear and orthosis variables upon plantar/forefoot pressure and pressure-time integrals (PTIs) have been studied experimentally, including shoe choice (Hennessy et al., 2007), FO customization (Hennessy et al., 2012), orthosis stiffness/rigidity and adaptations including metatarsal bars and domes (Tenten-Diepenmaat et al., 2019), and optimizing FOs based on pressure measurements (Tenten-Diepenmaat et al., 2020). These interventions typically reduced pressure but did not have a clear effect on pain or disability scores. One study found that FOs only significantly reduced peak pressures in a sub-group who had high in-shoe pressures without an FO (Tenten-Diepenmaat et al., 2020). Thus far, no single FO design is considered best practice to reduce pain and improve QoL in RA treatment, and the focus has primarily been on plantar pressure reductions even though other factors are involved (Hooper et al., 2012).

Computational modelling provides additional understanding of how loading affects the soft tissue and joints internally. Modelling studies have assessed the effectiveness of FO designs, though the studies tend to assess healthy individuals rather than those who would use the FOs (Chen et al., 2003; Cheung and Zhang, 2005; Goske et al., 2006). These models vary in configuration, using 2D or 3D geometry, linear elastic or hyperelastic properties for the soft tissue and orthosis, and a single bulk soft tissue group or including ligaments and tendons (Cheung et al., 2009). Another consideration is inclusion of the shoe. Despite evidence that shoe uppers also affect soft tissue loading (Woodburn and Helliwell, 1996; Dahmen et al., 2020), most studies only include the sole (Chen et al., 2003; Spirka et al., 2014; Chen et al., 2015; Telfer et al., 2017). Other studies have evaluated FO behavior without including the shoe (Cheung and Zhang, 2005; Zhang et al., 2020). As most of these models were based on a single healthy individual, the results relate only to that individual and may not apply to symptomatic populations, such as people with RA. There have been some exceptions where studies have assessed a pathological individual or multiple people. One study modelled a person with midfoot arthritis (Zhang et al., 2020), and another optimized FO design for 18 people with diabetes (Telfer et al., 2017). However, no studies have assessed people with RA, whose pathology, and thus orthotic requirements, differ from those with diabetes or post-traumatic midfoot arthritis.

In the present study, models were developed for people with RA affecting the forefoot. The aim was to ascertain whether simplified forefoot models would produce differing biomechanical predictions depending on RA severity, and relevant anatomical measures from magnetic resonance (MR) imaging. The RA model predictions were also compared to model predictions from a healthy individual for contrast. Such models would provide advantages over experimental studies where it is difficult to examine internal effects of loading, and pave the way for FO and footwear choices tailored to the requirements of individuals with RA.

MATERIALS AND METHODS

This study involved secondary analysis of patient imaging and clinical outcome data sets from established studies (FeeTURA) (Cherry et al., 2014) by image-based computational modelling.

Participants

MR and questionnaire data were obtained, which had been collected from participants with RA during FeeTURA (Cherry et al., 2014), including assessments of condition severity through subjective means such as the Leeds Foot Impact Scale. The scale consists of two subsections: the impairment/footwear section (LFIS-IF) includes pain and footwear choices, while the second section covers activity limitation and participation restriction (LFIS-AP) (Helliwell et al., 2005). Instances of bursae between and beneath the MTP joints were also recorded, along with joint erosion and synovial hypertrophy. Detailed methodology for how these parameters were determined was published previously by

Cherry et al. (2014). Of the original 30 participants for whom MR data were available, 13 (aged 29-73, all female) were selected for the present study, purposively sampled to represent a range of LFIS-IF scores. These participants will henceforth be referred to as P1-13. The purpose of this study was to assess the performance of the models across a range of condition presentations. As such, the selection of participants was not controlled in any other way, so that potentially influencing factors would not be excluded.

A healthy individual, with no known medical conditions or history of musculoskeletal injuries to the foot and ankle, was assessed for comparison (female, aged 31 years). MR data for this individual had been collected in a previous study at the Cardiff University Brain Research Imaging Centre (CUBRIC, Dr Bethany Keenan). Ethical approval was granted by the relevant institutional and local authority committees for the original studies and secondary analysis purposes.

The participant selection and subsequent segmentation, measurement and FE modelling processes were completed by different researchers (ASD and ESK respectively) so that the study could be carried out blinded to the participants' reported condition severities.

MR Segmentation and Morphological Measurements

MR data for the RA participants had been collected specifically for the FeeTURA study in 2010–2011. The MR sequencing is detailed in the FeeTURA study in full (Cherry et al., 2014). The T1-weighted spin echo sequence taken in the coronal plane was used for this study (repetition time/echo time (TR/TE): 656 ms/15 ms, slice thickness: 3mm, in-plane resolution: 0.52 × 0.52 mm). The distal slices consisting of only the toes were removed, leaving only the metatarsal and MTP joint regions. MR data for the healthy volunteer had been collected with a Dual Echo Steady State (DESS) sequence in the sagittal plane (TR/TE: 13.48 ms/4.79 ms, resolution: 0.6 × 0.6 × 0.6 mm). This was carried out using a 3T scanner (Magnetom Prisma, Siemens, Erlangen, Germany) with a foot/ankle and four-channel flex coil with the plantar forefoot rested against a flat support.

The MR data were segmented using ScanIP (Simpleware ScanIP N-2018.03-SP2 Build 55, Synopsys, Mountain View, United States). The RA participants' MR data had been collected using a standardized foot position, with the coronal slices perpendicular to the metatarsal parabola. However, as the data were not originally collected for modelling purposes, the images were not orientated within the coronal plane, in positions appropriate for gait. Thus, the data were rotated in the coronal plane using ScanIP to ensure all the forefoot sections were appropriately and similarly orientated, using the metatarsal heads as references. Masks were created for the skin, underlying soft tissue and bone using greyscale thresholds. The same threshold values were used across all participants except for the healthy volunteer, where the values were adapted to suit the different MR sequencing that had been used. Where the scans included the proximal phalanges, these were fused to the metatarsals. A 2 mm thick sock was generated by dilating the skin mask in-plane. This was repeated to form a footwear model, representing a simplified leather shoe. This was given a 3 mm thick upper and 6 mm sole, allowing space for a total contact FO with a 3 mm minimum depth (**Figure 1A**). The simplified foot anatomy present in these models was deemed appropriate as the study purpose was comparison between models built using the same methods, rather than determination of absolute values.

Morphological measurements were taken using ScanIP's linear measurement tool, to be used as potential indicators of condition severity (**Figure 1B**). The first metatarsal head (MH1) region was investigated as a key bony prominence, potentially increasing the risk of damage to the surrounding tissue. Assessments were made regarding the sesamoid bone orientations, observing whether they were neutrally positioned under MH1 (normal position) or shifted laterally beyond MH1 (displaced position) (**Figure 1C**), and measuring the lateral distance from the medial edge of MH1 to the medial edge of the sesamoid. This measure was presented as a percentage of MH1 width. The depth of tissue under MH1 was measured to indicate tissue migration. Surface meshes of MH1 were exported to MATLAB (R2020b, MathWorks, Massachusetts, USA), to calculate the average principal curvature of the medial plantar quarter of MH1, using code sourced from MathWorks File Exchange (Rusinkiewicz, 2004; Ben Shabat and Fischer, 2015).

FE Model

The segmented geometries were imported into COMSOL Multiphysics v.5.5 (COMSOL Inc., Stockholm, Sweden) for FE analysis (**Figure 2**). Material properties of the shoe upper, sock and bone were assumed to be linear elastic (**Table 1**). The skin and soft tissue were modelled using a first order Ogden hyperelastic model for incompressible materials, using the following strain energy function W_s:

$$W_s = \frac{\mu}{\alpha}\left(\lambda_1^{\alpha} + \lambda_2^{\alpha} + \lambda_3^{\alpha} - 3\right) \tag{1}$$

The orthosis and shoe sole materials were modelled using Storakers model for highly compressible foam:

$$W_s = \frac{2\mu}{\alpha^2}\left(\lambda_1^{\alpha} + \lambda_2^{\alpha} + \lambda_3^{\alpha} - 3 + \frac{1}{\beta}\left(J_{e\tau}^{-\alpha\beta} - 3\right)\right) \tag{2}$$

For both equations, μ represents the shear modulus, α the deviatoric exponent, β the volumetric exponent, J_{el} the elastic volume ratio, and λ_i the principal stretches in each direction.

A fixed constraint was applied to all bones except the sesamoids, which were allowed to move freely as they would anatomically where they are embedded within the flexor hallucis brevis. The cut boundaries of the modelled foot section were assigned a fixed displacement perpendicular to the cutting plane. Friction was applied between the orthosis and upper and the sock with a static coefficient of 0.55 (Carlson, 2006). The orthosis, shoe sole and upper were bonded together, as were the bones, soft tissue and skin.

Vertical and medial ground reaction forces (GRF) were applied to the external boundary of the shoe sole in contact with the ground, to represent midstance of gait. The medial force was 5% of the participant's body weight (Jung et al., 2016). The

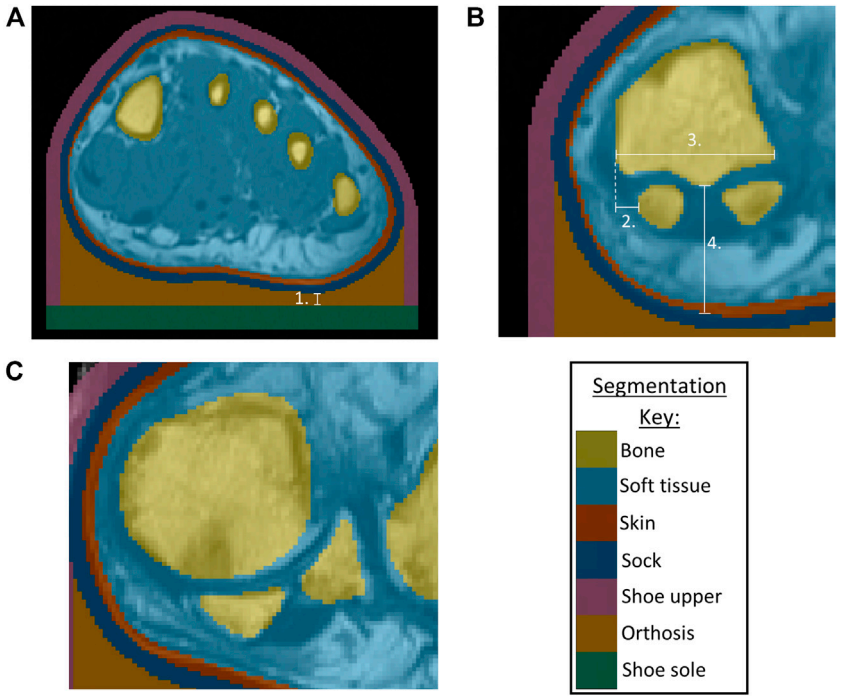

FIGURE 1 | (A) Segmentation of bones, skin, soft tissue from P3 MRI, with addition of sock, shoe upper, orthosis, shoe sole, indicating minimum orthosis depth (1.) **(B)** Morphological measurements for P3 showing sesamoids in a normal position, with 2. Lateral distance from MH1 edge to sesamoid, 3. MH1 width, 4. Tissue depth under MH1 **(C)** P1 MRI showing example of sesamoids in a displaced position.

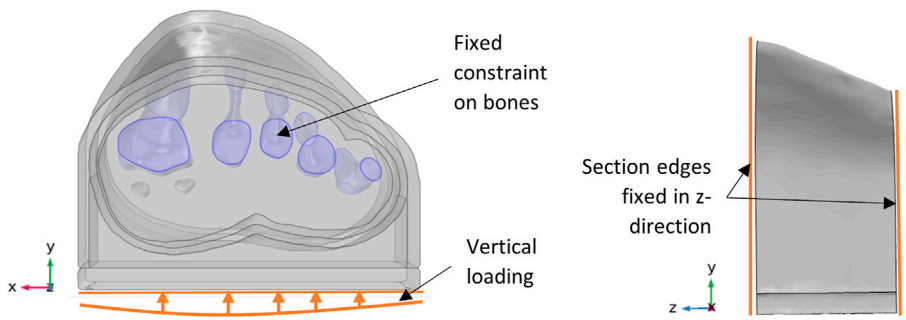

FIGURE 2 | P3 model, indicating vertical loading and boundary conditions.

TABLE 1 | Material Properties for linear elastic shoe sides, sock, bone and hyperelastic soft tissue, orthosis, shoe sole.

Material	Elastic parameters		Hyperelastic parameters			References
	Young's modulus (MPa)	Poisson's ratio	μ (kPa)	α	β	
Shoe upper (leather)	200	0.3	—	—	—	Goske et al. (2006)
Sock (cotton)	1.8	0.4	—	—	—	Zhou et al. (2010); Tian et al. (2019)
Bone	7,300	0.3	—	—	—	Cheung and Zhang, (2005)
Skin	—	—	452	5.6	—	Ahanchian et al. (2017)
Soft Tissue (exc. skin)	—	—	36	4.5	—	Ahanchian et al. (2017)
Orthosis (Poron)	—	—	144	4.013	0.057	Petre et al. (2006)
Shoe sole	—	—	1,588	7.708	0.292	Petre et al. (2006)

vertical force was scaled, using the participant weight and comparative length of forefoot section:

$$GRF_{vertical}(N) = Participant\ Weight(kg) \times 9.81 \times \frac{Forefoot\ section\ length}{Full\ foot\ length} \times 1.4 \quad (3)$$

The multiplier of 1.4 represented the proportion of load distributed to the forefoot during midstance (van der Leeden et al., 2006). This single load value was adjusted across the forefoot's width, using multipliers of 1.05, 1.26, 1.06, 0.88 and 0.75 for the load under the first to fifth metatarsal heads, respectively (**Figure 2**). This distribution was determined using gait pressure data of healthy individuals, collected with F-scan in-shoe sensors (Tekscan, Massachusetts, USA), and agreed with literature for people with RA (van der Leeden et al., 2006).

A second order tetrahedral mesh was used with local refinement in the narrow skin and sock domains, and at the orthosis/sock boundary (**Appendix 1**). Mesh convergence was assessed using P1 models. For the mesh used, percentile shear strain and pressure results were within 2.5% of the finest mesh results. Similarly, a sensitivity analysis was performed to ensure that the proximity of the forefoot section's cut edges to the region of interest would not affect the model results (**Appendix 2**).

Data Analysis

Four parameters were used to provide indications of tissue damage risk, that had been used previously in literature (Oomens et al., 2013; Bader and Worsley, 2018; Steer et al., 2021). Data from the models were processed in MATLAB to calculate the following:

1. 99th percentile shear strain (calculated from Green-Lagrange strain tensor) in the soft tissues,
2. volume of tissue above 10% shear strain,
3. 99th percentile plantar pressure,
4. maximum plantar pressure gradient.

The percentile calculations were based on soft tissue volume for shear strain and orthosis/limb interface area for pressure. 99th % values were used rather than maximums so that outliers due to highly localized peaks were excluded and so did not affect the model comparisons. The percentile value itself (99th) was chosen based on examination of the relevant histograms, so that the majority of the pressure or strain was included. For the pressure gradient calculations, the plantar pressure data was resampled to a 5 × 5mm resolution to reflect experimental F-scan sensor measurements. The pressure results along the cut edges of the forefoot sections were omitted from this resampling process as they were affected by the boundary conditions. The maximum pressure gradient was then found by calculating the pressure difference between each point and its neighbours, divided by the distance between points. Alongside these model results, clinical data for the participants were assessed including body mass index (BMI), LFIS-IF scores, instances of bursae, erosion and synovial hypertrophy at the joints, and the MRI-based anatomical measures mentioned above. For some analyses, the BMI was grouped into normal BMI ($18.5 \leq$ BMI <25 kg/m^2) and high BMI (BMI ≥ 25 kg/m^2).

SPSS Statistics (v.27, IBM Corp., Armonk, NY, United States) was used to carry out statistical analyses of the model results and participant data. Shapiro-Wilk normality tests were performed to determine whether parametric or non-parametric tests were appropriate. Disease duration, lateral sesamoid offset and volume of tissue over 10% shear strain were found to be non-parametric. The remaining FE model predictions, morphological measurements and clinical data were found to be parametric. Pearson correlation analyses were performed to determine the relationships between parametrically distributed variables, and where variables were skewed, Spearman's correlations were used.

RESULTS

Demographic and Morphological Comparisons

All 13 RA participants selected for this secondary analysis had relatively established disease, of duration over 1year and varying morphological presentations (**Figure 3**). Longer disease duration was correlated with sesamoid bones offset (r = 0.698, p = 0.008) (**Figure 4A**). The sesamoid offset also correlated with soft tissue depth under MH1 (r = -0.721, p = 0.005). Longer disease duration did not correlate significantly with reduced soft tissue depth, potentially due to the confounding effects of foot size and BMI (**Figure 4B**). Despite this, longer disease duration was not necessarily associated with a worse clinical presentation (**Figure 4C, D**). For example, in participants with RA for over 10 years, there was an even split of people with low vs moderate to high foot impairment (LFIS-IF threshold of 7 (Turner et al., 2006)). P6 and P10 had low LFIS-IF scores and instances of bursae, erosion and hypertrophy despite their longer disease durations and thus higher sesamoid offset and lower tissue depth under MH1. The opposite was observed for P1 and P8.

RA and Healthy Model Comparisons

The healthy participant had a normal BMI and sesamoid bones in a neutral position, confirming their suitability as a control. The healthy participant's FE model predictions generally fell at the lower end of the RA models' range, either just within or below the inter-quartile range (IQR) (**Table 2**). The exception was the pressure gradient predictions where the healthy participant fell towards the upper end of the IQR. Note that n = 12 for instances of bursae, erosion, and synovial hypertrophy, as data was unavailable for P12.

FE Model Predictions Across Participants With RA

Across all participants, the highest plantar pressures were located under the first or second metatarsal heads (**Figure 5**). Peak shear strains were concentrated in the soft tissue around the bones, particularly the medial first metatarsal head aspect and sesamoid bones.

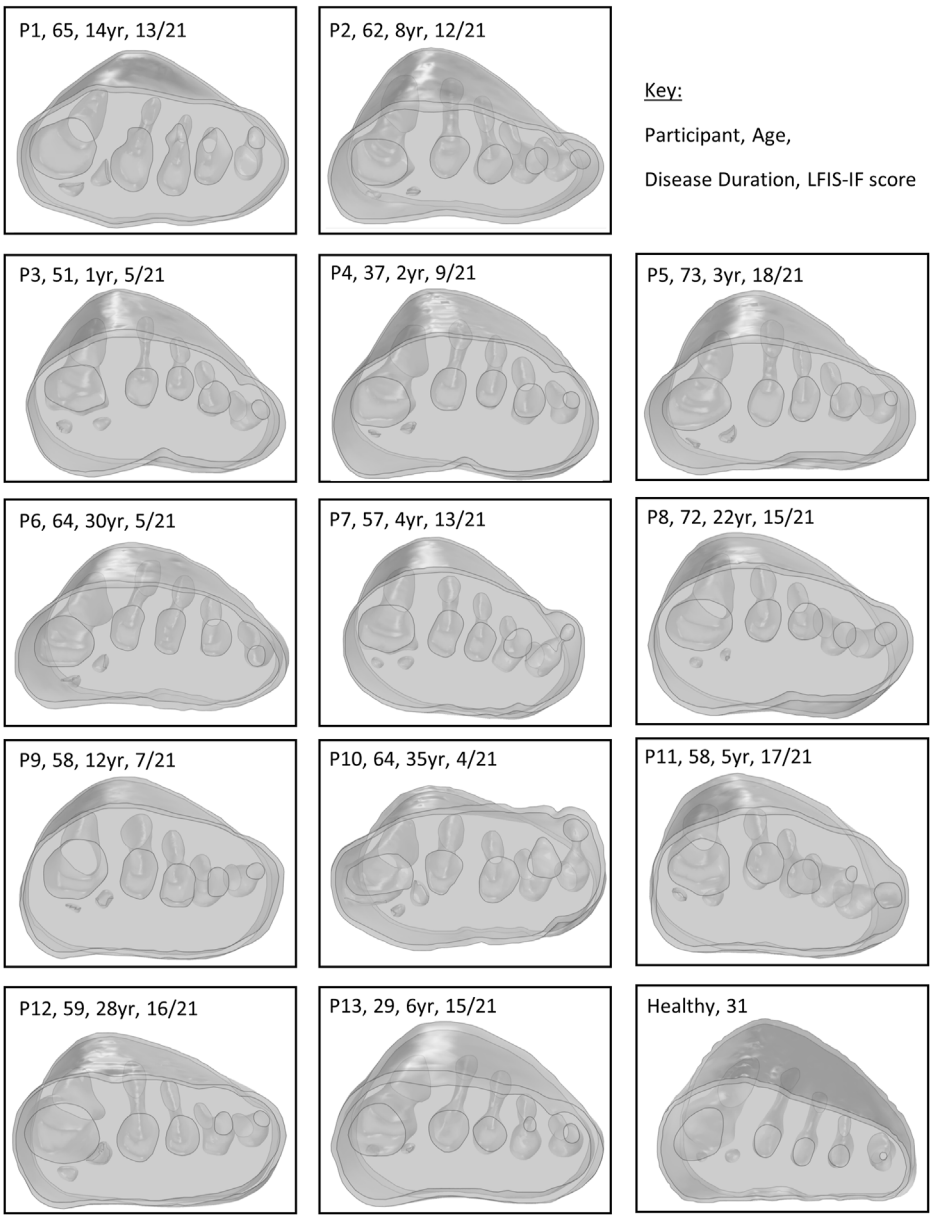

FIGURE 3 | Modelled forefeet (skin, encapsulated bulk soft tissue, bones) of the 13 participants with RA and one healthy participant, with age and disease duration indicated.

The model results displayed differences between participants with RA for some parameters, with BMI and MH1 curvature appearing to have the greatest impact (**Figure 6**). The four participants with the highest BMIs all produced model predictions above the median values (P3, P7, P11, P13). There was no discernible trend in model results for the participants with the four lowest BMIs (P5, P6, P8, P9). Overall, there were strong significant correlations between BMI and 99th% shear strain, volume of tissue over 10% shear strain, and 99th% plantar pressure ($0.600 < r < 0.652$, $p < 0.05$) (**Table 3**).

Similarly, three of the four participants with the lowest MH1 curvature (i.e., highest radius) accounted for three of the four lowest model predictions for strain and pressure gradient metrics (P1, P10, P12). Those with the four highest curvatures also had two to three of the highest pressure and strain predictions, with a clear distinction between those with high curvature and high BMI (P3, P7) and high curvature but normal BMI (P5, P6). Overall, MH1 curvature was moderately correlated with borderline significance to all four model predictions ($0.529 < r < 0.574$, $0.040 < p < 0.063$). This was the only parameter to produce a significant correlation with the pressure gradients.

Sesamoid offset and tissue depth under MH1 also displayed moderate to strong correlations with the shear strain variables and to a lesser extent the 99th% plantar pressure ($-0.578 < r < -0.758$,

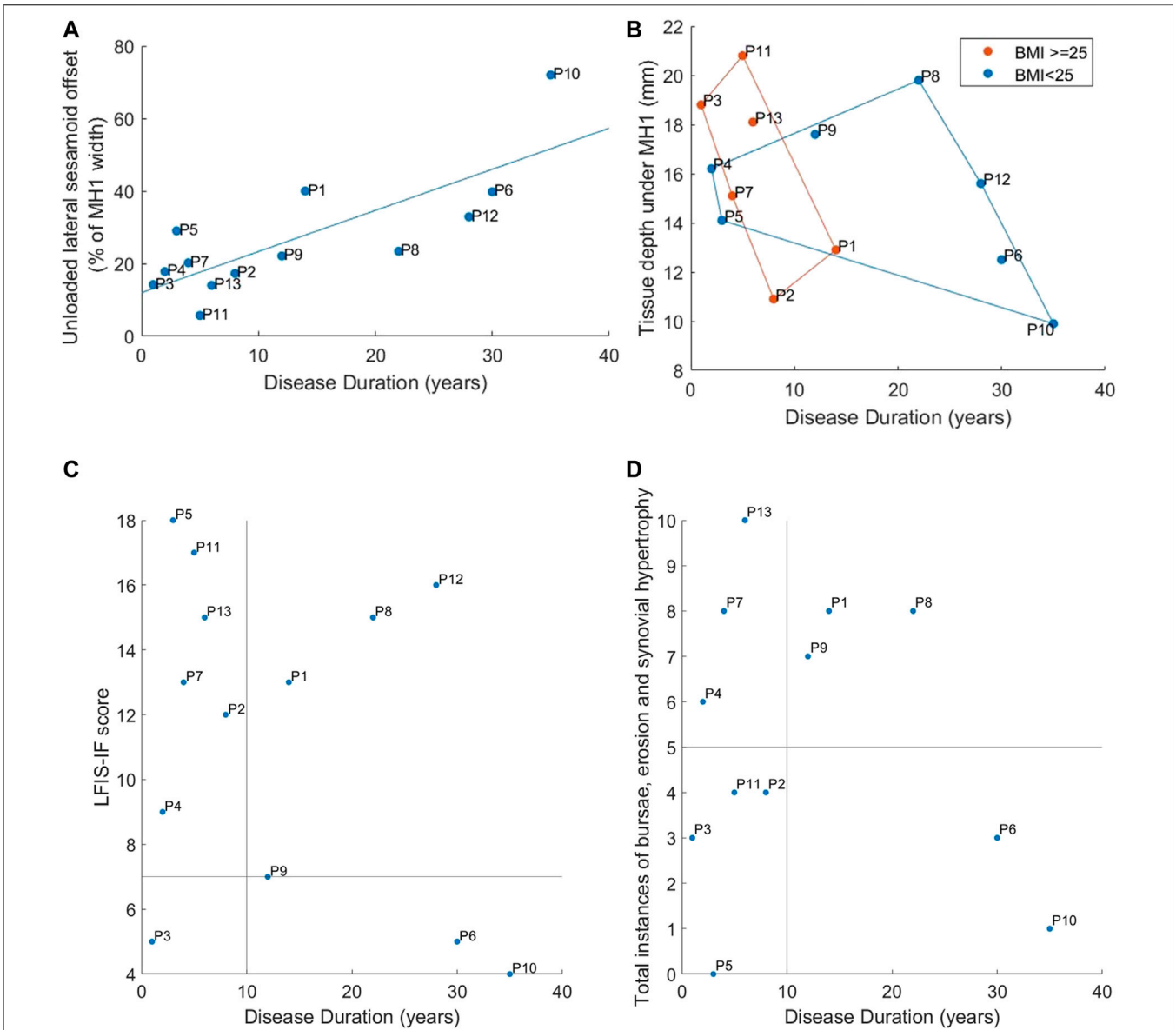

FIGURE 4 | Correspondence of disease duration to: **(A)** Lateral offset of the sesamoid bones **(B)** Tissue depth under MH1 with groupings for normal vs high BMI using marker colors and convex hull boundaries **(C)** LFIS-IF score with quadrants indicating short vs long duration and low vs moderate/high LFIS score **(D)** Instances of bursae, erosion and synovial hypertrophy at the MTP joints, with quadrants showing short vs long duration and low vs high instances. Note: data for P12 was missing for instances of bursae, erosion and hypertrophy and so n = 12.

$p < 0.05$ and $0.464 < r < 0.627$, $0.022 < p < 0.110$ respectively). This would suggest that higher pressure and strain results stemmed from reduced sesamoid offset and higher tissue depths, which would be associated with more normal anatomy. However, it should be noted that the four participants with the lowest sesamoid offsets (P2, P3, P11, P13) all had BMIs in the top five of the group, and those with the highest sesamoid offsets (P1, P6, P10, P12) all had either MH1 curvature or BMI within the lowest four of the group. Similar trends were found with the tissue depth variable.

Neither the LFIS-IF score or instances of bursae, erosion and synovial hypertrophy correlated with model predictions. Where there were potential trends for low or high rankings within the dataset, these could also be attributed to MH1 curvature and BMI. Full results for each participant, indicating the highest and lowest ranked participants for each variable, can be found in the Supplementary Data–Section A.

DISCUSSION

The aim of this study was to determine whether simplified computational forefoot models would produce differing biomechanical predictions depending on condition severity in

TABLE 2 | Median (IQR) results for the clinical data, morphological measurements and model predictions. The healthy participant rank indicates where they fell within the RA dataset, with one being lowest and 14 highest. X = denotes where rankings where tied.

	Measure	RA participants (n = 13)	Healthy participant (n = 1)	
		Median (IQR)	Median (IQR)	Rank (out of 14)
Clinical Data	BMI	24.8 (22.3–28.4)	22.3	4 =
	Disease duration (years)	8 (4–22)	NA	NA
	LFIS-IF (0-21)	13 (7–15)	NA	NA
	Instances of bursae (0-9), erosion (0-5), synovial hypertrophy (0-5)	5 (3–8)	NA	NA
Morphological Measurements	Depth of tissue under MH1 (mm)	15.6 (12.9–18.1)	16.7	9
	Unloaded lateral offset of sesamoid from MH1 edge (% of MH1 width)	22.1 (17.3–32.9)	14.4	2 =
	Average principal curvature of MH1 (mm^{-1})	0.149 (0.128–0.163)	0.079	1
Model Predictions	99th% shear strain in limb (%)	13.7 (12.3–16.7)	12.3	5
	Volume of tissue over 10% shear strain (mm^3)	3,214 (2,359–6,407)	1,418	4
	99th% plantar pressure (kPa)	62.9 (59.3–65.6)	55.6	4
	Maximum plantar pressure gradient (kPa/mm)	3.1 (2.6–3.4)	3.4	10

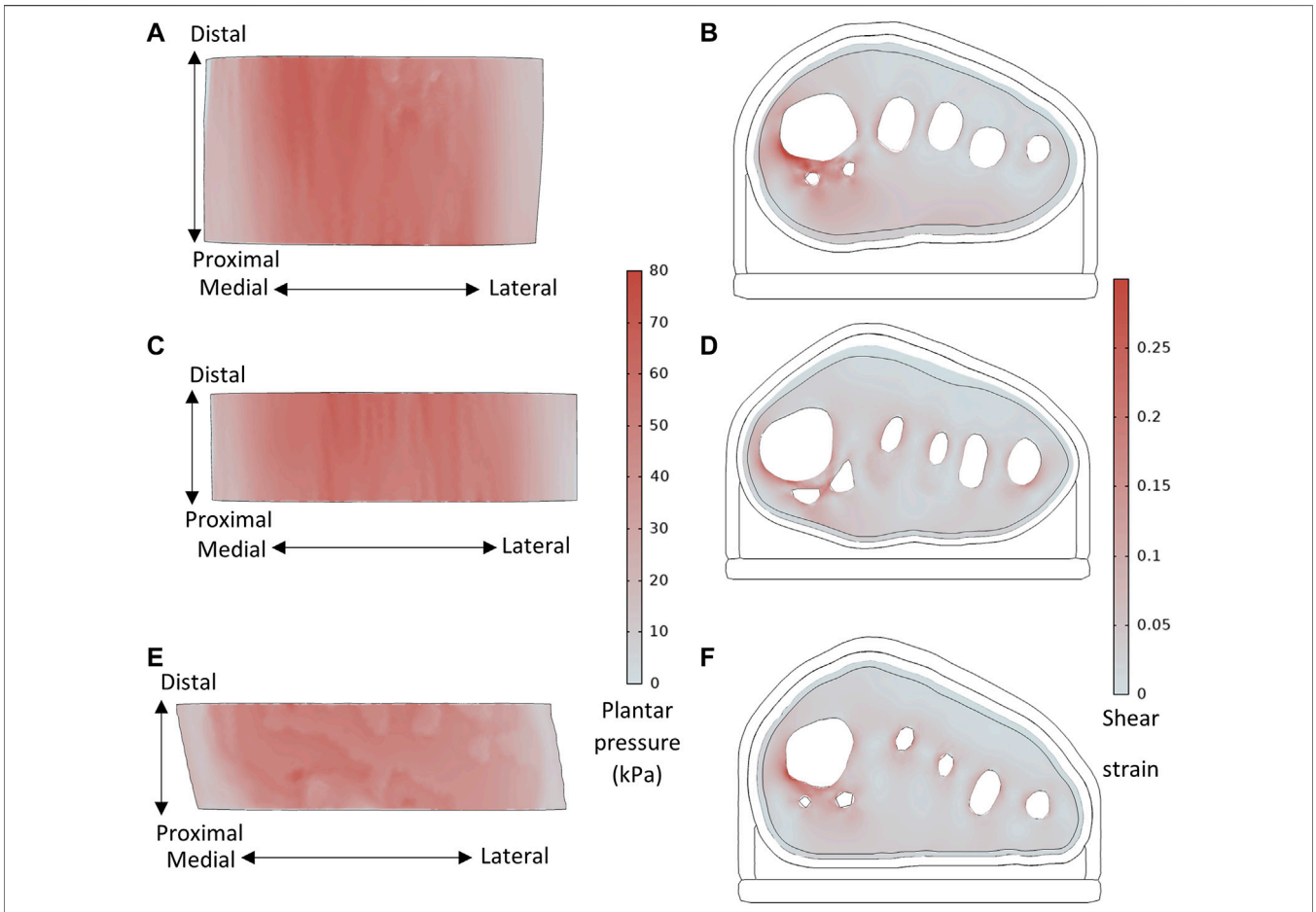

FIGURE 5 | Plantar pressure and shear strain (taken from slice through sesamoid center) distributions, for **(A,B)** P8 with sesamoids in neutral position, BMI = 21.7, MH1 curvature = 0.144 mm^{-1}, and **(C,D)** P1 with displaced sesamoids, BMI = 26.7, MH1 curvature = 0.112 mm^{-1}, and **(E,F)** Healthy participant, BMI = 22.3, MH1 curvature = 0.079mm^{-1}.

people with RA, e.g. LFIS-IF score and morphological measures, or other relevant factors such as BMI. These predictions were also compared to model predictions from a healthy individual to determine any differences. Models capable of producing different predictions between these individuals would allow for personalised FO design to improve treatment. The model predictions differed between the foot MR data for a healthy individual and the data for those with RA, as seen in the

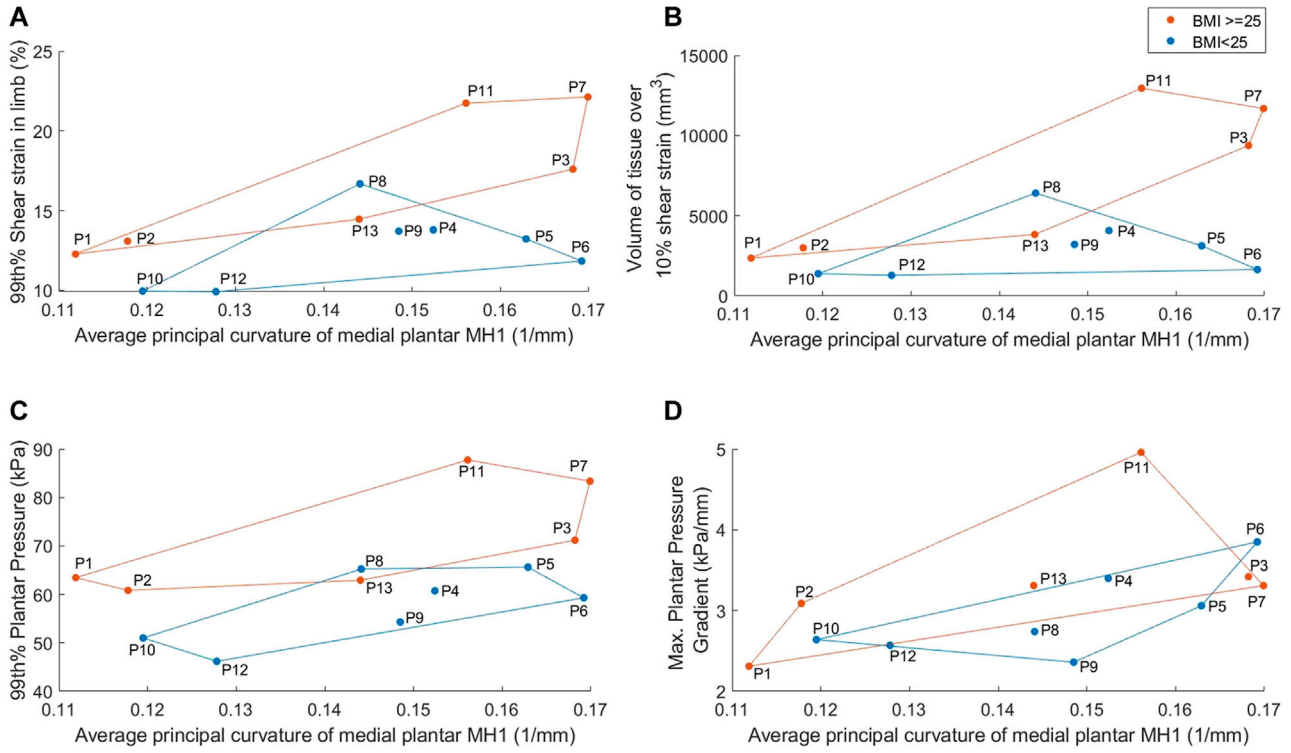

FIGURE 6 | Average medial plantar MH1 curvature results, separated into normal vs high BMI groups, for: **(A)** 99th% shear strain in the limb **(B)** volume of tissue in the limb over 10% shear strain **(C)** 99th% plantar pressure **(D)** maximum plantar pressure gradient. Groups identified by marker color and convex hull boundaries.

pressure and strain results (**Table 2**). Comparing to a single healthy individual does not confirm the models would distinguish between cohorts of healthy vs RA, but the results do provide another point of comparison for condition severity. Within the RA group, higher BMIs corresponded to higher model predictions of soft tissue shear strain and plantar pressure, as did higher medial plantar MH1 curvature (indicating a less rounded, more sharply curved bone contour). The models could not distinguish between LFIS-IF score or instances of bursae, erosion and synovial hypertrophy. RA prevalence is significantly higher in women than men (Symmons et al., 2002), and all participants in this study were female. However, this does mean the findings are only applicable to women with RA and may not apply to men with RA. The predicted pressure and strain varied considerably across the participants, emphasizing the importance of evaluating multiple individuals. Previous studies using single cases or healthy cohorts are unlikely to provide a robust assessment of interventions.

The plantar pressures predicted by the models (median: 63kPa, IQR: 59–66kPa) fell within the expected bounds of forefoot pressures during midstance in the presence of an FO. Experimental testing of in-shoe midstance pressures of five healthy participants recorded median peak forefoot pressures of 131kPa (IQR: 95–151kPa), see Supplementary Data–Section B for details of the testing. Though higher than the pressure results in the present study, the experimental pressures were measured without an FO. FOs have been shown to reduce plantar pressures by 56% during stance (Kato et al., 1996), which would bring the experimental results far more in line with the model predictions. A recent study by Simonsen et al. (Simonsen et al., 2021) measured in-shoe plantar pressures for people with RA wearing orthoses, and found that at 50% of the stance phase, peak pressures ranged from approximately 17–54kPa, with a mean of around 29kPa with a custom FO. Previous studies of healthy individuals have found mean midstance forefoot pressures of approximately 70kPa (Aliberti et al., 2011) and 132kPa (s.d. 65kPa) (Kanatli et al., 2008), though these values were obtained barefoot which causes higher plantar pressures than when shod. Additionally, the shear strains in the present models were concentrated around the bones, with lower tissue strains elsewhere (**Figure 5**). These strain distributions are a well-established occurrence in the foot (Luboz et al., 2014), and correspond to common sites of ulceration due to RA (Firth et al., 2008). The models predicted results within the expected range, and produced trends based on participant clinical and morphological data. This is a promising sign that the models would be suitable for assessing FO and footwear choices across at least a female population, as the group represented in the present study.

One of the clearest trends observed was the effect of BMI on pressure and shear strain predictions, with high BMI (≥25 kg/m^2) posing more risks. The differences in model results between participants were not just due to the applied loading conditions, which were based on participant weight. Three

TABLE 3 | Correlations for model predictions with the clinical data and morphological measurements. Moderate to strong correlations (>0.4) are bolded. *indicates significant ($p < 0.05$) correlation.

Variable 1	Variable 2	Correlation (*p* value)
99th% Shear strain in limb	BMI	**0.600 (0.030)***
	Unloaded lateral offset of sesamoid	**-0.662 (0.014)***
	Tissue Depth under MH1	**0.623 (0.023)***
	LFIS-IF	0.271 (0.370)
	Disease Duration	**-0.601 (0.030)***
	Instances of bursae, erosion, synovial hypertrophy	0.284 (0.372)
	Average principal curvature of MH1	**0.574 (0.040)***
Volume of tissue over 10% shear strain	BMI	**0.652 (0.016)***
	Unloaded lateral offset of sesamoid	**-0.758 (0.003)***
	Tissue Depth under MH1	**0.627 (0.022)***
	LFIS-IF	0.222 (0.467)
	Disease Duration	**-0.709 (0.007)***
	Instances of bursae, erosion, synovial hypertrophy	0.157 (0.627)
	Average principal curvature of MH1	**0.543 (0.055)**
99th% Plantar pressure	BMI	**0.644 (0.018)***
	Unloaded lateral offset of sesamoid	**-0.578 (0.038)***
	Tissue Depth under MH1	**0.464 (0.110)**
	LFIS-IF	0.323 (0.281)
	Disease Duration	**-0.621 (0.023)***
	Instances of bursae, erosion, synovial hypertrophy	0.128 (0.691)
	Average principal curvature of MH1	**0.529 (0.063)**
Max. plantar pressure gradient	BMI	**0.452 (0.121)**
	Unloaded lateral offset of sesamoid	**-0.485 (0.093)**
	Tissue Depth under MH1	0.374 (0.208)
	LFIS-IF	0.126 (0.681)
	Disease Duration	-0.335 (0.264)
	Instances of bursae, erosion, synovial hypertrophy	-0.206 (0.520)
	Average principal curvature of MH1	**0.557 (0.048)***

participants (P1, P3, P7) had identical weights and thus similar applied loads, but their BMIs differed as did the model results. Individuals with both RA and increased BMI experience increased pain, MTP joint swelling, activity limitation, and in-shoe pressures but little change to barefoot pressures (Dahmen et al., 2020). Thus, restricting the foot within a shoe caused more issues for those with higher BMIs, who may already be adversely affected due to higher loads going through the foot (Mickle and Steele, 2015). Additionally, people with high BMI may have different requirements for an FO to provide the necessary shock absorption. The importance of including the shoe in modelling of this nature is clear, and the present approach could be adapted for future FO design research in different groups at high risk of soft tissue injury in the foot, because the models can assess the effects of varying morphology, disease presentation and footwear choice.

The curvature of the medial plantar MH1 was also related to the model predictions. Individuals with a more rounded MH1 tended to produce lower model results and vice versa. The highest shear strains were also observed in the tissue surrounding this region. This was likely due to a combination of the medially skewed loading, and compression of the tissue between the bony prominence and orthosis/shoe. This parameter is not currently considered during FO or footwear assessments, but could provide additional information for such a use, particularly in identifying individuals with higher bone curvatures who may require more protection.

MH1 curvature was the only parameter that significantly correlated with the model pressure gradient predictions. Again, this likely relates to it being a bony prominence, where pressure gradients are higher and indicative of shear strain (Mueller et al., 2005; Lung et al., 2019). The lack of relationship between pressure gradients and other variables is understandable, particularly for BMI, given that the measure is not magnitude-based. Additionally, the FO may have reduced pressure gradients across all participants, including the healthy individual, limiting differences between them.

Increased tissue depth under MH1 and reduced sesamoid offset were also connected to increased pressure and shear strain predictions. However, this may have been an indirect effect due to BMI and MH1 curvatures. The majority of participants with longer disease durations had normal BMIs, while most with shorter durations had high BMIs (**Figure 4B**). Sesamoid offset increased with duration, so trends observed for normally positioned sesamoid bones may have been due to high BMIs instead, through artefacts of the small population. Similar overlaps were found with high sesamoid offset and low MH1 curvature. It should also be noted that the participants with highly displaced sesamoid bones (P1, P6, P10, P12) did not necessarily have worse conditions according to LFIS-IF scores and instances of bursae, erosion and synovial hypertrophy (**Figure 4C, D**).

The strength of this study was the consideration of these inhomogeneities and variations within the study population,

however a few limitations should be acknowledged, which arise because the images used to develop the models were not originally collected for the purposes of simulation. First, the MR data used for the RA models had been collected in unloaded positions. Thus, the shape of the plantar foot varied considerably between participants, affecting the thickness of orthotic present in different forefoot regions, including where reduced tissue depth may have resulted in increased FO thickness (**Figure 3**). Given that FO thickness may influence pressure and strain (Goske et al., 2006; Chen et al., 2015), inter-participant comparisons may have been affected by differing FO thicknesses due to the varying plantar profiles. These limitations in the dataset make it difficult to draw conclusions on the effect of sesamoid offset and tissue depth under MH1 in these models. Further work with imaging collected in stance position but low, nominal loading, or a larger sample size, would be required to ascertain if these two RA-related variables were truly identifiable in participants' model results. The small sample size in the present study may also have affected the other correlations, and so assessment of a larger cohort would confirm those results.

The models were not capable of distinguishing between participant's LFIS-IF scores or instances of bursae, erosion or synovial hypertrophy, though there are possible explanations. First, the LFIS-IF score is a subjective measure, based on each individual's perception of their experience and pain threshold. A clear example of this was P5, who's LFIS-IF score was highest at 18 despite having no instances of bursae, erosion or synovial hypertrophy visible on ultrasound (**Figure 4**). Second, simplifications in the model geometries may not have allowed for distinguishing these parameters. Any bursae present were not included in the models, nor was detailed anatomy of the MTP joints. More complex models including these features may show relationships between the model results and the above parameters. The model simplifications, such as use of a bulk soft tissue group and fused MTP joints, were thought suitable for the purpose of this study and future purpose of the models which centers on comparisons between FO design, for which the absolute values of pressure and strain are not necessary. However, the simplifications may have limited the differences in predictions between the models.

Other model limitations stemmed from the loading conditions, such as the ground reaction forces that were applied to the models. As previously mentioned, a key improvement would be the use of forefoot MR data with the soft tissues and bones in a loaded position, as well as collecting kinetic data for the participants being modelled. In the present study, the GRFs applied to the models were based on a set load distribution across the forefoot, albeit scaled to the participant's weight and relative locations of the metatarsal heads. Thus, the pressure and strain predictions may be inaccurate, particularly given that some individuals with RA adapt their gait to off-load painful or affected forefoot regions (Bowen et al., 2011; Carroll et al., 2015). To use these models to assess FO design on a personalised level, load distributions based on the individual's gait pattern would be beneficial.

Additionally, using static midstance loads does not encompass the peak pressures experienced by the forefoot during toe-off, or the full sesamoid bone movement as would occur during dynamic gait influencing pressure and strain distributions. However, as conditions were consistent across participants, comparisons were still valid. Another drawback of using static models was that PTI differences between participants could not be examined. Given the importance of sustained loading and how it can relate to pain experienced by those with RA (van der Leeden et al., 2006), and risk of tissue damage (Gefen, 2009; Lung et al., 2016), dynamic modelling should also be explored.

CONCLUSION

The model predictions for those with RA were highly influenced by the participant's BMI and the medial plantar MH1 curvature. Due to limitations of the dataset, it was unclear whether the tissue depth under MH1 and the unloaded lateral offset of the sesamoids bone directly impacted model results. No relation was found between the model's pressure or strain predictions and LFIS-IF score or instances of bursae, erosion and synovial hypertrophy. The wide ranges observed in the model predictions emphasizes the importance of modelling interventions across multiple pathological individuals rather than a single healthy case.

The simplified forefoot models produced differing biomechanical predictions between people with RA, with the variation relating to some condition-related factors but not to others. The models also produced differing results for a healthy individual and people with RA. Thus, with the limitations from the present study addressed, the models could provide a suitable basis for comparing FO designs based on individual requirements, particularly as they relate to BMI and alleviating internal tissue strains around bony prominences.

DATA AVAILABILITY STATEMENT

The datasets presented in this study can be found in the University of Southampton repository: https://doi.org/10.5258/SOTON/D2061.

ETHICS STATEMENT

The studies involving human participants were reviewed and approved by Southampton and South West Hampshire Local Research Ethics Committee (NIHR ref. 24,427), Cardiff University School of Psychology Ethics Committee (EC.18.03.13.5264), and University of Southampton (ERGO ID: 48,707 and 48,710), United Kingdom. The patients/participants provided their written informed consent to participate in this study.

AUTHOR CONTRIBUTIONS

EK, PW, CB, AD were involved in conception of the study, data analysis and interpretation. CB, CE, LC, LK, BK, NO were involved in data collection and preparation of the original datasets. EK collected further data and drafted the manuscript. All authors reviewed and approved the manuscript.

FUNDING

The authors would like to thank the following for their financial support:

- ESK: the University of Southampton's EPSRC Doctoral Training Program (ref EP/R513325/1)
- PRW: the EPSRC-NIHR "Medical Device and Vulnerable Skin Network" (ref EP/N02723X/1)
- CB, CE, LC, LK: Pfizer Inc., "The epidemiology of MRI-detected rheumatoid arthritis disease activity within the forefoot"
- ASD: the Royal Academy of Engineering, United Kingdom, (ref RF/130).

The FeeTURA study received funding from Pfizer Inc. The funder was not involved in the present study design, collection, analysis, interpretation of data, the writing of this article or the decision to submit it for publication.

ACKNOWLEDGMENTS

We would like to thank all of the individuals who participated in this study and CUBRIC who facilitated the MR data collection for the healthy volunteer at Cardiff University.

SUPPLEMENTARY MATERIAL

The Supplementary Material for this article can be found online at: https://www.frontiersin.org/articles/10.3389/fbioe.2021.803725/full#supplementary-material

REFERENCES

Ahanchian, N., Nester, C. J., Howard, D., Ren, L., and Parker, D. (2017). Estimating the Material Properties of Heel Pad Sub-layers Using Inverse Finite Element Analysis. *Med. Eng. Phys.* 40, 11–19. doi:10.1016/j.medengphy.2016.11.003

Aliberti, S., Costa, M. D. S. X., Passaro, A. D. C., Arnone, A. C., Hirata, R., and Sacco, I. C. N. (2011). Influence of Patellofemoral Pain Syndrome on Plantar Pressure in the Foot Rollover Process during Gait. *Clinics* 66 (3), 367–372. doi:10.1590/s1807-59322011000300001

Bader, D. L., and Worsley, P. R. (2018). Technologies to Monitor the Health of Loaded Skin Tissues. *Biomed. Eng. Online* 17 (1), 40. doi:10.1186/s12938-018-0470-z

Ben Shabat, Y., and Fischer, A. (2015). Design of Porous Micro-structures Using Curvature Analysis for Additive-Manufacturing. *Proced. CIRP* 36, 279–284. doi:10.1016/j.procir.2015.01.057

Bowen, C. J., Culliford, D., Allen, R., Beacroft, J., Gay, A., Hooper, L., et al. (2011). Forefoot Pathology in Rheumatoid Arthritis Identified with Ultrasound May Not Localise to Areas of Highest Pressure: Cohort Observations at Baseline and Twelve Months. *J. Foot Ankle Res.* 4, 25. doi:10.1186/1757-1146-4-25

Bowen, C. J., Hooper, L., Culliford, D., Dewbury, K., Sampson, M., Burridge, J., et al. (2010). Assessment of the Natural History of Forefoot Bursae Using Ultrasonography in Patients with Rheumatoid Arthritis: a Twelve-Month Investigation. *Arthritis Care Res.* 62 (12), 1756–1762. doi:10.1002/acr.20326

Carlson, J. M. (2006). Functional Limitations from Pain Caused by Repetitive Loading on the Skin: A Review and Discussion for Practitioners, with New Data for Limiting Friction Loads. *JPO J. Prosthetics Orthotics* 18 (4), 93–103. doi:10.1097/00008526-200610000-00002

Carroll, M., Parmar, P., Dalbeth, N., Boocock, M., and Rome, K. (2015). Gait Characteristics Associated with the Foot and Ankle in Inflammatory Arthritis: a Systematic Review and Meta-Analysis. *BMC Musculoskelet. Disord.* 16 (1), 134. doi:10.1186/s12891-015-0596-0

Chen, W. M., Lee, S.-J., and Lee, P. V. S. (2015). Plantar Pressure Relief under the Metatarsal Heads - Therapeutic Insole Design Using Three-Dimensional Finite Element Model of the Foot. *J. Biomech.* 48 (4), 659–665. doi:10.1016/j.jbiomech.2014.12.043

Chen, W. P., Ju, C. W., and Tang, F.-T. (2003). Effects of Total Contact Insoles on the Plantar Stress Redistribution: a Finite Element Analysis. *Clin. Biomech.* 18 (6), S17–S24. doi:10.1016/S0268-0033(03)00080-9

Cherry, L., King, L., Thomas, M., Roemer, F., Culliford, D., Bowen, C. J., et al. (2014). The Reliability of a Novel Magnetic Resonance Imaging-Based Tool for the Evaluation of Forefoot Bursae in Patients with Rheumatoid Arthritis: the FFB Score. *Rheumatology (Oxford)* 53 (11), 2014–2017. doi:10.1093/rheumatology/keu232

Cheung, J. T.-M., and Zhang, M. (2005). A 3-dimensional Finite Element Model of the Human Foot and Ankle for Insole Design. *Arch. Phys. Med. Rehabil.* 86 (2), 353–358. doi:10.1016/j.apmr.2004.03.031

Cheung, J. T. M., Yu, J., Wong, D. W. C., and Zhang, M. (2009). Current Methods in Computer-Aided Engineering for Footwear Design. *Footwear Sci.* 1 (1), 31–46. doi:10.1080/19424280903002323

Dahmen, R., Konings-Pijnappels, A., Kerkhof, S., Verberne, S., Boers, M., Roorda, L., et al. (2020). Higher Body Mass index Is Associated with Lower Foot Health in Patients with Rheumatoid Arthritis: Baseline Results of the Amsterdam-Foot Cohort. *Scand. J. Rheumatol.* 49 (3), 186–194. doi:10.1080/03009742.2019.1663920

Firth, J., Hale, C., Helliwell, P., Hill, J., and Nelson, E. A. (2008). The Prevalence of Foot Ulceration in Patients with Rheumatoid Arthritis. *Arthritis Rheum.* 59 (2), 200–205. doi:10.1002/art.23335

Gefen, A. (2009). Reswick and Rogers Pressure-Time Curve for Pressure Ulcer Risk. Part 1. *Nurs. Stand.* 23 (45), 64–74. doi:10.7748/ns2009.07.23.45.64.c7115

Goske, S., Erdemir, A., Petre, M., Budhabhatti, S., and Cavanagh, P. R. (2006). Reduction of Plantar Heel Pressures: Insole Design Using Finite Element Analysis. *J. Biomech.* 39 (13), 2363–2370. doi:10.1016/j.jbiomech.2005.08.006

Helliwell, P., Reay, N., Gilworth, G., Redmond, A., Slade, A., Tennant, A., et al. (2005). Development of a Foot Impact Scale for Rheumatoid Arthritis. *Arthritis Rheum.* 53 (3), 418–422. doi:10.1002/art.21176

Hennessy, K., Burns, J., and Penkala, S. (2007). Reducing Plantar Pressure in Rheumatoid Arthritis: A Comparison of Running versus Off-The-Shelf Orthopaedic Footwear. *Clin. Biomech.* 22 (8), 917–923. doi:10.1016/j.clinbiomech.2007.04.011

Hennessy, K., Woodburn, J., and Steultjens, M. P. M. (2012). Custom Foot Orthoses for Rheumatoid Arthritis: A Systematic Review. *Arthritis Care Res.* 64 (3), 311–320. doi:10.1002/acr.21559

Hooper, L., Bowen, C. J., Gates, L., Culliford, D. J., Ball, C., Edwards, C. J., et al. (2012). Prognostic Indicators of Foot Related Disability in Patients with RA: Results of a Prospective Three-Year Study. *Arthritis Care Res.* 64 (8), 1116–1124. doi:10.1002/acr.21672

Jaakkola, J. I., and Mann, R. A. (2004). A Review of Rheumatoid Arthritis Affecting the Foot and Ankle. *Foot Ankle Int.* 25 (12), 866–874. doi:10.1177/107110070402501205

Jung, Y., Jung, M., Ryu, J., Yoon, S., Park, S.-K., and Koo, S. (2016). Dynamically Adjustable Foot-Ground Contact Model to Estimate Ground Reaction Force

during Walking and Running. *Gait & Posture* 45, 62–68. doi:10.1016/j.gaitpost.2016.01.005

Kanatli, U., Yetkin, H., Simşek, A., Oztürk, A. M., Esen, E., and Beşli, K. (2008). Pressure Distribution Patterns under the Metatarsal Heads in Healthy Individuals. *Acta Orthop. Traumatol. Turc* 42 (1), 26–30. doi:10.3944/aott.2008.026

Kato, H., Takada, T., Kawamura, T., Hotta, N., and Torii, S. (1996). The Reduction and Redistribution of Plantar Pressures Using Foot Orthoses in Diabetic Patients. *Diabetes Res. Clin. Pract.* 31 (1), 115–118. doi:10.1016/0168-8227(96)01214-4

Konings-Pijnappels, A. P. M., Tenten-Diepenmaat, M., Dahmen, R., Verberne, S. K., Dekker, J., Twisk, J. W. R., et al. (2019). Forefoot Pathology in Relation to Plantar Pressure Distribution in Patients with Rheumatoid Arthritis: A Cross-Sectional Study in the Amsterdam Foot Cohort. *Gait & Posture* 68, 317–322. doi:10.1016/j.gaitpost.2018.12.015

Linder-Ganz, E., Shabshin, N., Itzchak, Y., and Gefen, A. (2007). Assessment of Mechanical Conditions in Sub-dermal Tissues during Sitting: A Combined Experimental-MRI and Finite Element Approach. *J. Biomech.* 40 (7), 1443–1454. doi:10.1016/j.jbiomech.2006.06.020

Luboz, V., Perrier, A., Stavness, I., Lloyd, J. E., Bucki, M., Cannard, F., et al. (2014). Foot Ulcer Prevention Using Biomechanical Modelling. *Computer Methods Biomech. Biomed. Eng. Imaging Visualization* 2 (4), 189–196. doi:10.1080/21681163.2013.837410

Lung, C.-W., Yang, T. D., Liau, B.-Y., Cheung, W. C., Jain, S., and Jan, Y. K. (2019). Dynamic Changes in Seating Pressure Gradient in Wheelchair Users with Spinal Cord Injury. *Assistive Tech.* 32 (5), 277–286. doi:10.1080/10400435.2018.1546781

Lung, C. W., Hsiao-Wecksler, E. T., Burns, S., Lin, F., and Jan, Y. K. (2016). Quantifying Dynamic Changes in Plantar Pressure Gradient in Diabetics with Peripheral Neuropathy. *Front. Bioeng. Biotechnol.* 4, 54. doi:10.3389/fbioe.2016.00054

Mickle, K. J., and Steele, J. R. (2015). Obese Older Adults Suffer Foot Pain and Foot-Related Functional Limitation. *Gait & Posture* 42 (4), 442–447. doi:10.1016/j.gaitpost.2015.07.013

Mueller, M. J., Zou, D., and Lott, D. J. (2005). Pressure Gradient" as an Indicator of Plantar Skin Injury. *Diabetes Care* 28 (12), 2908–2912. doi:10.2337/diacare.28.12.2908

Nix, S. E., Vicenzino, B. T., Collins, N. J., and Smith, M. D. (2012). Characteristics of Foot Structure and Footwear Associated with Hallux Valgus: a Systematic Review. *Osteoarthritis and Cartilage* 20 (10), 1059–1074. doi:10.1016/j.joca.2012.06.007

Oomens, C. W. J., Zenhorst, W., Broek, M., Hemmes, B., Poeze, M., Brink, P. R. G., et al. (2013). A Numerical Study to Analyse the Risk for Pressure Ulcer Development on a Spine Board. *Clin. Biomech.* 28 (7), 736–742. doi:10.1016/j.clinbiomech.2013.07.005

Petre, M. T., Erdemir, A., and Cavanagh, P. R. (2006). Determination of Elastomeric Foam Parameters for Simulations of Complex Loading. *Comput. Methods Biomech. Biomed. Eng.* 9 (4), 231–242. doi:10.1080/10255840600747620

Rosenbaum, D., Schmiegel, A., Meermeier, M., and Gaubitz, M. (2006). Plantar Sensitivity, Foot Loading and Walking Pain in Rheumatoid Arthritis. *Rheumatology (Oxford)* 45 (2), 212–214. doi:10.1093/rheumatology/kei137

Rusinkiewicz, S. (2004). "Estimating Curvatures and Their Derivatives on triangle Meshes," in Proceedings. 2nd International Symposium on 3D Data Processing, Visualization and Transmission, 2004. 3DPVT 2004, Thessaloniki, Greece, 9-9 Sept. 2004. IEEE, 486–493.

Simonsen, M. B., Pessoto Hirata, R., Næsborg-Andersen, K., Derek Christian Leutscher, P., Hørslev-Petersen, K., Woodburn, J., et al. (2021). Different Types of Foot Orthoses Effect on Gait Mechanics in Patients with Rheumatoid Arthritis. *J. Biomech.*, 110496. , In Press. doi:10.1016/j.jbiomech.2021.110496

Spirka, T. A., Erdemir, A., Ewers Spaulding, S., Yamane, A., Telfer, S., and Cavanagh, P. R. (2014). Simple Finite Element Models for Use in the Design of Therapeutic Footwear. *J. Biomech.* 47 (12), 2948–2955. doi:10.1016/j.jbiomech.2014.07.020

Steer, J. W., Worsley, P. R., Browne, M., and Dickinson, A. (2021). Key Considerations for Finite Element Modelling of the Residuum-Prosthetic Socket Interface. *Prosthetics Orthotics Int.* 45 (2), 138–146. doi:10.1177/0309364620967781

Symmons, D., Turner, G., Webb, R., Asten, P., Barrett, E., Lunt, M., et al. (2002). The Prevalence of Rheumatoid Arthritis in the United Kingdom: New Estimates for a new century. *Rheumatology* 41 (7), 793–800. doi:10.1093/rheumatology/41.7.793

Takahashi, M. B. J., Dealey, C., and Gefen, A. (2010). "Pressure in Context," in *International Review: Pressure Ulcer Prevention: Pressure, Shear, Friction and Microclimate in Context. A Consensus Document*. (London: Wounds International), 2–10.

Telfer, S., Woodburn, J., Collier, A., and Cavanagh, P. R. (2017). Virtually Optimized Insoles for Offloading the Diabetic Foot: A Randomized Crossover Study. *J. Biomech.* 60, 157–161. doi:10.1016/j.jbiomech.2017.06.028

Tenten-Diepenmaat, M., Dekker, J., Heymans, M. W., Roorda, L. D., Vliet Vlieland, T. P. M., and van der Leeden, M. (2019). Systematic Review on the Comparative Effectiveness of Foot Orthoses in Patients with Rheumatoid Arthritis. *J. Foot Ankle Res.* 12, 32. doi:10.1186/s13047-019-0338-x

Tenten-Diepenmaat, M., Dekker, J., Twisk, J. W. R., Huijbrechts, E., Roorda, L. D., and van der Leeden, M. (2020). Outcomes and Potential Mechanism of a Protocol to Optimize Foot Orthoses in Patients with Rheumatoid Arthritis. *BMC Musculoskelet. Disord.* 21 (1), 348. doi:10.1186/s12891-020-03364-5

Tian, H., Jiang, Y., Qi, Y., Xiang, H., and Yan, J. (2019). Study of Knitted Fabrics with Ultra-low Modulus Based on Geometrical Deformation Mechanism. *Textile Res. J.* 89 (5), 891–899. doi:10.1177/0040517518758004

Tuna, H., Birtane, M., Taştekin, N., and Kokino, S. (2005). Pedobarography and its Relation to Radiologic Erosion Scores in Rheumatoid Arthritis. *Rheumatol. Int.* 26 (1), 42–47. doi:10.1007/s00296-004-0504-7

Turner, D. E., Helliwell, P. S., Emery, P., and Woodburn, J. (2006). The Impact of Rheumatoid Arthritis on Foot Function in the Early Stages of Disease: a Clinical Case Series. *BMC Musculoskelet. Disord.* 7, 102. doi:10.1186/1471-2474-7-102

van der Leeden, M., Steultjens, M., Dekker, J. H. M., Prins, A. P. A., and Dekker, J. (2006). Forefoot Joint Damage, Pain and Disability in Rheumatoid Arthritis Patients with Foot Complaints: the Role of Plantar Pressure and Gait Characteristics. *Rheumatology (Oxford)* 45 (4), 465–469. doi:10.1093/rheumatology/kei186

Van Hul, E., Vanhoenacker, F., Van Dyck, P., De Schepper, A., and Parizel, P. M. (2011). Pseudotumoural Soft Tissue Lesions of the Foot and Ankle: a Pictorial Review. *Insights Imaging* 2 (4), 439–452. doi:10.1007/s13244-011-0087-2

Woodburn, J., and Helliwell, P. S. (1996). Relation between Heel Position and the Distribution of Forefoot Plantar Pressures and Skin Callosities in Rheumatoid Arthritis. *Ann. Rheum. Dis.* 55 (11), 806–810. doi:10.1136/ard.55.11.806

Zhang, H. W., Miko, L., Yang, J. Y., Niu, W. X., James, C. W. C., Sun, W. J., et al. (2020). Computational Modelling of Foot Orthosis for Midfoot Arthritis: a Taguchi Approach for Design Optimization. *Acta Bioeng. Biomech.* 22 (4), 75–83. doi:10.37190/Abb-01694-2020-03

Zhou, J. Y., Li, Y., Lam, J., and Cao, X. Y. (2010). The Poisson Ratio and Modulus of Elastic Knitted Fabrics. *Textile Res. J.* 80 (18), 1965–1969. doi:10.1177/0040517510371864

Conflict of Interest: The authors declare that the research was conducted in the absence of any commercial or financial relationships that could be construed as a potential conflict of interest.

Publisher's Note: All claims expressed in this article are solely those of the authors and do not necessarily represent those of their affiliated organizations, or those of the publisher, the editors and the reviewers. Any product that may be evaluated in this article, or claim that may be made by its manufacturer, is not guaranteed or endorsed by the publisher.

APPENDIX 1: COMSOL INPUT PARAMETERS USED FOR MESHING THE FOREFOOT MODELS

This appendix details the mesh input parameters that were used to develop the FE models in the study (**Table A1**).

APPENDIX 2: SENSITIVITY ANALYSIS

A sensitivity analysis was performed to ensure that the proximity of the forefoot section's cut edges to the region of interest would not affect the model results. Example models were run, removing a coronal MR slice at a time from both edges of the data. It was determined that as long as there was a slice between the region of interest (e.g., the sesamoid bones) and the section edge, the results were unaffected by the edge proximity (<0.5% difference in percentile strain and pressure, **Table A2**).

TABLE A1 | Mesh input parameters.

Mesh input parameter	Region 1: Sock, skin	Region 2: Soft tissue and bone	Region 3: Orthosis upper boundary	Region 4: Orthosis and shoe sides	Region 5: Shoe sole
Maximum element size (mm)	1.68	4	1	5	5.5
Smallest element size allowed (mm)	1.68–1.68/3	4–4/3	1–1/3	5–5/3	5.5–5.5/3
Maximum element growth rate	1.3	1.3	1.3	1.3	1.3
Curvature factor	0.3	0.3	0.3	0.3	0.9
Resolution of narrow regions	1.2	1.2	1.2	1.2	0.4

TABLE A2 | Results from the sensitivity analysis of removing coronal MR slices from the forefoot section model.

Model prediction parameter	Original model	Model with 1 slice removed from edges	Model with 2 slices removed from edges
99th% shear strain in limb (%)	12.28	12.33	11.88
Volume of limb over 10% shear strain (mm^3)	2,359	2,392	1,406
99th% plantar pressure (kPa)	63.47	63.63	62.65

frontiers in Bioengineering and Biotechnology

ORIGINAL RESEARCH
published: 28 January 2022
doi: 10.3389/fbioe.2021.786615

Thermal Analysis of Blood Flow Alterations in Human Hand and Foot Based on Vascular-Porous Media Model

Yue-Ping Wang, Rui-Hao Cheng, Ying He and Li-Zhong Mu*

School of Energy and Power Engineering, Dalian University of Technology, Dalian, China

Microvascular and Macrovascular diseases are serious complications of diabetic mellitus, which significantly affect the life quality of diabetic patients. Quantitative description of the relationship between temperature and blood flow is considerably important for non-invasive detection of blood vessel structural and functional lesions. In this study, thermal analysis has been employed to predict blood flow alterations in a foot and a cubic skin model successively by using a discrete vessel-porous media model and further compared the blood flows in 31 diabetic patients. The tissue is regarded as porous media whose liquid phase represents the blood flow in capillaries and solid phase refers to the tissue part. Discrete vascular segments composed of arteries, arterioles, veins, and venules were embedded in the foot model. In the foot thermal analysis, the temperature distributions with different inlet vascular stenosis were simulated. The local temperature area sensitive to the reduction of perfusion was obtained under different inlet blood flow conditions. The discrete vascular-porous media model was further applied in the assessment of the skin blood flow by coupling the measured skin temperatures of diabetic patients and an inverse method. In comparison with the estimated blood flows among the diabetic patients, delayed blood flow regulation was found in some of diabetic patients, implying that there may be some vascular disorders in these patients. The conclusion confirms the one in our previous experiment on diabetic rats. Most of the patients predicted to be with vascular disorders were diagnosed as vascular complication in clinical settings as well, suggesting the potential applications of the vascular-porous media model in health management of diabetic patients.

Keywords: thermal analysis, vascular disorder, blood flow estimation, diabetic foot, porous media model

OPEN ACCESS

Edited by:
Fang Pu,
Beihang University, China

Reviewed by:
Natalya Kizilova,
Warsaw University of Technology, Poland
Corina Stefania Drapaca,
The Pennsylvania State University (PSU), United States

****Correspondence:***
Ying He
heying@dlut.edu.cn

Specialty section:
This article was submitted to Biomechanics, a section of the journal Frontiers in Bioengineering and Biotechnology

Received: *30 September 2021*
Accepted: *20 December 2021*
Published: *28 January 2022*

Citation:
Wang Y-P, Cheng R-H, He Y and Mu L-Z (2022) Thermal Analysis of Blood Flow Alterations in Human Hand and Foot Based on Vascular-Porous Media Model. Front. Bioeng. Biotechnol. 9:786615. doi: 10.3389/fbioe.2021.786615

INTRODUCTION

Due to lifestyle changes, reduced physical activity, and increased obesity, the prevalence of diabetes has increased from 4.7% in 1980 to 8.5% in 2014. It is estimated that there will be more than 629 million adult diabetic patients in 2045 (Glovaci et al., 2019). Diabetic foot is one of the common and dangerous complications of diabetes mellitus, with an incidence rate of 6.3% worldwide (Zhang et al., 2017). All layers of tissues from the skin to bones will be affected by ulcers. In severe cases, amputations are required and even contralateral foot wound or repeated amputations may be induced, which not only reduces the life qualities of patients but also causes huge medical pressure

and economic losses. Therefore, early detection of diabetic foot is of vital importance. Diabetic complications are always accompanied with structural and functional disorders of the peripheral vascular system. Orchard and Strandness, (1993) found that calcification occurs in the posterior tibial artery, anterior tibial artery, and the arteries at the plantar level among diabetic patients through X-ray. The atherosclerotic plaque leads to occlusion of blood vessels. The vascular occlusion may reduce blood flow and further obstruct the transport of active substances which induce the onset of foot ulceration. Additionally, abnormal hemodynamic and metabolic dysfunctions contribute to the autoregulation of vasomotion disorders and eventually result in ischemia which would intensify ulceration. Therefore, the key factor of early diagnosis of diabetic foot is to detect the dysfunctions of macro/microvasculature as early as possible.

The methods for clinical evaluation of the lower extremity arterial disease include intermittent claudication observation, foot arterial pulsation measurement, ankle-brachial blood pressure index measurement, and so on. Among them, the ankle-brachial index (ankle-brachial index, ABI) is a proven reproducible inspection method. A hand-held Doppler probe can be used to measure the systolic blood pressure of the ankle and arms, and then calculate the ratio of the two. This operation is simple and non-invasive, and the results have been verified in the lesions confirmed by angiography. However, in some elderly patients, calcium deposition in the middle arteries and poor vascular compressibility may occur, resulting in an increase in the ABI, leading to false normals. The mainstream non-invasive methods for detecting the microcirculation blood perfusion rate include the Doppler effect–based laser Doppler flowmetry (laser Doppler flowmetry, LDF) direct detection and the transcutaneous oxygen content that indirectly reflects the perfusion rate through the partial pressure of oxygen. The high price of the abovementioned instruments and poor portability limit their wide application. On the other hand, plethysmograph (Schürmann et al., 2001), laser speckle imager (Briers, 1996), and other blood perfusion rate detection methods based on mechanical and ultrasound technology are still immature. Therefore, effective methods for non-invasive detection of vascular disease in diabetic patients still need further study.

Skin temperature variation is closely associated with the blood perfusion rate, suggesting that monitoring temperature alterations may be employed to study vascular reactivity. Through wavelet cross-correlation analysis of laser Doppler flowmetry (LDF) and skin temperature signal in healthy subjects, Frick et al. pointed out skin temperature monitoring can be used as a tracer of microvessel tone (Frick et al., 2015). The response to the cold pressor test in patients with type 2 diabetes differs essentially from that of healthy subjects in the endothelial frequency range (Smirnova et al., 2013). Podtaev et al. analyzed the correlation degree and phase shift between skin temperature fluctuations and periodic changes of the blood flow caused by oscillations in vasomotor smooth muscle tone (Podtaev et al., 2008). Thermography can be conveniently transformed into skin blood flow through a new developed spectral filter approach (Sagaidachnyi et al., 2017). Nieuwenhoff et al. (2016) also found the time constant expressing skin temperature variation rate can reflect the blood flow of the skin through the skin temperature heating test and heat transfer modeling. Reproducibility was confirmed in the assessment of axon reflex-related vasodilation. Coupling with thermography of tongue and bioheat transfer analysis, the state of the lingual circulation system can be assessed, which provides evidence for the traditional diagnosis method *via* observing the tongue surface state in Chinese medicine (Zhang and Zhu, 2010).

In the past 2 decades, various medical instruments for detecting pathological conditions in the circulatory system have been developed based on the correlation between temperature and blood flow, some of which are listed in **Table 1** showing the devices, experimental thermal environment, experimental subjects, and analytical models. Haga et al. (2012) developed an instrument and algorithm for estimation of blood perfusion from the measured skin temperature. A similar fingertip temperature measurement instrument has been also designed, which can record the temperature change within 75 s after the fingertip touches the sensor (Nagata et al., 2009). The developed heat transfer model was in analogy with the circuit where the thermal conductivity corresponds to the electrical resistance. As blood flow of capillaries affect the effective thermal conductivity of the skin, blood perfusion could be further inferred from the resistance value in the circuit model. In Wang et al.'s heating experiments on diabetic rats implemented by a microtest device, the blood perfusion before and after heating was evaluated by coupling a 1D bioheat transfer model and genetic algorithm (Wang et al., 2020). Apart from the conventional genetic algorithm, the Box–Kanemasu method (Ricketts et al., 2008) was also employed for prediction of blood perfusion from measured temperatures in Rickettes et al.'s study. It is seen a common feature from the abovementioned studies that various optimization algorithms have been used to estimate the blood perfusion rate or thermophysical parameters based on the surface temperature. This approach can be categorized as inverse analysis which is distinguished from the forward one to compute the surface and depth temperature distributions by using the given boundary conditions. In order to estimate these parameters, choosing a suitable heat transfer model for matching the added surface heating source is a key factor as well.

With the development of thermal imaging technology, a lot of research practices have been carried out around computer-aid diagnosis of diabetic foot by infrared thermography (Hernandez-Contreras et al., 2016; Muhammad et al., 2017). Comparing with other imaging modalities such as MRI, CT, and ultrasound, infrared thermal imaging is safer and more convenient (Bandalakunta Gururajarao et al., 2019). In the circumstance of critical ischemia, as a non-invasive method, thermal imaging is more effective than the toe brachial pressure index (Kevin et al., 2019). Sivanandam et al. (2012) collected the infrared thermal image of plantar among healthy people and diabetic patients with and without early signs of ulceration. It is found that the foot temperature of a diabetic subject without the complication of ulceration was 2°C lower than that of the healthy subjects. The average foot skin temperature in diabetic patients with early signs

TABLE 1 | Experimental study on the thermal method of vasomotor function.

Experimental device	Thermal environment	Experimental subject	Analytical method	References
Holdable heat-stimulated blood flow test instrument	Temperature measurement with local heating and recovery	Healthy people's hand	2-D cylindrical tissue model in a cylindrical coordinate system	Haga et al. (2012)
Fingertip temperature dual sensor	No external thermal stimulation	Healthy people's finger tip	0-D parametric model analogous to a circuit	Nagata et al. (2009)
Microtest	Temperature measurement with local heating and recovery	Healthy and diabetic SD rats' paw	1-D vascular-porous media bioheat transfer model	Wang et al. (2020)
A laminated flat thermocouple sensor	No external thermal stimulation	Healthy rats' liver tissue	2-D finite difference tissue heat transfer model	Ricketts et al. (2008)
14-node thermal mapping sensors	Temperature measurement with local heating and recovery	Healthy people's arm	2-D finite element bioheat transfer model	Webb et al. (2015)
Coupling of the optical probe with the Peltier element	Temperature measurement with local heating and recovery	Healthy and diabetic people's lower limb	Spectral analysis by using a wavelet transform	Mizeva et al. (2018)
Infrared thermography and photoplethysmography	No external thermal stimulation	Healthy people's fingertip	Morelet wavelet transfrom	Sagaidachnyi et al. (2014)
Temperature sensorHRTS-5760, Honeywell International, Inc., United States	Temperature measurement with local heating and recovery	Healthy and diabetic people's palm	Wavelet analysis of temperature	Podtaev et al. (2014)
Microtest	Temperature measurement with local heating and recovery	Healthy people's/ diabetic patients' finger tip	Wavelet analysis of temperature	Zubareva et al. (2019), Parshakov et al. (2016), Parshakov et al. (2017), Antonova et al. (2016)

of ulceration decreased by 0.5°C when compared with control subjects. The results suggest that diabetic patients with vascular complications and early signs of ulceration present different variation mechanisms in temperature distribution, of which one is mainly due to blood flow rate decreasing, but another may be caused by the occurrence of inflammation. Bagavathiappan et al. (2008) observed temperature gradients in the influenced regions of patients with vascular disorders and ischemic gangrene from thermal imaging. It was also displayed that diabetic subjects with neuropathy had higher mean foot temperature than non-neuropathic subjects (Bagavathiappan et al., 2010). The thermal imaging analyses show that there is usually a rapid rise about 0.7°C in skin temperature when a local wound occurs. If an inflammation occurs, the skin temperature will increase by 2.2°C (Chen et al., 2021). Van Netten et al. (2013) explored the applicability of infrared thermal imaging for detection of signs of diabetic foot by comparing the mean temperature between the lateral and the contralateral foot and found that the mean temperature difference of the feet in diabetic patients with diffusive complications is larger than 3°C.

Astasio et al. obtained thermograms of the sole in 277 diabetics and analyzed the temperature distribution patterns in four areas of the soles (Astasio et al., 2018) Additionally, they found a much lower mean temperature of soles in diabetics by further comparisons of the thermal maps with those of nondiabetics (Astasio-Picado et al., 2020). Using combined discrete wavelet transform and higher order spectra techniques (Muhammad et al., 2018a) or double density-dual tree-complex wavelet transform (Muhammad et al., 2018b), original foot thermal images can be decomposed for providing various valuable information in the diagnosis of the diabetic foot. The application of machine learning into infrared image processing can improve the accuracy and speed for classification of diabetic foot thermograms (He et al., 2021). In the future, a neural network model can be inserted into mobile phones for early detection of diabetic ulcers after training by using numerous foot temperature data for diabetic ulcer patients and healthy subjects (Serlina et al., 2020) (Amith et al., 2021). New techniques continuously appear to help identifying risk zones of diabetic foot, such as using a retrained MASK-R-CNN mode (Maldonado et al., 2020). In choosing the training data, it is pointed out that the temperatures of toes and the upper half of foot are better than those in other regions (Carlos Padierna et al., 2020) Although average skin temperature is a meaningful index for early diagnosis of diabetic foot in diabetic patients, it is rather insufficient to distinguish different stages of early signs. The foot temperature of diabetic patients with only vascular disease is frequently lower than that of healthy people. However, when it further develops into neuropathy, there will be an increase in the local foot temperature, which is associated with early inflammation in some places. Moreover, multiple vascular stenoses will have varying degrees of impact on each local foot temperature. Therefore, spatial variations of skin temperature should be more concerned. It is without doubt to see that the thermography-based diagnosis technique is powerful for detection of early stages of diabetic foot. However, few research studies concern with the underlying mechanisms associated with diabetic foot, such as the coherence between the altered foot vasculatures and tissue wound or the influence of arterial occlusion on blood perfusion in tissues. It has been known that skin temperature variations are closely associated with the variations of blood perfusion. Despite that detailed temperature changes can be detected using current

thermography-based techniques, it is still difficult to define the serious degrees of the diseased vascular system simply based on thermal images.

In this regard, bio-heat transfer modeling is helpful for establishment of a quantitative relationship between blood flow rates and temperature distribution. This kind of work has been extensively explored in numerous available literature reports. Ma et al. (2015) simplified foot tissue as a three-layer structure of skin, fat, and a core zone and gave an analytical mathematical solution for the simplified one-dimensional case. In Copetti et al.'s study (Copetti et al., 2017), thermal analysis on the foot was carried out by using a two-dimensional finite element model. However, dimensionality reduction results in the loss of complete three-dimensional (3D) temperature information. Rafael et al. (2016) presented a 3D-finite element simulation to predict the temperature variations of the foot with 5 ulcers at the depth of 5 mm away from the sole of the foot. Although the remarkably higher temperatures in ulcers have been achieved, the influence of altered blood flow and vasculatures on tissue temperatures has not been taken into account. No matter the above 2D or 3D heat transfer computation, they were all performed by using a one Pennes equation, and the thermal effect of blood phase is reflected in the blood perfusion term (Pennes, 1998). Due to the simplicity of the Pennes equation, it has been widely used in macroscale bio-heat transfer computation such as hand (Shao et al., 2014) and even thermal characteristics of the whole body (Tang et al., 2016) which has clinical significance such as the treatment of breast tumor by using hyperthermia therapy (Barrios et al., 2019). However, determination of the local blood perfusion rate in the tissue is always a challenging work, especially in pathological conditions when the blood perfusion rate becomes non-uniform. Another limitation of the Pennes equation is that the influence of blood flow directions is neglected, resulting in over or under estimations of blood perfusion in some conditions. The discrete vascular bioheat transfer model provides an alternative method to compute the non-uniform local blood perfusion.

The important feature of the discrete vascular bioheat transfer model is to consider the vessels as a separate domain and calculate the heat exchange between the surrounding tissues. Among them, embedded 1D/3D multiscale modeling has been extensively employed to deal with heat transfer between vessels and tissues. By using this kind of model, Tang et al. (2020) computed the distribution of oxygen and temperature distribution in microcirculation. The influence of the red blood cell on oxygen transport can be further addressed in the work of Wang et al. (2021). He and Liu, (2017) proposed a coupled continuum-discrete model (CCD) for thermal analysis. They classified the blood vessels as visible vessels and invisible vessels. The thermal effect of visible vessels includes blood heat transfer and the conduction between the blood vessel and the surrounding tissue. The effect of invisible vessels was converted to the blood perfusion term corresponding to the continuum parts. The CCD model can well capture a richer and complex thermal interaction of the vascular network and solid tissue compared to the conventional bioheat transfer model. Stephen studied the effect of surface cooling on the internal temperature of the brain by inserting a one-dimensional vascular structure into the brain region (Blowers, 2018; Blowers et al., 2018). The 1D vascular model contains the arteries, arterioles, veins, and venules. The capillaries were represented by the liquid phase of porous media whose solid phase corresponds to the white or gray matter of the brain. It is found from their study that due to the inclusion of the directional flow, scalp cooling has a larger impact on cerebral temperatures than the predictions by previous bioheat transfer models. Although the discrete vascular-porous media model is more complex than the Pennes equation, it can describe the biological heat transfer process more realistically, and the inversion of the blood flow is more reliable. Image-based voxel mesh generation provides an easy-implemented way to apply the discrete vascular-porous media model in the analysis of the real geometric structure.

In this study, the discrete vascular-porous media bioheat transfer model has been applied in thermal analysis on a cubic tissue model and a foot to evaluate the influence of the blood flow with various vasculatures. The tissue is regarded as a porous media, while the embedded vasculature includes arteries, arterioles, venules, and veins. The conductive and convective effects of blood flow in multi-scaled blood vessels on tissue temperature are well-addressed in the model. The temperature distributions for various degrees of foot vascular stenosis were simulated, and the relationship between the foot temperature distribution and blood flow was quantitatively correlated. A cubic porous media model embedded with the vessel network was also coupled with the measured skin temperature data for analysis of blood flow regulation in diabetic patients. The blood flow in the conditions of skin heating and power off were estimated according to the test setting, and comparisons of the predicted blood flow were made between healthy people and diabetic patients.

METHODS

The Developed Portable Thermal Sensor for Skin Temperature Measurement

In order to compare the automatic regulation of the blood flow between diabetic patients and healthy people, a programmable heating and temperature measurement device using a flexible material has been developed which is named by the superficial perfusion assessment system (SPAS). As shown in **Figure 1A**, the substrate of the SPAS is made of a double-layer flexible printed circuit (FPC) board, which is formed by 3 layers of polyimide, 2 layers of copper foil, and 4 layers of adhesive bonding. The top layer is welded with a high-precision temperature sensor chip si7051 and FPC connector. The circuit that is coiled into a loop near the center of the bottom layer generates heat when energized, which thermally stimulates the surface of the skin. The detailed content about the production and debugging of the film can be obtained from Cheng's master thesis (Cheng, 2020).

In the measurement, a medical tape was used to fix the SPAS on the skin of a hand, as shown in **Figure 1B**. Since the movement of a hand may cause the deviation of the flexible sensor, the

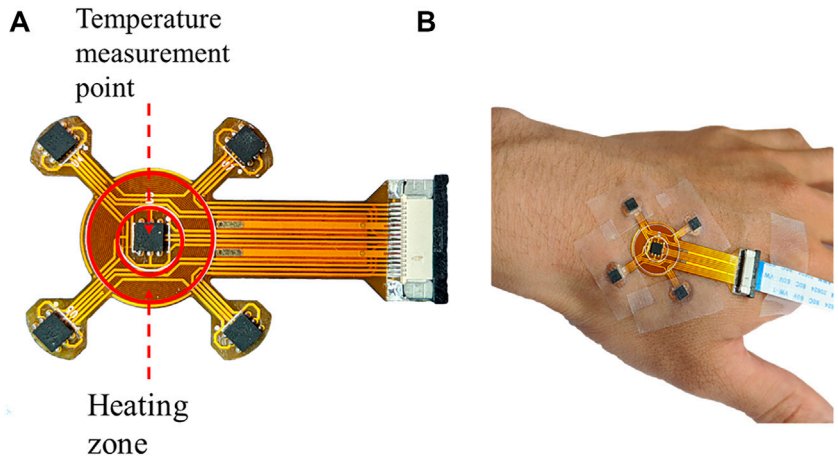

FIGURE 1 | (A) Display of the SPAS sensor and **(B)** its temperature measurement process during fixed at a hand.

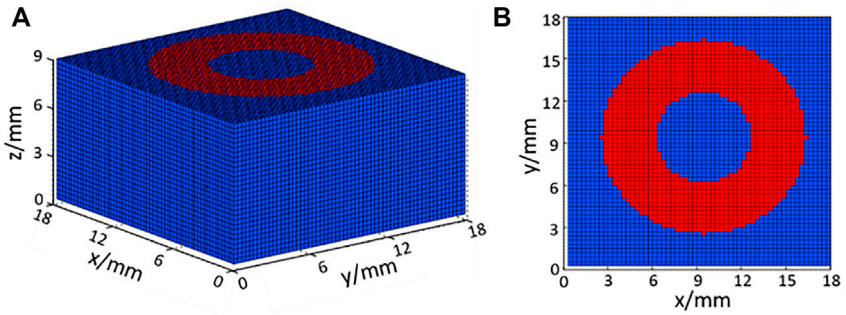

FIGURE 2 | (A) Three-dimensional cubic tissue model with voxel meshes and **(B)** its bottom view.

subject should remain as stable as possible during the test. After manually turning on the device, the measurement will start and end automatically when the setting period is reached. The duration of an experiment is set to 2,750 s including 3 stages. In the first 750 s, the heating power is 0 W/m2, which is called the resting phase. Then, it comes to the heating phase by heating the skin with a power of 150 W/m^2 for 1,000 s. After the power is switched off, the SPAS continues to record the temperature for another 1,000 s referring to the recovery phase.

Geometric Models and Mathematical Descriptions of the Vascular Porous Media Model

According to the shape and size of the SPAS equipment, a cubic tissue model was designed, as shown in **Figure 2A** which could describe the heat exchange between the skin surface and deeper tissue. The volume of the tissue model is 1.8 × 1.8 × 0.9 cm^3, and the voxel size is set as 0.3 mm. The upper surface of the model is the skin and conducts convective heat exchange with the surrounding environment. As shown in **Figure 2B**, the red area corresponds to the heating ring of the SPAS whose inner radius is 3.5 mm, and the outer one is 6.9 mm. An input heat flux as 150 W/m^2 is imposed on the red region at the heating phase, and zero is set in resting and recovery phases.

The subcutaneous tissue includes a large number of blood vessels to satisfy material and energy transport. As it is difficult to determine the specific structure of the blood vessels under the skin, an angiogenesis algorithm was used to generate blood vessels to fill the tissue area. In this tissue model, an inlet artery and an outlet vein were assumed inside the tissue model, as shown in **Figure 3A**. Then, the rapidly exploring random tree (RRT) algorithm was implemented as that in the work by Blowers et al. (Blowers, 2018) where it was used to generate brain vasculature. The procedures of the algorithm are as follows:

1) A new node is generated randomly inside the target tissue space.
2) Previous nodes are searched completely to find the closest segment or node.
3) A new segment is created by linking the created node with the closest point or with the nearest node of the nearest segment.
4) If the generated segment is connected to an existing segment (not at a node), a new node will be generated on the existing segment and will be divided in two segments.

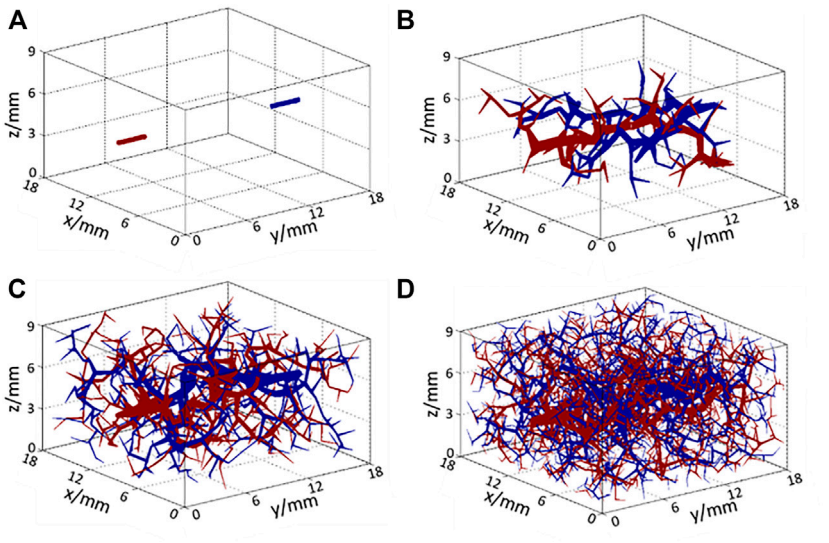

FIGURE 3 | Structure of arteries (red) and veins (blue) **(A)** at the initial state and after **(B)** 100 iterations, **(C)** 500 iterations, and **(D)** 2,000 iterations of the RRT algorithm.

5) The procedures 1–4 are repeated until the set number of iterations is completed.

The structures of the generated vessels after 100, 500, and 2,000 iterations of the RRT algorithm are shown in **Figures 3B–D**, respectively, where red lines represent arteries and arterioles, and blue lines represent veins and venules. As the number of iterations increased, blood vessels filled the entire space gradually so that blood could be perfused adequately to each part of the target tissue. In the generation of smaller vessels from the main arteries, two iteration criteria were set to end the RRT computation. If the numbers of vessels have no significant changes and the blood flow rate in the smallest vessel equals to a known value in the arteriole or venule, the computation will stop. In **Figure 3D**, the diameter of the smallest size of the vessel is 34 μm, which matches the size of the smallest arteriole. Additionally, to incorporate the thermal effects of capillaries, the voxel volume is regarded as a porous medium, whereby the liquid phase represents the blood in capillaries and the solid phase represents the solid tissue. Using this method, a complete multi-scale vascular and porous media model is formed. In the work, a cubic tissue and real geometric foot model have been constructed for the applications of the vascular porous media model.

Computation of Flow Rates in the 1D Vessel Network

Blood flow in 1D vessels is described by Poiseuille's law. The relationship between blood velocity and pressure is described by **Eq. 1**:

$$\boldsymbol{u_b} = -\frac{R^2}{8\mu}\frac{\partial P_b}{\partial \boldsymbol{s}}, \tag{1}$$

where R is the vessel radius, P_b is the blood pressure, $\boldsymbol{s}$ is the direction of the blood flow, μ is the blood viscosity, and $\boldsymbol{u_b}$ is the blood velocity. The continuity equation of blood in 1D blood vessels is:

$$\pi R^2 \nabla \cdot \boldsymbol{u_b} = -q_a + q_v, \tag{2}$$

where q_a and q_v denote the arterial outflow and venous inflow of blood. As blood can flow across the vessel wall and exchange with tissue at the capillary scale, q_a and q_v are set as 0 for non-terminal branches and assigned some values according to actual situations for terminal branches.

Computation of Flow Rates in Porous Media

In porous media, the capillary blood flow is assumed to occur *via* several thin capillaries. As such, the momentum equation can be simplified as the Darcy equation, which can be expressed as follows:

$$\nabla P = -\frac{\mu}{K}\boldsymbol{V_{Darcy}}, \tag{3}$$

where K is the permeability of porous media, and V_{Darcy} is the Darcy velocity. The Darcy velocity is related to the actual velocity V by: $V_{\mathrm{Darcy}} = \varepsilon V$ and ε represents the liquid volume fraction in the porous media. The continuity equation for the porous media is given as follows:

$$\rho_b \nabla \cdot \boldsymbol{V_{Darcy}} = Q_a - Q_v, \tag{4}$$

where Q_{a} and Q_{v} are the exchanged blood flows between tissue and arteries/veins, respectively. There is no velocity perpendicular to the skin. Therefore, the boundary pressure for skin can be given as:

$$\left.\frac{\partial P}{\partial n}\right|_{skin} = 0. \tag{5}$$

The blood flow at the interconnection between the discrete vascular and porous media are determined by the outflow of the arteries (q_{a}) and the inflow of veins (q_{v}) into the total ones into the

tissue (Q_a) and out of the tissue (Q_v). The relationship between them could be written as:

$$q_a = Q_a/n;\ qv = Q_v/m,$$

where n and m are the number of nodes that the peripheral arteries and peripheral veins intersect with a voxel. Outflow or inflow from the surrounding blood vessels are evenly distributed to each coupling node in this study.

Computation of Blood and Tissue Temperature

For simplicity, the 1D arterial vessel network, the 3D solid tissue phase, the 3D capillary phase, and the 1D venous vessel structure are denoted 1, 2, 3, and 4, respectively. The heat transfer processes in these four regions are expressed as follows:

$$V_1\rho_b c_b\frac{\partial T_1}{\partial t} = V_1K_b\left(\nabla^2T_1\right) - V_1\rho_b c_b\boldsymbol{U}_1\left(\nabla T_1\right) + \beta_{1-2}\left(T_2 - T_1\right) + \beta_{1-3}\left(T_3 - T_1\right), \tag{6}$$

$$V_2\varepsilon_2\rho c\frac{\partial T_2}{\partial t} = V_2\varepsilon_2K_c\left(\nabla^2T_2\right) + \beta_{1-2}\left(T_1 - T_2\right) + \beta_{2-3}\left(T_3 - T_2\right) + \beta_{2-3}\left(T_3 - T_2\right) + \beta_{2-4}\left(T_4 - T_2\right) + V_2Q_{gen}, \tag{7}$$

$$V_3\varepsilon_3\rho_b c_b\frac{\partial T_3}{\partial t} = V_3\varepsilon_3K_b\left(\nabla^2T_3\right) - V_3\rho_b c_b\boldsymbol{U}_3\left(\nabla T_3\right) + \beta_{1-3}\left(T_1 - T_3\right) + \beta_{2-3}\left(T_2 - T_3\right) + \beta_{3-4}\left(T_4 - T_3\right) + c_bM_{1-3}\left(T_3 - T_1\right), \tag{8}$$

$$V_4\rho_b c_b\frac{\partial T_4}{\partial t} = V_4K_b\left(\nabla^2T_4\right) - V_4\rho_b c_b\boldsymbol{U}_4\left(\nabla T_4\right) + \beta_{2-4}\left(T_2 - T_4\right) + \beta_{3-4}\left(T_3 - T_4\right) + c_bM_{3-4}\left(T_4 - T_3\right), \tag{9}$$

where V_{1-4} denotes the volume of the domain, and $U_{1,\,2,\,4}$ are the blood velocities in different regions. As the soft tissue is the solid phase in the porous media, U_3 does not exist. ε_2 is the volume fraction of the tissue within the porous domain, and ε_3 is the volume fraction of the blood; therefore, $\varepsilon_2 + \varepsilon_3 = 1$. K and K_b are the conduction coefficients for the tissue and blood phases, respectively. c_b and c are the heat capacities for blood and tissue. The tissue parameters include two components which are the soft tissue and bone. M_{1-3} and M_{3-4} represent the mass exchange from domain 3 to domain 1 and from domain 3 to domain 4, reflecting convective heat transfer from arteries to voxels and from voxels to veins, respectively. Q_{gen} represents tissue metabolic heat generation. Heat exchange between the blood and the surrounding tissue through the vessel wall is described by the heat exchange coefficient $\beta_{x\text{-}y}$ which is defined as follows:

$$\beta_{x-y} = \varepsilon hA_{surf}, \tag{10}$$

where h is the convection coefficient of the blood and vessel wall, and A_{surf} is the surface area of the blood vessels. Vascular blood flow can be approximated as the laminar flow in a rigid pipe, so this convection coefficient can be deduced from the Nusselt number:

$$Nu = \frac{hD_v}{2K_b}. \tag{11}$$

It is well established that for a laminar flow in a pipe, Nu can be approximated to be a constant with the value of 4 (Blowers, 2018). At the surface of the foot model and the top surface of the cubic model, there is heat exchange with the environment and a Robin boundary condition can be prescribed as:

$$-K_c\frac{\partial T}{\partial n} = h\left(T - T_\infty\right), \tag{12}$$

where T_∞ is the environment temperature, and h is the convective heat transfer coefficient. The adiabatic boundary condition was set for the plane connecting the foot to the leg in the foot model and the other surface of the cubic model:

$$-K_c\frac{\partial T}{\partial n} = 0. \tag{13}$$

Having set the boundary conditions for the heat and mass transfer equations, the temperatures of the four domains could be solved with the given flow rates within domains 1, 3, and 4. A MATLAB program was developed based on an open-source code on GitHub [https://github.com/sblowers/VaPor] for the implementation of numerical computation. The physical parameters used in this computation are described in **Table 2**.

In this model, $\boldsymbol{u_b}$ represents the velocities in blood vessels including the velocities in arteries ($\boldsymbol{U_1}$) and veins ($\boldsymbol{U_4}$) which are solved by **Eqs 1** and **2**. The vessel network model used in this work is a 1-dimensional one with the information of radii and lengths. In the computation of the blood flow of the 1D model, the velocity in every segment is computed by **Eq. 1**, while the velocities at the bifurcation nodes should be computed by combining **Eqs 1, 2** to satisfy the continuity condition of mass flow at these points. The direction of the blood flow in every segment depends on the known position of every vessel segment generated by the RRT algorithm. The direction of vector $\boldsymbol{u_b}$ refers to the one in the 3D information of the network. Similar implementation can be found in the works of Pozrikidis (Pozrikidis, 2009) and Blowers, (2018) for blood flow simulation through vascular networks. On the other hand, $\boldsymbol{U_3}$ can be obtained by solving **Eqs 3, 4**. $\boldsymbol{V_{Darcy}}$ represents the Darcy velocity in the porous medium model which is related to the velocity of the blood flow in a capillary ($\boldsymbol{U_3}$).

Since voxel-based meshes are employed, the finite difference method (FDM) can be easily employed for the discretization of **Eqs 6–9**. The real geometric 3D model reconstructed from medical images can also be directly transformed into a voxel mesh for the computation by the FDM. Currently, the steady-state temperature is considered; thus, the discretization of the time derivative term is not needed. The convection term is discretized using the first-order upwind difference scheme. The diffusion terms of the equations are discretized using the central difference scheme. The discrete governing equation can be then written as a stiffness-matrix form as:

TABLE 2 | Physical parameters used in the foot model.

Physical parameter	Value	Unit	References
Blood viscosity, μ	3.5	mPa s	Bagavathiappan et al. (2008)
Permeability of porous media, K	1.5×10^{-13}	m^2	Bagavathiappan et al. (2008)
Blood density, ρ_b	1,050	kg/m^3	Bagavathiappan et al. (2008)
Specific heat capacity of blood, c_b	3,800	J/(kg K)	Bagavathiappan et al. (2008)
Thermal conductivity of blood, K_b	0.50	W/m^3	Bagavathiappan et al. (2008)
Tissue density, $\rho_{soft\ tissue}$	1,270	kg/m^3	Antonova et al. (2016)
Specific heat capacity of the soft tissue, $c_{soft\ tissue}$	3,768	J/(kg K)	Antonova et al. (2016)
Thermal conductivity of the soft tissue, $K_{soft\ tissue}$	0.35	W/m^3	Antonova et al. (2016)
Bone density, ρ_{bone}	1,418	kg/m^3	Antonova et al. (2016)
Specific heat capacity of the bone, c_{bone}	2,409	J/(kg K)	Antonova et al. (2016)
Thermal conductivity of the bone, K_{bone}	2.21	W/m^3	Antonova et al. (2016)
Metabolism, Q_{gen}	368	W/m^3	Antonova et al. (2016)

$$\boldsymbol{Ax} = \boldsymbol{B}, \tag{14}$$

where $\boldsymbol{x}$ is the temperature matrix, A is the coefficient matrix of temperature, and B is the loading term derived from the known terms in the governing equations. Through the built-in Gaussian elimination algorithm in MATLAB, the above algebraic equation can be solved. It takes about 10 min in MATLAB on a PC with an Intel i7 6700k QuadCore processor and 32 GB of RAM for a foot model with a 1.5 mm-voxel size and 50,000 generated vessels.

RESULTS

The process of the thermal analysis on the cubic tissue and foot model are basically the same, among which the heating source should be taken into account for the cubic model. Since the measurement period is sufficiently long, the stable heating and power-off instance were chosen for the analysis in the cubic tissue model. The blood temperature of the inlet artery is constant at 37°C. The convective and radiative boundary condition is assigned at the skin of which the total heat transfer coefficient was set to be 8.0 W/m^2 K. The environmental temperature was set as 23°C, following the same environmental condition of Sivanandam et al. (2012). The results of the heat transfer computation in the two models are presented in *Tissue Temperature Distributions Under Heating and Power-Off Condition and Temperature Distributions for Different Vasculatures on Foot* sections, respectively. The inversion of blood flow for healthy people and diabetic patients is illustrated in *Inverse Analysis of Skin Blood Flow in Healthy People and Diabetic Patients* section.

Tissue Temperature Distributions Under Heating and Power-Off Condition

When there is no external heat stimulation on the skin (resting and recovery stage), the computed tissue temperature distribution is shown in **Figure 4A**, and the temperature distribution of internal tissue sections coupling with vessels is displayed in **Figure 4B**. In this phase, blood flow is the heat source; thus the highest temperature is located at the arterial entrance. As illustrated in **Figure 4B**, the temperatures of blood vessels gradually decrease along the flow direction due to the heat exchange between the blood vessel and the surrounding tissue. At the skin surface, it is seen that the skin temperature in the upstream is slightly higher than that in the downstream position.

When the skin surface is heated by the SPAS (heating stage), the temperature of the heated ring zone at the skin surface increases significantly, as shown in **Figure 4C**. At this time, blood plays a role of heat dissipation; thus, the coolest area is located at the arterial inlet. **Figure 4D** shows the temperature distribution of the inner section and blood vessels. As the blood is heated during flowing, the temperature of blood at the downstream is increasing; thus, the cooling effect of the blood flow in the downstream is weaker than that in the upstream of the blood flow. This effect is also reflected in the skin surface that the surface skin temperature in the downstream area of the heating ring is higher than that in other areas.

Temperature Distributions for Different Vasculatures on the Foot

The vascular—porous media model has been applied in the thermal analysis on the foot and for establishing a quantitative relationship between the blood flow and temperature distribution. The foot model in this study was reconstructed from sequential medical images. Simpleware software (Exeter, United Kingdom) was used to identify the bone and soft tissue automatically from CT images. The structure of the basic blood vessel of this foot model was obtained from the available website (https://human.biodigital.com). and further developed by using the RRT algorithm. **Figure 5** shows the foot skin temperature distribution from a dorsal, side, and plantar view. The temperature ranges from 24.28°C to 32.12°C. In **Figure 5A**, it can be observed that the temperature of the skin near the large blood vessels is higher, and it decreases gradually to the distal end. In **Figure 5C**, the computed average temperature of the foot plantar region is 29.42°C, which is 0.5°C higher than the experimental data (Sivanandam et al., 2012). In addition, the computed temperature distribution shows the temperature of the arch is higher than that of the sole and heel, and the toes are the coldest area of the whole foot. Specifically, the 1st and 5th toes are warmer than the 2nd, 3rd, and 4th toes. The computed temperature values closely approach the experimental data, and the abovementioned characteristics for the temperature distribution are consistent with the standard thermographic

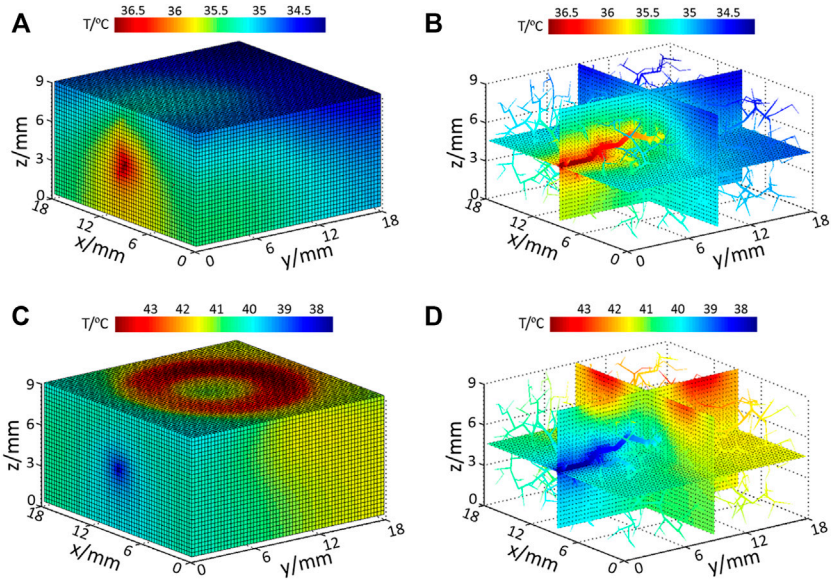

FIGURE 4 | Temperature distribution of **(A)** model surface with no input heating power; **(B)** internal tissue and vessel temperature distribution with no extra heating power; **(C)** model surface temperature under heating and **(D)** internal tissue and vessel temperature under heating.

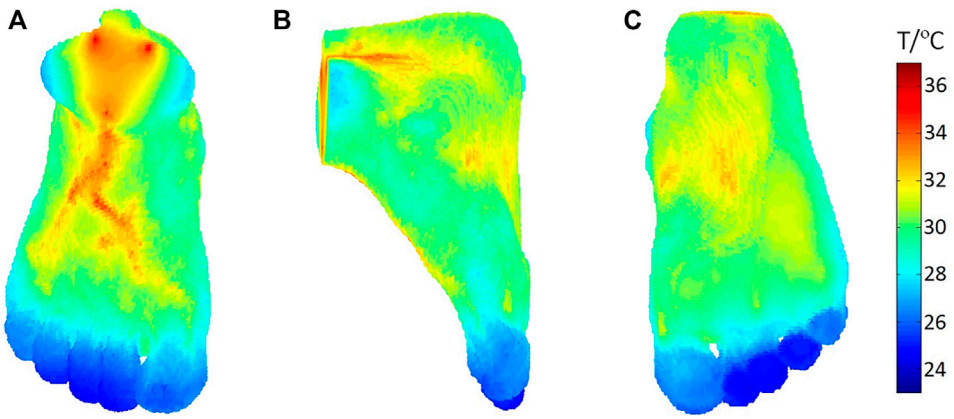

FIGURE 5 | Temperature distribution of a foot from **(A)** dorsal, **(B)** side, and **(C)** plantar view.

patterns of feet (Alfred et al., 2015), confirming the validity of the vascular porous media model.

Figures 6A–C show the distribution of arterial blood flow when occlusion occurs in the anterior tibial artery, posterior tibial artery, and peroneal artery, respectively. The occlusion positions in the three inlet arteries were specifically marked, wherein the anterior tibial artery supplies blood to the dorsal part of the foot, the posterior tibial artery supplies blood to the plantar region, and the peroneal artery supplies blood to the lateral areas. The vasculature in the foot model can be also seen clearly. As the total number of vessels is more than 1×10^6, it is difficult to visualize all vessels concurrently; only the vessels with diameter >100 μm are displayed. It is observed that the blood flow in the non-blocked inlet vessels and its downstream vessels gradually decreases along with the bifurcation generations. Apart from the blood flow in the major blood vessels, the arteriole and venule flow rates are <0.01 ml/s, indicating that the blood had been perfused to all parts of the foot. In contrast, no blood flows through the downstream area of the blocked vessel which will affect the distribution of the foot temperature.

The temperature distributions on the surface of the foot when the three inlet vessels are blocked, as shown in **Figure 7**, where the rows indexed (a–c), (d–f), and (g–i) correspond to the temperature contours for the occlusion of the anterior tibial artery, posterior tibial artery, and peroneal artery, respectively. When the anterior tibial artery is occluded, the temperature of the upper surface of the foot decreases considerably, especially in the

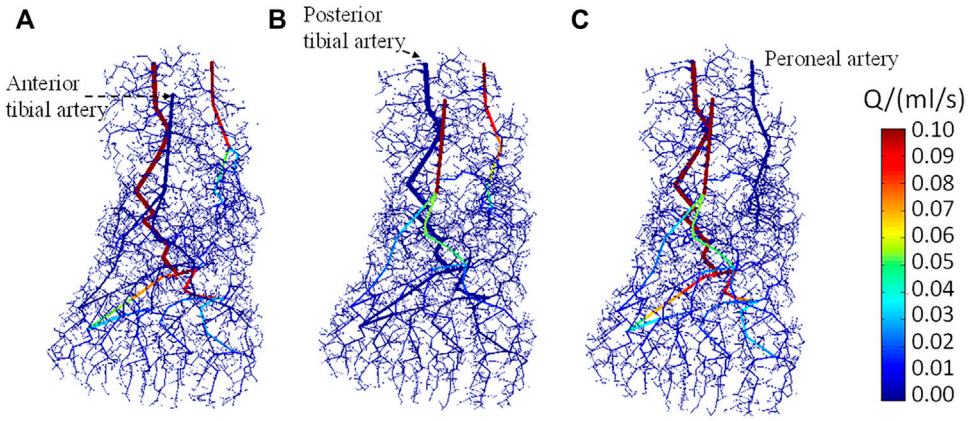

FIGURE 6 | Dorsal view of the blood flow in arteries when stenosis occurs in **(A)** anterior tibial artery, **(B)** posterior tibial artery, and **(C)** peroneal artery, respectively.

central region more influenced by the occluded feeding artery. If observed from the lateral side and foot sole, as shown in **Figures 7B,C**, there are no remarkable changes in the temperature compared to the healthy case. As the blood flow in the peroneal artery is at the normal state, the temperature decreases in the heel are small. This means when occlusion occurs in the anterior tibial artery, the most affected area in the skin temperature is the plantar surface. Moreover, in the middle and lower part of the foot, especially the toes, the lower temperature areas are enlarged which can even be seen from the dorsal and side view. Similarly, as seen in **Figures 7D–I**, the occlusions of the posterior tibial and peroneal artery have the impacts on the sole and lateral side of the foot. Meanwhile, it is noted that the occlusion in the posterior tibial artery seems to result in the largest lower temperature area, suggesting that the occlusion in the posterior tibial artery should be paid more attention to.

Inverse Analysis of the Skin Blood Flow in Healthy People and Diabetic Patients

The vascular porous media model has applied in the thermal analysis of blood flow regulation in the SPAS test. The measurements by using the SPAS were implemented on five healthy people denoted by N1~N5 and 31 diabetic patients denoted by DM1~DM31. The experiments have been approved by the Biological and Medical Ethics Committee of Dalian University of Technology. The data collection of diabetic patients was performed in the First Affiliated Hospital of Anhui Medical University. The ages, BMI indices, and blood glucose levels of the subjects are shown in **Table A1** as an **Appendix**. The temperature curves of a typical diabetic patient (DM1) and healthy people (N2) are shown in **Figure 8**. In each phase, the temperature of the diabetic patient is higher than that of the healthy person. In the heating phase, both the temperature rises rapidly and then stabilizes for a sufficiently long period. However, after heating is over, the temperature of the healthy person returns to the level before heating, but the temperature of the diabetic patient has not declined to the resting stage range.

The ambient temperature varies slightly in different tests, as shown in **Figure 8**, since the tests were carried out during a short period of several days. In order to estimate the blood flow in each test, the temperature distributions of the cubic tissue model were computed for various inlet flow rates from 0 to 0.01 ml/s, and the ambient temperature was set to 20 to 24°C, respectively. The skin temperature at the center point surrounded by the heating ring was subsequently extracted. A set of curves for the relationships between the skin temperature, blood flow, and ambient temperature were achieved and could be fitted as a two-dimensional graph by using the surface fitting tool toolbox in MATLAB. **Figures 9A,B** give the temperature variations at the recovery and heating phase. It is clear to see that the skin temperature increases with the input blood flow rate without external heating; meanwhile, the increase of the environmental temperature can also lead to the slight increase of the skin temperature. If an external constant heat is added, the center-point skin temperature decreases with the input blood flow rate. Temperature varies significantly when the input blood flow changes from 0 to 0.002 ml/s and then tends to vary slowly when the blood flow is further increased. Having the set of fitted curves, the input arterial blood flow rate could be determined from the measured environmental and skin temperatures.

In order to analyze the blood flow during the stable period of each stage, the measured temperature data of the last 100 s in each stage were extracted to evaluate the average blood flow during resting, heating, and recovery stages. The obtained results for the healthy people are displayed in **Figure 10**. The typical blood flow variation pattern for the healthy subjects is the blood flow rates at the resting and recovery phases, which are distinctly lower than that at the heating stage although there are slight differences among the healthy subjects. The blood flow increases at the heating stage since the blood vessels dilate for heat dissipation when the skin is heated. The smallest blood flow at the heating phase is 0.32 ml/s which is larger than the largest blood flow rate of 0.23 ml/s at the resting phase among healthy people. At the

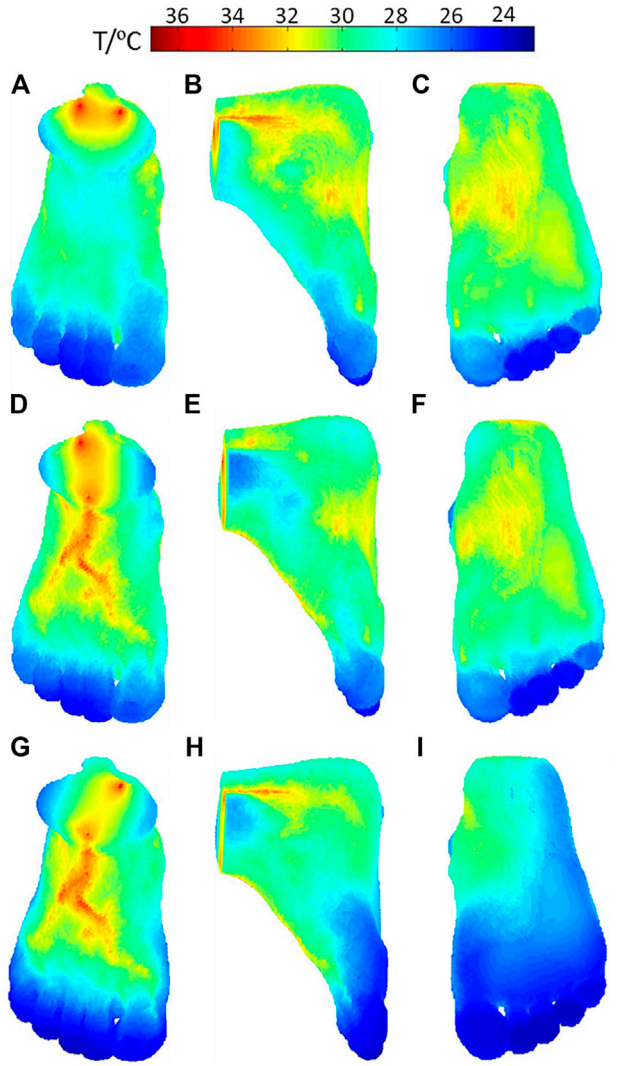

FIGURE 7 | Temperature distribution of the foot model when stenosis occurs in **(A–C)** anterior tibial artery occlusion, **(D–F)** posterior tibial artery, and **(G–I)** peroneal artery.

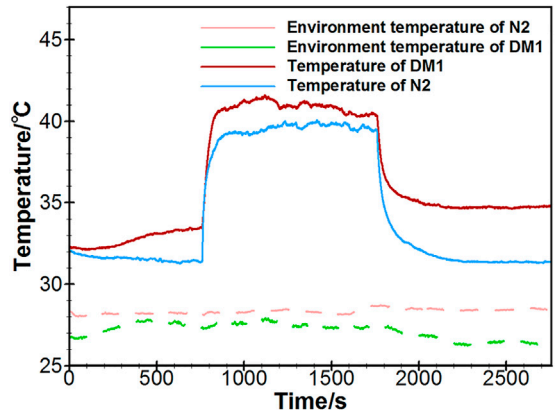

FIGURE 8 | Measured temperature curves by the SPAS for a healthy person and a diabetic patient.

recovery phase after the power is off, the blood flow returns to the resting level before heating with the difference of less than 10%.

However, the blood flow variation patterns of individuals with diabetes vary greatly, especially at the recovery stage. According to the blood flow alteration patterns at the resting and recovery stage, the estimated results can be classified into three groups shown in **Figures 11A–C**, respectively. In **Figure 11A**, the blood flow rate during heating is greater than that of the resting phase, but the increment is smaller compared to that of healthy people. It is noticeable that the blood flow rate at the recovery stage is even larger than that at the heating stage. In **Figure 11B**, the variation pattern of the blood flow rate at the resting and heating stage is close to that of healthy subjects; however, the blood flow rate at the recovery stage is only slightly reduced from the value at the heating stage, whose value is close to the average one of the resting and heating stage. Seven sets of data in the third group are shown in **Figure 11C**. The pattern of the blood flow variation for the group of diabetic patients is similar to that of healthy subjects that the blood flow rate at the resting and recovery stage are remarkably lower than the one at the heating stage.

DISCUSSION

In this study, thermal analysis of blood flow was performed in a cubic tissue and a real geometric foot model by using a discrete vascular-porous media model. The discrete vascular-porous media model was first put forward by Blowers et al. in analyzing the effect of therapeutic hypothermia of the human brain. It is our opinion that the advantage of the model is to take into account the influence of the vasculature more precisely. Hence, a MATLAB program was further extended to allow the model to calculate more complex conditions with a ring-mounted vessel structure and a vascular stenosis. The blood flow rates in vasculatures and temperature distributions have been achieved under various thermal conditions, providing the possibilities to analyze blood flow conditions in the tissue from the surface temperature.

In analyzing the thermal responses measured by the SPAS, the inlet arterial blood flow of the three stages was estimated and compared between healthy subjects and diabetic patients. It is seen that the blood flow rate at the recovery phase fell back to the level at the resting phase for healthy subjects. However, in the diabetic group, the blood flow in the recovery phase is close to the blood flow rate at the heating phase and even larger than it, which manifests that the vasodilation under a thermal stimulation is delayed in some of the diabetic patients. The results further support our previous studies (Wang et al., 2020) on SD rats that the blood flow drops rapidly after thermal stimulation for all healthy rats, but the delay of the declination occurs in some diabetic rats. Compared to the 2nd blood flow variation pattern in diabetic patients, the 1st blood flow variation pattern suggests more delayed time to thermal response. It is implied that the diabetes with delayed autoregulated vasomotion may be suffering

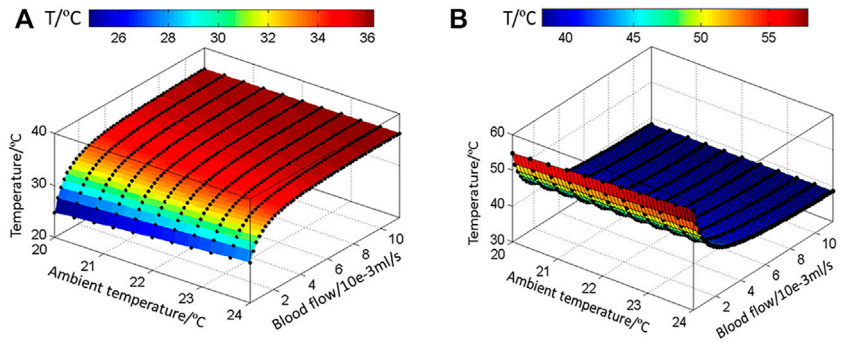

FIGURE 9 | Fitted curves to express the relationships of the blood flow, ambient temperature, and skin temperature in the **(A)** recovery and **(B)** heating phase.

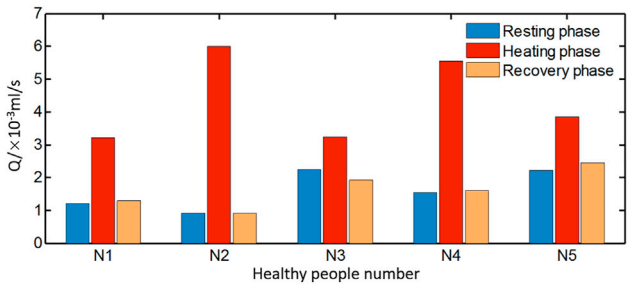

FIGURE 10 | Average blood flow rate of healthy subjects during rest, heating, and recovery phases.

from peripheral vascular diseases and needs to be more concerned. By comparing the analytical results to the clinical diagnoses by the First Affiliated Hospital of Anhui Medical University for the 15 diabetic subjects, it is found that except one patient, the other patients are suffering different kinds of complications, including hypertension, peripheral vascular disease, or peripheral neuropathy.

Both the skin temperature variation in diabetic patients and rats in our experiments show the similar pattern that the severe the diabetic mellitus is, the faster the skin temperature increases. Although constant thermal conductivity and the same vasculature were assigned in the work, it will not affect the estimated blood flow pattern in healthy and diabetic patients. Nonetheless, the possibility still exists that some estimated healthy blood flow patterns may have some abnormalities due to neglecting the impacts of aging and fat thickness.

Aging may cause the decrease of the microvasculature density and increase of vessel stiffness, leading to the increase of peripheral resistance. This kind of alteration can be also reflected in the change of effective conductivity. If microvasculature density decreases, the effective thermal resistance will increase. Similarly, fat thickness increasing will increase the thermal resistance as well. These factors can lead to faster temperature increasing in the heating stage of the test and reinforce the predicted blood flow variation pattern, which is with a higher ratio of the blood flow in the recovery phase to that in the heating phase. In addition, the increase of thermal resistance can result in a damping of the magnitude of the skin temperature oscillation and a larger phase lag to the blood flow (Tang et al., 2017).

It is commonly known that the foot temperature of diabetic patients is lower which is caused by the lower blood perfusion rate (Uraiwan et al., 2018). **Equations 6–9** have the similar form of the Pennes equation, but they describe the heat transfer process of arteries, tissue, capillaries, and veins more in detail rather than using a lumped source/sink term in the Pennes equation. The vascular-porous media model captures the thermal effect of heat conduction and convection within their regions and between blood vessels and their surrounding tissues. The alterations of blood vessel structures could also be explored. The Pennes equation could be applied in thermal analysis of foot, but it needs more assumptions for blood perfusion. The computed temperature of the foot *via* the vascular-porous media model is in a favorable agreement with thermography, showing the prospective applications in the assessment of vascular alterations for a diabetic foot.

With the development of medical imaging technology such as laser speckle flowmetry or thermography, it has been possible to directly obtain structural lesions of the blood vessels of body parts. However, early detection of the diabetic foot needs to be performed at a high frequency. Medical imaging testing is not yet suitable for daily inspections due to the high cost. Thermography is a prospective way for screening the microvasculature, but a more reliable algorithm for converting the temperature to blood flow is needed. The voxel-based vascular-porous media model provides a useful way for the conversion. Additionally, the medical image could only reflect the structural lesions but not functional lesions. It is found that the diabetic vascular functional lesions may appear before structural lesions through rat experiments (Wei et al., 2021). Coupling with thermography and the porous media model, the stenosis degree of peripheral vessels, vascular density variation, or vasodilation dysfunction may be detected, which are meaningful for the early diagnosis of a diabetic foot.

In our previous study, we measured the foot and finger temperature simultaneously and found that the foot skin

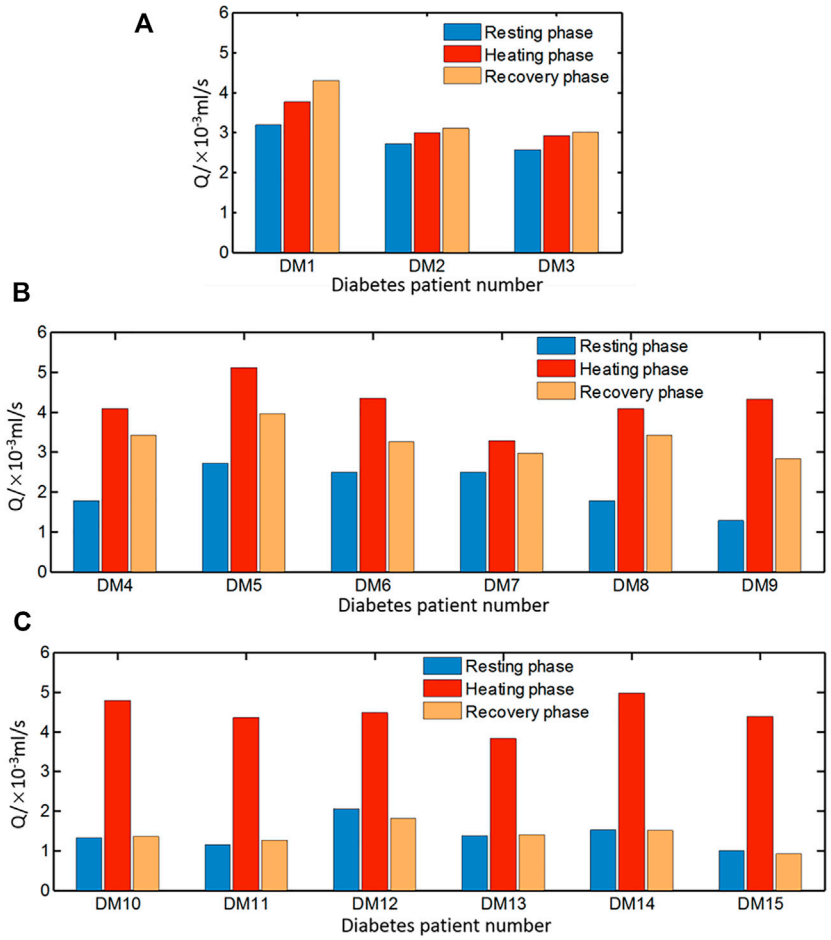

FIGURE 11 | Average blood flow rate of diabetic patients in three groups **(A)** DM1–DM3, **(B)** DM4–DM9, and **(C)** DM10–DM15 during resting, heating, and recovery phases.

temperature is more sensitive to reflect the endothelial dysfunction, but finger temperature can also give the same information (Tang, 2017). Since vascular abnormalities frequently occur in a similar fashion (Abularrage et al., 2005), abnormal vasomotion of hand could reflect the foot vascular disease to a certain extent. Compared to foot, hand is more accessible for measurement. Despite that, we did not focus on the coherence between the data in the hand and foot; there are three patients suffering peripheral neuropathy among the screened abnormal blood flow patients through the thermal analysis of SPAS data. This reveals that the hand skin temperature can also be a tracer for the early detection of the diabetic foot. More data from hand and foot should be collected simultaneously and compared for showing the coherence between them in detecting the endothelial dysfunction.

Additionally, although the relationship between the temperature and blood flow distribution was established in the foot model, the inversion of the blood flow of inlet arteries of the foot is not as simple as the process in the cubic model. Different inlet blood vessels or intermediated blood vessels own their respective temperature influencing areas, and the abnormal temperature distribution is a combined result of multiple blood flow under different degrees of stenosis. Therefore, in the future, it is necessary to divide the foot into several areas and apply available optimization methods to comprehensively investigate the coupling effect of various vascular disorders on temperature.

In generation of the foot vasculature, the nodes of the main blood vessels of the foot were manually set with reference to the physiological model obtained from the website, where the distance between the vessel and bone can be determined from the slices of the foot. After setting the arterial and venous nodes, the vessel network was compared to the physiological model again. Although the website provides the detailed structure of the foot including all tissues, the specific data could not be obtained. Thus, we manually made a vessel network according to the relative distance and size of the physiological model and inserted into the voxel-based model. The names and positions of the foot blood vessels in our model are also in agreement with the ones in the literature (Manzi et al., 2011).

The RRT algorithm was implemented to generate the blood vessels so that the blood is perfused into various regions of the tissue. **Figure 12** shows the number of vessel elements and relative

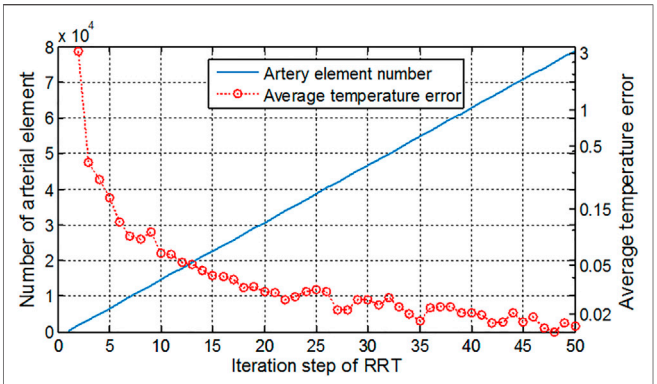

FIGURE 12 | Artery element number and average temperature error along with the increment of iteration steps in the RRT algorithm.

temperature errors along with the increasing RRT iterations. The number of iteration steps increases by 1,000 step each time, and the mean square error of the surface temperature between the newly computed temperature and original one was computed. The initial average error reached 3°C and gradually reduced as the iteration number increases. It is seen that the more iteration steps are used, the smaller blood vessels can be included and larger computational burden is resulted in. At the 50,000 s′ step, the average temperature error has been reduced to 0.01°C, and temperature distribution has hardly changed even with more iteration steps. Therefore, the iteration of this foot model is set as 50,000. In the computation for the cubic tissue model, the iteration step is set as 2,000 due to the smaller model size.

Despite of the reasonable structure and sizes of the vessels, it should be noted that the model has not reflected the individual differences in the foot structure. Our rat experimental study has shown that the microvasculature alteration occurs after the endothelial dysfunction (Wei et al., 2021). In the current study, it is assumed that the microvasculature has not been changed since the blood flow alterations due to the change of vasodilation is the first aim of the work. On the other hand, the iteration number of the RRT algorithm may give an impact on the structure of the vascular network and further influence the blood flow in a one-dimensional straight tube model. In the future we may optimize the RRT algorithm in the setting of the bifurcation angle of blood vessels and fractional dimensions so that various altered vasculatures in pathological conditions can be generated. Using MR angiography for showing the main vessels is an alternative way as well.

CONCLUSION

In this study, a vascular-porous media model has been applied in the thermal analysis of foot and a cubic tissue. Since the blood flow and the heat exchange within tissues during the flow process was considered by using a multiscale model, the temperature distributions under various thermal and blood flow conditions can be achieved so that the non-linear relationship between the blood flow and skin temperature can be further deduced. The computed results in the foot model reveals that the stenosis of feeding arteries can lead to temperature decreases in the downstream for different degrees, among which the occlusion of the posterior tibial artery has the largest lower-temperature area.

Then, analysis of the thermal response test imposed on type 2 diabetic patients and healthy subjects show that for a healthy subject, the blood flow rate after heating power is off at the recovery stage decreases to the level as that of the resting condition, whereas in some diabetic patients, the blood flow rates solely decrease slightly or even increase further at this stage. This implies that the vasodilation function to the thermal stimulus is delayed in the subject, which verifies the conclusions in our previous studies on diabetic rats. Most of the screened diabetic patients with peripheral vascular or neuropath disease are in agreement with those diagnosed clinically. It is believed that the discrete vascular-porous media model may have more applications, especially to studies of the diabetic foot by coupling with thermography imaging.

DATA AVAILABILITY STATEMENT

The raw data supporting the conclusions of this article will be made available by the authors, without undue reservation.

ETHICS STATEMENT

The studies involving human participants were reviewed and approved by the Biological and Medical Ethics Committee of Dalian University of Technology. Written informed consent for participation was not required for this study in accordance with the national legislation and the institutional requirements.

AUTHOR CONTRIBUTIONS

Y-PW drafted the manuscript and analyzed the data of this work. YH made substantial contributions to the design of this work and revised it critically for important intellectual content. R-HC made efforts in the data acquisition. L-ZM collected the raw data of foot CT images.

FUNDING

This work is supported by the National Natural Science Foundation of China No. 51976026 and the Fundamental Research Funds for the Central Universities (No. DUT20GJ203).

REFERENCES

Abularrage, C. J., Sidawy, A. N., Aidinian, G., Singh, N., Weiswasser, J. M., and Arora, S. (2005). Evaluation of the Microcirculation in Vascular Disease. *J. Vasc. Surg.* 42 (3), 574–581. doi:10.1016/j.jvs.2005.05.019

Alfred, G., Cynthia, F., Kevin, C., Camilleri, K. P., Raffaele, C. D., Mizzi, A., et al. (2015). Thermographic Patterns of the Upper and Lower Limbs: Baseline Data. *Int. J. Vasc. Med.* 2015, 831369. doi:10.1155/2015/831369

Amith, K., Muhammad, E. H. C., Mamun, B. I. R., Sawal, H. M. A., Md, A. H., Serkan, K., et al. (2021). A Machine Learning Model for Early Detection of Diabetic Foot Using Thermogram Images. *Comput. Biol. Med.* 137, 104838. doi:10.1016/j.compbiomed.2021.104838

Antonova, N., Tsiberkin, K., Podtaev, S., Paskova, V., Velcheva, I., and Chaushev, N. (2016). Comparative Study between Microvascular Tone Regulation and Rheological Properties of Blood in Patients with Type 2 Diabetes Mellitus. *Clin. Hemorheol. Microcirc.* 64, 837–844. doi:10.3233/CH-168000

Astasio, A., Escamilla, M. E., Martínez, N., Sánchez Rodríguez, R., and Gómez–Martín, B. (2018). Thermal Map of the Diabetic Foot Using Infrared Thermography. *Infrared Phys. Techn.* 93, S1350449518302512. doi:10.1016/j.infrared.2018.07.008

Astasio-Picado, Á., Escamilla Martínez, E., and Gómez-Martín, B. (2020). Comparative thermal Map of the Foot between Patients with and without Diabetes through the Use of Infrared Thermography. *Enfermería Clínica (English Edition)* 30 (2), 119–123. doi:10.1016/j.enfcle.2018.11.004

Bagavathiappan, S., Philip, J., Jayakumar, T., Raj, B., Rao, P. N. S., Varalakshmi, M., et al. (2010). Correlation between Plantar Foot Temperature and Diabetic Neuropathy: A Case Study by Using an Infrared Thermal Imaging Technique. *J. Diabetes Sci. Technol.* 4 (6), 1386–1392. doi:10.1177/193229681000400613

Bagavathiappan, S., Saravanan, T., Philip, J., Jayakumar, T., Raj, B., Karunanithi, R., et al. (2008). Investigation of Peripheral Vascular Disorders Using thermal Imaging. *Diabetes Vasc. Dis.* 8 (2), 102–104. doi:10.1177/1474651408080020901

Bandalakunta Gururajarao, S., Venkatappa, U., Shivaram, J. M., Sikkandar, M. Y., and Al Amoudi, A. (2019). Infrared Thermography and Soft Computing for Diabetic Foot Assessment. *Infrared Thermography Soft Comput. Diabetic Foot Assess.*, 73–97. doi:10.1016/b978-0-12-816086-2.00004-7

Barrios, A., Debnath, O. B., Ito, K., Saito, K., and Uesaka, M. (2019). "Blood Flow Effect in Combination of Hyperthermia with Radiation Therapy for Treatment in Breast Tumor," in 2019 URSI Asia-Pacific Radio Science Conference (AP-RASC), New Delhi, India, 9-15 March 2019.

Blowers, S. J. (2018). *Modelling Brain Temperatures in Healthy Patients and Those with Induced Hypothermia* Edinburgh: The University of Edinburgh.

Blowers, S., Marshall, I., Thrippleton, M., Andrews, P., Harris, B., Bethune, I., et al. (2018). How Does Blood Regulate Cerebral Temperatures during Hypothermia. *Sci. Rep.* 8 (1), 7877. doi:10.1038/s41598-018-26063-7

Briers, J. D. (1996). Laser Speckle Contrast Analysis (LASCA): a Nonscanning, Full-Field Technique for Monitoring Capillary Blood Flow. *J. Biomed. Opt.* 1 (2), 174–179. doi:10.1117/12.231359

Carlos Padierna, L., Fabián Amador-Medina, L., Olivia Murillo-Ortiz, B., and Villaseñor-Mora, C. (2020). Classification Method of Peripheral Arterial Disease in Patients with Type 2 Diabetes Mellitus by Infrared Thermography and Machine Learning. *Infrared Phys. Techn.* 111, 103531. doi:10.1016/j.infrared.2020.103531

Chen, Z. Z., Gao, M. J., and Zhang, W. Z. (2021). Analytic Strategies for Early Diagnosis of Diabetic Foot Using Infrared thermal Imaging Technology. *China J. Traditional Chin. Med. Pharm.* 36 (2), 963–967.

Cheng, R. H. (2020). *Development of Thermal Response Measuring System for Assessing Blood Perfusion in Microcirculation*. Dalian: Dalian University of Technology.

Copetti, M. I. M., Durany, J., Fernández, J. R., and Poceiro, L. (2017). Numerical Analysis and Simulation of a Bio-thermal Model for the Human Foot. *Appl. Maths. Comput.* 305, 103–116. doi:10.1016/j.amc.2017.01.067

Frick, P., Mizeva, I., and Podtaev, S. (2015). Skin Temperature Variations as a Tracer of Microvessel Tone. *Biomed. Signal Process. Control.* 21, 1–7. doi:10.1016/j.bspc.2015.04.014

Glovaci, D., Fan, W., and Wong, N. D. (2019). Epidemiology of Diabetes Mellitus and Cardiovascular Disease. *Curr. Cardiol. Rep.* 21 (4), 21–28. doi:10.1007/s11886-019-1107-y

Haga, T., Ibe, A., Aso, Y., Ishizawa, M., Miyajima, M., and Takeda, K. (2012). Development of Methodology for Estimation of Skin Blood Perfusion by Applying Inverse Analysis of Skin Model. *Biomed. Eng.* 50 (4), 317–328. doi:10.11239/jsmbe.50.317

He, Y., Deng, B., Wang, H., Cheng, L., Zhou, K., Cai, S., et al. (2021). Infrared Machine Vision and Infrared Thermography with Deep Learning: A Review. *Infrared Phys. Techn.* 116 (2), 103754. doi:10.1016/j.infrared.2021.103754

He, Z.-Z., and Liu, J. (2017). A Coupled Continuum-Discrete Bioheat Transfer Model for Vascularized Tissue. *Int. J. Heat Mass Transfer* 107, 544–556. doi:10.1016/j.ijheatmasstransfer.2016.11.053

Hernandez-Contreras, D., Peregrina-Barreto, H., Rangel-Magdaleno, J., and Gonzalez-Bernal, J. (2016). Narrative Review: Diabetic Foot and Infrared Thermography. *Infrared Phys. Techn.* 78, 105–117. doi:10.1016/j.infrared.2016.07.013

Kevin, C., Falzon, O., and Sturgeon, C. (2019). Thermography to Assess Success of Lower Limb Endovascular Revascularisation in Diabetics with Critical Ischaemia. *Eur. J. Vasc. Endovascular Surg.* 58 (6), e36. doi:10.1016/j.ejvs.2019.06.545

Ma, W., Liu, W., and Li, M. (2015). Modeling Heat Transfer from Warm Water to Foot: Analytical Solution and Experimental Validation. *Int. J. Therm. Sci.* 98, 364–373. doi:10.1016/j.ijthermalsci.2015.07.030

Maldonado, H., Bayareh, R., Torres, I. A., Vera, A., Gutiérrez, J., and Leija, L. (2020). Automatic Detection of Risk Zones in Diabetic Foot Soles by Processing Thermographic Images Taken in an Uncontrolled Environment. *Infrared Phys. Techn.* 105, 103187. doi:10.1016/j.infrared.2020.103187

Manzi, M., Cester, G., Palena, L. M., Alek, J., Candeo, A., and Ferraresi, R. (2011). Vascular Imaging of the Foot: The First Step toward Endovascular Recanalization. *Radiographics* 31 (6), 1623–1636. doi:10.1148/rg.316115511

Mizeva, I., Zharkikh, E., Dremin, V., Zherebtsov, E., Makovik, I., Potapova, E., et al. (2018). Spectral Analysis of the Blood Flow in the Foot Microvascular Bed during thermal Testing in Patients with Diabetes Mellitus. *Microvasc. Res.* 120, 13–20. doi:10.1016/j.mvr.2018.05.005

Muhammad, A., Eddie, Ng., and Shu, Oh. (2018a). Automated Characterization of Diabetic Foot Using Nonlinear Features Extracted from Thermograms. *Infrared Phys. Techn.* 89, 325–337. doi:10.1016/j.infrared.2018.01.022

Muhammad, A., Eddie, Ng., Shu, Oh., Heng, M. L., Hagiwara, Y., Tan, J. H., et al. (2018b). Automated Detection of Diabetic Foot with and without Neuropathy Using Double Density-Dual Tree-Complex Wavelet Transform on Foot Thermograms. *Infrared Phys. Techn.* 92, 270–279. doi:10.1016/j.infrared.2018.06.010

Muhammad, A., Eddie, N. G., Tan, J. H., Heng, M. L., Tong, J. W. K., and Rajendra Acharya, U. (2017). Computer Aided Diagnosis of Diabetic Foot Using Infrared Thermography: A Review. *Comput. Biol. Med.* 91, 326. doi:10.1016/j.compbiomed.2017.10.030

Nagata, K., Hattori, H., Sato, N., Ichige, Y., and Kiguchi, M. (2009). Heat Transfer Analysis for Peripheral Blood Flow Measurement System. *Rev. Scientific Instr.* 80 (6), 064902. doi:10.1063/1.3155458

Nieuwenhoff, M. D., Wu, Y., Huygen, F. J. P. M., Schouten, A. C., van der Helm, F. C. T., and Niehof, S. P. (2016). Reproducibility of Axon Reflex-Related Vasodilation Assessed by Dynamic thermal Imaging in Healthy Subjects. *Microvasc. Res.* 106, 1–7. doi:10.1016/j.mvr.2016.03.001

Orchard, T. J., and Strandness, D. E. (1993). Assessment of Peripheral Vascular Disease in Diabetes. Report and Recommendations of an International Workshop Sponsored by the American Heart Association and the American Diabetes Association 18-20 September 1992, New Orleans, Louisiana. *J. Am. Podiatr Med. Assoc.* 83 (2), 685–695. doi:10.7547/87507315-83-12-685

Parshakov, A., Zubareva, N., and Frick, S. P. (2016). Detection of Endothelial Dysfunction Using Skin Temperature Oscillations Analysis during Local Heating in Patients with Peripheral Arterial Disease. *Microcirculation* 23 (6), 406–415. doi:10.1111/micc.12283

Parshakov, A., Zubareva, N., Podtaev, S., and Frick, P. (2017). Local Heating Test for Detection of Microcirculation Abnormalities in Patients with Diabetes-Related Foot Complications. *Adv. Skin Wound Care* 30 (4), 158–166. doi:10.1097/01.asw.0000508635.06240.c9

Pennes, H. H. (1998). Analysis of Tissue and Arterial Blood Temperatures in the Resting Human Forearm. *J. Appl. Physiol.* 85 (1), 5–34. doi:10.1152/jappl.1998.85.1.5

Podtaev, S., Stepanov, R., Smirnova, E., and Loran, E. (2014). Wavelet-analysis of Skin Temperature Oscillations during Local Heating for Revealing Endothelial Dysfunction. *Microvasc. Res.* 97, 109–114. doi:10.1016/j.mvr.2014.10.003

Podtaev, S., Morozov, M., and Frick, P. (2008). Wavelet-based Correlations of Skin Temperature and Blood Flow Oscillations. *Cardiovasc. Eng.* 8 (3), 185–189. doi:10.1007/s10558-008-9055-y

Pozrikidis, C. (2009). Numerical Simulation of Blood Flow through Microvascular Capillary Networks. *Bull. Math. Biol.* 71 (6), 1520–1541. doi:10.1007/s11538-009-9412-z

Rafael, B., Arturo, V., Lorenzo, L., and Gutierrez, M. I. (2016). "Simulation of the Temperature Distribution on a Diabetic Foot Model: A First Approximation," in 13th International Conference on Electrical Engineering, Computing Science and Automatic Control (CCE), IEEE, Mexico City, Mexico, 24 November 2016, 1–5.

Ricketts, P. L., Mudaliar, A. V., Ellis, B. E., Pullins, C. A., Meyers, L. A., Lanz, O. I., et al. (2008). Non-invasive Blood Perfusion Measurements Using a Combined Temperature and Heat Flux Surface Probe. *Int. J. Heat Mass. Transf* 51 (23-24), 5740–5748. doi:10.1016/j.ijheatmasstransfer.2008.04.051

Sagaidachnyi, A. A., Skripal, A. V., Fomin, A. V., and Usanov, D. A. (2014). Determination of the Amplitude and Phase Relationships between Oscillations in Skin Temperature and Photoplethysmography-Measured Blood Flow in Fingertips. *Physiol. Meas.* 35 (2), 153–166. doi:10.1088/0967-3334/35/2/153

Sagaidachnyi, A. A., Fomin, A. V., Usanov, D. A., and Skripal, A. V. (2017). Thermography-based Blood Flow Imaging in Human Skin of the Hands and Feet: a Spectral Filtering Approach. *Physiol. Meas.* 38 (2), 272–288. doi:10.1088/1361-6579/aa4eaf

Schürmann, M., Zaspel, J., Gradl, G., Wipfel, A., and Christ, F. (2001). Assessment of the Peripheral Microcirculation Using Computer-Assisted Venous Congestion Plethysmography in Post-Traumatic Complex Regional Pain Syndrome Type I. *J. Vasc. Res.* 38 (5), 453–461. doi:10.1159/000051078

Serlina, S., Saldy, Y., Cahyono, K., and Mukhtar, M. (2020). Evaluation Risk of Diabetic Foot Ulcers (DFUs) Using Infrared Thermography Based on mobile Phone as Advanced Risk Assessment Tool in the Community Setting: A Multisite Cross-Sectional Study. *Enfermería Clínica* 30, 453–457. doi:10.1016/j.enfcli.2019.07.136

Shao, H., He, Y., and Mu, L. (2014). Numerical Analysis of Dynamic Temperature in Response to Different Levels of Reactive Hyperaemia in a Three-Dimensional Image-Based Hand Model. *Comput. Methods Biomech. Biomed. Engin* 17 (5-8), 865–874. doi:10.1080/10255842.2012.723698

Sivanandam, S., Anburajan, M., Venkatraman, B., Menaka, M., and Sharath, D. (2012). Medical Thermography: a Diagnostic Approach for Type 2 Diabetes Based on Non-contact Infrared thermal Imaging. *Endocrine* 42 (2), 343–351. doi:10.1007/s12020-012-9645-8

Smirnova, E., Podtaev, S., Mizeva, I., and Loran, E. (2013). Assessment of Endothelial Dysfunction in Patients with Impaired Glucose Tolerance during a Cold Pressor Test. *Diabetes Vasc. Dis. Res.* 10 (6), 489–497. doi:10.1177/1479164113494881

Tang, Y., He, Y., Shao, H., and Ji, C. (2016). Assessment of Comfortable Clothing thermal Resistance Using a Multi-Scale Human Thermoregulatory Model. *Int. J. Heat Mass Transfer* 98, 568–583. doi:10.1016/j.ijheatmasstransfer.2016.03.030

Tang, Y. L. (2017). *Mechanism Study of Thermal Methods for the Detection of Diabetic Microvascular Dysfunction* (Dalian: Dalian University of Technology). PhD thesis.

Tang, Y. L., Mizeva, I., and He, Y. (2017). A Modeling Method on the Influence of Blood Flow Regulation on Skin Temperature Pulsations. *Proc. SPIE* 10337, 1–6. doi:10.1117/12.2267952

Tang, Y., Mu, L., and He, Y. (2020). Numerical Simulation of Fluid and Heat Transfer in a Biological Tissue Using an Immersed Boundary Method Mimicking the Exact Structure of the Microvascular Network. *Fluid Dyn. Mater. Process.* 16 (2), 281–296. doi:10.32604/fdmp.2020.06760

Uraiwan, C., Patsakorn, N., Tanchanok, D., and Yamauchi, J. (2018). An Exploration of the Relationship between Foot Skin Temperature and Blood Flow in Type 2 Diabetes Mellitus Patients: a Cross-Sectional Study. *J. Phys. Ther. Sci.* 30 (11), 1359–1363. doi:10.1589/jpts.30.1359

Van Netten, J. J., Van Baal, J. G., Liu, C., van der Heijden, F., and Bus, S. A. (2013). Infrared thermal Imaging for Automated Detection of Diabetic Foot Complications. *J. Diabetes Sci. Technol.* 7 (5), 1122–1129. doi:10.1177/193229681300700504

Wang, Y.-P., Tang, Y.-L., and He, Y. (2021). Numerical Analysis of the Influence of RBCs on Oxygen Transport within a Tissue with an Embedded Capillary Network. *Proc. Inst. Mech. Eng. C: J. Mech. Eng. Sci.* 235 (2), 412–427. doi:10.1177/0954406220954482

Wang, Y., Mu, L., He, Y., Tang, Y., Liu, C., Lu, Y., et al. (2020). Heat Transfer Analysis of Blood Perfusion in Diabetic Rats Using a Genetic Algorithm. *Microvasc. Res.* 131, 104013. doi:10.1016/j.mvr.2020.104013

Webb, R. C., Ma, Y., Krishnan, S., Li, Y., Yoon, S., Guo, X., et al. (2015). Epidermal Devices for Noninvasive, Precise, and Continuous Mapping of Macrovascular and Microvascular Blood Flow. *Sci. Adv.* 1 (9), e1500701. doi:10.1126/sciadv.1500701

Wei, Y., Chen, H., Chi, Q., He, Y., Mu, L., Liu, C., et al. (2021). Synchronized Research on Endothelial Dysfunction and Microcirculation Structure in Dorsal Skin of Rats with Type 2 Diabetes Mellitus. *Med. Biol. Eng. Comput.* 59 (5), 1151–1166. doi:10.1007/s11517-021-02363-5

Zhang, P., Lu, J., Jing, Y., Tang, S., Zhu, D., and Bi, Y. (2017). Global Epidemiology of Diabetic Foot Ulceration: a Systematic Review and Meta-Analysis. *Ann. Med.* 49 (2), 106–116. doi:10.1080/07853890.2016.1231932

Zhang, Y., and Zhu, K. (2010). Relationship between Tongue Temperature and Lingual Circulation System in Blood Stasis Syndrome and Blood Deficiency Syndrome. *Space Med. Med. Eng.* 23 (4), 267–273.

Zubareva, N., Parshakov, A., Podtaev, S., Frick, P., and Mizeva, I. (2019). "Recovery of Endothelial Function in Microvessels in Patients with Peripheral Artery Disease (PAD) after Conservative and Surgery Treatment," in Saratov Fall Meeting 2018: Computations and Data Analysis: from Nanoscale Tools to Brain Functions.

Conflict of Interest: The authors declare that the research was conducted in the absence of any commercial or financial relationships that could be construed as a potential conflict of interest.

Publisher's Note: All claims expressed in this article are solely those of the authors and do not necessarily represent those of their affiliated organizations, or those of the publisher, the editors, and the reviewers. Any product that may be evaluated in this article, or claim that may be made by its manufacturer, is not guaranteed or endorsed by the publisher.

APPENDIX

TABLE A1 | Information on healthy people and diabetic patients in the experiments.

Number of subject	Age	BMI
N1	52	22.0
N2	23	20.55
N3	23	18.21
N4	25	25.09
N5	28	28.34
DM1	35	20.99
DM2	48	33.14
DM3	44	25.0
DM4	32	25.69
DM5	57	28.88
DM6	64	28.7
DM7	47	26.85
DM8	49	29.39
DM9	50	30.0
DM10	34	28.53
DM11	37	32.57
DM12	50	26.9
DM13	51	22.14
DM14	66	27.9
DM15	57	25.25

frontiers | Frontiers in Bioengineering and Biotechnology

ORIGINAL RESEARCH
published: 04 April 2022
doi: 10.3389/fbioe.2022.836018

Relationship Between Plantar Tissue Hardness and Plantar Pressure Distributions in People With Diabetic Peripheral Neuropathy

Yijie Duan[1†], *Weiyan Ren*[2†], *Wei Liu*[1], *Jianchao Li*[1], *Fang Pu*[1*] *and Yih-Kuen Jan*[3*]

[1]*Key Laboratory of Biomechanics and Mechanobiology, Ministry of Education, Beijing Advanced Innovation Center for Biomedical Engineering, School of Biological Science and Medical Engineering, Beihang University, Beijing, China,* [2]*Key Laboratory of Rehabilitation Technical Aids for Old-Age Disability, Key Laboratory of Human Motion Analysis and Rehabilitation Technology of the Ministry of Civil Affairs, National Research Center for Rehabilitation Technical Aids, Beijing, China,* [3]*Department of Kinesiology and Community Health, University of Illinois at Urbana-Champaign, Champaign, IL, United States*

OPEN ACCESS

Edited by:
Rezaul Begg,
Victoria University, Australia

Reviewed by:
Karen Mickle,
The University of Newcastle, Australia
M. Tarik Arafat,
Bangladesh University of Engineering and Technology, Bangladesh

****Correspondence:***
Fang Pu
pufangbme@buaa.edu.cn
Yih-Kuen Jan
yjan@illinois.edu

†These authors have contributed equally to this work and share first authorship

Specialty section:
This article was submitted to Biomechanics, a section of the journal Frontiers in Bioengineering and Biotechnology

Received: *15 December 2021*
Accepted: *14 March 2022*
Published: *04 April 2022*

Citation:
Duan Y, Ren W, Liu W, Li J, Pu F and Jan Y-K (2022) Relationship Between Plantar Tissue Hardness and Plantar Pressure Distributions in People With Diabetic Peripheral Neuropathy. Front. Bioeng. Biotechnol. 10:836018. doi: 10.3389/fbioe.2022.836018

Objective: People with diabetic peripheral neuropathy (DPN) are usually accompanied with increased plantar pressure. Such high plantar loading during daily activities may cause changes in the biomechanical properties of plantar soft tissue, whose viability is critical to the development of foot ulcers. This study aimed to investigate the relationship between plantar tissue hardness and plantar pressure in people with and without DPN, and preliminarily explore the influence of plantar loading patterns on the plantar pressure and tissue hardness.

Methods: The study was conducted on 14 people with DPN and 14 diabetic people without DPN. The Shore durometer and MatScan System were used to measure the plantar tissue hardness and plantar pressure, respectively. The plantar loading level was evaluated by the duration of daily weight-bearing activity and was used to group diabetic participants with and without DPN into two subgroups (lower loading group and higher loading group).

Results: The plantar tissue hardness was significantly correlated with static peak plantar pressure (PPP, $p < 0.05$) and dynamic pressure-time integral (PTI, $p < 0.05$) in the forefoot region in people with DPN. Results of variance analysis showed a significant interaction effect between peripheral neuropathy and plantar loading on tissue hardness ($p < 0.05$), but not plantar pressure. For people with DPN, significant differences in tissue hardness between the higher loading group and lower loading group were observed in the forefoot, midfoot and hindfoot regions. In the higher loading group, people with DPN had significantly greater tissue hardness than that in people without DPN in the toes, forefoot, midfoot and hindfoot regions ($p < 0.05$).

Conclusions: There is a significant correlation between tissue hardness and PPP, and between tissue hardness and PTI in people with DPN. Plantar loading associated with daily activities plays a significant role on the plantar tissue hardness in people with DPN. The findings of this study contribute to further understand the relationship between increased plantar tissue hardness and high plantar pressure in people with diabetic peripheral neuropathy.

Keywords: diabetic peripheral neuropathy, foot ulcers, plantar soft tissue hardness, plantar pressure, plantar loading

INTRODUCTION

Diabetic foot ulcers (DFUs) are one of the most serious complications of diabetes, with a global prevalence of 6.3% (Zhang et al., 2017). Studies have shown that the amputation rate in diabetics is much higher than non-diabetics (Ahmad et al., 2016; Claessen et al., 2018; Gurney et al., 2018), which seriously affects the physical health and imposes additional financial burden for people with diabetes.

Peripheral neuropathy is an important risk factor for DFUs (Monteiro-Soares et al., 2012; Armstrong et al., 2017), which may lead to foot deformities, biomechanical abnormalities, and the loss of protective sensation (Volmer-Thole and Lobmann, 2016). Several studies demonstrated that people with diabetic peripheral neuropathy (DPN) have a higher peak plantar pressure (Sacco et al., 2014; Halawa et al., 2018) and show an imbalance in plantar pressure distribution (Caselli et al., 2002; Kernozek et al., 2013; Al-Angari et al., 2017), compared with people without DPN. The loss of protective sensation caused by neuropathy also prevents people with DPN from responding promptly to abnormal mechanical stress during daily activities (Armstrong et al., 2017). These factors may affect their ambulatory function.

Plantar soft tissue is the first contact with the ground during daily activities, such as standing and walking, and plays a key role in shock-absorbing and protecting foot from external mechanical damage. The accumulation of advanced glycation end-products in people with diabetes can lead to histological changes in plantar soft tissue (Ramasamy et al., 2005). Abnormal microvascular function and dysfunctional secretion of sweat caused by peripheral neuropathy may further aggravate histological changes (Volmer-Thole and Lobmann, 2016). Several studies have found that plantar soft tissue of people with DPN was thinner and stiffer than healthy people (Klaesner et al., 2002; Chao et al., 2011; Sun et al., 2011; Jan et al., 2013). Periyasamy et al. further reported significant differences in plantar tissue hardness between diabetic people with and without DPN using a shore durometer (Periyasamy et al., 2012a; Periyasamy et al., 2012b). Increased tissue hardness in people with DPN may be accompanied by stress concentration during daily activities (Klaesner et al., 2002; Chatzistergos et al., 2014). Over time, the dry skin and abnormal plantar pressure may cause hyperkeratosis under repeated and elevated plantar pressure loading (Volmer-Thole and Lobmann, 2016), which may affect the biomechanical properties of the soft tissue, and increase the vulnerability of plantar tissue to trauma and ulceration.

Several studies have shown the potential link between plantar pressure and the biomechanical properties of soft tissue (Gefen, 2003; Jan et al., 2013; Helili et al., 2021). Jan et al.'s study demonstrated a correlation between the soft tissue biomechanical properties and plantar pressure gradient in the first metatarsal region in people with DPN (Jan et al., 2013). Helili et al. also reported a correlation between plantar soft tissue hardness and average dynamic pressure in healthy people (Helili et al., 2021). However, the whole plantar regions and more plantar pressure characteristics (both peak plantar pressure and pressure-time integral (Duckworth et al., 1985; Patry et al., 2013; Chatwin et al., 2020) in static and dynamic conditions) need to be considered, in order to better understand the relationship between the biomechanical properties of soft tissue and plantar pressure distribution in people with DPN.

In daily activities, plantar loading may be an important factor affecting the plantar pressure and tissue hardness of people with DPN. Limited joint mobility, muscular alterations and foot deformities associated with peripheral neuropathy may altered the postural control and balance function during gait (Simoneau et al., 1994; Periyasamy et al., 2012a; Volmer-Thole and Lobmann, 2016), which results in an insecure gait. Such deficit of balance and posture may exacerbate their plantar biomechanical abnormalities under the excessive mechanical stress stimulus. In addition, studies showed that different levels of plantar loading have an effect on microvascular regulation (Wu et al., 2020; Duan et al., 2021). Excessive plantar pressure load may increase the degree of compression of plantar tissue and the occlusion duration of microvessels, which leads to an insufficient blood perfusion and a lack of nutrients in soft tissue. These factors may jointly influence the biomechanical properties of plantar soft tissue. It is of great significance to explore the effects of plantar loading on plantar pressure and tissue hardness for understanding the changes of soft tissue biomechanical properties on the development of ulceration in people with DPN.

Therefore, this study aimed to investigate the relationship between plantar tissue hardness and plantar pressure in people with and without DPN, and preliminarily explore the influence of plantar loading on plantar pressure and tissue hardness. This study hypothesized that the increased plantar tissue hardness was related to plantar pressure, and the plantar loading associated with daily activities has an effect on the plantar pressure and tissue hardness.

MATERIALS AND METHODS

Participants

People with type 2 diabetes were recruited from nearby hospitals and communities. The inclusion criteria were: 1) diagnosed type 2 diabetes mellitus, 2) no symptoms such as redness, inflammation, or wounds on the skin of the feet or legs, 3) no history of amputation, and 4) performed regular moderate-intensity physical activities at least 150 min/week over the course of one year on the basis of self-report (American Diabetes Association, 2021). Moderate-intensity physical activity was defined as a metabolic equivalent (MET) of 3–5.9 Mets, according to the compendium of physical activities (Ainsworth et al., 2011).

The 10 g Semmes-Weinstein monofilament was used to identify peripheral neuropathy in people with diabetes. Participants who were unable to sense the touch of the 10 g monofilament at all four areas on the plantar surface (1st, 3rd and 5th metatarsal heads and distal hallux) were assigned to the diabetic peripheral neuropathy group (DPN group) (Boulton et al., 2008), otherwise, the participant was assigned to the non-diabetic peripheral neuropathy group (Non-DPN group).

The criterion of physical activities is the minimum weekly physical activity level recommended by ADA guidelines for

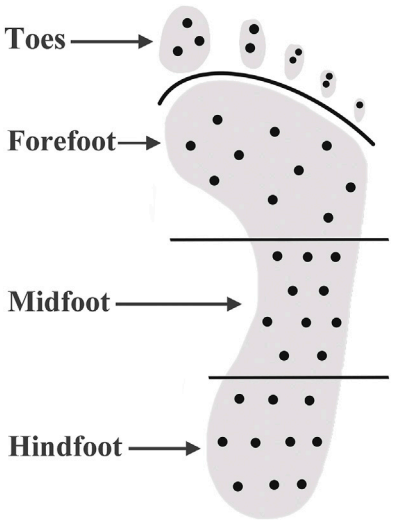

FIGURE 1 | Measurement of plantar soft tissue hardness by using the Shore (OO) durometer. The black dots indicate the measurement site of plantar tissue hardness.

people with diabetes (American Diabetes Association, 2021). The type, frequency and duration of daily physical activities of each participant were firstly recorded using the International Physical Activity Questionnaire (IPAQ) (Mynarski et al., 2012), which has been proven to be a validated tool for physical activity assessment. The median duration of weight-bearing physical activity per day of all participants (LeMaster et al., 2003) was used to divided participants of each group into two subgroups (lower loading group and higher loading group).

This study was conducted in accordance with clinical protocols approved by the institutional review board of Affiliated Hospital of National Research Center for Rehabilitation Technical Aids (20190101) and the Declaration of Helsinki (2013 revision). All participants were briefed on the study purposes and procedures and gave written informed consent prior to participation.

Measurement of Plantar Tissue Hardness and Plantar Pressure

All tests were performed in a climate-controlled room at 24°C.

A Shore durometer (Model 1600, Type OO, Rex Co., Buffalo Grove, USA) was used to measure the plantar tissue hardness, which has been used in several studies (Periyasamy et al., 2012b; Helili et al., 2021). During measurement, the durometer was pressed perpendicular to the plantar skin surface and expresses the hardness in degrees of Shore (unit: °Shore). A lower Shore value indicates a softer material. The plantar surface was divided into four regions: toes, forefoot, midfoot and hindfoot. Ten sites were selected for each of four regions of interest. Plantar tissue hardness over these sites were measured and mean values of tissue hardness were calculated for comparisons to investigate the relationship between plantar tissue hardness and plantar pressure. All measurements were performed by one skilled experimenter. **Figure 1** shows the measurement sites of plantar tissue hardness by using the Shore (OO) durometer. The locations and area of callus were special recorded.

A MatScan System (HR Mat, Tekscan, Inc., Boston, USA) was used to measure plantar pressure. It has a spatial resolution of 4 Sensels™/cm^2 (25 Sensels/in^2) with 8,448 individual pressure sensing locations. After calibration based on the manufacturer recommendations, the pressure was recorded at static conditions (standing) and dynamic conditions (taking one step on the MatScan) (Sacco et al., 2014). Recordings were made at 50 Hz for 30 s, and the analysis was made using the FootMat Research software. Plantar pressure parameters included static peak plantar pressure (PPP), dynamic peak plantar pressure (PPP) and dynamic pressure-time integral (PTI).

Data and Statistical Analyses

The plantar foot was divided into four regions, including toes, forefoot, midfoot, and hindfoot. The plantar tissue hardness of the whole foot was the average value of the tissue hardness in the regions of toes, forefoot, midfoot and hindfoot. Static PPP, dynamic PPP and PTI of corresponding area (toes, forefoot, midfoot, hindfoot, and whole foot) were calculated to assess plantar pressure distribution. The average values of tissue hardness and plantar pressure in the corresponding regions of the left and right feet were calculated and compared.

The correlations between tissue hardness and plantar pressure in each plantar region were determined using Pearson correlation analysis. When taking the plantar loading into consideration, two-way analysis of variance (ANOVA) was used to compare the plantar tissue hardness and plantar pressure between four subgroups to investigate the effect of plantar loading and neuropathy on tissue hardness and plantar pressure in people with diabetes. If there was a significant interaction between neuropathy and plantar loading, the simple effect (examined through univariate ANOVA) was used to assess the effect of neuropathy with restricted levels of plantar loading and vice versa. If no interaction was found, the main effects of neuropathy and plantar loading on tissue hardness and plantar pressure were assessed, respectively. The main effect is defined as an integrated effect of neuropathy, which disregard the levels of plantar loading, and vice versa.

The significant level was set as 0.05. All statistical analyses were performed in SPSS (Version 26.0, IBM, Armonk, NY, USA).

RESULTS

A total of 28 people with diabetes volunteered in this study, including 14 people with DPN (DPN group) and 14 people without DPN (Non-DPN group). Participants' characteristics are shown in **Table 1**. The median duration of daily weight-bearing activities of all participants was 2 h per day. In the DPN group, nine participants were divided into the higher loading group, and five participants were divided into the lower loading group. In the Non-DPN group, eight

TABLE 1 | Demographic and physiological information of participants in DPN group and Non-DPN group (Mean ± SD).

Variables	DPN Group	Non-DPN Group
Gender (Male/Female)	5/9	7/7
Age (years)	67.93 ± 5.72	67.86 ± 6.20
BMI (kg/m^2)	25.95 ± 2.77	25.91 ± 2.77
Systolic blood pressure (mmHg)	136.92 ± 11.54	132.43 ± 11.88
Diastolic blood pressure (mmHg)	71.38 ± 6.47	69.29 ± 7.39
Heart rate (bpm)	71.15 ± 7.94	73.36 ± 7.69
Duration of diabetes (years)	17.64 ± 11.88	14.82 ± 6.52
Fasting blood glucose (mmol/L)	7.90 ± 1.79	8.09 ± 1.65
ABI (left)	1.08 ± 0.12	1.03 ± 0.08
ABI (right)	1.00 ± 0.13	1.08 ± 0.06

There was no significant difference in all parameters between the DPN group and Non-DPN group (p > 0.05). BMI: body mass index; ABI: Ankle-brachial index. DPN: people with diabetic peripheral neuropathy; Non-DPN: people without diabetic peripheral neuropathy.

participants were divided into the higher loading group, and six participants were divided into the lower loading group. Except for one participant in the Non-DPN group engaged in square dancing and walking, the other participants only performed walking during daily activities. The daily weight-bearing physical activities duration of DPN group and Non-DPN group was 1.93 ± 0.92 h/day and 1.75 ± 0.80 h/day, respectively.

In DPN group, three participants had callus over the forefoot region, two participants had callus over the big toe, and one participant had callus over both forefoot region and big toe. In the Non-DPN group, none of them had callus in their feet.

Relationships Between Soft Tissue Hardness and Plantar Pressure

For all participants, tissue hardness in the forefoot region was significantly correlated with static PPP and dynamic PTI (Static PPP: r = 0.556, p = 0.002, and Dynamic PTI: r = 0.447, p = 0.017). No significant correlations between tissue hardness and plantar pressure in other plantar regions were observed ($p > 0.05$).

Figure 2 shows the correlations between the soft tissue hardness and plantar pressure in each plantar region of people with DPN. The tissue hardness of the forefoot region was significantly correlated with static PPP and dynamic PTI (tissue hardness and static PPP: r = 0.599, p = 0.024, tissue hardness and Dynamic PTI: r = 0.573, p = 0.032). No significant correlations between the soft tissue hardness and

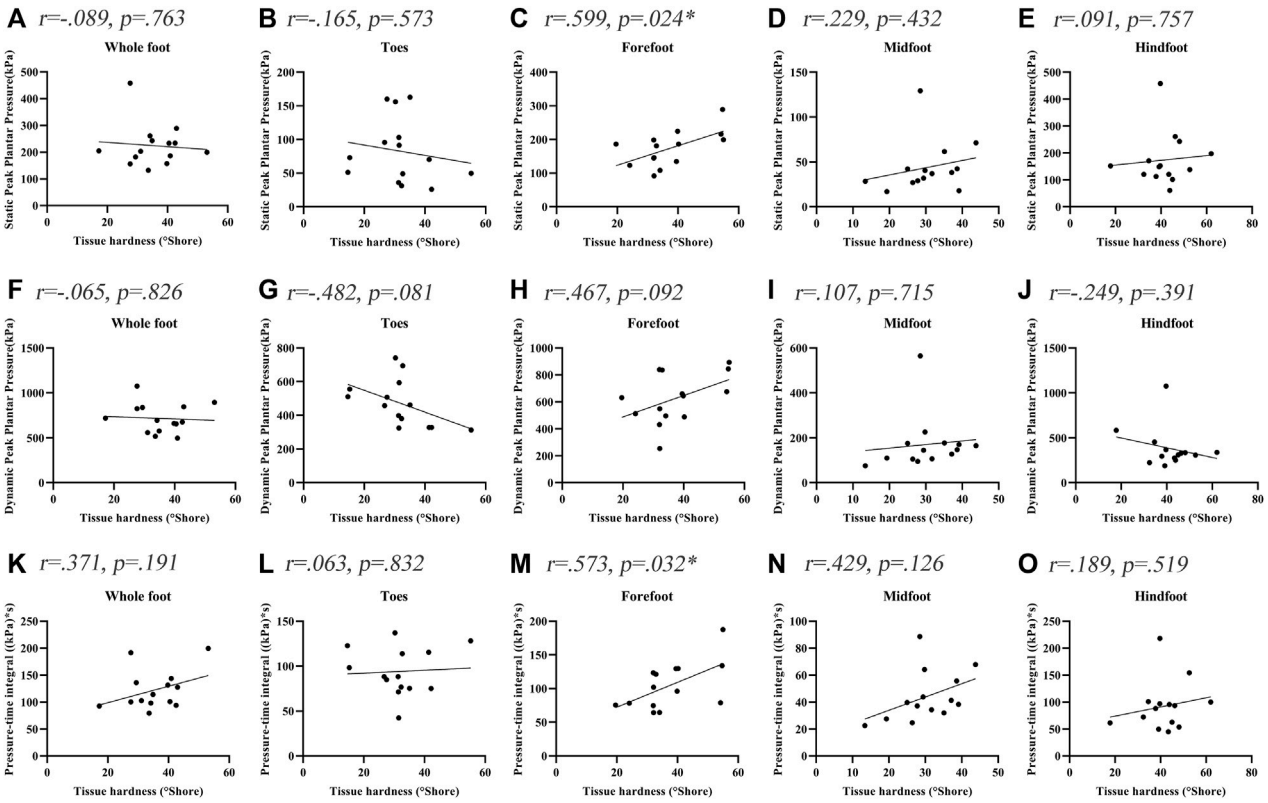

FIGURE 2 | Correlation coefficients between plantar tissue hardness and plantar pressure in people with DPN. * indicates a significant correlation ($p < 0.05$). **(A-E)** represent the correlation coefficients between plantar tissue hardness and static peak plantar pressure in the whole foot, toes region, forefoot region, midfoot region and hindfoot region, respectively. **(F-J)** represent the correlation coefficients between plantar tissue hardness and dynamic peak plantar pressure in the whole foot, toes region, forefoot region, midfoot region and hindfoot region, respectively. **(K-O)** represent the correlation coefficients between plantar tissue hardness and pressure-time integral in the whole foot, toes region, forefoot region, midfoot region and hindfoot region, respectively.

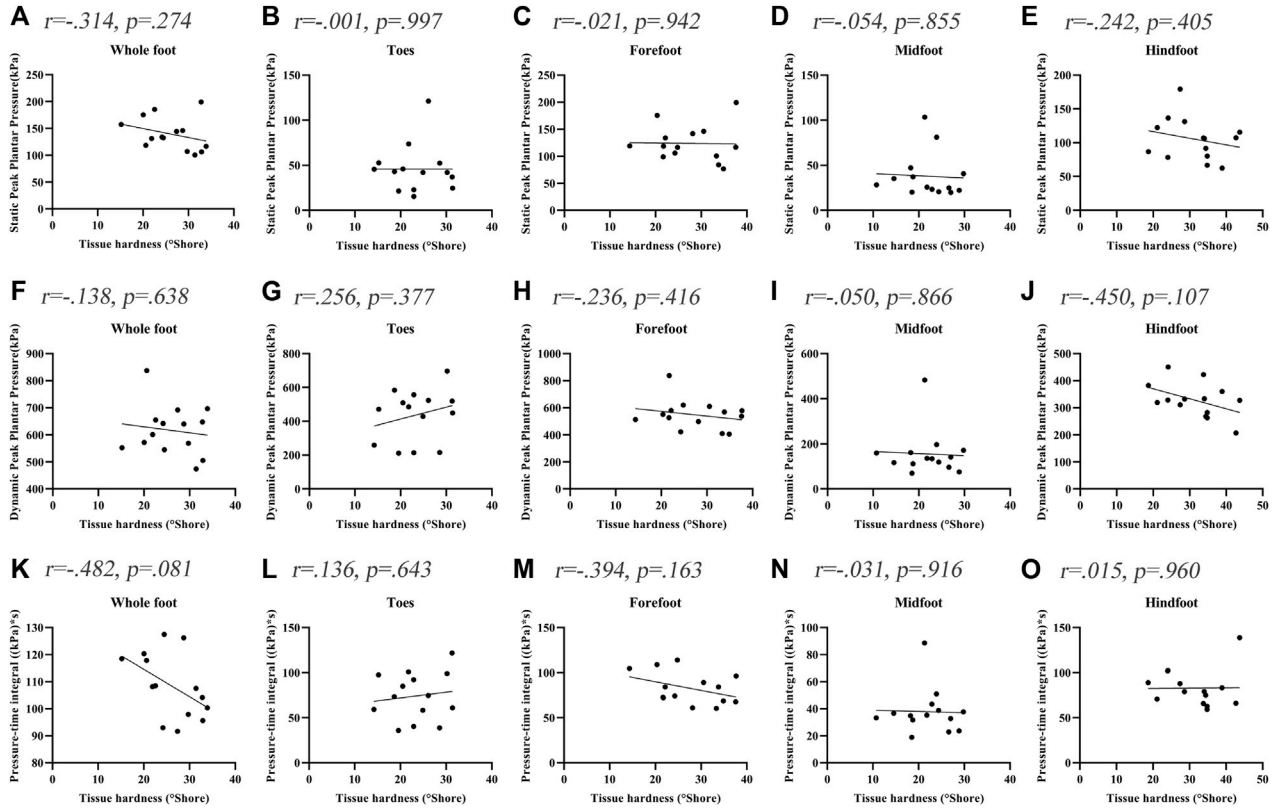

FIGURE 3 | Correlation coefficients between plantar tissue hardness and plantar pressure in people without DPN. **(A-E)** represent the correlation coefficients between plantar tissue hardness and static peak plantar pressure in the whole foot, toes region, forefoot region, midfoot region and hindfoot region, respectively. **(F-J)** represent the correlation coefficients between plantar tissue hardness and dynamic peak plantar pressure in the whole foot, toes region, forefoot region, midfoot region and hindfoot region, respectively. **(K-O)** represent the correlation coefficients between plantar tissue hardness and pressure-time integral in the whole foot, toes region, forefoot region, midfoot region and hindfoot region, respectively.

plantar pressure in other plantar regions were observed ($p > 0.05$).

Figure 3 shows the correlations between the soft tissue hardness and plantar pressure in each plantar region of people without DPN. The correlations between the soft tissue hardness and plantar pressure both did not reach statistical significance in each plantar region ($p > 0.05$).

Effect of Plantar Loading and Neuropathy on Tissue Hardness and Plantar Pressure

The interaction and main effect of peripheral neuropathy and plantar loading on tissue hardness and plantar pressure was showed in **Table 2**.

There was an interaction between the peripheral neuropathy and plantar loading on tissue hardness, with a statistical significance over the whole foot, forefoot, midfoot, and hindfoot region ($p < 0.05$). The results of simple effect on tissue hardness showed that people with DPN and higher loading had significantly higher tissue hardness, compared with people without DPN and higher loading ($p < 0.05$, **Table3**). Similarly, significant differences were also found between people with DPN and higher loading and people with DPN and lower loading, and between people with DPN and higher loading people and people without DPN and lower loading ($p < 0.05$). No significant differences in tissue hardness were observed among other subgroups ($p > 0.05$).

There was no significant interaction between the peripheral neuropathy and plantar loading on plantar pressure ($p > 0.05$). Peripheral neuropathy and plantar loading caused a significant main effect on plantar pressure, respectively (**Table 2**). The static PPP of participants in the DPN group was higher than Non-DPN group, with a significant difference over the whole foot, toes, forefoot, and hindfoot region ($p < 0.05$). The PTI of participants in the DPN group was significantly higher than Non-DPN group over the toes region ($p < 0.05$). In comparison to participants in lower loading group, people with higher loading showed significantly higher static PPP, dynamic PPP and PTI over the midfoot region and lower dynamic PPP over the toes region ($p < 0.05$).

In addition, people with callus over the forefoot region had significantly greater values of tissue hardness compared people without callus in the DPN group (50.94 ± 7.37 vs. 31.87 ± 6.19 Shore, $p < 0.05$). Their plantar pressure also higher than people without callus (static PPP: 232.18 ± 39.33 *vs.* 149.99 ± 36.69 kPa, $p < 0.05$, dynamic PPP: 764.69 ± 123.29 *vs.* 569.73 ± 179.61 kPa,

TABLE 2 | The interaction and main effects of peripheral neuropathy and plantar loading patterns on plantar tissue hardness and plantar pressure (Mean ± SD).

		DPN	Non-DPN	Lower Loading	Higher Loading	ANOVA *p* Value		
						P_I	P_N	P_L
Tissue hardness (°Shore)	Whole foot	35.39 ± 8.81	26.12 ± 5.72	27.24 ± 5.61	33.03 ± 9.67	**0.019**	**0.006**	**0.043**
	Toes	31.94 ± 10.29	23.44 ± 5.61	24.39 ± 6.17	29.82 ± 10.35	0.261	**0.026**	0.127
	Forefoot	37.32 ± 10.91	27.51 ± 7.24	28.25 ± 6.05	35.11 ± 11.78	**0.019**	**0.022**	0.053
	Midfoot	30.34 ± 8.14	21.94 ± 5.44	23.31 ± 6.21	27.97 ± 8.7	**0.045**	**0.009**	0.099
	Hindfoot	41.58 ± 10.19	31.5 ± 7.74	33.86 ± 8.99	38.27 ± 10.9	**0.016**	**0.018**	0.225
Static PPP (kPa)	Whole foot	224.15 ± 79.87	139.61 ± 30.56	177.22 ± 41.92	184.9 ± 89.14	0.170	**0.003**	0.918
	Toes	82.49 ± 48.01	45.68 ± 26.56	78.55 ± 49.51	54.72 ± 35.64	0.473	**0.009**	0.075
	Forefoot	173.47 ± 52.67	123.79 ± 33.64	140.16 ± 41.24	154.11 ± 55.76	0.060	**0.018**	0.497
	Midfoot	43.75 ± 28.75	37.79 ± 24.92	28.03 ± 6.77	49.01 ± 31.29	0.777	0.703	**0.049**
	Hindfoot	173.98 ± 97.63	105.15 ± 31.32	137.65 ± 51.78	140.79 ± 94.52	0.541	**0.035**	0.961
Dynamic PPP (kPa)	Whole foot	716.27 ± 162.5	616.08 ± 92.34	658.84 ± 109.2	670.92 ± 158.93	0.712	0.062	0.941
	Toes	471.09 ± 138.3	437.01 ± 153.78	547.55 ± 95.13	393.54 ± 140.38	0.568	0.306	**0.004**
	Forefoot	625.43 ± 184.92	546.46 ± 108.96	521.65 ± 151.07	627.55 ± 145.65	0.472	0.283	0.087
	Midfoot	170.56 ± 120.44	154.94 ± 100.86	107.66 ± 21.81	198.39 ± 128.16	0.809	0.865	**0.037**
	Hindfoot	380.85 ± 222.22	327.43 ± 63.78	331.2 ± 106.24	368.98 ± 192.42	0.686	0.394	0.618
Dynamic PTI (kPa*s)	Whole foot	122.24 ± 36.23	108.36 ± 12.07	107.02 ± 14.73	120.65 ± 32.49	0.243	0.326	0.217
	Toes	94.08 ± 26.41	74.09 ± 26.46	92.87 ± 20.78	78.41 ± 30.88	0.993	**0.048**	0.127
	Forefoot	104.3 ± 35.16	82.67 ± 17.69	85.16 ± 21.19	98.88 ± 33.22	0.053	0.121	0.218
	Midfoot	44.09 ± 18.72	37.77 ± 16.82	32.17 ± 7.16	46.6 ± 20.32	0.645	0.484	**0.042**
	Hindfoot	92.2 ± 46.09	82.86 ± 20.97	83.68 ± 22.44	90.02 ± 42.31	0.573	0.621	0.683

P_I, *is the interaction between plantar loading and peripheral neuropathy;* P_N, *is the main effect of peripheral neuropathy;* P_L, *is the main effect of plantar loading. P value in bold text indicate the significant interaction or main effect. DPN: people with diabetic peripheral neuropathy; Non-DPN: people without diabetic peripheral neuropathy.*

TABLE 3 | The effect of peripheral neuropathy and plantar loading patterns on plantar tissue hardness (Mean ± SD).

	DPN Group		Non-DPN Group		ANOVA *p* Value		
	Lower Loading	Higher Loading	Lower Loading	Higher Loading	P_{LH}	P_{HH}	P_{HL}
Whole foot	27.92 ± 6.47	39.54 ± 7.13[a,b,c]	26.68 ± 5.35	25.7 ± 6.31	**0.011**	**0.001**	**0.002**
Toes	26.46 ± 6.72	34.98 ± 10.96[b,c]	22.67 ± 5.67	24.01 ± 5.89	0.144	**0.024**	**0.026**
Forefoot	28.15 ± 5.96	42.41 ± 9.69[a,b,c]	28.34 ± 6.68	26.89 ± 8.02	**0.012**	**0.003**	**0.009**
Midfoot	24.31 ± 7.7	33.69 ± 6.53[a,b,c]	22.48 ± 5.27	21.54 ± 5.9	**0.032**	**0.001**	**0.004**
Hindfoot	33.76 ± 10.35	45.92 ± 7.46[a,b,c]	33.95 ± 8.72	29.66 ± 6.92	**0.025**	**<0.001**	**0.014**

P_{LH}, *is the significance test between people with DPN and lower loading, and people with DPN and higher loading;* P_{HH}, *is the significance test between people with DPN and higher loading, and people without DPN and higher loading;* P_{HL}, *is the significance test between people with DPN and higher loading, and people without DPN and lower loading.*
[a]*Indicates a significant difference between people with DPN and lower loading, and people with DPN and higher loading (*$p < 0.05$*).*
[b]*Indicates a significant difference between people with DPN and higher loading, and people without DPN and higher loading (*$p < 0.05$*).*
[c]*Indicates a significant difference between people with DPN and higher loading, and people without DPN and lower loading (*$p < 0.05$*). P value in bold text indicate the significant difference. DPN: people with diabetic peripheral neuropathy; Non-DPN: people without diabetic peripheral neuropathy.*

$p < 0.05$, dynamic PTI: 124.25 ± 48.15 *vs.* 96.32 ± 27.66 kPa*s, $p = 0.188$).

DISCUSSION

This study investigated the relationship between plantar tissue hardness and plantar pressure in people with and without DPN, and preliminarily explored the influence of plantar loading associated with daily activities on plantar pressure and tissue hardness. The results showed significant correlations between tissue hardness and static PPP, and between tissue hardness and dynamic PTI in the forefoot region in people with DPN. Peripheral neuropathy and plantar loading caused a significant interaction effect on tissue hardness, but not plantar pressure. The plantar pressure distribution was independently associated with peripheral neuropathy and plantar loading. In comparison to people without DPN, significant differences in tissue hardness were only found in people with DPN and higher loading.

The results of this study showed that plantar tissue hardness of people with DPN was significantly correlated to static PPP and dynamic PTI over the forefoot region. This suggested the potential relationship between increased plantar tissue hardness and high plantar pressure. This study is an important supplement to Jan et al.'s study (Jan et al., 2013) that did not pay attention to the static plantar pressure. Static plantar pressure, reflecting the contact force of the foot with the ground during standing, is as important as dynamic plantar pressure in assessing the risk of DFUs (Duckworth et al., 1985; Patry et al., 2013). Thus, both static plantar pressure (during

standing) and dynamic plantar pressure (during walking) were measured in this study. However, except the forefoot region, no significant correlation was observed between tissue hardness and plantar pressure in other plantar regions, which may be due to the fact that the forefoot is the main load-bearing area during daily activities. There was no significant correlation in the heel region may be related to the imbalanced plantar pressure distribution (Caselli et al., 2002; Kernozek et al., 2013; Al-Angari et al., 2017), which may lead to change of plantar load-bearing position. Besides, the different correlation trend between plantar pressure and tissue hardness in different plantar regions may be related to different injury thresholds, which should be explored in future studies. It should also be mentioned that no significant correlation between plantar pressure and tissue hardness was observed in people without DPN. This may be due to their relatively normal plantar pressure distribution and postural control during walking. The changes of the soft tissue biomechanical properties in diabetic people without DPN may be more influenced by the accumulation of advanced glycation end-products. Therefore, foot deformities, postural control and balance function may be considered in future studies. In this study, a significant correlation between increased plantar tissue hardness and plantar pressure could contribute to understand the changes of soft tissue biomechanical properties in people with DPN.

The findings of this study also found that increased plantar tissue hardness associated with peripheral neuropathy was affected by plantar loading level. People with DPN and higher loading had higher tissue hardness compared with people with DPN and lower loading in the forefoot, midfoot and hindfoot regions. It indicated a low shock-absorbing capacity to distribute mechanical stress during daily activities, especially weight-bearing activities (e.g. walking) in people with DPN. Excessive and repetitive plantar pressure loading may aggravate the stiffness of plantar soft tissue due to their weak ability to evenly distribute abnormal plantar pressure (Chatzistergos et al., 2014) during daily activities. Klaesner et al. demonstrated that the plantar soft tissue of people with DPN over the metatarsal heads was stiffer than healthy people using an indentor system (Klaesner et al., 2002). Several studies have also reported consistent findings using ultrasound palpation system (Sun et al., 2011). However, none of these studies involved diabetic people without DPN, which makes it difficult to determine the changes in biomechanical properties of plantar soft tissue associated with pure neuropathy. Only one study reported a significant difference in tissue hardness between diabetic people with and without DPN (Periyasamy et al., 2012b), which was consistent with the results in this study. Increased plantar tissue hardness in people with DPN and higher loading indicated a warning that excessive plantar loading during weight-bearing activities may increase the burden of fragile soft tissue caused by peripheral neuropathy (Sun et al., 2011) and make a negative effect on plantar soft tissue.

However, no significant difference was observed in plantar tissue hardness between people without DPN and lower loading and people without DPN and higher loading, which indicated the specificity and importance of the safe threshold for plantar loading during daily activities. The Physical Stress Theory (PST) proposed by Muller and his group assumes a window of "increased tolerance" between function maintenance threshold and injury threshold of plantar soft tissue. Physical stress within this window may be beneficial to enhance the adaptability of plantar soft tissue to external stress stimulus (Mueller and Maluf, 2002; Kluding et al., 2017) for people with DPN. The most important and challenging thing, however, is how to determine this safe threshold. In addition, Chao et al. showed that the stiffness of plantar soft tissue was increased in all diabetic people (diabetics with foot ulceration group, diabetics with neuropathy group, and pure diabetics group) compared healthy people, but no significant difference was reported between people with neuropathy and pure diabetics (Chao et al., 2011). This may be due to a lack of consideration of various plantar loading levels on soft tissue. In this study, no significant differences in tissue hardness were found between people with DPN and lower loading and people without DPN and lower loading. It indicated that appropriate plantar loading (e.g. performing weight-bearing physical activities) may be useful to improve the soft tissue biomechanical properties in people with DPN (Otterman et al., 2011; Mueller et al., 2013). Otterman et al. demonstrated the benefits of a 12-weeks exercise programme, consisting 30 min of aerobic exercise (e.g. cycling, walking, etc.) per day for people with DPN (Otterman et al., 2011). Mueller et al.'s study conducted a 12-weeks exercise programme for 1-h exercise sessions with 3 times per week (Mueller et al., 2013), and demonstrated the benefits of weight-bearing exercise in ambulatory function. Future studies may need to clarify the effects of different levels of plantar loading on plantar soft tissue, in order to seek the safety thresholds in people with and without DPN and guide physicians to develop exercise program for people with diabetes.

In addition, the static PPP of people with DPN were significantly higher than people without DPN, which was consistent with previous studies (Sacco et al., 2014; Halawa et al., 2018). However, no significant difference in dynamic PPP between people with and without DPN was observed in this study. Such differences may be influenced by different patient characteristics such as severity stages of diabetic peripheral neuropathy (Sacco et al., 2014) and skin health characteristics (i.e. callus presence). Because Sacco et al. found that plantar pressure gradually increased with the aggravation of neuropathy (Sacco et al., 2014). People with higher loading had higher plantar pressure in the midfoot region and lower plantar pressure in the toes region, suggesting changes of plantar pressure distribution under repeated mechanical stress stimulus. Therefore, the influence of such changes of plantar pressure distribution on diabetic foot ulcers still needs to be further studied.

In people with DPN, the forefoot region with callus had higher peak plantar pressure compared with people without callus. Studies suggested high shear stress near callus could cause abnormal peak plantar pressure and plantar pressure gradient in plantar soft tissues (Chao et al., 2011). Plantar soft tissue in callus area has impaired shock-absorbing function, which may result in tissue inflammation, skin breakdown and ulceration (Sun et al., 2011). Therefore, callus presence should be noticed immediately for people with DPN. It is

necessary to ensure proper footwear and perform weight-bearing physical activities selectively.

The power analysis was performed to validate the statistical results of comparisons. There are large different effects for the comparisons of plantar tissue hardness in the whole foot and forefoot region between people with DPN and higher loading and people without DPN and higher loading (whole foot: 97.91%, forefoot region: 92.49%). In addition, the power of the difference in plantar tissue hardness in the whole foot and forefoot region between people with DPN and lower loading and people with DPN and higher loading was 80.77 and 88.55%, respectively. This may suggest an important influence of plantar loading level (i.e. weight-bearing physical activity duration) on the biomechanical properties of plantar soft tissue in people with DPN.

This study has some limitations. Firstly, plantar loading caused by exercise may result in different plantar pressures between people with and without DPN. It is necessary to examine the relationship between plantar loading and plantar pressure in a larger cohort of participants with DPN. Besides, plantar loading patterns were only divided into two levels based on the duration of daily weight-bearing activities, due to the limited sample size. More groups of plantar loading levels should be explored in the future. Secondly, this study explored the influence of plantar loading caused by exercise on plantar tissue hardness and plantar pressure in people with DPN. Future research should perform longitudinal studies to further explore the changes in the soft tissue biomechanical properties under long-term physical activities. Thirdly, walking was the main type of weight-bearing activities among the participants enrolled in this study. Other types of physical activities should be considered in future studies. Fourthly, the shore durometer has limitations in characterizing nonlinear viscoelastic behavior and tissue thickness of soft tissue. Ultrasound imaging may provide additional information on the biomechanical properties of plantar soft tissue (e.g. skin thickness). In addition, body weight and duration of diabetes may affect the results observed in our study (Abouaesha et al., 2001; Pirozzi et al., 2014; Jeong et al., 2021). Thus, our finding may not be generalized to people with DM who have different durations of diabetes and BMI. The influence of other covariates on plantar pressure and tissue hardness should be investigated in the future, such as body weight and skin quality on different regions of foot. Fifthly, the plantar surface was divided into four regions in order to explore the potential relationship between tissue hardness and plantar pressure in the whole plantar region in people with diabetes. Subdivision of plantar regions (e.g. the five metatarsal regions of the forefoot, big toe and little toes) should be considered in future studies.

CONCLUSION

In conclusion, this study found that the plantar tissue hardness was correlated to plantar pressure in people with DPN. Peripheral neuropathy and plantar loading patterns associated with various physical activities are important factors affecting the biomechanical properties of plantar soft tissue. The findings of this study contribute to further understand the relationship between increased plantar tissue hardness and high plantar pressure in people with diabetic peripheral neuropathy.

DATA AVAILABILITY STATEMENT

The original contributions presented in the study are included in the article/Supplementary Material, further inquiries can be directed to the corresponding authors.

ETHICS STATEMENT

The studies involving human participants were reviewed and approved by the institutional review board of Affiliated Hospital of National Research Center for Rehabilitation Technical Aids. The patients/participants provided their written informed consent to participate in this study.

AUTHOR CONTRIBUTIONS

Methodology, FP and Y-KJ; formal analysis, YD and WR; investigation, YD, WL, and JL; data curation, YD, WL, and WR; writing—original draft preparation, YD and WR; writing—review and editing, FP and Y-KJ; funding acquisition, FP and WR. All authors have read and agreed to the published version of the manuscript.

FUNDING

This research was funded by the National Natural Science Foundation of China (grant numbers 11902089, 11672027, and 12072019).

ACKNOWLEDGMENTS

The authors thank all subjects who participated in this study.

REFERENCES

Abouaesha, F., van Schie, C. H. M., Griffths, G. D., Young, R. J., and Boulton, A. J. M. (2001). Plantar Tissue Thickness is related to Peak Plantar Pressure in the High-Risk Diabetic Foot. *Diabetes Care* 24 (7), 1270–1274. doi:10.2337/diacare.24.7.1270

Ahmad, N., Thomas, G. N., Gill, P., and Torella, F. (2016). The Prevalence of Major Lower Limb Amputation in the Diabetic and Non-diabetic Population of England 2003-2013. *Diabetes Vasc. Dis. Res.* 13 (5), 348–353. doi:10.1177/1479164116651390

Ainsworth, B. E., Haskell, W. L., Herrmann, S. D., Meckes, N., Bassett, D. R., Tudor-Locke, C., et al. (2011). 2011 Compendium of Physical Activities. *Med. Sci. Sports Exerc.* 43 (8), 1575–1581. doi:10.1249/MSS.0b013e31821ece12

Al-Angari, H. M., Khandoker, A. H., Lee, S., Almahmeed, W., Al Safar, H. S., Jelinek, H. F., et al. (2017). Novel Dynamic Peak and Distribution Plantar Pressure Measures on Diabetic Patients during Walking. *Gait & Posture* 51, 261–267. doi:10.1016/j.gaitpost.2016.11.006

American Diabetes Association (2021). 5. Facilitating Behavior Change and Well-Being to Improve Health Outcomes: Standards of Medical Care in Diabetes-2021. *Diabetes Care* 44 (Suppl. ment_1), S53–S72. doi:10.2337/dc21-S005

Armstrong, D. G., Boulton, A. J. M., and Bus, S. A. (2017). Diabetic Foot Ulcers and Their Recurrence. *N. Engl. J. Med.* 376 (24), 2367–2375. doi:10.1056/NEJMra1615439

Boulton, A. J. M., Armstrong, D. G., Albert, S. F., Frykberg, R. G., Hellman, R., Kirkman, M. S., et al. (2008). Comprehensive Foot Examination and Risk Assessment. *Endocr. Pract.* 14 (5), 576–583. doi:10.4158/ep.14.5.576

Caselli, A., Pham, H., Giurini, J. M., Armstrong, D. G., and Veves, A. (2002). The Forefoot-To-Rearfoot Plantar Pressure Ratio is increased in Severe Diabetic Neuropathy and Can Predict Foot Ulceration. *Diabetes Care* 25 (6), 1066–1071. doi:10.2337/diacare.25.6.1066

Chao, C. Y. L., Zheng, Y.-P., and Cheing, G. L. Y. (2011). Epidermal Thickness and Biomechanical Properties of Plantar Tissues in Diabetic Foot. *Ultrasound Med. Biol.* 37 (7), 1029–1038. doi:10.1016/j.ultrasmedbio.2011.04.004

Chatwin, K. E., Abbott, C. A., Boulton, A. J. M., Bowling, F. L., and Reeves, N. D. (2020). The Role of Foot Pressure Measurement in the Prediction and Prevention of Diabetic Foot Ulceration-A Comprehensive Review. *Diabetes Metab. Res. Rev.* 36 (4)e3258. doi:10.1002/dmrr.3258

Chatzistergos, P. E., Naemi, R., Sundar, L., Ramachandran, A., and Chockalingam, N. (2014). The Relationship between the Mechanical Properties of Heel-Pad and Common Clinical Measures Associated with Foot Ulcers in Patients with Diabetes. *J. Diabetes Its Complications* 28 (4), 488–493. doi:10.1016/j.jdiacomp.2014.03.011

Claessen, H., Narres, M., Haastert, B., Arend, W., Hoffmann, F., Morbach, S., et al. (2018). Lower-extremity Amputations in People with and without Diabetes in Germany, 2008–2012 – an Analysis of More Than 30 Million inhabitants. *Clep* 10, 475–488. doi:10.2147/clep.S146484

Duan, Y., Ren, W., Xu, L., Ye, W., Jan, Y.-K., and Pu, F. (2021). The Effects of Different Accumulated Pressure-Time Integral Stimuli on Plantar Blood Flow in People with Diabetes Mellitus. *BMC Musculoskelet. Disord.* 22 (1)554. doi:10.1186/s12891-021-04437-9

Duckworth, T., Boulton, A., Betts, R., Franks, C., and Ward, J. (1985). Plantar Pressure Measurements and the Prevention of Ulceration in the Diabetic Foot. *The J. Bone Jt. Surg. Br. volume* 67 (1), 79–85. doi:10.1302/0301-620x.67b1.3968150

Gefen, A. (2003). Plantar Soft Tissue Loading under the Medial Metatarsals in the Standing Diabetic Foot. *Med. Eng. Phys.* 25 (6), 491–499. doi:10.1016/s1350-4533(03)00029-8

Gurney, J. K., Stanley, J., York, S., Rosenbaum, D., and Sarfati, D. (2018). Risk of Lower Limb Amputation in a National Prevalent Cohort of Patients with Diabetes. *Diabetologia* 61 (3), 626–635. doi:10.1007/s00125-017-4488-8

Halawa, M. R., Eid, Y. M., El-Hilaly, R. A., Abdelsalam, M. M., and Amer, A. H. (2018). Relationship of Planter Pressure and Glycemic Control in Type 2 Diabetic Patients with and without Neuropathy. *Diabetes Metab. Syndr. Clin. Res. Rev.* 12 (2), 99–104. doi:10.1016/j.dsx.2017.09.010

Helili, M., Geng, X., Ma, X., Chen, W., Zhang, C., Huang, J., et al. (2021). An Investigation of Regional Plantar Soft Tissue Hardness and its Potential Correlation with Plantar Pressure Distribution in Healthy Adults. *Appl. Bionics Biomech.* 2021, 1–9. doi:10.1155/2021/5566036

Jan, Y.-K., Lung, C.-W., Cuaderes, E., Rong, D., and Boyce, K. (2013). Effect of Viscoelastic Properties of Plantar Soft Tissues on Plantar Pressures at the First Metatarsal head in Diabetics with Peripheral Neuropathy. *Physiol. Meas.* 34 (1), 53–66. doi:10.1088/0967-3334/34/1/53

Jeong, H., Johnson, A. W., Feland, J. B., Petersen, S. R., Staten, J. M., and Bruening, D. A. (2021). Added Body Mass Alters Plantar Shear Stresses, Postural Control, and Gait Kinetics: Implications for Obesity. *Plos One* 16 (2), e0246605. doi:10.1371/journal.pone.0246605

Kernozek, T. W., Greany, J. F., and Heizler, C. (2013). Plantar Loading Asymmetry in American Indians with Diabetes and Peripheral Neuropathy, with Diabetes Only, and without Diabetes. *J. Am. Podiatr Med. Assoc.* 103 (2), 106–112. doi:10.7547/1030106

Klaesner, J. W., Hastings, M. K., Zou, D., Lewis, C., and Mueller, M. J. (2002). Plantar Tissue Stiffness in Patients with Diabetes Mellitus and Peripheral Neuropathy. *Arch. Phys. Med. Rehabil.* 83 (12), 1796–1801. doi:10.1053/apmr.2002.35661

Kluding, P. M., Bareiss, S. K., Hastings, M., Marcus, R. L., Sinacore, D. R., and Mueller, M. J. (2017). Physical Training and Activity in People with Diabetic Peripheral Neuropathy: Paradigm Shift. *Phys. Ther.* 97 (1), 31–43. doi:10.2522/ptj.20160124

LeMaster, J. W., Reiber, G. E., Smith, D. G., Heagerty, P. J., and Wallace, C. (2003). Daily Weight-Bearing Activity Does Not Increase the Risk of Diabetic Foot Ulcers. *Med. Sci. Sports Exerc.* 35 (7), 1093–1099. doi:10.1249/01.Mss.0000074459.41029.75

Monteiro-Soares, M., Boyko, E. J., Ribeiro, J., Ribeiro, I., and Dinis-Ribeiro, M. (2012). Predictive Factors for Diabetic Foot Ulceration: a Systematic Review. *Diabetes Metab. Res. Rev.* 28 (7), 574–600. doi:10.1002/dmrr.2319

Mueller, M. J., and Maluf, K. S. (2002). Tissue Adaptation to Physical Stress: A Proposed "physical Stress Theory" to Guide Physical Therapist Practice, Education, and Research. *Phys. Ther.* 82 (4), 383–403. doi:10.1093/ptj/82.4.383

Mueller, M. J., Tuttle, L. J., LeMaster, J. W., Strube, M. J., McGill, J. B., Hastings, M. K., et al. (2013). Weight-Bearing versus Nonweight-Bearing Exercise for Persons with Diabetes and Peripheral Neuropathy: A Randomized Controlled Trial. *Arch. Phys. Med. Rehabil.* 94 (5), 829–838. doi:10.1016/j.apmr.2012.12.015

Mynarski, W., Psurek, A., Borek, Z., Rozpara, M., Grabara, M., and Strojek, K. (2012). Declared and Real Physical Activity in Patients with Type 2 Diabetes Mellitus as Assessed by the International Physical Activity Questionnaire and Caltrac Accelerometer Monitor: A Potential Tool for Physical Activity Assessment in Patients with Type 2 Diabetes Mellitus. *Diabetes Res. Clin. Pract.* 98 (1), 46–50. doi:10.1016/j.diabres.2012.05.024

Otterman, N. M., van Schie, C. H. M., van der Schaaf, M., van Bon, A. C., Busch-Westbroek, T. E., and Nollet, F. (2011). An Exercise Programme for Patients with Diabetic Complications: a Study on Feasibility and Preliminary Effectiveness. *Diabetic Med.* 28 (2), 212–217. doi:10.1111/j.1464-5491.2010.03128.x

Patry, J., Belley, R., Cote, M., and Chateau-Degat, M.-L. (2013). Plantar Pressures, Plantar Forces, and Their Influence on the Pathogenesis of Diabetic Foot Ulcers. *J. Am. Podiatr Med. Assoc.* 103 (4), 322–332. doi:10.7547/1030322

Periyasamy, R., Anand, S., and Ammini, A. (2012a). Association of Limited Joint Mobility and Increased Plantar Hardness in Diabetic Foot Ulceration in north Asian Indian: A Preliminary Study. *Proc. Inst. Mech. Eng. H* 226 (4), 305–311. doi:10.1177/0954411911435613

Periyasamy, R., Anand, S., and Ammini, A. C. (2012b). Investigation of Shore Meter in Assessing Foot Sole Hardness in Patients with Diabetes Mellitus - a Pilot Study. *Int. J. Diabetes Dev. Ctries* 32 (3), 169–175. doi:10.1007/s13410-012-0085-z

Pirozzi, K., McGuire, J., and Meyr, A. J. (2014). Effect of Variable Body Mass on Plantar Foot Pressure and Off-Loading Device Efficacy. *J. Foot Ankle Surg.* 53 (5), 588–597. doi:10.1053/j.jfas.2014.02.005

Ramasamy, R., Vannucci, S. J., Yan, S. S. D., Herold, K., Yan, S. F., and Schmidt, A. M. (2005). Advanced Glycation End Products and RAGE: a Common Thread in Aging, Diabetes, Neurodegeneration, and Inflammation. *Glycobiology* 15 (7), 16R–28R. doi:10.1093/glycob/cwi053

Sacco, I. C. N., Hamamoto, A. N., Tonicelli, L. M. G., Watari, R., Ortega, N. R. S., and Sartor, C. D. (2014). Abnormalities of Plantar Pressure Distribution in Early, Intermediate, and Late Stages of Diabetic Neuropathy. *Gait & Posture* 40 (4), 570–574. doi:10.1016/j.gaitpost.2014.06.018

Simoneau, G. G., Ulbrecht, J. S., Derr, J. A., Becker, M. B., and Cavanagh, P. R. (1994). Postural Instability in Patients with Diabetic Sensory Neuropathy. *Diabetes care* 17 (12), 1411–1421. doi:10.2337/diacare.17.12.1411

Sun, J.-H., Cheng, B. K., Zheng, Y.-P., Huang, Y.-P., Leung, J. Y., and Cheing, G. L. (2011). Changes in the Thickness and Stiffness of Plantar Soft Tissues in People with Diabetic Peripheral Neuropathy. *Arch. Phys. Med. Rehabil.* 92 (9), 1484–1489. doi:10.1016/j.apmr.2011.03.015

Volmer-Thole, M., and Lobmann, R. (2016). Neuropathy and Diabetic Foot Syndrome. *Ijms* 17 (6), 917. doi:10.3390/ijms17060917

Wu, F.-L., Wang, W. T.-J., Liao, F., Elliott, J., Jain, S., and Jan, Y.-K. (2020). Effects of Walking Speeds and Durations on Plantar Skin Blood Flow Responses. *Microvasc. Res.* 128, 103936. doi:10.1016/j.mvr.2019.103936

Zhang, P., Lu, J., Jing, Y., Tang, S., Zhu, D., and Bi, Y. (2017). Global Epidemiology of Diabetic Foot Ulceration: a Systematic Review and Meta-Analysis. *Ann. Med.* 49 (2), 106–116. doi:10.1080/07853890.2016.1231932

Conflict of Interest: The authors declare that the research was conducted in the absence of any commercial or financial relationships that could be construed as a potential conflict of interest.

Publisher's Note: All claims expressed in this article are solely those of the authors and do not necessarily represent those of their affiliated organizations, or those of the publisher, the editors and the reviewers. Any product that may be evaluated in this article, or claim that may be made by its manufacturer, is not guaranteed or endorsed by the publisher.

Advantages of publishing in Frontiers

OPEN ACCESS
Articles are free to read for greatest visibility and readership

FAST PUBLICATION
Around 90 days from submission to decision

HIGH QUALITY PEER-REVIEW
Rigorous, collaborative, and constructive peer-review

TRANSPARENT PEER-REVIEW
Editors and reviewers acknowledged by name on published articles

Frontiers
Avenue du Tribunal-Fédéral 34
1005 Lausanne | Switzerland

Visit us: www.frontiersin.org
Contact us: frontiersin.org/about/contact

REPRODUCIBILITY OF RESEARCH
Support open data and methods to enhance research reproducibility

DIGITAL PUBLISHING
Articles designed for optimal readership across devices

FOLLOW US
@frontiersin

IMPACT METRICS
Advanced article metrics track visibility across digital media

EXTENSIVE PROMOTION
Marketing and promotion of impactful research

LOOP RESEARCH NETWORK
Our network increases your article's readership